

Indenyl Rhodium N-Heterocyclic Carbene Complexes for Catalytic C-H Borylation

Kieren J. Evans

Submitted for the degree of Doctor of Philosophy

Heriot-Watt University

School of Engineering and Physical Sciences

Institute of Chemical Sciences

July 2020

The copyright in this thesis is owned by the author. Any quotation from the thesis or use of any of the information contained in it must acknowledge this thesis as the source of the quotation or information.

Abstract

Metal-catalysed C-H activation offers the ability to access key synthetic targets in more straightforward reactions than previously used methods. However, undirected activation pathways face issues of selectivity and low rates of reaction that make substituting simple hydrocarbons difficult. Indenyl (Ind) and fluorenyl ligands offer increased reactivity compared to cyclopentadienyl groups, which have been used previously in C-H borylation, and combining these donors with electron-donating NHC ligands was investigated for the borylation of arenes and alkanes. Additionally, the effects of tethered systems were explored to see whether the catalytic ability is enhanced.

[Rh(Ind)(SIPr)(C₂H₄)], [Rh(Ind)(SIPr)(COE)] and [Rh(Ind)(SIPr)(CO)] (SIPr = 1,3-bis(2,6-diisopropylphenyl)-4,5-dihydroimidazol-2-ylidene, COE = *cis*-cyclooctene) were synthesised and characterised by multinuclear NMR spectroscopy and X-ray diffraction. Only the ethylene and cyclooctene complexes were found to be reactive under photolytic conditions and towards silanes. Photolysis led to the loss of coordinated alkenes and the formation of a cyclometallated species due to C-H activation of the NHC substituents. With reducing silanes or hydrogen, a rhodium dihydride complex was observed, that is hypothesised to form via the reaction of the cyclometallated species, while less reducing silanes led to the formation of the oxidative addition product.

Both [Rh(Ind)(SIPr)(C₂H₄)] and [Rh(Ind)(SIPr)(COE)] were found to be catalytically competent for the borylation of benzene, while the carbonyl complex was found to be unreactive under these conditions. Borylation of a selection of arenes showed that the selectivity was comparable to previously reported rhodium catalysts, which is dominated by steric effects, however, the reactivity was lower compared to previously reported catalysts such as [RhCp*(C₆Me₆)]. Borylation of decane and octane showed that the cyclooctene complex was capable of borylating alkanes, albeit in low yields. Stoichiometric experiments monitored by NMR spectroscopy provided evidence that the catalysis proceeds via rhodium boryl hydride species, with the previously identified cyclometallated species also likely to play a role.

The synthesis of fluorenyl-tethered saturated-NHC ligands required the development of homobimetallic synergic bases in order to bring about a ring-opening deprotonation of a spirocyclic intermediate. The structure of [Li₂(μ²-Ph){μ²-N(SiMe₃)₂}] was crystallographically characterised as a coordination polymer, and reaction with the

spirocyclic compound led to the formation of dialkali metal complexes of a fluorenone-bridged NHC ligand that incorporated a bridging amide group. The use of these bimetallic complexes as ligand transfer reagents gave rhodium carbonyl and ethene complexes in low yields. Initial testing of these complexes in the borylation of benzene found that the carbonyl species was inactive while the ethene complex was less active than the related monodentate species.

Overall, this research has demonstrated that NHC ligands can be used to develop Rh-complexes capable of C-H activation, the oxidative addition of silanes and the catalytic borylation of hydrocarbons. This supports the idea that a $[\text{Rh}(\text{Ind})(\text{NHC})]$ fragment (16 electron for η^5 -indenyl, or 14 electron with η^3 -indenyl) can mimic the reactivity of the previously successful $[\text{Rh}(\text{Cp})(\text{L})]$ and $[\text{Rh}(\text{Cp}^*)]$ fragments. Although the compounds synthesised in this thesis were not better catalysts than literature examples, they hold much promise because the incorporation of a tuneable NHC ligand on the metal centre can lead to future improvements, especially considering the potential importance of cyclometallated species in C-H activation reactivity.

Acknowledgements

Firstly, I would like to thank my supervisor Dr Stephen Mansell for allowing me to undertake this project, for his constant support over the years, and for his guidance during the course of my research. His help with experimental ideas and crystallography has been invaluable during my PhD, and has helped me reach this point. I also thank Dr Mairi Haddow for her help with the more difficult crystal structure solutions.

I also thank the members of Mansell group, past and present for providing a helpful and engaging environment for research. Particular thanks to go to Dr Peter Cleaves and Dr Robert Newland for putting up with me at the beginning of my PhD, and helping in transition up to postgraduate level research. I have been lucky to work with several undergraduate project students, namely Stephen Belford, Ben Potrykus, Cameron Campbell, Paul Morton, William Walker, Callum Miller and Olivia Raine. While their research does not feature in this work, it complemented much of my work and will hopefully be further developed in the Mansell group.

I thank Dr Jason Lynam at the University of York for assisting with my research and hosting me during my short research visit which provided a great degree of information for my research. Additional thanks goes to Chris and Jonny for their in-lab assistance.

My appreciation also goes to Dr David Ellis for his assistance with NMR spectroscopy, which was extensively used during this project, and to Dr Georgina Rosair for her assistance with performing X-ray crystallography used during the course of my research.

Research Thesis Submission

Please note this form should be bound into the submitted thesis.

Name:	Kieren Evans		
School:	EPS		
Version: (<i>i.e.</i> <i>First,</i> <i>Resubmission,</i> <i>Final</i>)	Final	Degree Sought:	PhD

Declaration

In accordance with the appropriate regulations I hereby submit my thesis and I declare that:

The thesis embodies the results of my own work and has been composed by myself

Where appropriate, I have made acknowledgement of the work of others

The thesis is the correct version for submission and is the same version as any electronic versions submitted*.

My thesis for the award referred to, deposited in the Heriot-Watt University Library, should be made available for loan or photocopying and be available via the Institutional Repository, subject to such conditions as the Librarian may require

I understand that as a student of the University I am required to abide by the Regulations of the University and to conform to its discipline.

I confirm that the thesis has been verified against plagiarism via an approved plagiarism detection application e.g. Turnitin.

* *Please note that it is the responsibility of the candidate to ensure that the correct version of the thesis is submitted.*

Signature of Candidate:	Kieren J. Evans	Date:	12/02/2021
-------------------------	-----------------	-------	------------

Submission

Submitted By (<i>name in capitals</i>):	KIEREN EVANS
Signature of Individual Submitting:	Kieren J. Evans
Date Submitted:	13/02/2021

For Completion in the Student Service Centre (SSC)

Limited Access	Requested	Yes		No		Approved	Yes		No	
<i>E-thesis Submitted (mandatory for final theses)</i>										
Received in the SSC by (<i>name in capitals</i>):						Date:				

Abbreviations

AM	Alkali Metal
APCI	Atmospheric Pressure Chemical Ionisation
App.	Apparent
Ar	Aryl, a derivative of the phenyl group
ASAP	Atmospheric Solids Analysis Probe
Bcat	Catecholboronate, $\text{BO}_2\text{C}_6\text{H}_4$
BF_4	Tetrafluoroborate
Bpin	Pinacolboronate, $\text{BO}_2\text{C}_2\text{Me}_4$
bpy	2,2'-bipyridine
br	Broad
^nBu	<i>normal</i> -Butyl, $\text{CH}_2\text{CH}_2\text{CH}_2\text{CH}_3$
^tBu	<i>tertiary</i> -Butyl, $\text{C}(\text{CH}_3)_3$
COD	Cyclooctadiene
COE	Cyclooctene
Cp	Cyclopentadienyl
Cp^*	Pentamethylcyclopentadienyl
d	Doublet
δ	Chemical shift
Δ	Heating a chemical reaction
Dipp	2,6-Diisopropylphenyl
DMAc	Dimethylacetamide

dtbpy	4,4'-di- <i>tert</i> -butyl-2,2'-bipyridine
EI	Electron Ionisation
ESD	Estimated Standard Deviation
ESI	Electrospray Ionisation
Et	Ethyl, CH ₂ CH ₃
Hz	Hertz
Ind	Indenyl
IR	Infra-Red
<i>J</i>	Coupling Constant
m	Multiplet
M	Generic metal atom
MeCN	Acetonitrile
Mes	Mesityl, 2,4,6-Me ₃ C ₆ H ₂
MS	Mass Spectrometry
<i>m/z</i>	Mass to Charge
NCS	National Crystallography Service
NHC	N-Heterocyclic Carbene
NMR	Nuclear Magnetic Resonance
Ph	Phenyl
<i>i</i> Pr	<i>iso</i> -propyl, CH(CH ₃) ₂
ppm	Parts Per Million
q	Quartet

sept.	Septet
SIPr	1,3-Bis(2,6-diisopropylphenyl)-4,5-dihydroimidazol-2-ylidene
t	Triplet
THF	Tetrahydrofuran
TLC	Thin Layer Chromatography
TM	Transition Metal
TMP	2,2,6,6-tetramethylpiperidide
TOF	Time of Flight (when describing mass spectrometry)
TOF	Turnover Frequency (when describing catalytic potential)
TON	Turnover Number
UV-vis	Ultraviolet-Visible (spectrum)

Table of Contents

Chapter 1: Introduction	1
1.1 Sustainable processes	1
1.2 Homogeneous catalysis	2
1.3 Metal-mediated C-H activation	3
1.3.1 Background	3
1.3.2 Historical perspective on C-H activation	6
1.3.3 Catalytic C-H activation	9
1.4 C-H borylation	14
1.4.1 Applications of borylation	14
1.4.2 Arene borylation	16
1.4.3 Alkane borylation	18
1.4.3 Substrate scope	23
1.5 Ligands in organometallic chemistry	26
1.5.1 Cyclopentadienyl-type ligands	26
1.5.2 Phosphines	29
1.5.3 N-Heterocyclic carbenes	30
1.5.4 Coordination chemistry of NHCs	34
1.5.5 NHCs in catalysis	36
1.5.6 Functionalised NHCs	37
1.5.7 Chelating functionalised NHCs	38
1.6 Hypothesis and project aims	45
Chapter 2: Indenylrhodium complexes with monodentate NHC ligands	47
2.1 Introduction	47
2.2 Synthesis of monodentate complexes	52
2.2.1 Synthesis of lithium NHC complexes	52
2.2.2 Synthesis of rhodium SIPr complexes	54
2.3 Reactivity	64

2.3.1 Stability	64
2.3.2 Photolysis studies	66
2.3.3 Hydrogenation and reaction with silanes	72
2.4 Conclusions	81
Chapter 3: Catalytic borylation	82
3.1 Introduction	82
3.2 Borylation of arenes	82
3.3 Borylation of alkanes	90
3.4 Stoichiometric reactions	93
3.5 Potential catalytic cycle	100
3.6 Conclusions	102
Chapter 4 : Fluorenyl-tethered NHC complexes.....	103
4.1 Introduction	103
4.2 Synthesis of imidazolium salts and spirocyclic compounds.....	106
4.3 Deprotonation and metallation attempts	112
4.4 Lithium amide complexes	116
4.5 Sodium and potassium amide complexes	122
4.6 Mixed-metal attempts.....	125
4.7 Complexation to rhodium	128
4.8 Initial catalytic studies for tethered complexes	134
4.8 Conclusions	136
Chapter 5: Conclusions	137
Chapter 6: Future work	140
6.1 Expansion of catalysis substrate scope	140
6.2 Ligand modification	141
6.3 Alternative metals	142
Chapter 7: Experimental	144
7.1 General remarks	144

7.2 Synthetic methods	146
7.2.1 Monodentate complexes.....	146
7.2.2 Photolysis	153
7.2.3 Reactions with hydrogen and silanes	153
7.2.4 Catalysis	155
7.2.5 Tethered ligands and complexes	160
7.3 Tables of crystallographic data	170
Chapter 8: References	180

List of Figures, Schemes and Tables

Figure 1.1: Cyclopentadienyl-type ligands.	26
Figure 1.2: Phosphine-metal interactions.....	30
Figure 1.3: Generalised molecular orbitals of singlet (A), triplet (B & C) and N-heterocyclic carbenes (D).	31
Figure 1.4: General structure of common NHCs and precursor salts.	31
Figure 1.5: Molecular orbitals for an idealised NHC and transition metal interaction. .	35
Figure 1.6: 2 nd generation Grubbs catalyst featuring SIMes.	36
Figure 1.7: SIMes variation of Hoveyda-Grubbs system 1.52 and 3 rd generation Grubbs catalyst 1.53	37
Figure 1.8: Early transition complexes with indenyl and fluorenyl functionalised NHCs.	39
Figure 1.9: Nickel complex 1.67 with an indenyl-tethered NHC and the corresponding monodentate complex 1.68	41
Figure 1.10: Chiral Cp-NHC complexes of Rh and Ir.	44
Figure 1.11: General structures for the target complexes; R = Dipp, L = COE, C ₂ H ₄ , CO.	46
Figure 2.1: X-ray determined structure for Li NHC complex 2.3 . All H atoms, except for H11A/B and H12A/B, as well as a benzene solvate molecule have been omitted for clarity.....	53
Figure 2.2: X-ray determined structure for Li NHC complex 2.4 . All H atoms, except for H16A/B and H15A/B, as well as a benzene solvate molecule have been omitted for clarity. The fluorenyl ring was found to be disordered over three positions and thus was only able to be refined isotropically, with only one position shown for clarity.....	54
Figure 2.3: X-ray determined molecular structure of complex 2.5 (thermal ellipsoids at 50%). All H atoms except for H10A/B, H1A/B, H13A/B and H14A/B have been omitted for clarity.....	56
Figure 2.4: X-ray determined structure of complex 2.6 (thermal ellipsoids at 50%). All H atoms except for H10, H11, H19A/B and H20A/B have been omitted for clarity.	56

Figure 2.5: X-ray determined structure of complex 2.7 (thermal ellipsoids at 50%). All H atoms except for H11A/B and H12A/B have been omitted for clarity.	58
Figure 2.6: X-ray determined structure of Cp* Rh ethene dimer 2.8 (thermal ellipsoids at 50%). All H-atoms, except for H11 and H12A/B, have been omitted for clarity.....	60
Figure 2.7: View along the Rh-Rh bond in 2.8 showing the staggered conformation of the Cp* methyl groups.	60
Figure 2.8: X-ray determined structure of 2.9 (thermal ellipsoids at 50%). All H-atoms, except for H2A/B, H3A/B, H28 and H29, and a benzene solvate molecule have been omitted for clarity.....	62
Figure 2.9: X-ray determined structure for complex 2.10 (thermal ellipsoids at 50%). All H atoms, except for H2, H2A/B and H3A/B have been removed for clarity in addition to two benzene solvate molecules.	65
Figure 2.10: UV-vis spectra for 2.2 and 2.5 – 2.7 obtained from a solution in toluene. The solvent cut-off for toluene occurs at 284 nm; data from this wavelength or lower is therefore omitted.	67
Figure 2.11: Proposed structures for the species observed by LIFDI mass spec.....	70
Figure 2.12: UV-vis spectra following the photolysis of 2.6 in toluene.	71
Figure 2.13: UV-vis difference spectra showing change upon photolysis of 2.6 (t-0'). Positive values indicate increased absorption relative to the initial spectrum of 2.6 in toluene, negative values indicate decreased absorption relative to the initial spectrum.	72
Figure 2.14: X-ray determined structure for Rh silyl hydride complex 2.16 (thermal ellipsoids at 50%). All H atoms except for the hydride and NHC backbone have been removed for clarity.....	77
Figure 2.15: ¹ H NMR spectrum of the hydride region for the reaction between 2.6 and (EtO) ₂ MeSiH.....	79
Figure 2.16: Summary of proposed products with the associated hydridic resonance chemical shift and J-coupling values for the reaction of 2.6 with trisubstituted silanes.	80
Figure 3.1: ¹¹ B NMR spectrum of reaction of B ₂ pin ₂ with 2.6 in C ₆ H ₆ /C ₆ D ₆	84
Figure 3.2: Mass spectrum (EI) for the borylation of C ₆ H ₆ /C ₆ D ₆ with 2.6	85
Figure 3.3: Low-field region of the ¹ H NMR spectrum in a reaction between B ₂ pin ₂ and 2.5 , including possible assignments.	86

Figure 3.4: ^1H NMR spectrum of decylBpin obtained after purification.....	91
Figure 3.5: ^1H NMR spectrum of octylBpin obtained after purification.	92
Figure 3.6: Mass spectrum for the crude reaction mixture of the borylation of decane with B_2pin_2	92
Figure 3.7: Mass spectrum for the crude reaction mixture of the borylation of octane with B_2pin_2	93
Figure 3.8: X-ray determined structure for Rh boryl hydride complex 3.7 (thermal ellipsoids at 50%). All H atoms except for the hydride and NHC backbone have been removed for clarity in addition to a benzene solvate molecule.....	98
Figure 3.9: Alternative view of 3.7 showing the bridging boryl groups.....	99
Figure 4.1: Tethered indenyl/fluorenyl-NHC complexes with important features highlighted.	103
Figure 4.2: Molecular structure for 4.2-BF₄ (thermal ellipsoids at 50%). All H-atoms except for H1, H16, H17A/B and H18A/B have been omitted for clarity.....	107
Figure 4.3: X-ray determined structure of spirocycle 4.3 (thermal ellipsoids at 50% probability). All H-atoms (except imidazoline H16) have been removed for clarity. .	110
Figure 4.4: X-ray determined molecular structure of the LiPh/LiTMP aggregate 4.6 (thermal ellipsoids at 50% probability). ²⁷³ All H atoms have been omitted for clarity.	116
Figure 4.5: X-ray determined structure of dilithium complex 4.7 (thermal ellipsoids at 50% probability). All H-atoms (except for those on the NHC backbone) have been omitted for clarity.....	118
Figure 4.6: X-ray determined structure of dilithium complex 4.8 (thermal ellipsoids at 50% probability). All H-atoms (except for those on the NHC backbone) have been omitted for clarity.....	119
Figure 4.7: X-ray determined structure of LiPh/LiN(SiMe ₃) ₂ 1:1 adduct 4.9 with the interactions to neighbouring units shown (thermal ellipsoids at 50% probability). All H-atoms have been omitted for clarity.....	121
Figure 4.8: Reactions of spirocycle 4.3 with MCH ₂ Ph and MN(SiMe ₃) ₂ (M = Na, K).	122

Figure 4.9: X-ray determined structure of disodium complex 4.10 with interactions of Na ₂ to the neighbouring unit shown (thermal ellipsoids at 50% probability). All H-atoms (except for those on the NHC backbone) in addition to solvating benzene molecules have been omitted for clarity.	123
Figure 4.10: X-ray determined structure of dipotassium complex 4.11 with interactions of K ₂ to the neighbouring unit shown (thermal ellipsoids at 50% probability). All H atoms (except for those on the NHC backbone) in addition to solvating benzene molecules have been omitted for clarity.	124
Figure 4.11: Attempted reactions of 4.3 with mixed bimetallic bases with Li.	125
Figure 4.12: ¹ H NMR (400 MHz, C ₆ D ₆) spectra for the reaction between 4.3 and LiPh/NaN(SiMe ₃) ₂ , with highlighted similarities. A is isolated 4.8 , B-E shows the reaction upon heating up to 20 hrs.	125
Figure 4.13: ⁷ Li NMR (155 MHz, C ₆ D ₆) spectra for the reaction between 4.3 and LiPh/NaN(SiMe ₃) ₂ (red) compared to 4.8 (black).	126
Figure 4.14: ¹ H NMR (400 MHz, C ₆ D ₆) spectra for the reaction of 4.3 with LiPh/KN(SiMe ₃) ₂ compared to the spectrum for isolated 4.8 (A).	126
Figure 4.15: ⁷ Li NMR (155 MHz, C ₆ D ₆) spectra comparing the reaction between LiPh/KN(SiMe ₃) ₂ and 4.3 with spectrum for 4.8	127
Figure 4.16: Stacked plot of ¹ H NMR (400 MHz, C ₆ D ₆) spectra for NMR scale reactions of 4.3 with A : KCH ₂ Ph/KHMDS, B : NaCH ₂ Ph/NaHMDS, C : KCH ₂ Ph/NaHMDS, D : NaCH ₂ Ph/KHMDS. The spectra for C and D are very similar in nature suggesting the same product(s) are being formed.	127
Figure 4.17: ¹³ C{ ¹ H} NMR (101 MHz, C ₆ D ₆) spectrum of the reaction between 4.8 and [Rh(CO) ₂ Cl] ₂ , with peaks assigned to different structures.	129
Figure 4.18: ¹ H NMR (400 MHz, C ₆ D ₆) spectrum of isolated 4.12	130
Figure 4.19: X-ray determined structure of rhodium carbonyl complex 4.12 (thermal ellipsoids at 50% probability). All H-atoms (except for those on the NHC backbone) have been omitted for clarity.	131
Figure 4.20: X-ray determined structure of rhodium ethene complex 4.13 (thermal ellipsoids at 50% probability). All H-atoms (except for H17A/B, H18A/B, H31A/B and H32A/B) have been omitted for clarity.	133

Figure 4.21: $^{13}\text{C}\{^1\text{H}\}$ NMR (101MHz, C_6D_6) spectrum for the reaction of 4.8 with $[\text{Rh}(\text{COE})_2\text{Cl}]_2$ with the carbene and bound alkene resonances highlighted.....	134
Figure 6.1: An expanded range of substrates for borylation.	140
Figure 6.2: Common NHC ligands.	141
Figure 6.3: Alternative anionic donors.....	142
Figure 6.4: Variation of tethered NHC ligands.	142
Scheme 1.1: C-H activation step (oxidative addition) and subsequent functionalisation as the overall process of C-H functionalisation.....	3
Scheme 1.2: Mechanisms for activation of EH bonds.....	5
Scheme 1.3; A: Formation of a σ -complex prior to oxidative addition. B: general bonding scheme for σ -complexes.	6
Scheme 1.4: In-situ reduction of $\text{Ru}(\text{dmpc})_2\text{Cl}_2$ to $\text{Ru}(0)$, subsequent reaction with naphthalene and thermolysis.	7
Scheme 1.5: Addition of hydrocarbons to the Cp^*Ir fragment under photochemical conditions with different ligands, PMe_3 (A) and PPh_3 (B).....	8
Scheme 1.6: Photochemical reactions with group 9 $\text{M}(\text{I})$ complexes [A: $\text{M} = \text{Ir}$, $\text{L} = \text{CO}$, $\text{R} = \text{Me}$ 1.13 ; $\text{M} = \text{Rh}$, $\text{L} = \text{C}_2\text{H}_4$, $\text{R} = \text{H}$ 1.14].....	9
Scheme 1.7: Rh catalysed alkylation of aryl-substituted imines, with proposed catalytic cycle featuring oxidative addition of the aryl C-H bond.....	11
Scheme 1.8: Base-promoted C-H arylation of phenylpyridines (A) and tryptophan (B) catalysed by $\text{Pd}(\text{OAc})_2$	12
Scheme 1.9: Based promoted $\text{Mn}(\text{I})$ alkenylation of phenylpyridines, with the proposed C-H activation transition state highlighted.	12
Scheme 1.10: Rh-catalysed cyclisation and alkene insertion, with control of product formation depending on reaction conditions (DMAc = dimethylacetamide).	13
Scheme 1.11: Non C-H borylation based synthesis of boronic acids and esters.....	14
Scheme 1.12: General borylation of arenes ($\text{X} = \text{H}$ or BR_2).	15

Scheme 1.13: Photolytically activated C-H borylation reactions ($B_{cat}^* = BO_2C_6H_2Me_2$, $M = Re$ or Mn , $Cp^R = Cp^*$, C_5H_4Me).	15
Scheme 1.14: Borylation of benzene with Ir complex 1.16 and Rh complex 1.17	16
Scheme 1.15: Isolation of Ir intermediate 1.18 and subsequent reaction with d_6 -benzene.	18
Scheme 1.16: Borylation of substituted arenes and heteroarenes by $[Ir(COD)Cl]_2/dtbp$ in hexane.	18
Scheme 1.17: Borylation of alkanes with Cp^*RhL_2 complexes ($L_2 = \eta^4-C_6Me_6$ 1.17 or $L = C_2H_4$ 1.19).	19
Scheme 1.18: Proposed catalytic cycle for the borylation of alkanes via an oxidative addition mechanism ($X, Y = Bpin$ or H).	21
Scheme 1.19: Reactions of bis- and trisboryl complexes with benzene.	21
Scheme 1.20: σ -CAM description of the mechanism for C-H borylation with 1.17 ($X = H$ or $Bpin$).	22
Scheme 1.21: Possible bonding descriptions for 1.20 and 1.21	22
Scheme 1.22: Mechanism for the C H activation of THF by Ir system 1.24 or 1.29 ($mes = mesitylene$).	25
Scheme 1.23: Indenyl ring-slippage.	26
Scheme 1.24: Substitution of $[Mo(Ind)X(CO)_3]$ with phosphines via a 7-coordinate intermediate (A) or via a 5-coordinate intermediate (B).	27
Scheme 1.25: Thermolysis of Ir complexes 1.32 and 1.9 ($Cy = cyclohexyl$) in benzene leading to the formation of the phenyl hydride complexes 1.33 and 1.7	28
Scheme 1.26: Reactions of indenyl Ir complexes with CO and subsequent migratory insertion.	29
Scheme 1.27: Synthesis of imidazol(in)ium salts with cyclisation, ^{123, 124} or alkylation. ¹²⁵	33
Scheme 1.28: Deprotonation of an imidazolium salt to a NHC ($X = Cl, Br, BF_4, PF_6$, etc).	33
Scheme 1.29: Wanzlick equilibrium (A) and metallation to a metal complex via N,N' chelate (B) ($R = Me$ or Et).	34

Scheme 1.30: Example of synthesis of NHC-complexes via A) silver transfer agents, ¹³⁶ or B) NHC-carboxylates. ¹³⁵	35
Scheme 1.31: Different approaches for functionalised NHCs binding to metals.....	38
Scheme 1.32: Electrochemical alternative to deprotonation due to acidic substituents (highlighted in red).....	39
Scheme 1.33: Reactions with borane-protected NHC Mo complexes.	40
Scheme 1.34: Tetramethylcyclopentadienyl NHC Ni complexes (1.71-1.75).	41
Scheme 1.35: Synthesis of indenyl-tethered NHC complexes with Ru ₃ (CO) ₁₂	42
Scheme 1.36: Synthesis of tetramethyl- and tetrabenzyl-cyclopentadienyl NHCs with Ru.	42
Scheme 1.37: Synthesis of tetramethylcyclopentadienyl-NHC Ir complex 1.86	43
Scheme 1.38: Synthesis of Rh(III) and Ir(III) complexes 1.89 and 1.90 with a tetramethylcyclopentadienyl-NHC ligand.	43
Scheme 1.39: Synthesis of Rh and Ir iodide complexes and subsequent cyclometalated Ir species.	44
Scheme 1.40: Synthesis of Indenyl-NHC half sandwich complexes with Rh and Ir.	45
Scheme 2.1: Typical synthesis of Rh(III) half-sandwich complexes with Cp (R = H) and Cp* (R = Me).	47
Scheme 2.2: Synthesis of Rh(I) half-sandwich complexes.	48
Scheme 2.3: Synthesis of Cp and Cp* rhodium complexes featuring an NHC ligand. .	49
Scheme 2.4: Synthesis of indenylrhodium(I) complexes (M = Li, Na, K).....	50
Scheme 2.5: Possible synthesis of indenylrhodium carbonyl complexes via CO substitution of an alkene complex.....	50
Scheme 2.6: Synthesis of SIPr (Dipp = 2,6-diisopropylphenyl).	51
Scheme 2.7: Synthesis of lithium NHC complexes with indenyl and fluorenyl ligands.	52
Scheme 2.8: Reactions between indenylrhodium bis(alkene) complexes and SIPr.	55
Scheme 2.9: Reaction of 2.5 with CO to give 2.7	57

Scheme 2.10: Attempted reaction of SIPr with $[\text{Rh}(\text{Cp}^*)(\text{C}_2\text{H}_4)_2]$ to yield a $\text{Cp}^*\text{Rh}(\text{NHC})$ complex.	59
Scheme 2.11: Addition of SIPr to $[\text{Rh}(\text{COE})_2\text{Cl}_2]$ to give 2.9	61
Scheme 2.12: Addition of LiR to 2.9 (R = Ind, Flu) to give 2.6	63
Scheme 2.13: Reaction of 2.7 with water to generate hydroxide bridged Rh dimer 2.10	64
Scheme 2.14: General photochemical reaction for Rh complexes with R-H substrates [R = H, Ph, SiR' ₃].	66
Scheme 2.15: Proposed photochemical products from the photolysis of 2.6 . One diisopropylphenyl group is displayed for clarity.	69
Scheme 2.16: The anticipated addition of H ₂ to 2.6 with the formation of cyclooctane (COA).	73
Scheme 2.17: Proposed steps in the reaction between 2.6 and H ₂ . Only one isomer of 2.12 and one diisopropylphenyl group is displayed for clarity where appropriate.	74
Scheme 2.18: Reaction between 2.6 and (EtO) ₃ SiH forming 2.16	76
Scheme 2.19: Reaction between 2.6 and (EtO) ₂ MeSiH.	78
Scheme 3.1: General reaction for the borylation of arenes and alkanes with bis(pinacolato)diborane(4) (B ₂ pin ₂) and pincolborane (HBpin) using a rhodium complex.	82
Scheme 3.2: Borylation with complexes 2.5 – 2.7	83
Scheme 3.3: Preparative-scale borylation of arenes with 2.6	87
Scheme 3.4: Borylation of alkanes.	90
Scheme 3.5: Stoichiometric NMR-scale reactions.	94
Scheme 3.6: Reaction between 2.6 and HBpin and potential products.	95
Scheme 3.7: Reaction of $[\text{Rh}(\text{Ind})(\text{COE})_2]$ and HBpin.	95
Scheme 3.8: Reaction of 2.13 with HBpin and the proposed products.	96
Scheme 3.9: Reaction between 2.6 and HBcat, with the proposed oxidative addition product 3.6 and the isolated dirhodium complex 3.7	97
Scheme 3.10: Proposed catalytic cycle for the borylation of arenes with B ₂ pin ₂	101

Scheme 4.1: Proposed synthetic pathway to tethered-NHC transition metal complexes. AM is an alkali metal, M is a transition metal and L is a suitable ligand such as COE, C ₂ H ₄ or CO.....	104
Scheme 4.2: Previously synthesised indenyl-tethered NHC Rh complexes by Danopoulos and co-workers. ¹⁸¹	105
Scheme 4.3: Initial synthesis of imidazolinium salt 4.2-Cl	106
Scheme 4.4: Improved synthesis of imidazolinium salt 4.2 BF₄	107
Scheme 4.5: Attempted synthesis of indenyl-tethered NHC proligands.	108
Scheme 4.6: Formation of spirocycle 4.3 from the single deprotonation of 4.2-BF₄ via either deprotonation at the fluorenyl (pathway A) or deprotonation at the imidazolinium (pathway B), compared to the double deprotonation of N-methyl imidazolium C	109
Scheme 4.7: Optimised synthesis of spirocycle 4.3	111
Scheme 4.8: Reaction of spirocycle with water 4.3 to generate formamide 4.4	111
Scheme 4.9: Attempts to deprotonate 4.3 to generate an anionic NHC salt (MR is a generic alkyl metal reagent).	112
Scheme 4.10: Attempted reactions of 4.2-BF₄ with Ag ₂ O.....	114
Scheme 4.11: Reactions of 4.2-BF₄ with CuCl/KO ^t Bu and reduction with LiBEt ₃ H.	115
Scheme 4.12: Synthesis of dilithium amide complexes 4.7 and 4.8 with phenyl lithium/lithium amide mixtures.....	117
Scheme 4.13: Formation of 4.9 from mixing LiPh and LiHMDS.....	120
Scheme 4.14: Reaction of 4.8 with [Rh(CO) ₂ Cl] ₂	128
Scheme 4.15: Reaction of 4.8 with [Rh(alkene) ₂ Cl] ₂	132
Scheme 4.16: Borylation of benzene with 4.12/4.13	134
Scheme 6.1: Possible monodentate Co half-sandwich complexes with NHCs, with Cp* (A) and indenyl (B).	143
Table 1.1: The 12 principles of green chemistry.....	1
Table 1.2: Ir based catalysts for the borylation of benzene.....	17
Table 1.3: Bond dissociation energies for relevant bonds. ^{70, 71}	19

Table 1.4: Complexes for borylation of alkanes.	24
Table 2.1: Local λ_{max} for complexes 2.2 and 2.5 – 2.7 with their respective molar absorption coefficients.	67
Table 3.1: Conversion of benzene to phenylboronic acid pinacol ester by complexes 2.5 – 2.7 in NMR scale reactions.	87
Table 3.2: Borylation of a range of arenes with B ₂ pin ₂ catalysed by 2.6	89
Table 3.3: Borylation of alkanes using 2.6	91
Table 4.1: Summary of initial deprotonation attempts of 4.3	113
Table 4.2: Key bond lengths and angles for 4.8, 4.10 and 4.11	124
Table 4.3: Initial catalytic results of the borylation of benzene with 4.12 and 4.13	135

Chapter 1: Introduction

1.1 Sustainable processes

Sustainable chemistry focuses on ensuring that present chemical transformations can be carried out without compromising the ability of future generations to conduct them.¹ To this end, it is essential that the processes are compatible with the 12 Principles of Green Chemistry (**Table 1.1**), which set out the principles that chemical reactions should aim to achieve. Of note are the principles of Atom Efficiency, which calls for the minimisation of the amount of waste products formed,^{2,3} and the use of catalysis for the reduction in amount of waste over stoichiometric reactions.⁴

Table 1.1: The 12 principles of green chemistry.

Principle	Summary
Prevention	It is better to prevent formation of waste than treat or clean up waste after it has been created
Atom Economy	Synthetic methods should be designed to maximize incorporation of all materials used into the final product
Less Hazardous Chemical Syntheses	Designed to use and generate substances that possess little or no toxicity to human health and the environment
Designing Safer Chemicals	designed to preserve efficacy of function while reducing toxicity
Safer Solvents and Auxiliaries	Use of auxiliary substances (e.g., solvents, etc.) should be made unnecessary wherever possible + innocuous when used
Design for Energy Efficient	Synthetic methods should be conducted at ambient temperature and pressure
Use of Renewable Feedstocks	A raw material or feedstock should be renewable rather than depleting whenever technically and economically practicable.
Reduce Derivatives	Unnecessary derivatization (protection/deprotection, etc) should be minimized or avoided if possible
Catalysis	Catalytic reagents (as selective as possible) are superior to stoichiometric reagents
Design for Degradation	Chemical products should be designed so that at the end of their function they break down into innocuous degradation products and do not persist in the environment
Real-time analysis for Pollution Prevention	Analytical methodologies need to be further developed to allow for real-time, in-process monitoring and control prior to the formation of hazardous substances
Inherently Safer Chemistry for Accident Prevention	Substances and the form of a substance used in a chemical process should be chosen to minimize the potential for chemical accidents, including releases, explosions, and fires

1.2 Homogeneous catalysis

Catalysis using metals often involve the platinum group metals (Ru, Os, Rh, Ir, Pd, Pt) due to the wide-ranging reactivity and high selectivity that is often obtained by using these metals. While these metals are rare and expensive, their high activity can enable low catalytic loadings to be used, thus mitigating the cost of using precious metals to some extent. Their reactivity is dominated by two electron processes and have well-investigated mechanisms.

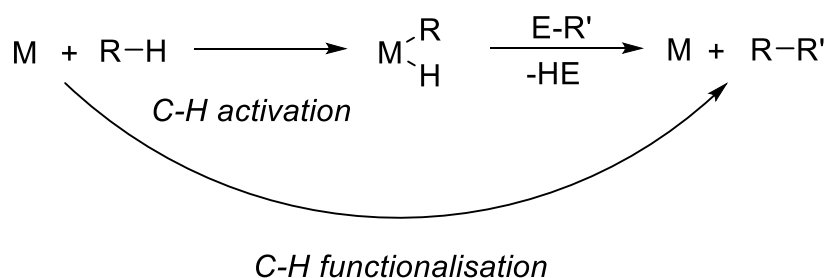
The alternative to the Pt group metals is using more abundant metals such as the first row transition metals, in particular titanium, iron, cobalt and nickel. However, use of these metals can be challenging due to the different behaviour between the first row and the second/third row transition metals. Whereas many of the catalytic processes for second and third row transition metals are well-defined, there is more uncertainty with first row metals, including the importance of different spin states [second and third row TMs (transition metals) are almost exclusively encountered as low spin] and one-electron processes. This means that reaction conditions and systems may not be directly compatible between these two different classes of complex, thus new systems will require extensive development. Ultimately, the reaction behaviour and scope may be very different as well.

As per the principles of green chemistry, the ideal system would involve a first row transition metal catalyst and have high selectivity and reactivity thus enabling a low loading to be used with few (if any) additives, which further decreases the amount of waste produced. Until this point is achieved, there is still a role to play for Pt group (Ru, Rh, Pd, Os, Ir, Pt) catalysts that are active, selective and give products that are not achievable by other systems.

1.3 Metal-mediated C-H activation

1.3.1 Background

C-H activation involves the direct reaction of a C-H bond, ideally facilitating subsequent functionalisation (**Scheme 1.1**).⁵ The C-H bond is a strong bond (*ca.* 400 kJ/mol, depending on substituents)⁶ and non-polar, thus it is widely acknowledged to be difficult to break. New, efficient methods are therefore desirable to enable direct access to useful chemicals from the large amount of simple hydrocarbons available from the petrochemical sector.^{7, 8} In addition it may prove useful in late-stage functionalisation of complicated molecules, as libraries of related compounds can be synthesised from shared highly-functionalised precursors, which allow rapid screening in drug discovery.⁹⁻¹¹ C-H activation can improve the synthesis of these libraries as it may be quicker, milder and produce less waste.^{12, 13}



Scheme 1.1: C-H activation step (oxidative addition) and subsequent functionalisation as the overall process of C-H functionalisation.

Early methods of C-H functionalisation relied on radical reactions or the use of directing groups to activate the C-H bond. The former has problems controlling the reactivity and selectivity of the reaction, which inhibits its use with functionalised substrates. In the latter case, the directing group coordinates to the metal centre and positions the substrate in the correct orientation for metallation and subsequent functionalisation at the directed position. This requires functionality to already be present in the molecule, which means that syntheses require careful development to enable the functionality to be introduced at the correct place, and that either the directing group is present in the final product or can be removed at a later point. This latter option adds in additional steps to the synthesis which requires more time and increases waste.

One well-understood mechanism for C-H activation uses an oxidative addition/reductive elimination pathway (**Scheme 1.2, A**).¹⁴ This involves the addition of a C-H bond across the metal centre with an increase in oxidation state of the metal centre by two. The reverse process is called reductive elimination due to the metal centre's oxidation state being reduced by two. Oxidative addition is favoured by electron-rich metals that have high electron density, such as the late transition metals (Rh, Pd, Ir, etc.). If in **Scheme 1.2, A** [M] was a CpRh fragment, it would increase in oxidation state from Rh(I) to Rh(III) and then to Rh(V), before reductive eliminations reverse the process. There is also evidence that an intermediate σ -complex exists in oxidative addition processes (**Scheme 1.3**).¹⁵⁻¹⁷

Another possible mechanism of C-H activation is σ -bond metathesis (**Scheme 1.2, B**), which involves the concerted exchange of groups in a 4-membered transition state.^{18, 19} This mechanism does not formally increase the oxidation state of the metal and thus is favoured by complexes of early transition metals and the f-block (such as Sc and Lu) which do not have accessible d electrons in their most commonly observed oxidation states, and thus for which oxidative addition is disfavoured.

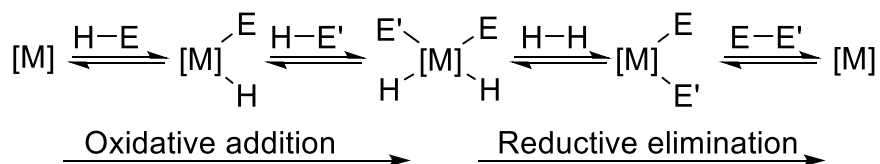
A third possibility is the σ -CAM mechanism (complex assisted metathesis; **Scheme 1.2, C**).²⁰ While this also features a 4-membered transition state, it differs in that a σ -complex is formed before the exchange such that the coordination number does increase but not the oxidation state. This mechanism has been shown to be active for late transition metals such as Rh and Ru,²¹⁻²³ and thus offers a pathway that does not require as high an oxidation state as traditional oxidative addition/reductive elimination mechanisms.

Radical oxidative addition involves the stepwise addition of radicals, formed from the homolytic cleavage of a E-H bond, to the metal centre leading to an increase in the oxidation state of the metal centre (**Scheme 1.2, D**).²⁴ To facilitate this, the metals are strongly oxidising and a variety of favoured oxidation states are common. Generally, these processes occur with alkyl halides or organometallic hydrides such as Bu₃SiH,^{25, 26} though addition of benzyl groups can proceed via radical addition.^{27, 28}

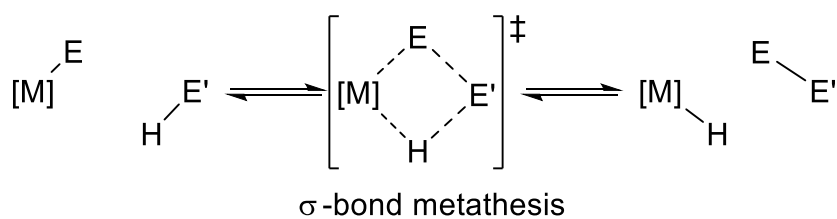
Complexes with M=E bonds can undergo 1,2-addition where a C-H bond can add across the double bond (**Scheme 1.2, E**).^{29, 30} Typically, imido (M=N), alkylidene (M=C), and alkylidyne (M \equiv C) complexes of early and middle transition metals operate via this C-H activation mode, partly due to this mechanism not requiring electron-rich metal centres, which are more typical of the late transition metals.

Additionally, base-assisted mechanisms also occur, typically with acetate or carboxylate used in a deprotonation step (**Scheme 1.2, F**).³¹ This mechanism is often used by late transition metals, such as Pd(II), Rh(III) and Ir(III), in higher oxidation states than those typically involved in oxidative addition pathways.

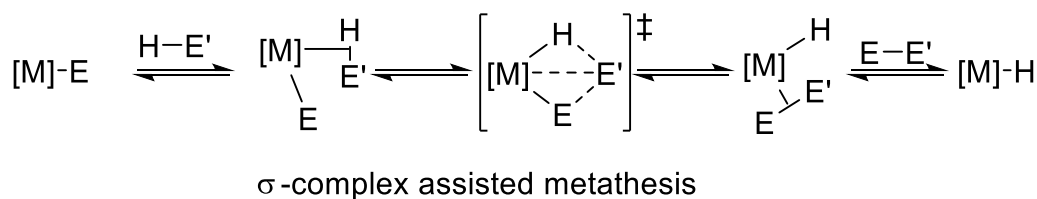
A



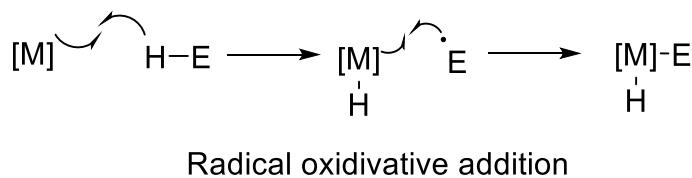
B



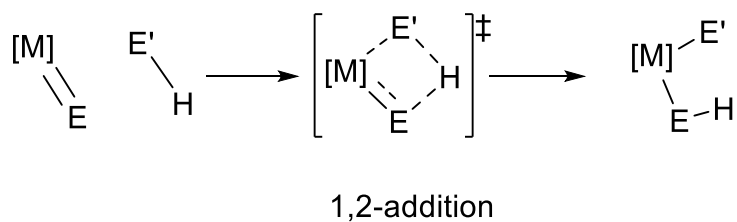
C



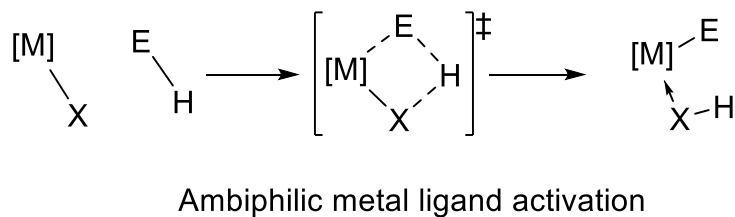
D



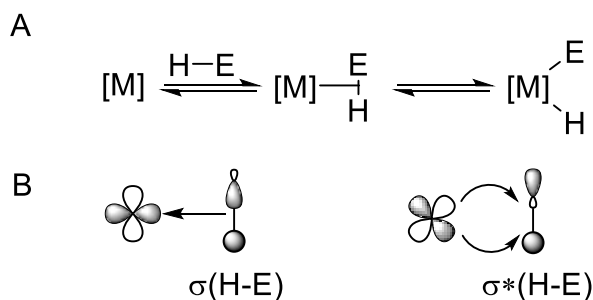
E



F



Scheme 1.2: Mechanisms for activation of EH bonds.

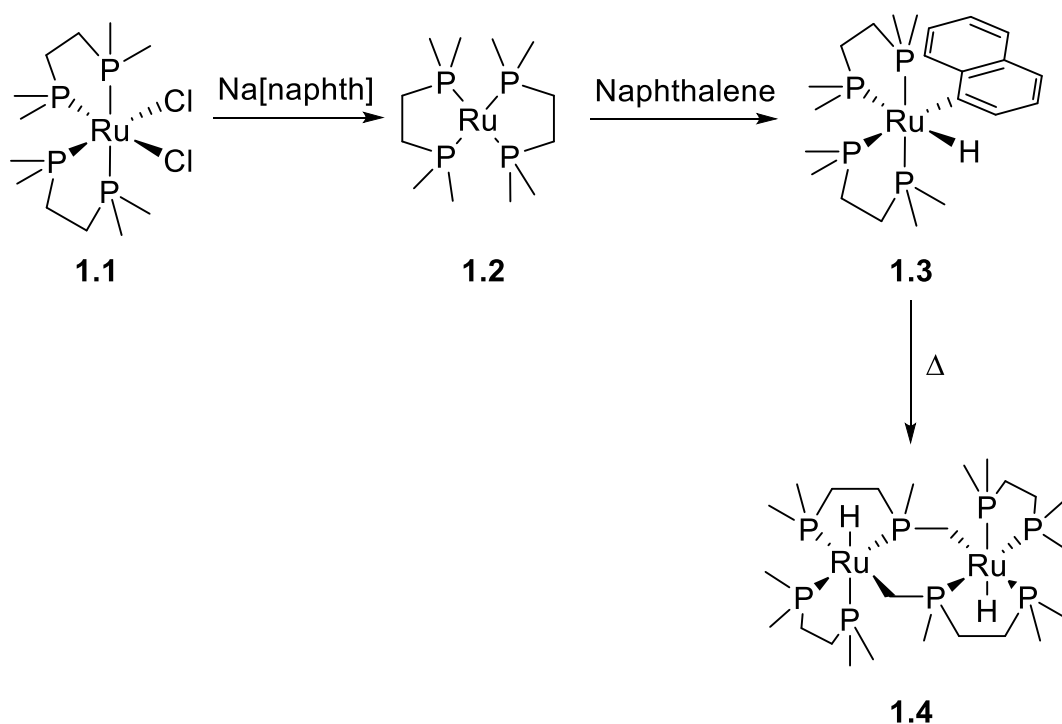


Scheme 1.3; A: Formation of a σ -complex prior to oxidative addition. B: general bonding scheme for σ -complexes.

1.3.2 Historical perspective on C-H activation

Early metal-mediated systems often involved stoichiometric amounts of metal complexes to facilitate the C-H addition step. Direct mercuration of arenes, including benzene, with $Hg(OAc)_2$ leads to $ArHgOAc$,³² from which other $ArHgX$ species can be readily accessed. The addition is irreversible hence the need for stoichiometric quantities of Hg, which is far from ideal.

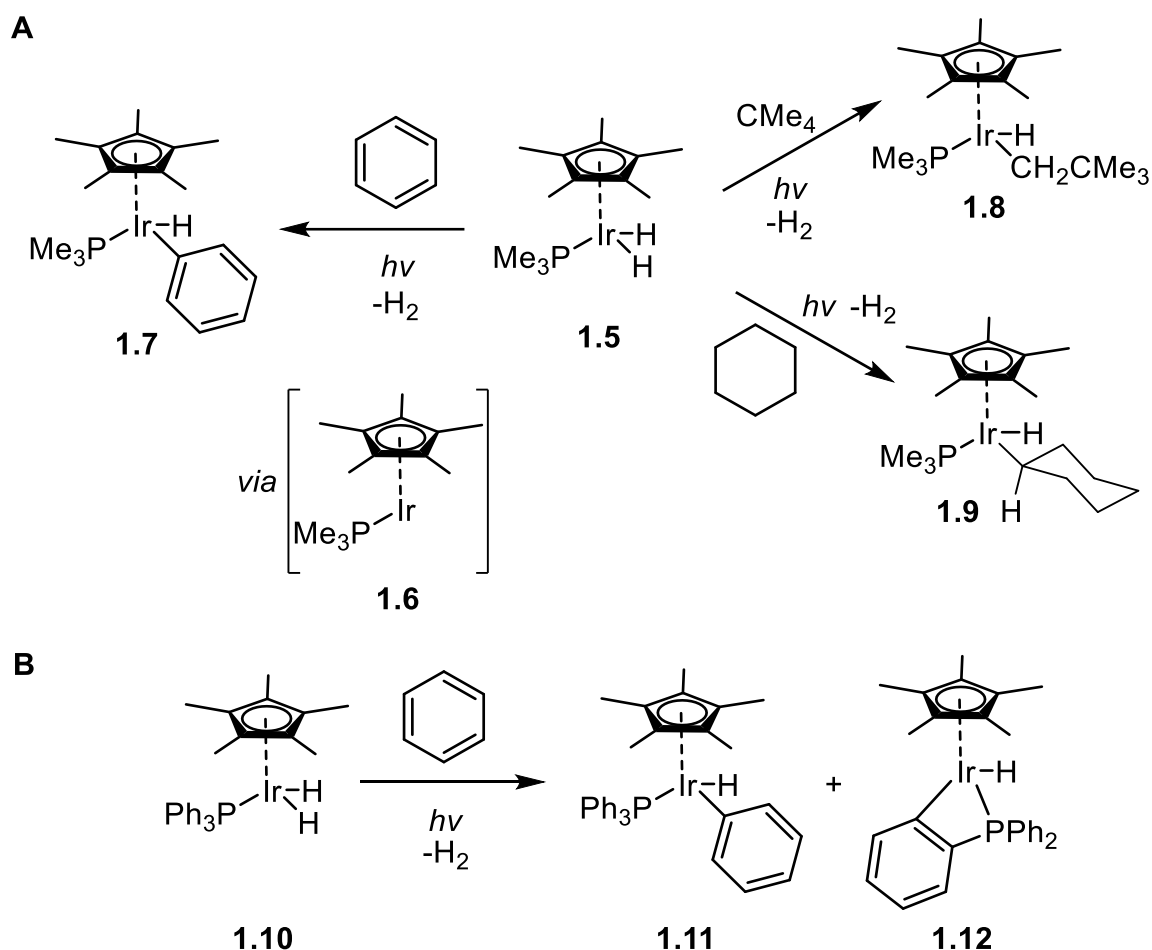
Electron-rich metal centres have been known to be able to oxidatively add C-H bonds since the 1960s. The addition of naphthalene to $Ru(0)$ was observed by Chatt and co-workers after reduction of $Ru(II)$ with $Na[naphth]$ (naphth = naphthalenide) (**Scheme 1.4**).³³ Subsequent thermolysis of the naphthalenyl species led to the loss of naphthalene and then dimerization via intermolecular oxidative addition of the phosphine methyl groups to give a bridged bimetallic product, **1.4**.



Scheme 1.4: In-situ reduction of $\text{Ru}(\text{dmpe})_2\text{Cl}_2$ to $\text{Ru}(0)$, subsequent reaction with naphthalene and thermolysis.

The use of Cp-based ligands with Rh and Ir also enabled the addition of C-H bonds to metal centres. Work by Bergman and co-workers featured Ir and started with a Ir(III) dihydride complex (**1.5**) that, under photolysis, induces the reductive elimination of H_2 forming a 16e Ir(I) species (**1.6**) in-situ, which can then oxidatively add CH bonds in a range of hydrocarbons including benzene (sp^2 CH, **1.7**), neopentane (sp^3 CH_3 , **1.8**) and cyclohexane (sp^3 CH_2 , **1.9**).^{34, 35} Due to the reactive nature of the intermediate, careful selection of the ligand system was required to prevent cyclometallation of the phosphine R groups.^{35, 36} The use of PMe_3 (**Scheme 1.5, A**) prevents cyclometallation as the product would contain a three-membered metallacycle. The analogous PPh_3 complex (**Scheme 1.5, B**) forms the cyclometallated complex in a competitive side-reaction to the intermolecular oxidative addition product in a 53:47 ratio. In this case, a four-membered metallacycle is formed, suggesting that the dividing line between the two reaction pathways is small. Computational calculations on the $[\text{Ir}(\text{Cp}^*)(\text{PPh}_3)]$ system estimates that there is only a 0.6 kcal/mol difference in the energy barriers between the intermolecular and intramolecular products, hence the nearly equal distribution of products.³⁶ Comparison to the less sterically-crowded but less electron-rich $[\text{Ir}(\text{Cp})(\text{PPh}_3)]$ system revealed that the intramolecular reaction was predicted to dominate

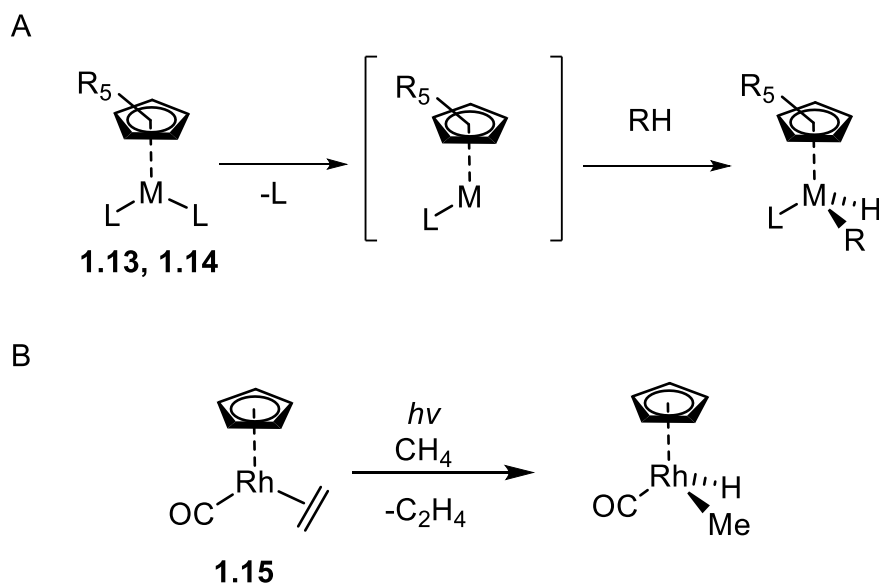
by a ratio of 99:1, indicating that sterics have a greater influence than electronics in this case.



Scheme 1.5: Addition of hydrocarbons to the Cp*Ir fragment under photochemical conditions with different ligands, PMe₃ (**A**) and PPh₃ (**B**).

An alternative approach is the photolysis-promoted cleavage of a M-L bond in a M(I) complex, usually either a Rh or Ir system with a labile L-type ligand, such as CO or C₂H₄, which can dissociate upon irradiation (**Scheme 1.6, A**).³⁷⁻³⁹ This generates a reactive 16e intermediate which can then add groups such as neopentane across the metal centre in an analogous manner to the Bergman system (**Scheme 1.5**). It should be noted that the Rh products required matrix isolation due to instability at room temperature, whereas Ir photoproducts were found to be stable at room temperature. This highlights a key difference in the CH activation chemistry between Rh and Ir. Photolysis of the heteroleptic complex **1.15** leads to the loss of ethene over CO (**Scheme 1.6, B**), which is expected as the latter is seen as the stronger ligand.⁴⁰ Complexes **1.13** – **1.15** are simpler

to synthesise but have less scope for variation in ligands than the Ir(III) route from **1.5**. The ability to change the ligands allows for the potential to tune the reactivity of the metal centre towards the addition of different CH bonds. Additionally, the reversible nature of the C-H addition is a key feature for catalytic applications, which is necessary for the wider implementation use of these transformations.



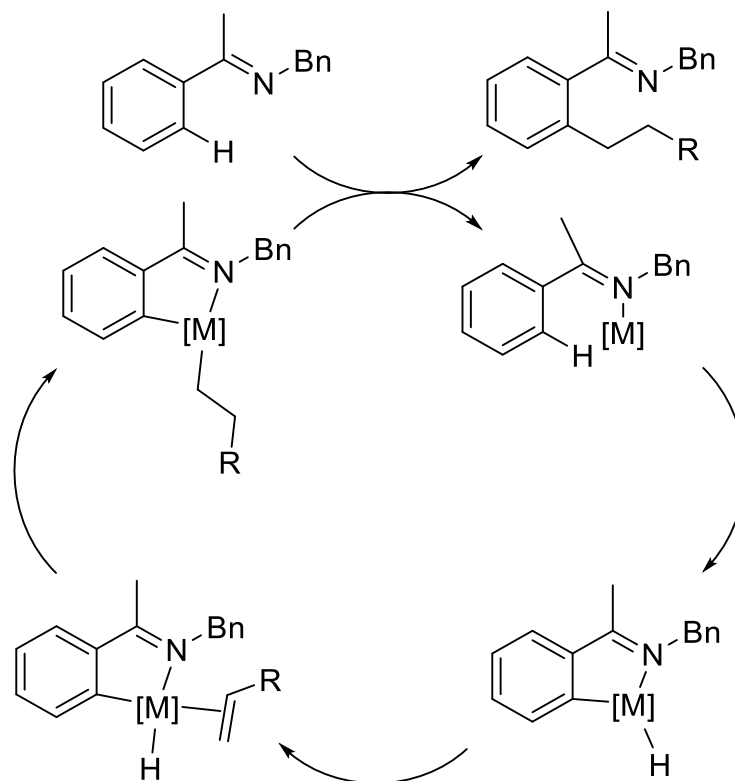
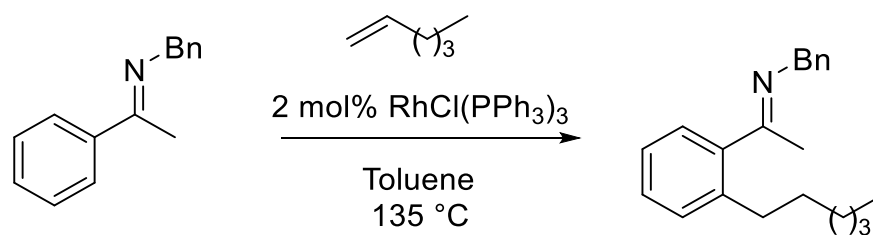
Scheme 1.6: Photochemical reactions with group 9 M(I) complexes [A: M = Ir, L = CO, R = Me **1.13**; M = Rh, L = C₂H₄, R = H **1.14**].

1.3.3 Catalytic C-H activation

The development of catalysis based on C-H activation enables reactions to be performed without the need for both substrates to be functionalised or activated beforehand. This enables two possibilities: more direct use of available starting materials, and late-stage functionalisation.⁹ In the former case, simple arenes and alkanes with no heteroatoms can be functionalised where traditional organic synthetic methods struggle. These simple compounds are readily available from the petrochemical industry and thus allow for a more efficient use of resources. In the latter case, late-stage functionalisation offers variation of substituents late in the synthesis of pharmaceutical compounds, enabling a library of compounds to be formed from a common point which is close to the end of the synthesis. This avoids the need to have multiple different routes that may require different

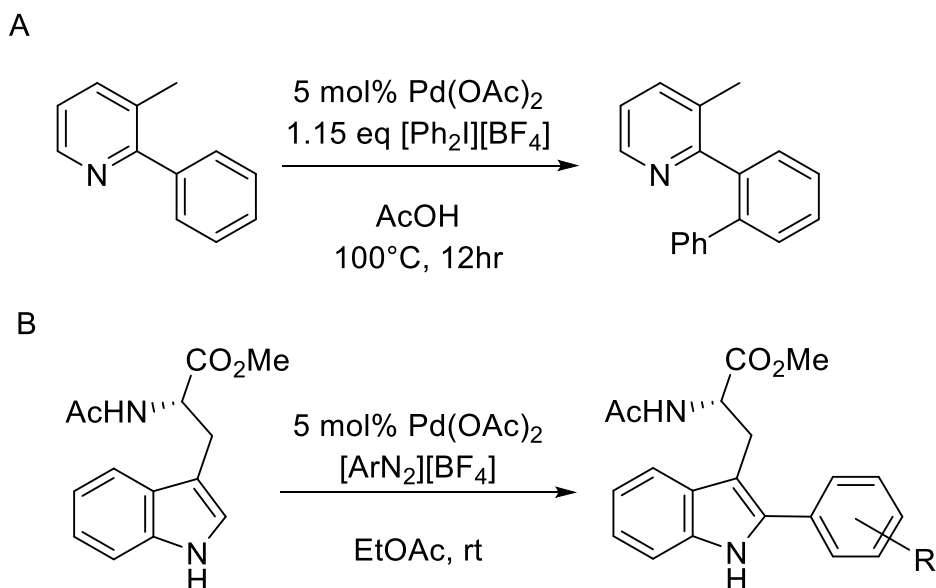
reaction and purification conditions, which increases the complexity of the synthesis and requires more time and resources to achieve. In addition, it would be possible to perform steps in the presence of reactive functional groups that allow protecting-group-free synthesis. Such protecting group usually need to be introduced before the functionalisation and then removed afterwards, and thus introduce extra steps which likely decreases overall yield and increases the potential amount of waste.

Some examples of C-H activation in catalysis include Rh-catalysed alkylations of aryl imine compounds,^{41, 42} which are proposed to proceed via cyclometallation of the arylimine with the C-H bond being oxidatively added (**Scheme 1.7**). The imine acts as a directing group for the selective ortho substitution, and the product can be converted via acid hydrolysis to a ketone. The Murai reaction is the analogous reaction using Ru-based catalysts which use carbonyl and other similar groups as directing groups.⁴³⁻⁴⁶

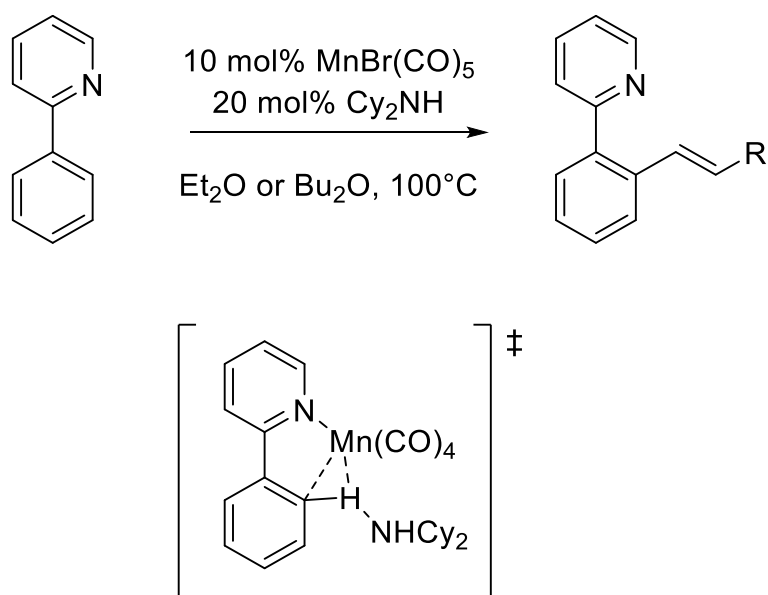


Scheme 1.7: Rh catalysed alkylation of aryl-substituted imines, with proposed catalytic cycle featuring oxidative addition of the aryl C-H bond.

Base-mediated C-H activation catalysis has been used for a variety of different transformations with Pd-based systems being exploited extensively. Many direct functionalisations of heterocycles such as pyridines and indoles/tryptophan have been reported (**Scheme 1.8**).^{47,48} The latter have extensive potential biological applications in the synthesis of modified peptides and proteins. Phenylpyridines have also been used in manganese(I) catalysed alkenylation with alkynes (**Scheme 1.9**),^{49,50} which is proposed to proceed via base-assisted activation with Cy_2NH .



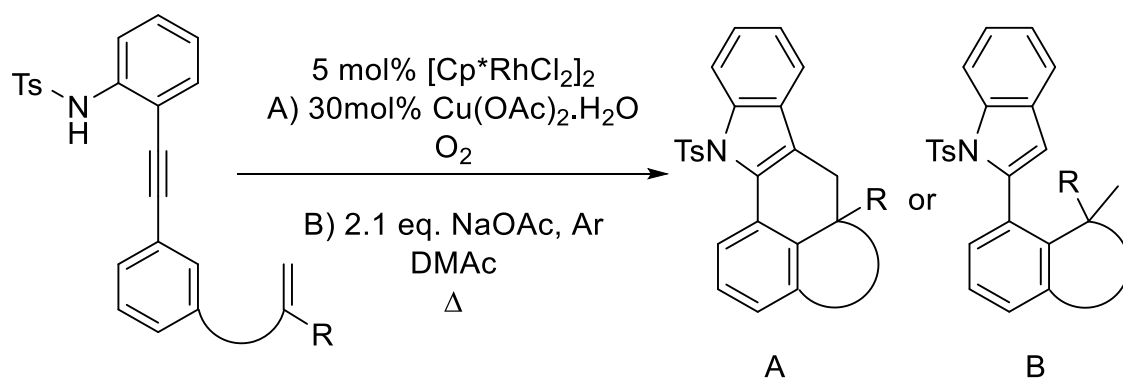
Scheme 1.8: Base-promoted C-H arylation of phenylpyridines (A) and tryptophan (B) catalysed by Pd(OAc)₂.



Scheme 1.9: Based promoted Mn(I) alkenylation of phenylpyridines, with the proposed C-H activation transition state highlighted.

In these examples, the C-H activation step is directed by a heteroatom coordinating to the metal centre which leads to selective C-H activation. As such these reactions are relatively easier than undirected reactions due to more favourable kinetic and entropic factors.⁵¹ In the rhodium-catalysed synthesis of fused indoles (**Scheme 1.10**),⁵² the formation of the two additional rings occurs with two undirected C-H activations.

Alteration of the reaction conditions with the use of NaOAc instead of Cu(OAc)₂ prevents the second C-H activation leading to the formation of product B.

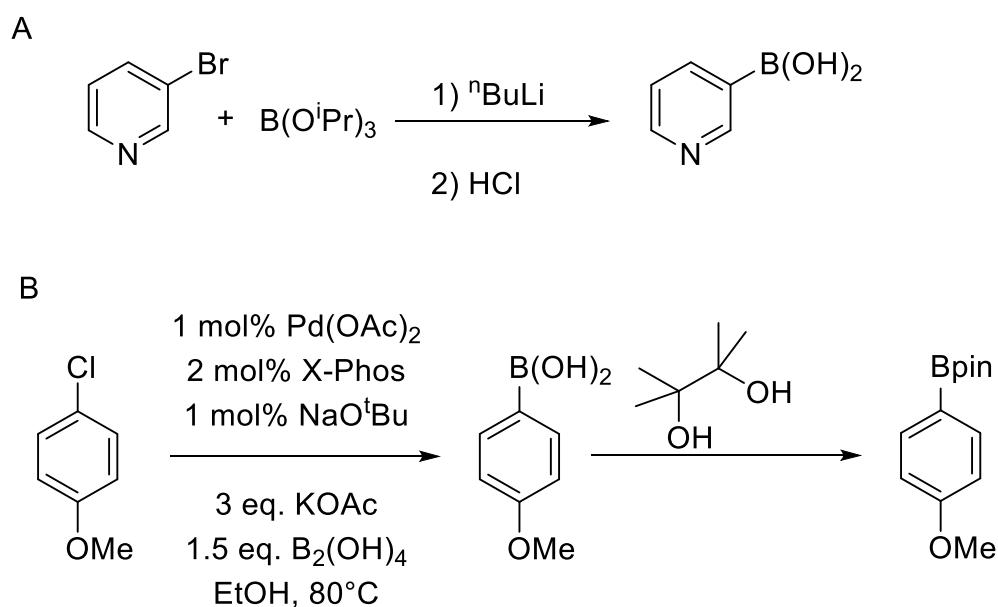


Scheme 1.10: Rh-catalysed cyclisation and alkene insertion, with control of product formation depending on reaction conditions (DMac = dimethylacetamide).

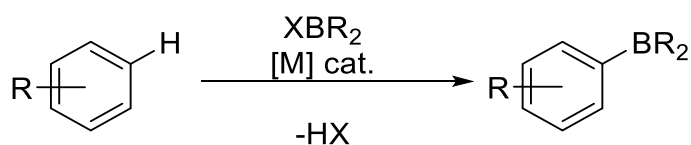
1.4 C-H borylation

1.4.1 Applications of borylation

Organoboron compounds have many important applications as cross-coupling reagents in organic synthesis. This includes their use in the synthesis of many compounds with medical applications such as (+)-Complanadine A,⁵³ and in the synthesis of tetracyclic drug agents.⁵⁴ Other applications of organoboron compounds include in supramolecular complexes for use in sensors for key targets such as sugars.⁵⁵ Formation of boronic acids and esters occurs either by the reaction of Grignard reagents (or lithium salts) with a borate ester,⁵⁶⁻⁵⁸ or the palladium-catalysed reaction of aryl halides with diboron reagents (**Scheme 1.11**).^{59, 60} Thus both reactions generate stoichiometric amounts of halogenated waste and have potential limitations due to sensitivity of other functional groups.

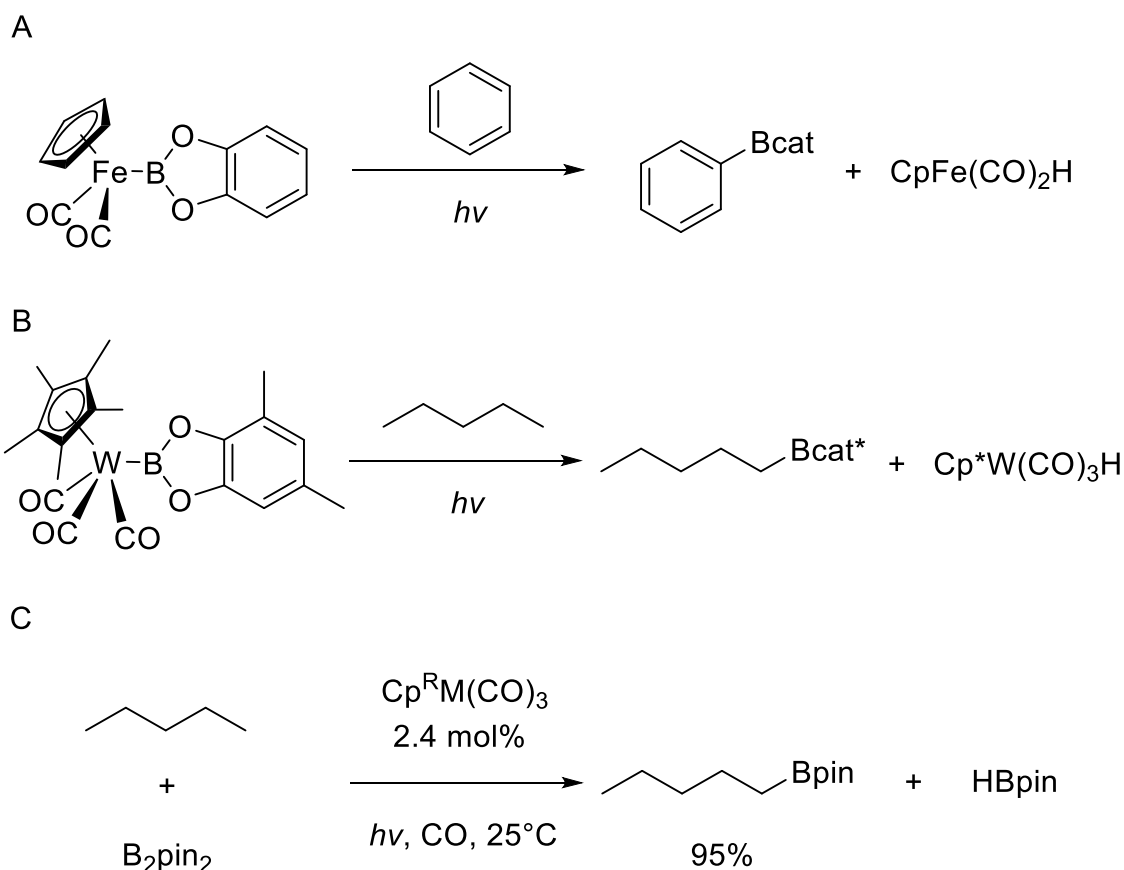


Thus, catalytic C-H borylation offers the ability to synthesise directly boronic esters without the need to use pre-functionalised substrates, which reduces the amount of waste generated from the synthesis of boronic esters (**Scheme 1.12**). Activation could be thermal or photolytic in nature;⁶¹ thermal activation is generally preferred due to difficulties in sourcing specialist light sources of the correct wavelength for photochemical reactions, problems in scaling up batch photochemical reactions and the avoidance of potential issues with photosensitive functional groups.



Scheme 1.12: General borylation of arenes (X = H or BR₂).

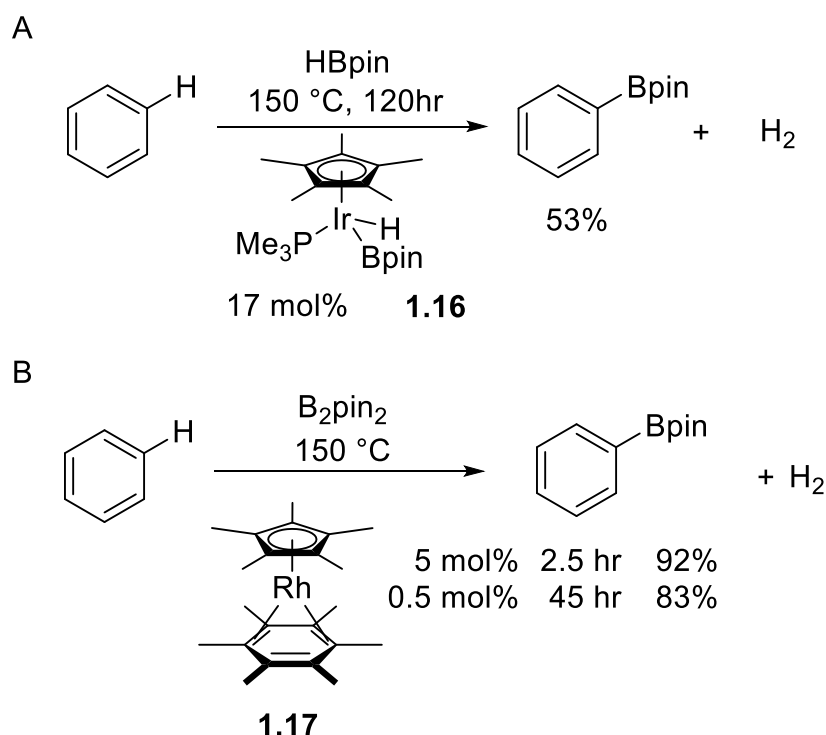
For C-H borylations, stoichiometric photolytic reactions were explored with iron and tungsten carbonyl complexes initially (**Scheme 1.13, A & B**),^{62, 63} before Mn and Re carbonyl complexes were used in catalytic reactions with arenes and alkanes (**Scheme 1.13, C**).⁶⁴ While the reactions occurred at room temperature, the use of powerful mercury arc lamps (450 W) for photolysis poses issues to its suitability for a general range of substrates. Additionally, it was found to be necessary to conduct the reaction under an atmosphere of CO in order to regenerate the active catalytic species, thus when the reaction was conducted without an atmosphere of CO, only a 22% yield of pentylboronate ester was achieved as opposed to the yield of 95% achieved with CO present.



Scheme 1.13: Photolytically activated C-H borylation reactions (Bcat* = BO₂C₆H₂Me₂, M = Re or Mn, Cp^R = Cp*, C₅H₄Me).

1.4.2 Arene borylation

The first recorded undirected thermal borylation of arenes was with Ir complex **1.16** for the borylation of benzene with HBpin (**Scheme 1.14, A**).⁶⁵ The reaction required a relatively high catalyst loading and very high temperatures (150 °C compared to 80 °C, the boiling point of benzene which was used as the reagent and solvent), thus it is not ideal due to safety concerns and energy costs.



Scheme 1.14: Borylation of benzene with Ir complex **1.16** and Rh complex **1.17**.

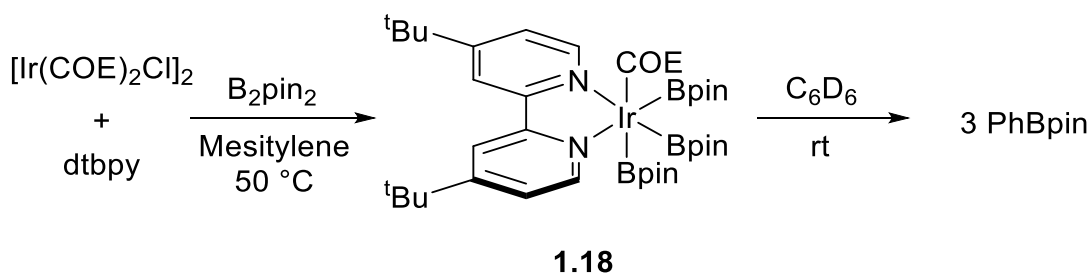
The Cp* Rh complex **1.17** was found to perform more efficiently than **1.16** with a reduced reaction time and requiring a lower catalytic loading,⁶⁶ however, the reaction was still carried out at elevated temperatures. Progress in arene borylation has mainly switched to iridium catalysts due to the serendipitous discovery that iridium centres with aromatic nitrogen ligands can form active catalysts that work at lower temperatures.⁶⁷ Thus, a range of Ir-based systems have been trialled for arene borylation (**Table 1.2**).⁶⁷⁻⁶⁹ The use of bipyridine (bpy) and the di-*tert*-butyl analogue (dtbpy) lead to a noticeable increase in reactivity with decreases in either reaction temperature or time. The iridium COD chloride dimer was found to be inactive at ambient conditions but reacts at 80°C. In contrast, the COE analogue was found to be active at room temperature, presumably due to COE being more labile than COD. Alternatively, changing the Cl ligand to an alkoxy (OPh, OMe) with COD as the alkene gave an effective system for the borylation of

benzene, with complete conversion of B₂pin₂ observed. The acetate analogue was found to be very poor at catalysing the reaction; this complex is less basic than the alkoxy analogues, which suggests that the nature of the anionic ligand is important to the activation process. Mesitylene was found to be unreactive towards aryl borylation (presumably due to the large degree of steric hindrance), and thus allowed the isolation of the product of the reaction of B₂pin₂ with [Ir(COE)₂Cl]₂/dtbpy as an octahedral trisboryl complex (**Scheme 1.15**). Addition of benzene to this species led to the formation of PhBpin.

Table 1.2: Ir based catalysts for the borylation of benzene.

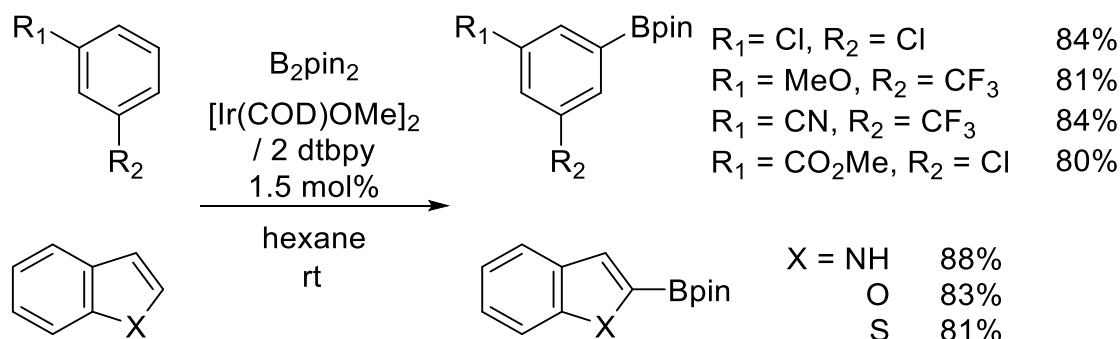
Complex	Ligand	Catalyst loading/ mol%	Temperature/ °C	Time/ hr	Conversion/ %
IndIr(COD)	PMe ₃	2	150	18	88 ^a
(MesH)Ir(Bpin) ₃	PMe ₃	2	150	15	98 ^a
0.5 [Ir(COD)Cl] ₂	bpy	3	80	16	80 ^b
0.5 [Ir(COD)Cl] ₂	bpy	6	rt	24	0 ^b
0.5 [Ir(COE) ₂ Cl] ₂	dtbpy	5	rt	4.5	83 ^b
0.5 [Ir(COE) ₂ Cl] ₂	dtbpy	0.02	100	16	80 ^b
0.5[Ir(COD)OMe] ₂	bpy	6	rt	4	100 ^b
0.5[Ir(COD)OPh] ₂	bpy	6	rt	4	100 ^b
0.5[Ir(COD)OH] ₂	bpy	6	rt	4	100 ^b
0.5[Ir(COD)OAc] ₂	bpy	6	rt	4	19 ^b

^a HBpin used as boron source, ^b B₂pin₂ used as boron source



Scheme 1.15: Isolation of Ir intermediate **1.18** and subsequent reaction with d_6 -benzene.

By using $[\text{Ir}(\text{COD})\text{OMe}]_2$ with dtbpy, it was found to be possible to borylate substrates in an inert solvent, which is more difficult than conducting the reactions in the neat arene.⁶⁷ This had been found to be usually disfavoured due to kinetic/concentration effects, but it is more synthetically useful to conduct these reactions in a solvent as it allows borylation of solids or expensive substrates for which neat reactions would be impractical. Borylation was found to be tolerant to halogen functionality as well as nitrile and ester groups with good to excellent yields (**Scheme 1.16**). In addition, heteroarenes such as benzothiophene, benzofuran and indole could also be borylated in good yields (81-88%). This system can be considered the current state of the art for undirected borylation of arenes with B_2Pin_2 .

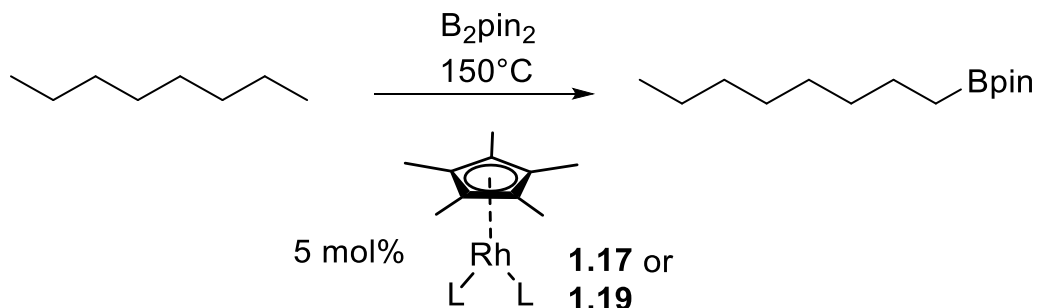


Scheme 1.16: Borylation of substituted arenes and heteroarenes by $[\text{Ir}(\text{COD})\text{Cl}]_2/\text{dtbpy}$ in hexane.

1.4.3 Alkane borylation

The catalytic C-H functionalisation of simple hydrocarbons was realised in the borylation of alkanes by a $\text{Cp}^*\text{Rh}(\text{I})$ based system (**Scheme 1.17**).⁶⁶ This reaction is more challenging than the activation of arenes. Although the arene C-H bond is stronger than an alkane C-H bond (**Table 1.3**), the resultant M-C bonds are stronger for arenes than

alkanes, thus the thermodynamic driving force is greater. Also, arenes are flat and thus less sterically hindered than sp^3 alkanes, and there are additional interactions between the metal and the arene π -systems which mean that arenes are more capable of complexation to the metal and thus will more readily C-H activate.



Scheme 1.17: Borylation of alkanes with Cp^*RhL_2 complexes ($L_2 = \eta^4-C_6Me_6$ **1.17** or $L = C_2H_4$ **1.19**).

Table 1.3: Bond dissociation energies for relevant bonds.^{70, 71}

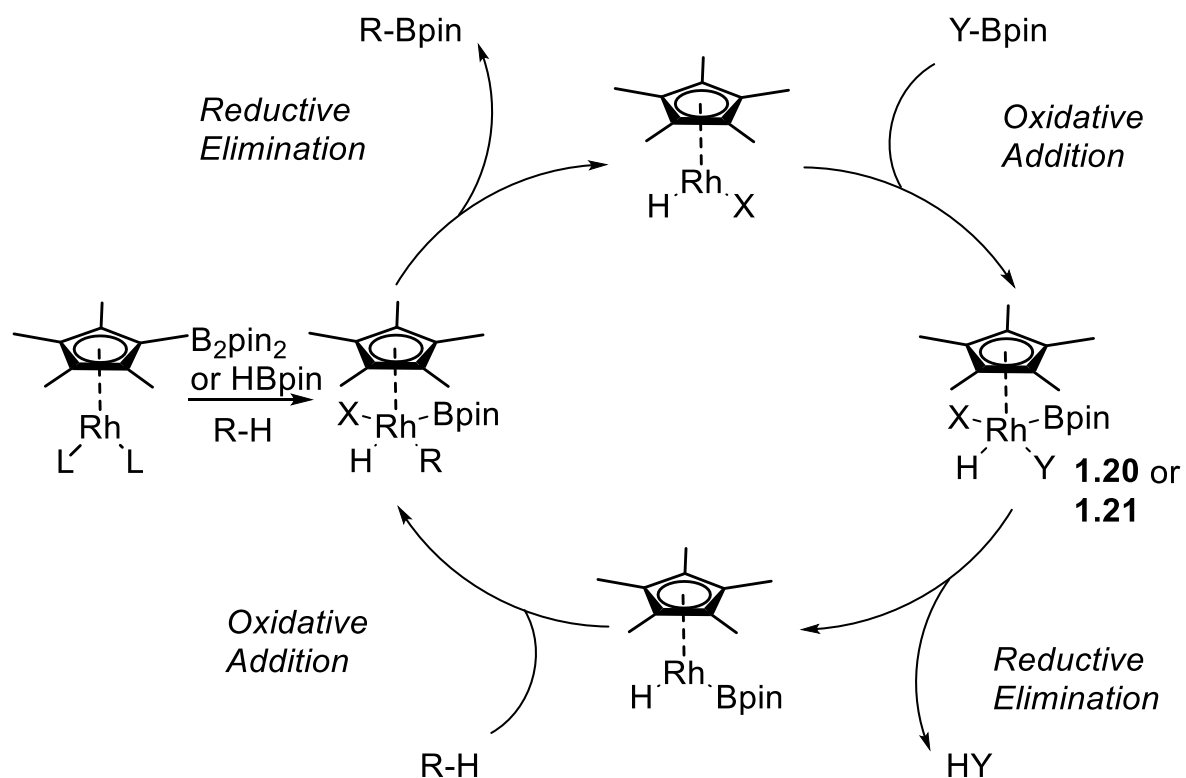
Bond type	Bond Dissociation Energy/ $KJmol^{-1}$
C-B	356
H-B	389
B-B	293
H-H	432
Alkane C-H (methane)	439
Alkane C-H (primary)	426
Alkane C-H (tertiary)	404
Alkene C-H	444
Arene C-H	464

While $[Rh(Cp^*)(C_2H_4)_2]$ (**1.19**) was found to be most active initially for alkane borylation, $[Rh(Cp^*)(\eta^4-C_6Me_6)]$ (**1.17**) was found to remain active for longer over the course of the reaction.⁶⁶ Reactions occur at the terminal position of the alkane, which is

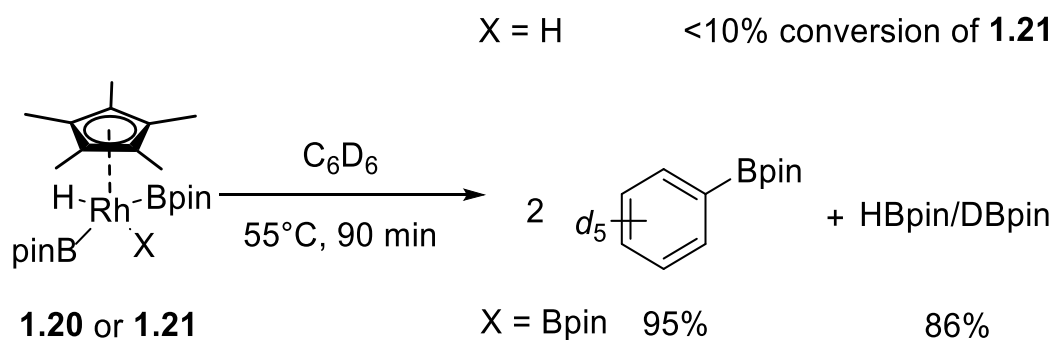
very different selectivity compared to radical functionalisation. This is because radical reactions favour the most stable radical, thus secondary and tertiary positions are preferred to primary (terminal). Borylation with B₂pin₂ (bis(pinacolato)diboron) generates an equivalent of HBpin, and dehydrogenative borylation with HBpin also can occur (with loss of H₂), which means that the total consumption of B₂pin₂ forming two C-B bonds is possible. It should be noted that the reaction temperature is ca. 25°C in excess of the boiling point of octane (125°C) indicating that quite forcing conditions are required.

If the mechanism is described as proceeding via an oxidative addition process, the resting state Rh species are thought to be [Rh(Cp*)(H)_n(Bpin)_{4-n}] (n = 1, **1.20**; n = 2, **1.21**), which can undergo reductive elimination to [Rh(Cp*)(H)(Bpin)] (**Scheme 1.18**).⁶⁶ From this, oxidative addition of alkanes (RH) give [Rh(Cp*)(H)₂(R)(Bpin)], from which loss of RBpin can occur via reductive elimination giving [Rh(Cp*)(H)₂]. Addition of B₂pin₂ then gives **1.21**. Complex **1.20** was independently synthesised via photolysis of either **1.17** or **1.19** with HBpin; subsequent heating in HBpin then generated complex **1.21**.²² Both complexes **1.20** and **1.21** were found to react with octane and benzene to give the respective pinacolboronate esters, with the bisboryl complex shown to be slower for both reactions compared to the trisboryl complex, which was confirmed by conducting the reactions at a lower temperature (**Scheme 1.19**).

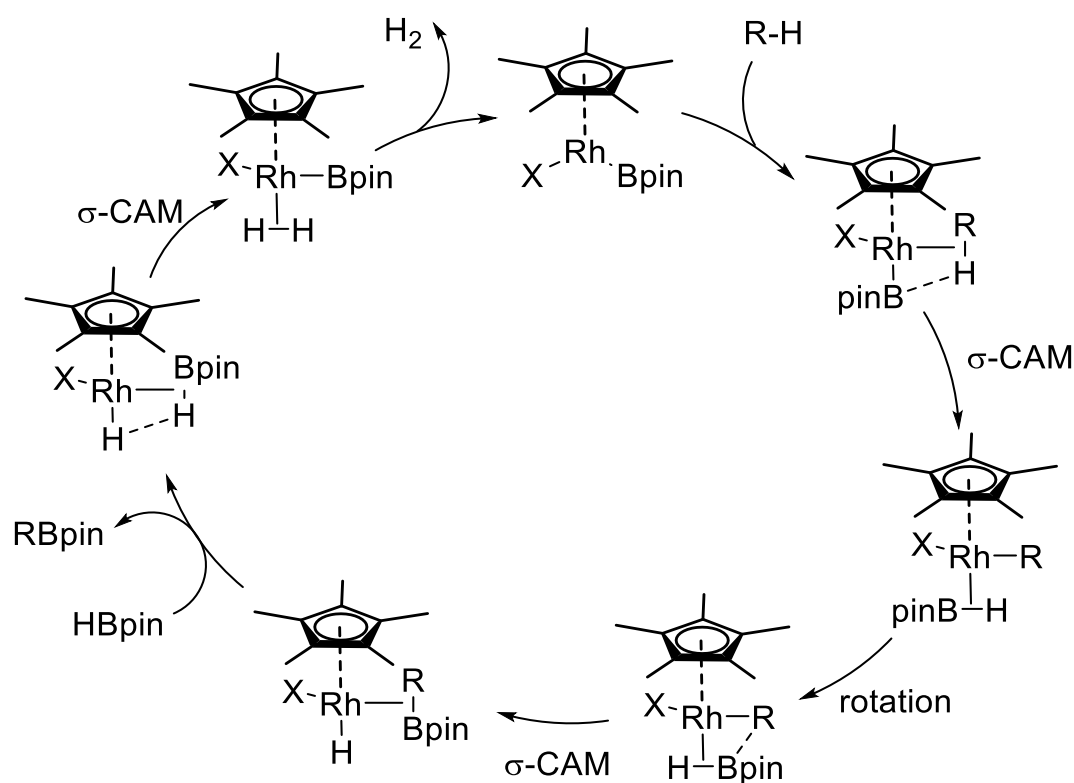
An alternative description of the mechanism involves σ -CAM processes rather than oxidative addition/reductive elimination steps (**Scheme 1.20**).^{20, 22} This description does not require high oxidation states and thus avoids invoking Rh(V) as the oxidative addition/reductive elimination mechanism does. This mechanism also implies an alternative description for complexes **1.20** and **1.21** (**Scheme 1.21**), which display distortions towards retaining H-B bonds in the X-ray determined structures.



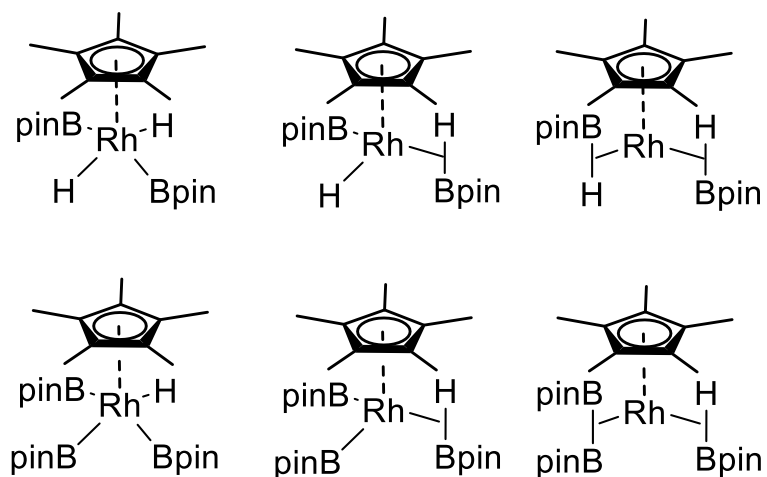
Scheme 1.18: Proposed catalytic cycle for the borylation of alkanes via an oxidative addition mechanism (X, Y = Bpin or H).



Scheme 1.19: Reactions of bis- and trisboryl complexes with benzene.



Scheme 1.20: σ -CAM description of the mechanism for C-H borylation with **1.17** ($X = H$ or Bpin).



Scheme 1.21: Possible bonding descriptions for **1.20** and **1.21**.

Additionally, **1.20** and **1.21** were observed by 1H NMR spectroscopy in the reaction mixture of **1.17** with B_2pin_2 in pentane. This combined with computational studies²² supports the mechanism that both are intermediates in the catalytic cycle (**Scheme 1.18**).

1.4.3 Substrate scope

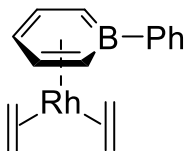
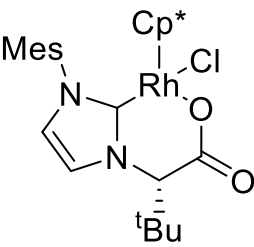
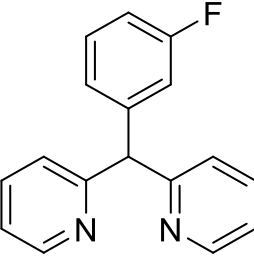
The borylation conditions were found to be tolerant to heteroatom-containing substrates with regiospecific reactions occurring at the least sterically hindered methyl group.⁷² In addition, borylation is preferred at the least electron-rich methyl group with selective reaction for (C₈F₁₇)C₂H₅ over C₈H₁₈ observed. These properties are interesting as it shows that the borylation is not affected by directing groups, which often induce additional reactivity/selectivity.

Other catalysts have been trialled for the CH activation of octane and are either Rh-, Ir- or Ru-based with an aromatic ligand (with the exception of **1.24** and **1.28** which use N,N ligands).⁷³⁻⁷⁷ These have a range of activities (**Table 1.4**) with all requiring either long reaction times, high temperatures or both. Some are able to perform borylation with B₂pin₂ and dehydrogenative borylation with HBpin, and thus are able to use all of the B reagent. Complex **1.28** was found to be the most active system for the borylation of octane achieving complete conversion of B₂pin₂ and HBpin to octylBpin, thus representing the current state-of-the-art system for alkane borylation. Additionally the increase in reactivity allowed the reaction to be attempted under non-neat conditions;⁷⁷ using 3 equivalents of octane in cyclohexane a yield of 52% was achieved which is greater than several neat reactions using other complexes (**Table 1.4**). This is possible due to the reaction being inactive towards secondary alkanes.

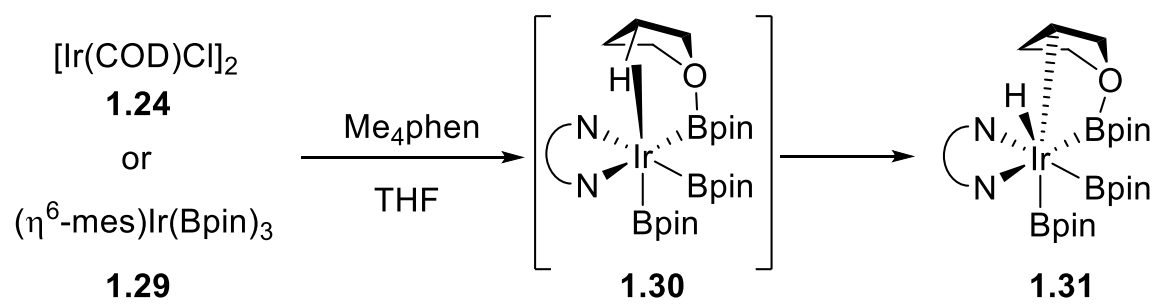
The Ir system **1.24** was found to be able to catalyse secondary C-H bond borylation in the reaction of THF and B₂pin₂. Interestingly, the product is 3-boryl tetrahydrofuran, and reactions with d₄-THF (2,2,5,5-tetradeuterotetrahydrofuran) showed no isotope scrambling between the 2- and 3-positions on the THF; ¹¹B NMR spectroscopy revealed the formation of HBpin, not DBpin. This indicates that the C-H activation step is directly at the 3-position, rather than activation at the 2-position followed by isomerisation to the 3-position. Complex **1.29** was found to be more active as a pre-catalyst for THF borylation, presumably because it more readily forms the active species **1.31**. The selectivity and deuterium labelling observations fit for the reaction proceeding via a 6-membered transition state (**Scheme 1.22**), with a THF-borane adduct (**1.30**) allowing pre-coordination of the THF prior to C-H activation step at the 3-position. Catalysis using either **1.24** or **1.29** has been used to borylate a range of saturated heterocycles including pyrrolidines, piperidines and lactones, and natural products such as menthol.⁷⁸ This

highlights how tolerant catalysts based upon these complexes can be towards functionality.

Table 1.4: Complexes for borylation of alkanes.

Complex	Catalyst loading/ mol%	Temperature/ °C	Time	Yield/ % ^b
[Ir(Cp*)(H) ₄] 1.22	10	200	^a	<20
[Ir(Cp*)(C ₂ H ₄) ₂] 1.23	10	200	10 days	58
[Ir{(OMe)(COD)} ₂] Me ₄ Phen 1.24	5	120	24 hrs	44
[Rh(Cp*)(C ₆ Me ₆)] 1.17	5	150	25 hrs	88
[Rh(Cp*)(C ₂ H ₄) ₂] 1.19	5	150	5 hrs	84
[{Ru(Cp*)Cl} ₂] 1.25	2	150	48 hrs	49
 1.26	5	50	100 hr	20
 1.27	5	150	16 hr	43
[(Mes)Ir(Bpin) ₃]/  1.28	1	120	24 hr	99

^a Time not given, ^b Yield with respect to consumption of B₂pin₂ & HBpin.



Scheme 1.22: Mechanism for the C H activation of THF by Ir system **1.24** or **1.29** (mes = mesitylene).

1.5 Ligands in organometallic chemistry

1.5.1 Cyclopentadienyl-type ligands

The cyclopentadienyl ligand (Cp) is the basis of many transition metal complexes capable of C-H activation. It is commonly thought of as taking up three cis coordination sites as an L₂X-type ligand (**Figure 1.1**). It is in general thought of as a very stable ligand and is unlikely to dissociate, although recent work has shown that this is not always the case.^{79, 80} The related pentamethylcyclopentadienyl (Cp*) ligand is more electron rich, which makes complexes of this ligand more electron rich and more reactive, as well as being more sterically bulky, and offers better solubility in hydrocarbon solvents.

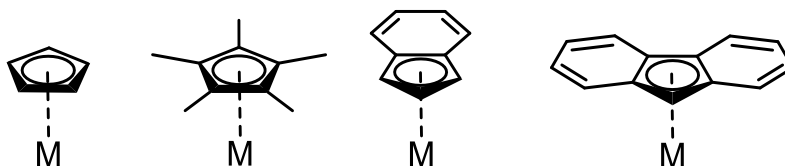
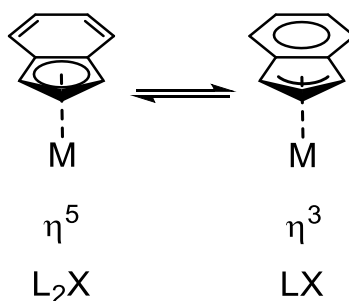


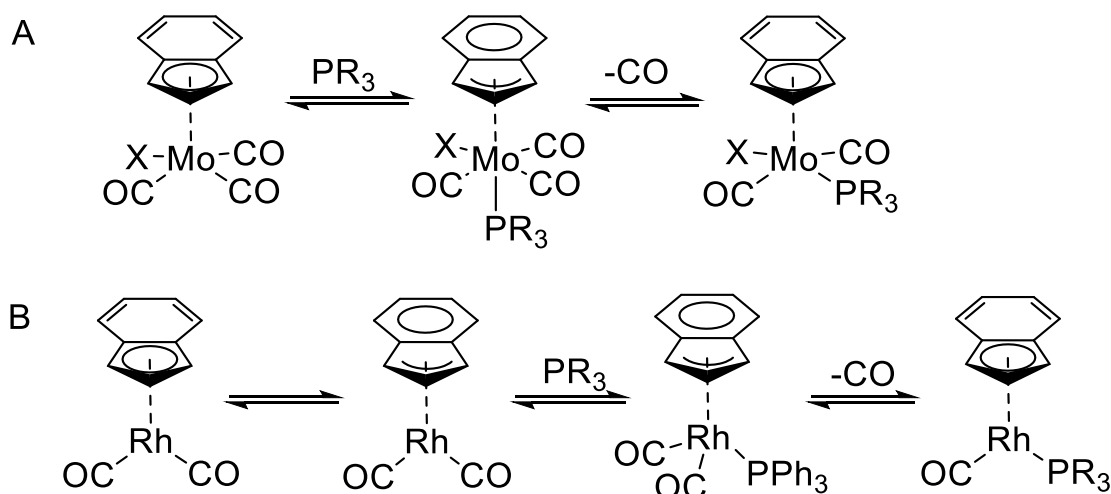
Figure 1.1: Cyclopentadienyl-type ligands.

Indenyl and fluorenyl are the mono- and di-benzannulated analogues respectively of the cyclopentadienyl ligand. The extra ring(s) lead to the stabilisation of the ‘ring slipped’ state (**Scheme 1.23**) due to reforming a discrete 6 π aromatic ring. Upon ring slippage, the indenyl changes from an L₂X donor to a LX ligand, thus the metal is no longer coordinatively saturated and is able to coordinate other ligands without the need to eject coordinated ligands.



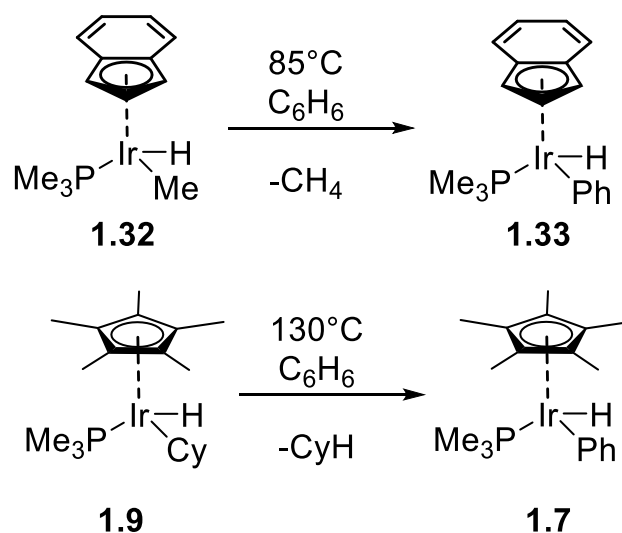
Scheme 1.23: Indenyl ring-slippage.

The ‘indenyl effect’ has been shown to lead to an increase in the rate of substitution reactions of $[\text{Mo}(\text{Ind})\text{X}(\text{CO})_3]$ ($\text{X} = \text{Me}, \text{Cl}, \text{Br}, \text{I}$) with phosphine ligands when compared to analogous Cp complexes (**Scheme 1.24**).^{81, 82} Hart-Davis and Mawby proposed a concerted associative mechanism with the phosphine attacking the η^5 -complex forming the η^3 complex followed by ligand dissociation to give the final η^5 -complex. An alternative mechanism proposed by Basolo involves the η^5 and η^3 complexes existing in a rapid equilibrium and the rate-determining step is the attack of the phosphine on to the η^3 species for Rh and Mn systems (**Scheme 1.24, B**).^{83, 84} Other ligands have been shown to display similar effects such as cyclohexadienyl and fluorenyl,⁸⁵ although they are generally less explored than indenyl.



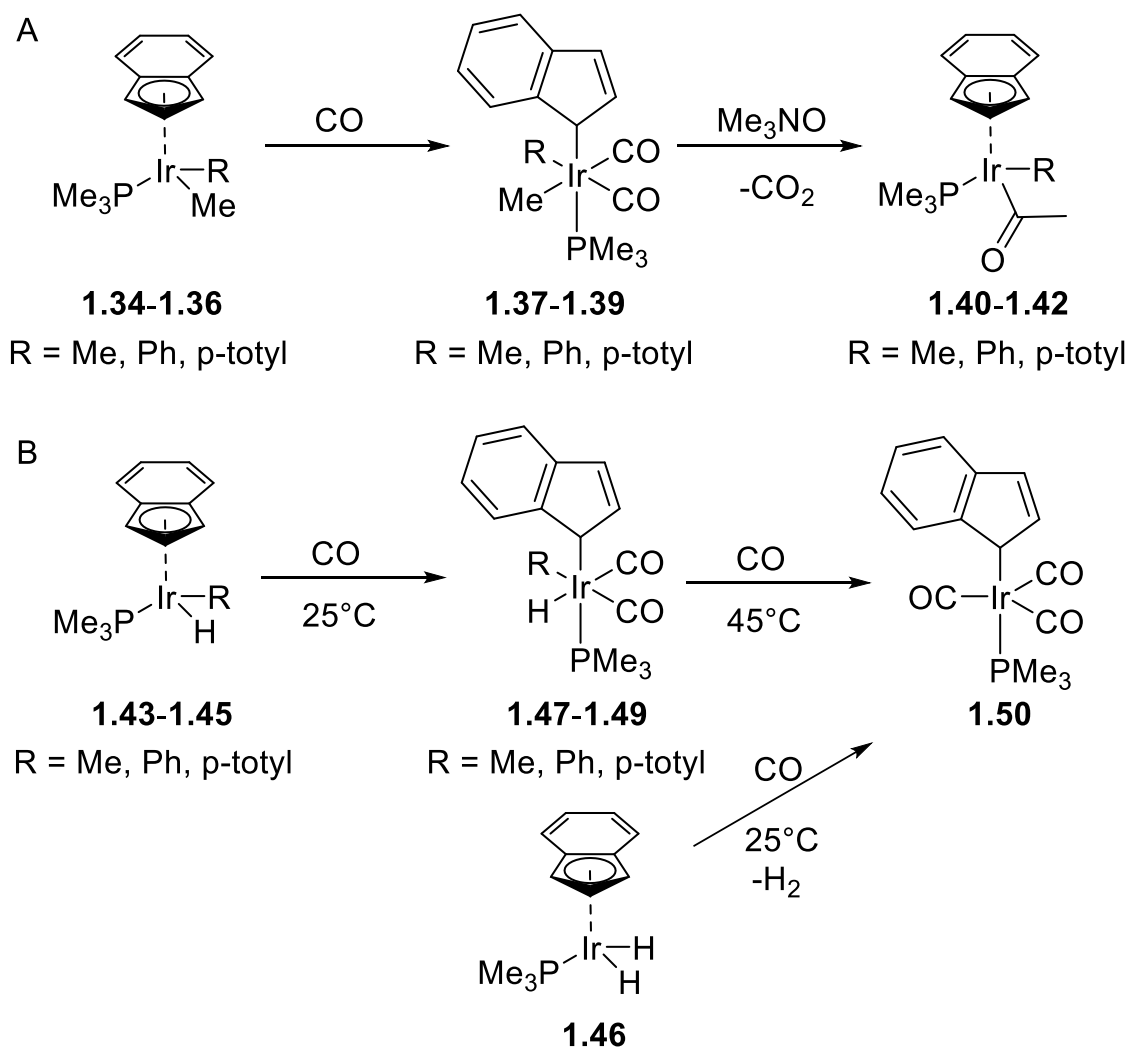
Scheme 1.24: Substitution of $[\text{Mo}(\text{Ind})\text{X}(\text{CO})_3]$ with phosphines via a 7-coordinate intermediate (A) or via a 5-coordinate intermediate (B).

Evidence for the differing reactivity of indenyl versus Cp is highlighted by comparison of the reactions of $[\text{Ir}(\text{Ind})(\text{PMe}_3)(\text{R})(\text{H})]$ to the Cp* analogues in the reduced temperatures required for the thermolysis of the Ir complexes (**Scheme 1.25**).^{86, 87} Thermolysis of $[\text{Ir}(\text{Ind})(\text{PMe}_3)(\text{Me})\text{H}]$ **1.32** in benzene readily occurs at 85°C affording the phenylhydride complex **1.33** with a reaction half-life of 25 hrs, while thermolysis of $[\text{Ir}(\text{Cp}^*)(\text{PMe}_3)(\text{Cy})\text{H}]$ in benzene required 130°C for convenient reaction times (the reaction at 100°C has a half-life of 4.5 days).



Scheme 1.25: Thermolysis of Ir complexes **1.32** and **1.9** (Cy = cyclohexyl) in benzene leading to the formation of the phenyl hydride complexes **1.33** and **1.7**.

The addition of CO to the dialkyl complexes **1.34** – **1.36** led to the η^1 -indenyl dicarbonyl complexes **1.37** – **1.39** (Scheme 1.26, A).⁸⁷ No intermediate η^3 complexes were observed, and limiting the amount of CO led to a mixture of starting η^5 and product η^1 complexes. Addition of Me_3NO induces the migratory insertion of the methyl into a M-CO bond to give η^5 -indenyl complexes **1.40**– **1.42**. This contrasts with the reactivity observed for hydride complexes **1.43** – **1.45** and dihydride complex **1.46** (Scheme 1.26, B). While the alkylhydride complexes do form the analogous η^1 -complex **1.47** – **1.49**, treatment with Me_3NO did not lead to migratory insertion. It was found that heating at 45°C led to reductive elimination and formation of the η^1 -indenyl tricarbonyl Ir complex **1.50**. Treatment of dihydride **1.46** with CO at 25°C also led to **1.50**, indicating that the presence of CO increases the potential for reductive elimination, a property previously observed for other systems with similar ligands.⁸⁸⁻⁹² These reactions show potential new reactivity that indenyl offers over Cp due to the former's ability to ring slip and form complexes other than the usual η^5 complexes typically observed for Cp.



Scheme 1.26: Reactions of indenyl Ir complexes with CO and subsequent migratory insertion.

1.5.2 Phosphines

Phosphines (PR_3) are commonly used as ligands in a variety of applications due to many being commercially available and the fact that they have very well defined properties. Phosphines act as σ -donors with the donation of the P lone pair into a transition metal empty d-orbital (**Figure 1.2**). They can also act as π -acceptor ligands with the donation of electron density from a filled metal d-orbital into a P-R σ^* -orbital.⁹³ More electron withdrawing groups such as F and aryl rings lead to increased π -acceptor character, while trialkylphosphines are strong σ -donors and poor π -acceptors. This variation in electronic properties allows for moderation of the electron density on the metal, which helps different steps such as oxidative addition and reductive elimination.

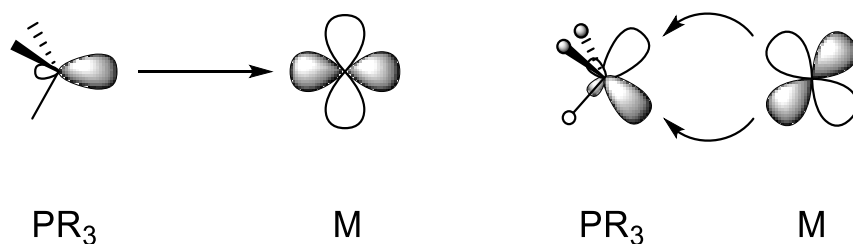


Figure 1.2: Phosphine-metal interactions.

In addition to electronics, steric parameters can be tuned easily by increasing the size of the R substituents. These changes can be quantified by a number of different methods that allow for the prediction of properties.⁹⁴ Bis(phosphines) are also commonly used as they often offer increased stability and/or reactivity in catalysis.⁹⁵ These enhancements arise from the chelate effect and distortion of bonding orbitals due to a small bite-angle.⁹⁶

Uses of phosphines in industrially-relevant catalysis include complexes with Rh for hydroformylation,⁹⁷ and with Pd for cross-coupling reactions that range in complexity to allow for a variety of transformations in applications including total synthesis.⁹⁸⁻¹⁰⁰

1.5.3 *N*-Heterocyclic carbenes

Carbenes are species that contain a divalent carbon atom. Two orbitals are involved in bonding to substituents while the remaining two electrons reside in the other orbitals. Carbenes exist in either the singlet, where the two electrons are in the same orbital and the remaining p-orbital is empty (**Figure 1.3, A**), or triplet state where one electron is in each orbital (**Figure 1.3, B**). Carbenes without heteroatom substituents are often triplets, sp-hybridised with the two unpaired electrons in separate p-orbitals (**Figure 1.3, C**). Triplet carbenes react in a stepwise manner as the unpaired electrons act independently of one another, whereas singlet carbenes react via concerted mechanisms with the electrons behaving more like a lone pair. In the absence of functionality at the α -position to the carbene C-atom, the triplet state is favoured as the spin-pairing energy provides an energetic penalty for the singlet state. In the presence of conjugated donor groups (+M), the singlet state is preferred as the p-orbital is filled with electron density from the donor groups.

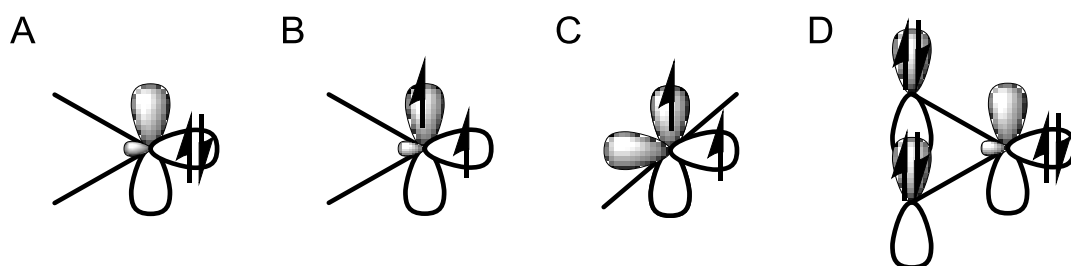


Figure 1.3: Generalised molecular orbitals of singlet (A), triplet (B & C) and N-heterocyclic carbenes (D).

Carbenes are often reactive species that have short lifetimes and can only be inferred by careful trapping experiments. ‘Stable carbenes’ are those that can be isolated and have moderate to long lifetimes. Although the phosphinocarbenes discovered by Bertrand showed increased stability,^{101, 102} the mostly widely used stable carbenes are based on those first isolated by the Arduengo group,¹⁰³ which featured a cyclic diaminocarbene with the very bulky adamantyl group (**Figure 1.4**). It was found to be stable in the absence of air and moisture and had a high melting point suggesting it does not readily decompose. Further examples showed that very bulky groups were not required for high stability,¹⁰⁴ and additionally the need for aromaticity of the ring was shown to be unnecessary with the synthesis of the dihydro-analogues.^{105, 106}

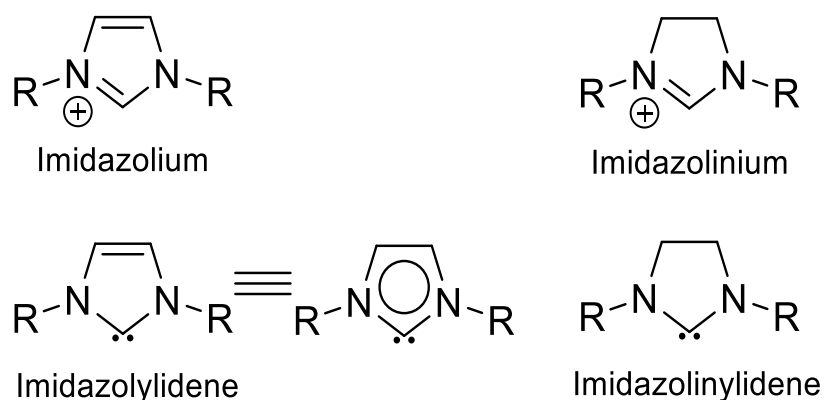


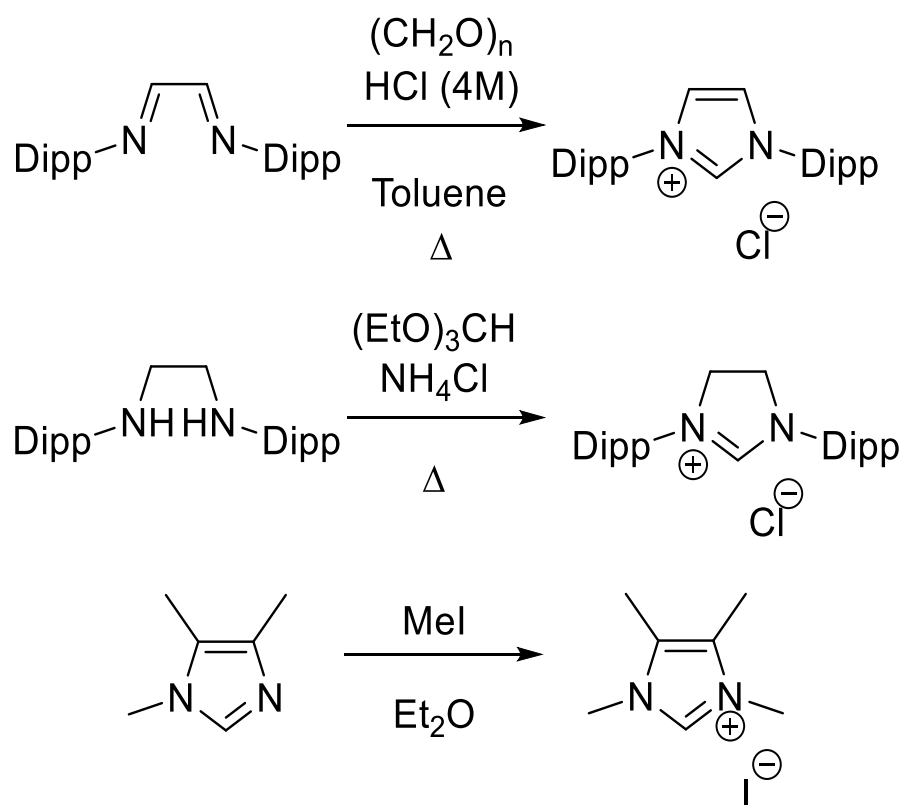
Figure 1.4: General structure of common NHCs and precursor salts.

The improved stability of NHCs is derived from the ability of the adjacent heteroatoms (usually N but not exclusively) to donate electron density into the p-orbital of the carbene thus leading to a singlet carbene (**Figure 1.3, D**).¹⁰⁷ This reduces the electrophilicity of the carbene to such a degree that they are classified as nucleophilic in nature.

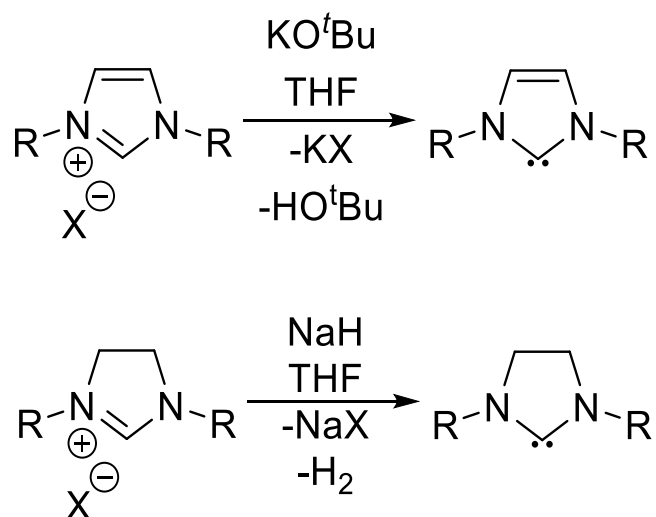
Unsaturation of the backbone of the NHC ring has been linked to increased stability due to Hückel's rule of aromaticity for imidazolylidene (**Figure 1.4**) and differing reactivity has been observed between saturated and unsaturated NHCs where other substituents are the same.^{106, 108, 109}

The steric and electronic properties of NHCs can be varied by changes to the N-substituents, substitution on the backbone, and switching from unsaturated to saturated backbones.¹¹⁰⁻¹¹² Quantification of these parameters can be achieved by a variety of methods, which each have different advantages and disadvantages, and provides useful information to aid the prediction of which NHC is most useful for a particular application. An example highlighting the need to choose the correct method of quantification is the comparison between the commonly used NHCs IPr and SIPr [1,3-bis(diisopropylphenyl)imidazol(in)ylidene], which only differ in structure at the backbone. The Tolman electronic parameter,¹¹³ a well-known measure which was originally developed for phosphines, is very similar for both (2051.5 cm⁻¹ and 2052.2 cm⁻¹ respectively),^{114, 115} however, there are many examples of differing reactivity between IPr and SIPr with metal complexes each showing differing reactivity.¹¹⁶⁻¹¹⁹ Alternative electronic parameter measurements, such as measurement of the NMR shift for P or Se adducts,^{120, 121} provide different values for IPr and SIPr, thus allowing for a better explanation of the different reactivities displayed by what are otherwise very similar compounds. There are similarities between NHCs and phosphines as both are σ -donors and can act as π -acceptors, which means that there are many applications for which both NHCs and phosphines have been investigated.

Multiple methods of synthesising NHCs have been reported, which allow for the synthesis of a wide variety of compounds.¹²² Most routes follow modular approaches so that different NHCs can have shared precursors allowing for efficient synthesis. Free NHCs are generally formed by deprotonation of the azolium salt with a base (**Scheme 1.28**). The azolium salts are typically synthesised by cyclisation of diimines or diamines with a suitable CH source to generate imidazolium or imidazolinium salts respectively,^{123, 124} though alkylation of substituted heterocycles have also been used to access these salts (**Scheme 1.27**).¹²⁵ For imidazolium salts, moderately strong bases such as KO^tBu may be used, while for imidazolinium salts much stronger bases are used, such as NaH and KH (**Scheme 1.28**).¹⁰⁶



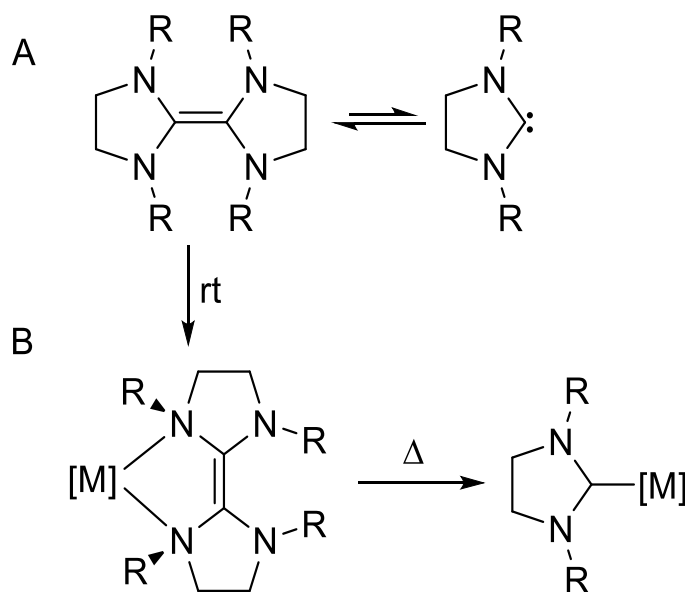
Scheme 1.27: Synthesis of imidazol(in)ium salts with cyclisation,^{123, 124} or alkylation.¹²⁵



Scheme 1.28: Deprotonation of an imidazolium salt to a NHC (X = Cl, Br, BF₄, PF₆, etc).

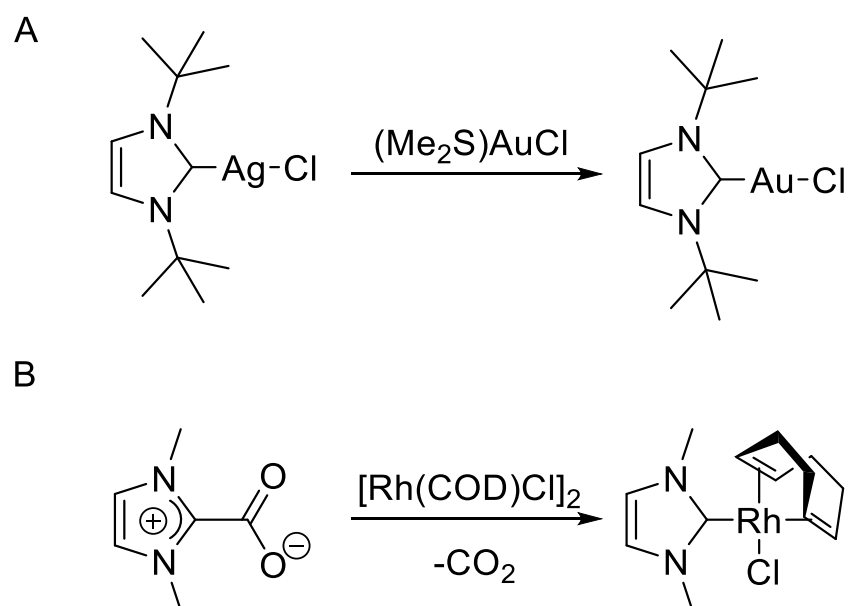
1.5.4 Coordination chemistry of NHCs

The first metal complexes of NHCs were reported before the isolation of free carbenes was achieved.¹²⁶ These were synthesised from ‘Wanzlick’ carbenes, tetraaminoethylenes which can be viewed as dimerised NHCs with too low an amount of steric bulk on the R groups to favour monomeric species. Heating these with metal complexes led to saturated NHC-metal complexes with many TMs (**Scheme 1.29**).¹²⁷ The mechanism is unlikely to go via the free carbene as the N,N' chelates are isolated from reactions at ambient temperature from which the NHC-complex is obtained after heating.¹²⁸⁻¹³⁰



Scheme 1.29: Wanzlick equilibrium (A) and metallation to a metal complex via N,N' chelate (B) (R = Me or Et).

Other syntheses of NHC complexes may involve the direct coordination of the free NHCs to a metal complex with either a leaving group or the breaking up of a multimeric structure to afford the target complex. A disadvantage of this route is the more limited range of solvents due to possible incompatibility with the free NHCs. To avoid this, alternative methods with the use of transfer agents have been developed, including the use of coinage metal complexes and NHC carboxylates. Both Cu(I) and Ag(I) NHC salts have been used as transfer complexes (**Scheme 1.30, A**),^{131, 132} with the NHC-M bond strength being weaker for Cu and Ag compared to other late transition metals,¹³³ therefore the range of metals applicable includes Au(I), Pd(II), Rh(I), Ir(I), and Ru(II).¹³⁴ NHC carboxylates can coordinate to a metal centre and then undergo decarboxylation to afford the NHC-metal complex (**Scheme 1.30, B**).¹³⁵



Scheme 1.30: Example of synthesis of NHC-complexes via A) silver transfer agents,¹³⁶ or B) NHC-carboxylates.¹³⁵

Metal complexes formed with stable NHCs are numerous and a wide scope of metals from the s, p, d, and f-blocks reported.^{137, 138} The bonding behaviour varies due to NHCs having a ‘soft’ character (according to HSAB theory) which leads to strong interactions with late transition metals, while weaker interactions to s-block and f-block metals where there is a low degree of covalency. The molecular orbitals of NHCs lead to a strong σ -donating interaction (**Figure 1.5**). While the potential π -acceptor interaction of a filled metal orbital donating electron density into the p-orbital on the carbene is possible, it is disfavoured due to overlap of the p-orbital with the lone pairs on the adjacent nitrogen atoms. The degree of π -acceptor character is therefore dependent on NHC and the metal centre.

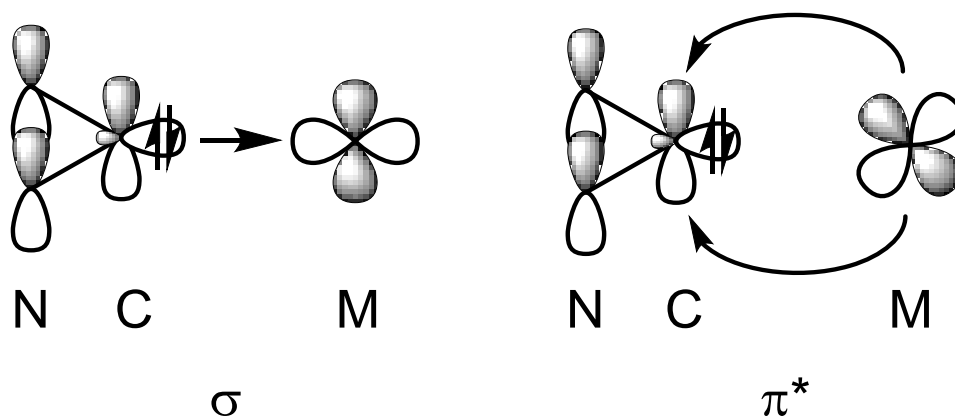


Figure 1.5: Molecular orbitals for an idealised NHC and transition metal interaction.

1.5.5 NHCs in catalysis

A wide range of NHC metal complexes have been used in transition metal based catalysis.¹³⁹ Well known examples include the commercially available second generation Grubbs catalyst **1.51** (**Figure 1.6**) which features the saturated NHC 1,3-bis(trimethylphenyl)imidazolin-2-ylidene (SIMes) for alkene metathesis reactions.¹⁴⁰ Using an NHC ligand was found to lead to an increased preference for the binding of the alkene substrate over the coordination of the free PCy₃ compared to the preference observed for the first generation bis(PCy₃) complex, thus leading to a greatly improved rate of metathesis.¹⁴¹ In this case, the analogous IMes complex was found to be significantly less reactive (5% yield vs 100% yield under the same conditions) indicating the importance of optimising the NHC properties.

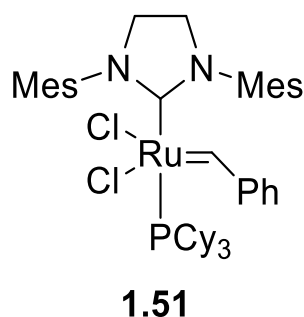


Figure 1.6: 2nd generation Grubbs catalyst featuring SIMes.

The use of SIMes was extended to the Hoveyda-Grubbs catalyst system giving the ‘2nd generation’ version **1.52** (**Figure 1.7**).¹⁴² This was shown to have different reactivity and selectivity to **1.51** with the former being more active towards CM (cross metathesis) than **1.51** which favours RCM (ring closing metathesis). Additionally, **1.52** is stable to oxygen and water and can be stored on the benchtop due to the O-chelating benzylidene group.¹⁴³

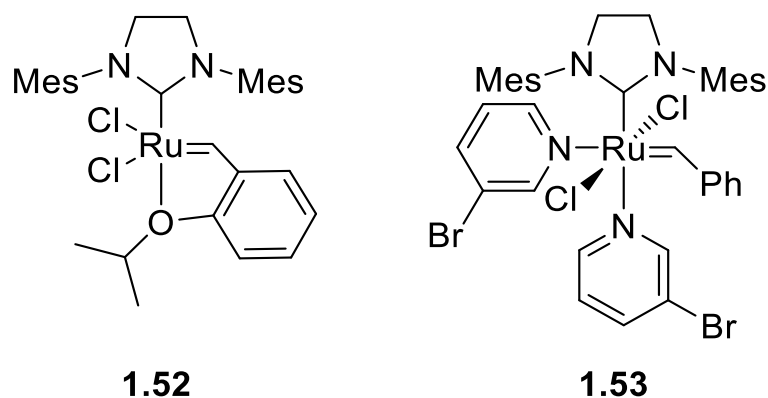


Figure 1.7: SIMes variation of Hoveyda-Grubbs system **1.52** and 3rd generation Grubbs catalyst **1.53**.

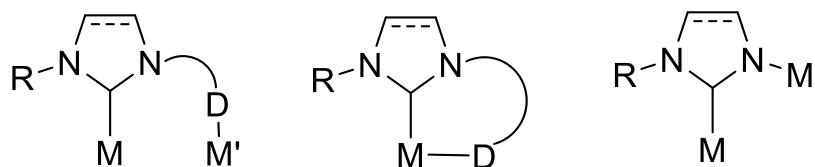
The ‘3rd generation’ Grubbs catalyst **1.53** still features SIMes but substitutes PCy₃ for pyridine, which is more weakly bound than PCy₃ thus leading to faster activation.¹⁴⁴ This allows the catalyst to achieve very low polydispersity values when used for ROMP (ring opening metathesis polymerisation) reactions.^{145, 146}

Pd NHC complexes have been used for a wide variety of cross-coupling reactions.¹⁴⁷⁻¹⁴⁹ These include Suzuki-Miyaura,¹⁵⁰⁻¹⁵³ Heck¹⁵⁴⁻¹⁵⁶ and Buchwald-Hartwig amination reactions.^{157, 158}

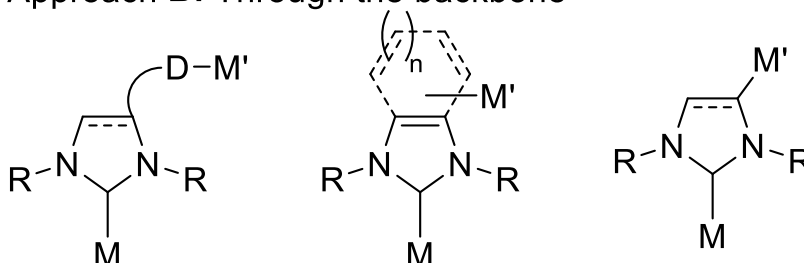
1.5.6 Functionalised NHCs

Functionalised carbenes feature additional donors that are attached to the NHC core, either as N-substituents or on the backbone. These enable additional coordination of metals and potential for reactivity by mixing different ligand classes. For example, NHCs are neutral and ‘soft’, so the addition of an alkoxide group gives a hard/soft X/L-type ligand system which will behave differently to early transition and f-block metals than late transition metals. These can lead to chelating complexes with one metal or multi-metallic complexes with the functionalised NHC coordinating to the different metal centres (**Scheme 1.31**). This topic has been recently reviewed.¹⁵⁹

Approach **A**: Through the N atom



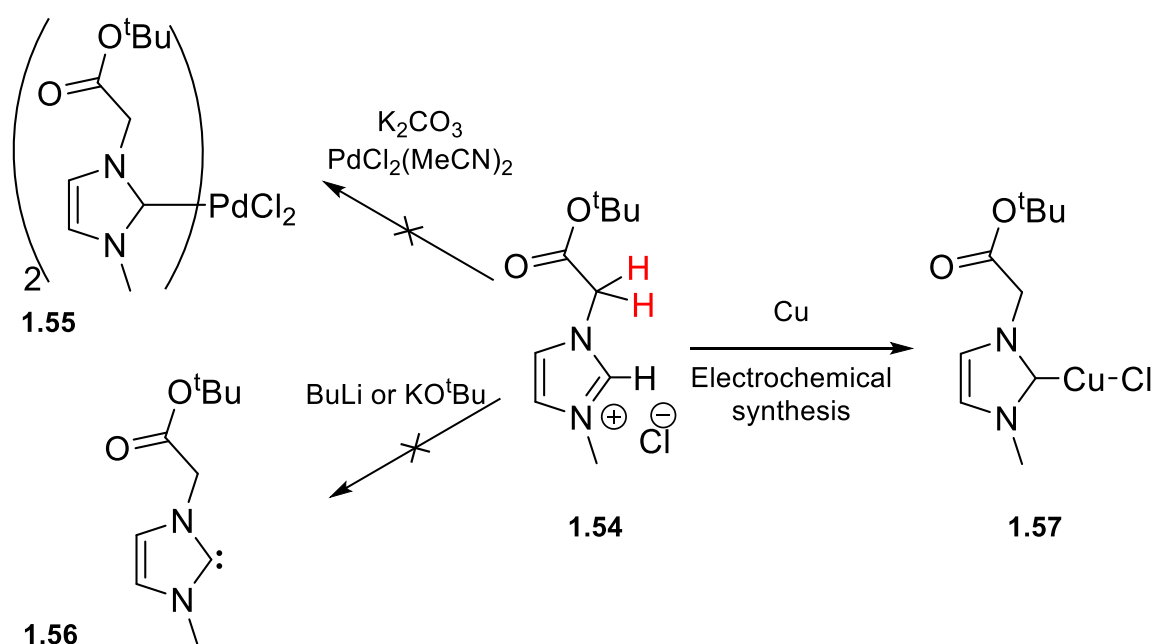
Approach **B**: Through the backbone



Scheme 1.31: Different approaches for functionalised NHCs binding to metals.

1.5.7 Chelating functionalised NHCs

Approaches to the synthesis of functionalised NHCs vary depending on the nature of the ring. Imidazoles can undergo alkylation/substitution reactions and thus a modular approach of varying the imidazole and the electrophile can generate a family of azolium salts.¹⁶⁰⁻¹⁶³ Other scaffolds, such as imidazolines and benzimidazoles, often need the functionality to be added in before the ring synthesis as these display reduced reactivity to electrophiles.¹⁶⁴ The generation of NHCs from azolium salts can be complicated by the added functionality due to potential base-sensitive groups or unforeseen reactivity. In some instances, electrochemistry has been used to generate the carbene by reduction with the loss of H₂.^{165, 166} An example of this was the generation of a Cu(I)-NHC complex **1.57** with an α -ester group (**Scheme 1.32**). This synthetic route was found to be incompatible with strong bases (BuLi) or in situ metallation with milder ones (K₂CO₃), while electrochemical synthesis was able to generate the desired complex. The protons α to the ester in **1.54** are more acidic than the C-2 H which leads to the failure for base-mediated synthesis due to competing deprotonation.



Scheme 1.32: Electrochemical alternative to deprotonation due to acidic substituents (highlighted in red).

Alternative approaches include the use of the transfer agents such as silver salts to metallate the NHC and then transfer it to the desired transition metal centre.^{131, 134, 167} The binding of the other donor group is dependent on its nature (anionic vs neutral) and the metal precursor used, with some precursors favouring different reactivity to others.

Several examples exist of Cp (or Cp-type) tethered NHC metal complexes.¹⁶⁸ Early transition-metal examples of tethered indenyl and fluorenyl complexes include Ti, V and Zr (**Figure 1.8**).^{163, 169} Complexes **1.60-1.62** were accessed from the relevant K salt of the tethered NHC ligand and the metal chloride THF adducts. Amido Ti complex **1.62** is of note due to it being in the Ti(III) oxidation state whilst the precursor was Ti(IV). An organic by-product was observed in the reaction mixture to balance the overall equation.

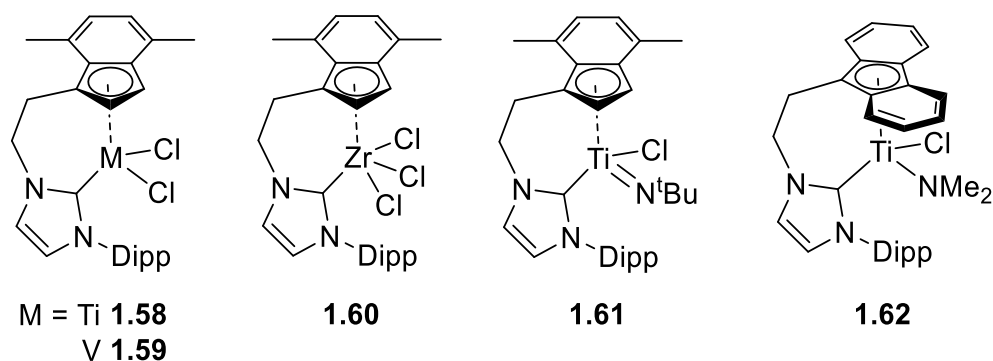
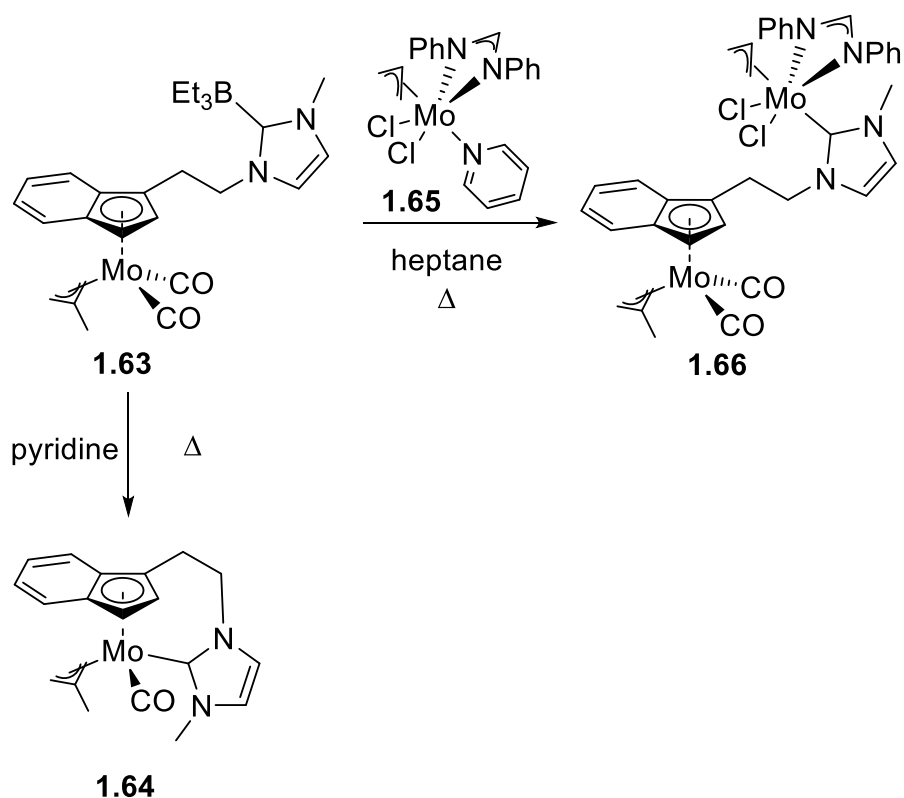


Figure 1.8: Early transition complexes with indenyl and fluorenyl functionalised NHCs.

The use of a borane-protecting group for the NHC enables the metallation of the indenyl ring with Mo forming a half-sandwich complex **1.63**, from which the chelated half-sandwich complex **1.64** can be accessed via borane deprotection (Scheme 1.33). Alternatively, treatment with an equivalent of another metal precursor **1.65** formed a bimetallic species **1.66**.



Scheme 1.33: Reactions with borane-protected NHC Mo complexes.

Nickel NHC complex **1.68** (Figure 1.9) was found to be more stable than its corresponding monodentate analogue, with **1.68** being stable in air for several days while **1.67** is only stable for a few hours.¹⁷⁰ This can be attributed to the chelate effect leading to greater stability when compared to monodentate complexes. Complex **1.68** was found to be more active in the polymerisation of styrene than **1.67** when using NaBPh₄ as an activator. Additionally, the polystyrene formed with **1.68** was more uniform in nature with a lower polydispersity index of 1.89 compared to 3.08 for the polystyrene formed by **1.67**.

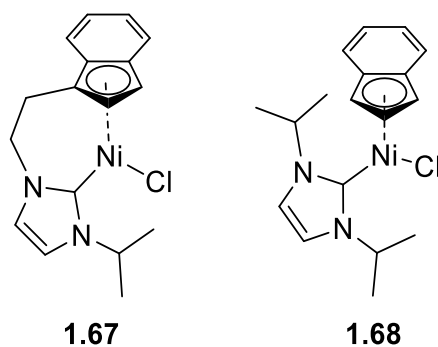
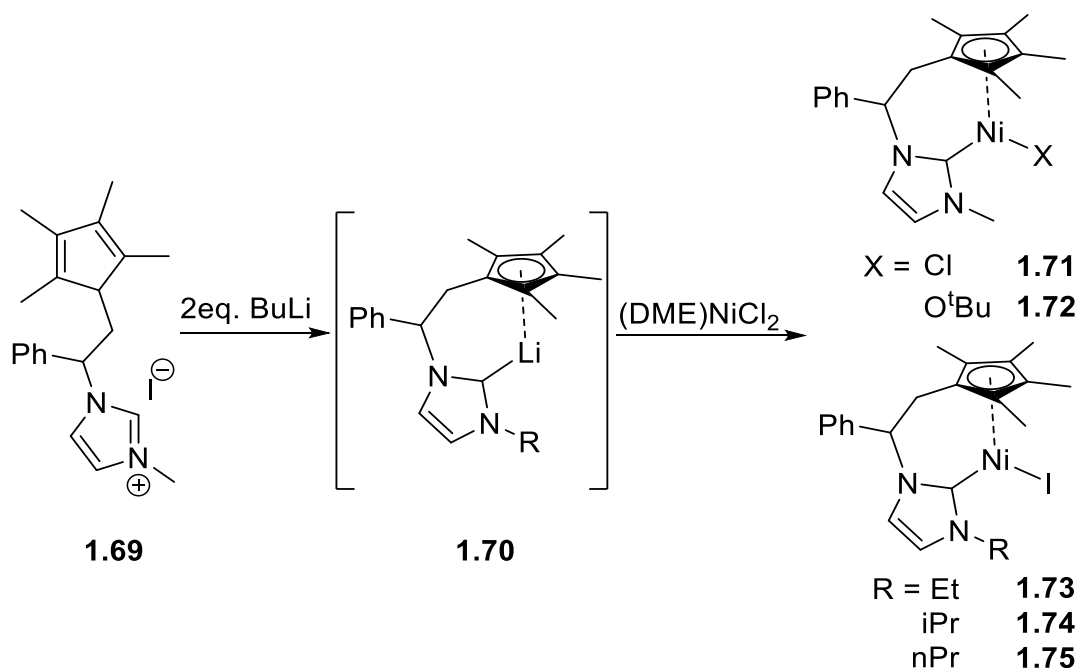


Figure 1.9: Nickel complex **1.67** with an indenyl-tethered NHC and the corresponding monodentate complex **1.68**.

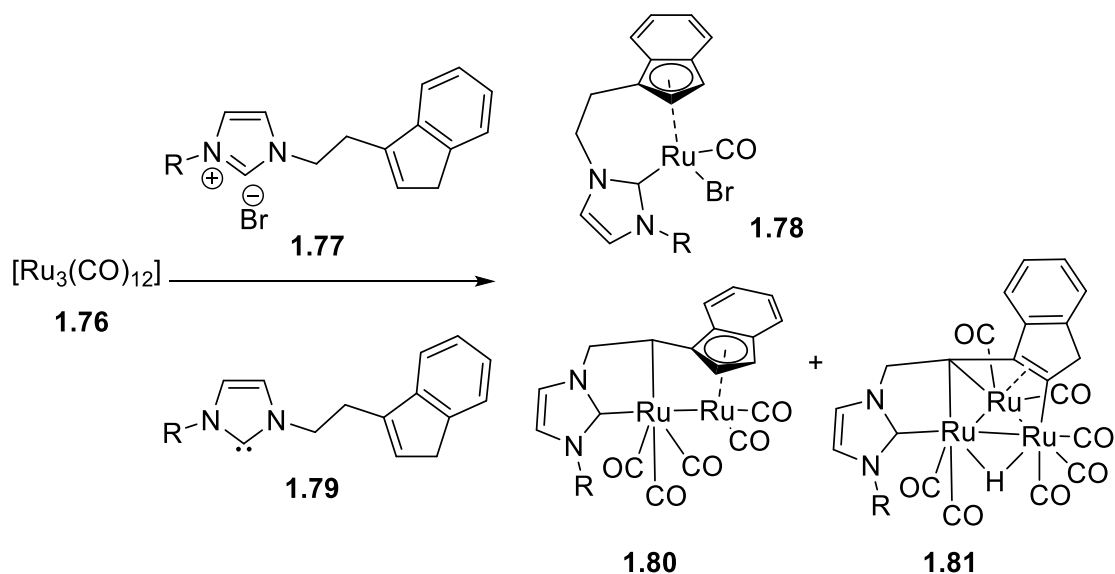
The tetramethylcyclopentadienyl-NHC Ni complex **1.71** (**Scheme 1.34**) was synthesised from (DME)NiCl₂ and the Li NHC salt **1.70** (synthesised in-situ with 2 eq. nBuLi and the relevant imidazolium salt **1.69**).^{171, 172} Reaction with KO^tBu affords the tert-butoxide complex **1.72**. Both were trialled for hydrosilylation reaction with aldehydes and ketones, with **1.72** found to be significantly more active than **1.71**. The related complexes **1.73-1.75** were tested for activity for dehydrogenative coupling of PhSH and Et₃SiH, with methyl-substituted **1.71** proving the least effective while the rest have similar activities.



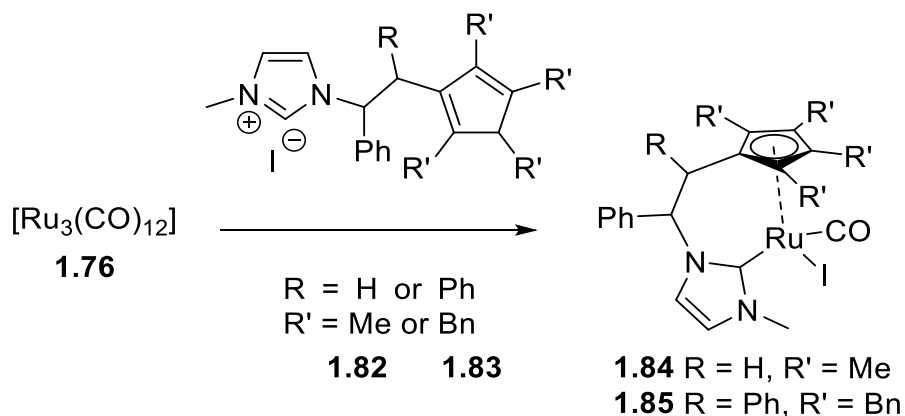
Scheme 1.34: Tetramethylcyclopentadienyl NHC Ni complexes (**1.71-1.75**).

Late transition-metal complexes with tethered Cp/C₅Me₄/indenyl/fluorenyl ligands include Ru, Rh and Ir examples. The synthesis of Ru(II) complexes typically involved metallation from the azolium salt via C-H activation to afford half-sandwich complexes

with carbonyl co-ligands (**Scheme 1.35** & **Scheme 1.36**).^{173, 174} Reactions with the neutral NHC lead to multi-metallic species **1.80** & **1.81** with a variety of coordination modes observed (**Scheme 1.35**).



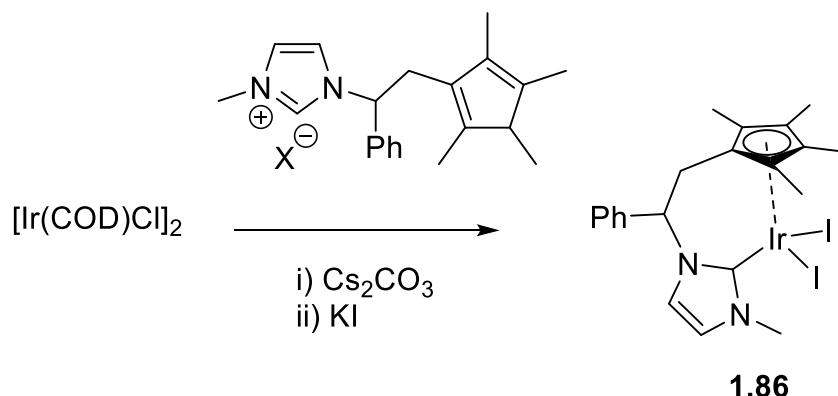
Scheme 1.35: Synthesis of indenyl-tethered NHC complexes with $Ru_3(CO)_{12}$.



Scheme 1.36: Synthesis of tetramethyl- and tetrabenzyl-cyclopentadienyl NHCs with Ru.

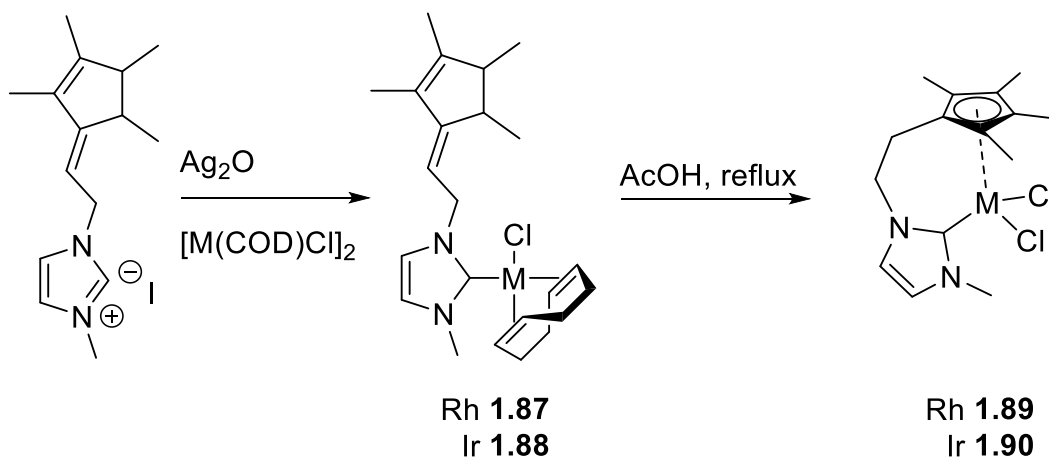
The Ru half-sandwich complexes **1.84** & **1.85** are chiral and are diastereomeric in nature due to additional stereogenic centres on the linker. These complexes have been trialled for the catalytic isomerisation of allylic alcohols, with the less sterically crowded **1.84** being quite active but the restricted **1.85** having very low activities.

Cp* Ir complex **1.86** was synthesised via deprotonation/metallation with Cs₂CO₃ and then heating with KI (**Scheme 1.37**).¹⁷⁵



Scheme 1.37: Synthesis of tetramethylcyclopentadienyl-NHC Ir complex **1.86**.

Complexes **1.87** and **1.88** were synthesised via formation of a silver transfer agent and transmetallation to the metal(I) cyclooctadiene chloride dimer (**Scheme 1.38**), which was followed by acetate-assisted addition of the Cp* ring and oxidation to M(III) to form complexes **1.89** and **1.90**.

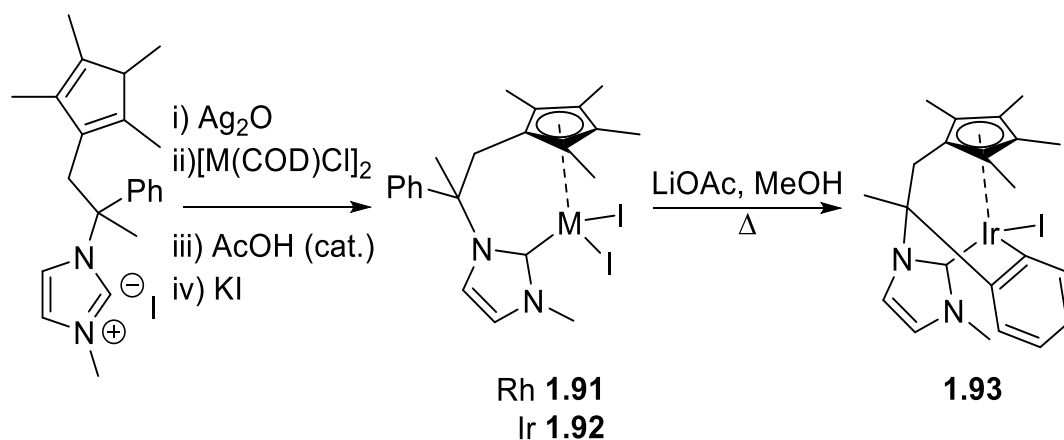


Scheme 1.38: Synthesis of Rh(III) and Ir(III) complexes **1.89** and **1.90** with a tetramethylcyclopentadienyl-NHC ligand.

Ir complexes **1.86** and **1.90** were tested for hydrogen borrowing reactions.^{176, 177} Both were found to be very active for transfer hydrogenation, β -alkylation of secondary alcohols and amination of primary alcohols.^{175, 178} The results were comparable to other “IrCp*(NHC)” type catalysts and were better than those observed for [IrCp*(Cl)₂].^{179, 180}

Cp*-NHC di-iodide complexes **1.91** and **1.92** were similarly prepared with the addition of KI to ensure Cl was exchanged for I (**Scheme 1.39**).¹⁷⁸ It was observed that Ir complex

1.92 would cyclometallate upon heating to reflux with LiOAc giving complex **1.93**. The Cp tethered complexes **1.94** and **1.95** (**Figure 1.10**) were synthesised in the analogous manner.



Scheme 1.39: Synthesis of Rh and Ir iodide complexes and subsequent cyclometalated Ir species.

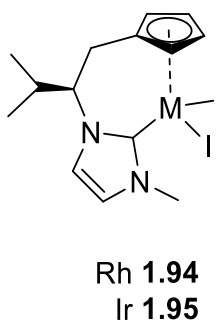
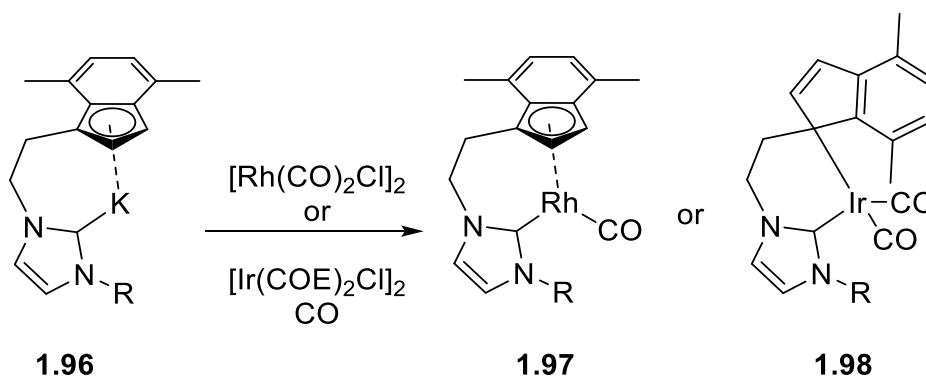


Figure 1.10: Chiral Cp-NHC complexes of Rh and Ir.

Reaction of K[NHC] salt **1.96** with the Rh carbonyl chloride dimer gave rise to the tethered half sandwich complex **1.97** (**Scheme 1.40**).¹⁸¹ However, reaction with $[\text{Ir}(\text{COE})_2\text{Cl}]_2$ under CO (isolated $[\text{Ir}(\text{CO})_2\text{Cl}]_2$ is not known)¹⁸² did not afford the analogous complex but gave rise to **1.98**, a 16e square planar complex with indenyl in a η^1 coordination mode. This is interesting as it suggests a notable difference between Rh and Ir when in the +1 oxidation state as to the preference for half-sandwich vs square planar complexes.



Scheme 1.40: Synthesis of Indenyl-NHC half sandwich complexes with Rh and Ir.

Rh complex **1.97** was tested for activity in hydroformylation of 1-octene and methanol carbonylation. For the former reaction, competing alkene isomerisation was observed with isomers also hydroformylated, giving a complex mixture. Carbonylation activity was more promising, with **1.97** being comparable to the electron rich $[\text{Rh}(\text{C}_5\text{Me}_4\text{-PEt}_2)(\text{CO})]$ complex,^{183, 184} but less active than $[\text{RhI}_2(\text{CO})_2]^-$, the standard Monsanto catalyst.

1.6 Hypothesis and project aims

The use of NHC ligands for undirected C-H activation is relatively unexplored compared to their use in directed C-H activation catalysis. This also contrasts with the extensive use of phosphine ligands in C-H activation catalysis. Half-sandwich complexes of Rh form the basis of the majority of catalysts used for alkane borylation, while indenyl or fluorenyl ligands have barely been explored in undirected C-H borylation catalysis, in stark contrast to the ubiquitous use of Cp and Cp* ligands. In addition, complexes with tethered NHCs have been rarely investigated in C-H activation-based catalysis, but have been shown to offer different properties to their monodentate analogues. Thus, individually, there is much to explore as well as the nexus of these ideas. The hypothesis behind this research is that an NHC-containing half-sandwich complex utilising the enhanced reactivity of indenyl is of interest to explore the differences that such a system presents over previous systems for C-H activation. The strong σ -donating properties of NHCs should give more electron rich, and potentially more reactive metal centres, and replacing Cp/Cp* with indenyl should also allow for different and potentially lower energy reactivity of half-sandwich complexes. In addition, tethering the NHC donor to the Cp/indenyl/fluorenyl donor will change the properties of the system, perhaps through

constraining the geometry and changing the energies of the metal orbitals, which can be contrasted with monodentate analogues. All of these complexes were then to be tested for C-H activation and C-H borylation.

Thus, the aims for this project were as follows:

- To synthesise a range of indenyl rhodium complexes featuring an NHC and a labile coligand to allow the identification of complexes capable of C-H activation.
- To test the reactivity of these complexes under photolysis conditions and with common reagents to enable comparisons with literature complexes that feature conventional Cp/Cp*/phosphine ligands such as those synthesised by Bergman and Hartwig.
- To test the reactivity of these complexes towards the borylation of arenes and alkanes, and to identify any catalytic systems with comparison to literature complexes particularly complexes **1.17** and **1.28.**,
- To synthesise tethered indenyl/fluorenyl NHC ligands and their complexes with Rh in order to explore the effects of tethering an NHC donor to the Cp-type donor.

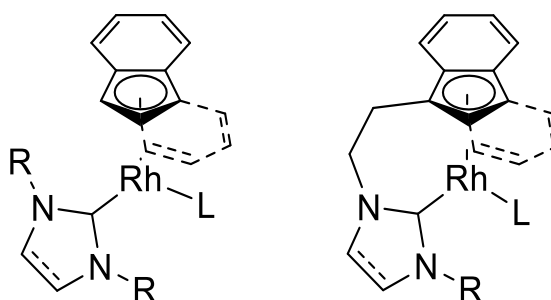
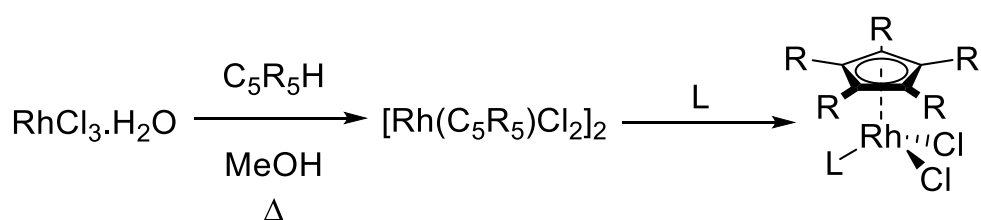


Figure 1.11: General structures for the target complexes; R = Dipp, L = COE, C₂H₄, CO.

Chapter 2: Indenylrhodium complexes with monodentate NHC ligands

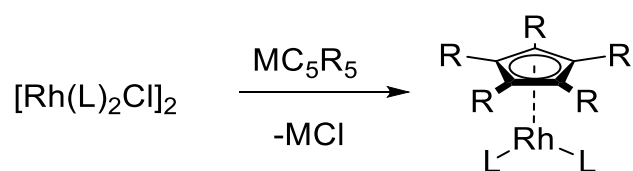
2.1 Introduction

Half-sandwich rhodium complexes are well known for both Rh(I) and Rh(III). The most common ligands are Cp and Cp*, with $[\{\text{Rh}(\text{Cp}^*)\text{Cl}_2\}_2]$ being an important precursor due to its relative ease of synthesis and stability,¹⁸⁵ and its use as a precatalyst for a variety of catalytic transformations including the synthesis of heterocycles¹⁸⁶⁻¹⁹¹ and directing-group-mediated C-H activation.¹⁹² Addition of the appropriate ligands can break up these dimers (**Scheme 2.1**), and the chloride ligands can be exchanged to other ligands such as hydrides by means of reaction with LiHBEt_3 or $\text{NaOH}/i\text{PrOH}$, or removed with AgPF_6 in MeCN to form $[\text{Rh}(\text{Cp}^*)(\text{MeCN})_3][\text{PF}_6]_2$, which is a source of dicationic $\text{Cp}^*\text{Rh}(\text{III})$.



Scheme 2.1: Typical synthesis of Rh(III) half-sandwich complexes with Cp (R = H) and Cp* (R = Me).

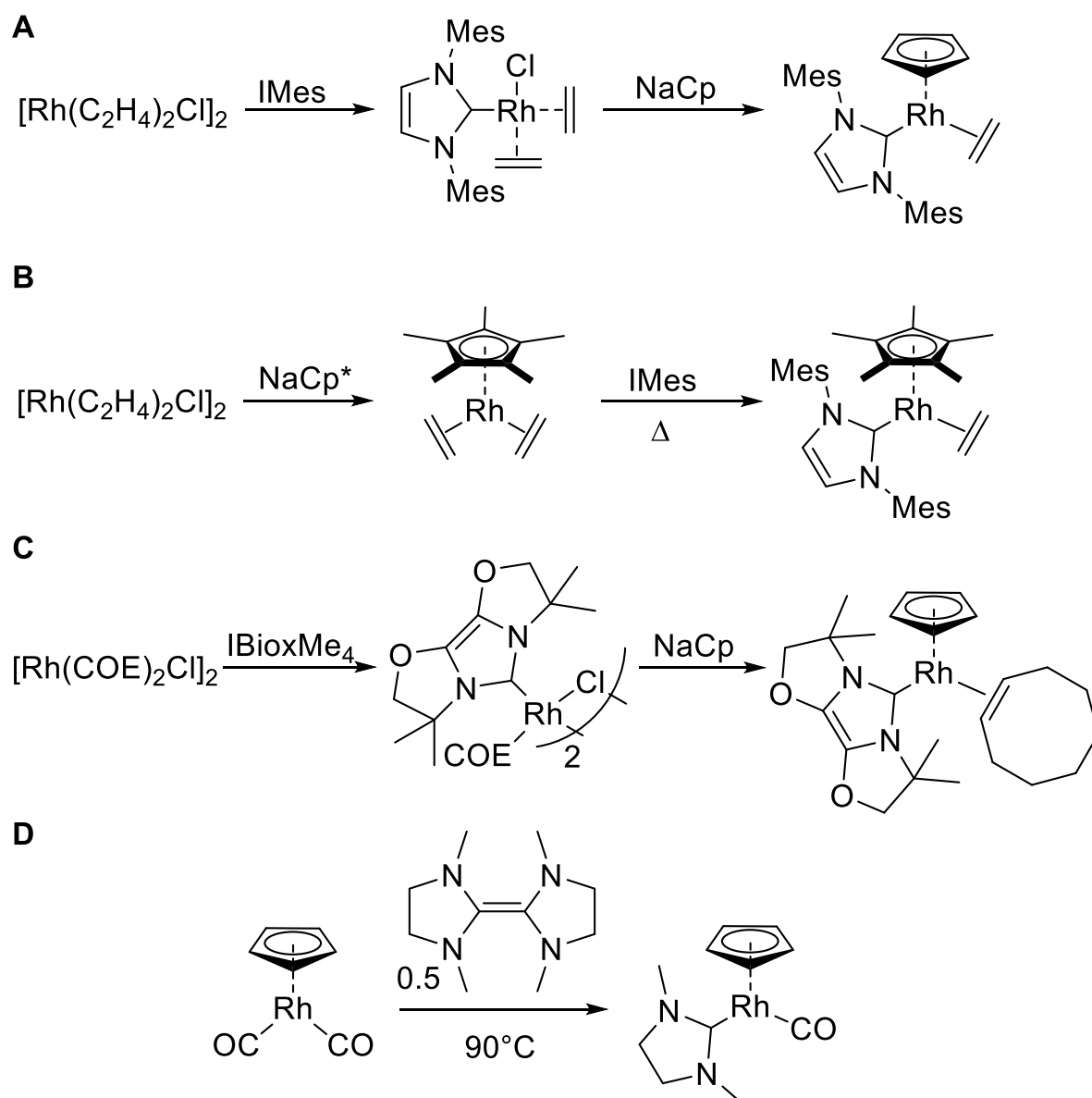
Rh(I) complexes with cyclopentadienyl ligands can either be synthesised from reduction of Rh(III) complexes or from the addition of MCp (M = alkali metal, Tl) to a Rh(I) chloride dimer which generates the half-sandwich Rh(I) complex with two L-type ligands (**Scheme 2.2**).^{40, 193-195} With the exception of where $(\text{L})_2 = \text{cyclooctadiene}$,¹⁹⁶ the Rh(I) alkene chloride dimers are generally less stable than $[\{\text{Rh}(\text{C}_5\text{R}_5)\text{Cl}_2\}_2]$. The cyclooctene dimer needs to be stored cold and under N_2 ,¹⁹⁷ and the ethene and CO dimers need to be kept cold or under an atmosphere of ethene / CO for long-term storage.¹⁹⁸⁻²⁰⁰ These considerations may explain why $[\{\text{Rh}(\text{Cp}^*)\text{Cl}_2\}_2]$ is widely used.



Scheme 2.2: Synthesis of Rh(I) half-sandwich complexes.

Half-sandwich complexes of Rh(I) that feature the coordination of an NHC have received minimal attention in the literature, with only four complexes having been reported (**Scheme 2.3**).^{127, 201} Two complexes feature IMes as the NHC and ethene as the other ligand (**Scheme 2.3, A & B**). It was found that the Cp complex required a different synthetic route to the Cp* complex as the temperature required to add the NHC to $[\text{Rh}(\text{Cp})(\text{C}_2\text{H}_4)_2]$ was above the decomposition temperature and led to very poor yields. Thus, the NHC was added to $[\text{Rh}(\text{C}_2\text{H}_4)_2\text{Cl}]_2$ to generate a square-planar complex, to which the addition of NaCp generated the Rh NHC half-sandwich complex.

The synthesis of an IBioxMe₄-substituted Cp-Rh half-sandwich complex proceeded via the addition of the NHC to $[\text{Rh}(\text{COE})_2\text{Cl}]_2$, from which COE is lost and a mono-NHC, mono-alkene Rh chloride dimer is formed (**Scheme 2.3, C**).²⁰² Reaction with NaCp forms the Cp half-sandwich complex.

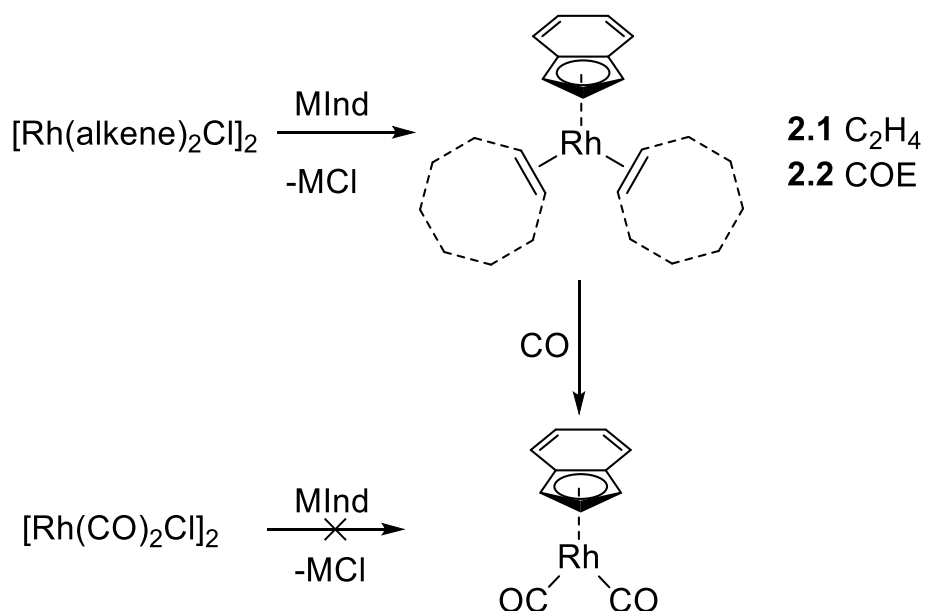


Scheme 2.3: Synthesis of Cp and Cp* rhodium complexes featuring an NHC ligand.

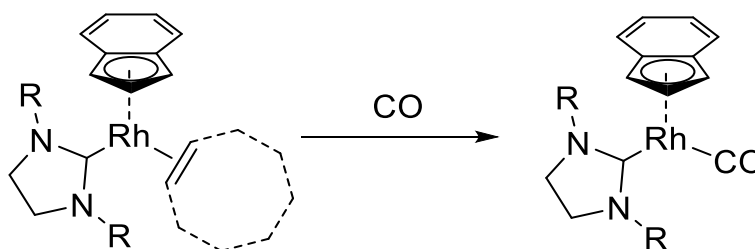
The synthesis of a SIME [1,3-bis(methyl)imidazolinylidene] complex was achieved by reaction of $[\text{Rh}(\text{Cp})(\text{CO})_2]$ with the appropriate Wanzlick-type carbene precursor, occurring with loss of CO (**Scheme 2.3, D**).¹²⁷ This is the only saturated-NHC-based Rh half-sandwich complex known in the literature, and was not synthesised from a free carbene, indicating a gap in the literature as to the behaviour of saturated NHCs in substitution reactions of half-sandwich complexes.

The analogous indenyl and fluorenyl Rh(III) dimers $[\text{Rh}(\text{R})\text{Cl}_2]_2$ (R = indenyl, fluorenyl) are not known, although substituted indenyl dimers have been synthesised and used in C-H functionalisation catalysis.^{203, 204} Indenylrhodium bis(alkene) complexes can be synthesised by the addition of MInd (M = alkali metal, Ind = indenyl) to $[\text{Rh}(\text{alkene})_2\text{Cl}]_2$

(**Scheme 2.4**).^{205, 206} The addition of MInd to $[\text{Rh}(\text{CO})_2\text{Cl}]_2$ does not proceed cleanly with di- and tri-rhodium species also formed.²⁰⁷ However, the addition of CO to $[\text{Rh}(\text{Ind})(\text{alkene})_2]$ proceeds well with the formation of $[\text{Rh}(\text{Ind})(\text{CO})_2]$. This suggests that it may be more convenient to synthesise carbonyl complexes from the mono alkene complexes (**Scheme 2.5**), rather than attempt addition of the NHC to $[\text{Rh}(\text{Ind})(\text{CO})_2]$. The loss of CO may be less favoured than loss of an alkene due to it being a stronger π -acceptor, and could affect the preference for the Rh(I) geometry between square planar or half-sandwich piano stool, which has been observed with Ir(I) where indenyl was observed in η^1 -coordination.^{181, 208}

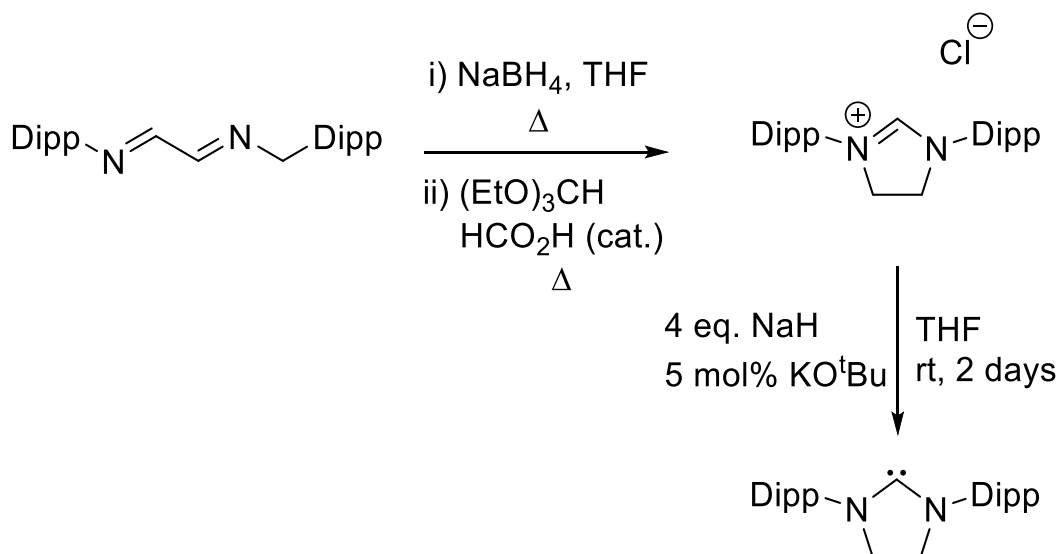


Scheme 2.4: Synthesis of indenylrhodium(I) complexes (M = Li, Na, K).



Scheme 2.5: Possible synthesis of indenylrhodium carbonyl complexes via CO substitution of an alkene complex.

The NHC used in the studies described below was 1,3-bis(2,6-diisopropylphenyl)imidazolin-2-ylidene (SIPr). SIPr was chosen due to the focus on saturated carbenes as part of the work on tethered systems (Chapter 4), as well as diisopropylphenyl substituents. SIPr can be synthesised as the free carbene via deprotonation of the parent imidazolium chloride salt (**Scheme 2.6**), which was formed via reduction and orthoformate cyclisation from the relevant bis-imine.¹⁰⁶

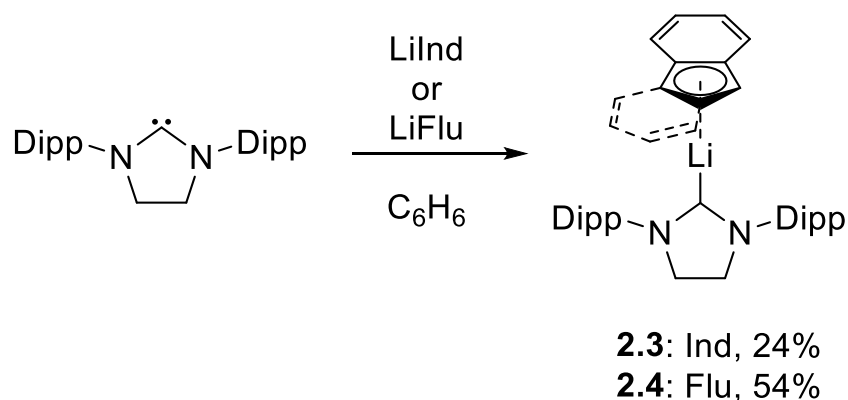


Scheme 2.6: Synthesis of SIPr (Dipp = 2,6-diisopropylphenyl).

2.2 Synthesis of monodentate complexes

2.2.1 Synthesis of lithium NHC complexes

As a test of the coordination chemistry of SIPr, and as a comparison to results achieved with tethered ligands (Chapter 4), lithium indenide and fluorenyl salts (LiInd, LiFlu) were added to SIPr (**Scheme 2.7**). After dissolution upon heating, [Li(Ind)(SIPr)] (**2.3**) and [Li(Flu)(SIPr)] (**2.4**) crystallised upon cooling, with single crystals suitable for X-ray diffraction being formed from benzene. ^7Li NMR spectroscopy showed resonances at -9.75 ppm and -8.95 ppm respectively for **2.3** and **2.4**. Symmetrical η^5 binding of lithium cations to fluorenyl and indenyl has previously been shown to give ^7Li chemical shifts between -7 and -8 ppm,²⁰⁹ and asymmetrical binding induced by a diamino-tethered fluorenyl was shown to increase the chemical shift to -5.7 ppm.²¹⁰ For unsaturated-NHC adducts of the Cp derivative $\text{C}_5\text{H}_2(\text{SiMe}_3)_3$, ^7Li NMR chemical shifts of $\delta = -7.78, -7.63$ and -9.01 ppm (NHC substituents = *tert*-butyl, 1-adamantyl and Mes, respectively) were observed, which is at lower chemical shift than for uncoordinated LiCp (-6.9 ppm).^{209, 211} Thus, the ^7Li chemical shifts for **2.3** and **2.4** are similar to the expected values for these type of complexes, although information about the exact coordination geometry is limited by the low sensitivity of the chemical shift differences to variation in donor properties. $^{13}\text{C}\{^1\text{H}\}$ NMR spectroscopy showed no clear resonances for the carbenic carbene atom in the direct observation experiment or by ^1H - ^{13}C HMBC experiments. This is likely to be due to the coordinated quadrupolar Li cations (Li has two quadrupolar isotopes), and thus the lack of downfield resonances point towards coordination of the NHC to Li.



Scheme 2.7: Synthesis of lithium NHC complexes with indenyl and fluorenyl ligands.

From the X-ray determined structure for **2.3** (**Figure 2.1**), there is a slight distortion in the η^5 coordination with the Li-C4/C9 distances being longer than to C1/C3 [2.265(2) and 2.272(2) Å compared to 2.218(2) and 2.204(2) Å respectively]. This is in-line with other indenyl complexes as benzannulation reduces the availability of p-orbitals on the C4/9 atoms to interact with the metal, thus driving a distortion towards η^3 coordination. The Li-NHC distance of 2.103(2) Å is similar although slightly shorter than that observed for other Li-NHC complexes.^{211, 212}

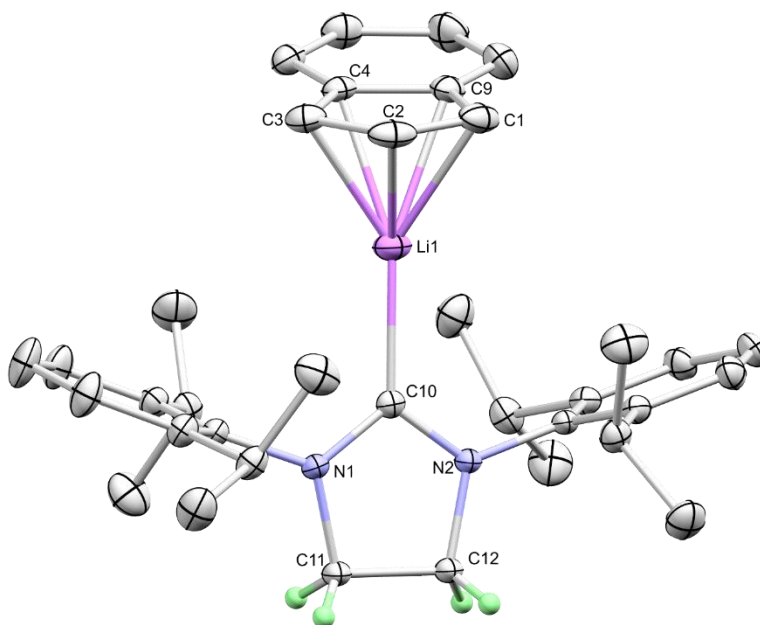


Figure 2.1: X-ray determined structure for Li NHC complex **2.3**. All H atoms, except for H11A/B and H12A/B, as well as a benzene solvate molecule have been omitted for clarity.

The X-ray determined structure for **2.4** displayed a disordered fluorenyl group over three positions (only one position is shown in Figure 2.2). This presumably arises due to a reduced energetic preference for the orientation of the fluorenyl ring compared to indenyl. This precludes further discussion of the Li-Flu bond distances. The NHC-Li distance is 2.102(3) Å, which is the same within error as the corresponding distance in **2.3**.

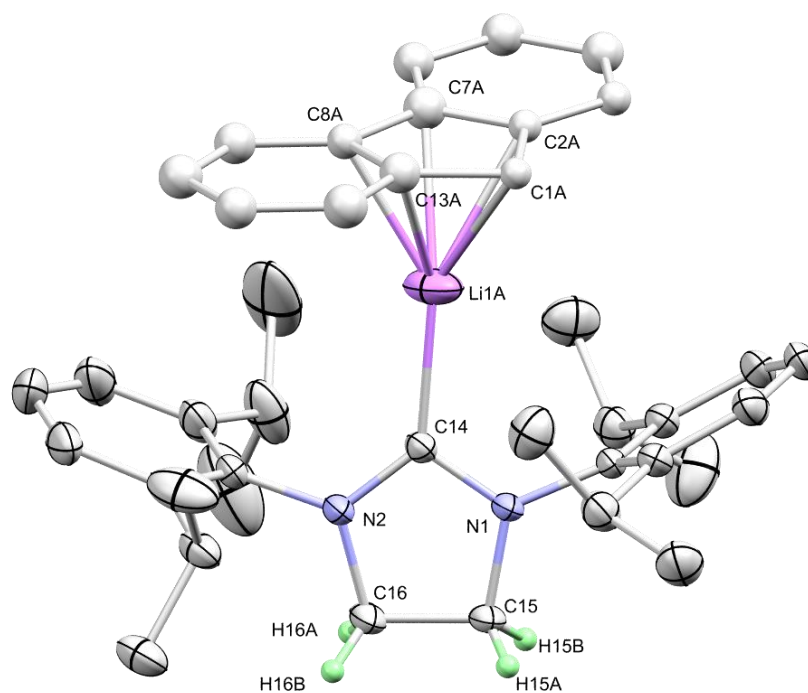
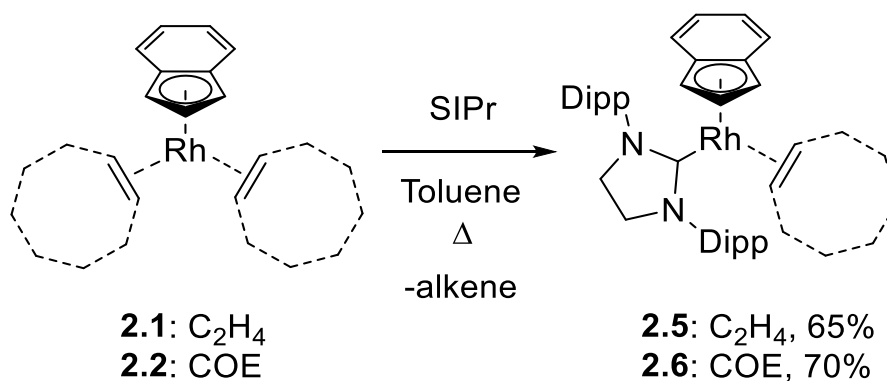


Figure 2.2: X-ray determined structure for Li NHC complex **2.4**. All H atoms, except for H16A/B and H15A/B, as well as a benzene solvate molecule have been omitted for clarity. The fluorenyl ring was found to be disordered over three positions and thus was only able to be refined isotropically, with only one position shown for clarity.

2.2.2 Synthesis of rhodium SIPr complexes

The indenylrhodium(I) bis(alkene) complexes $[\text{Rh}(\text{Ind})(\text{C}_2\text{H}_4)_2]$ (**2.1**) and $[\text{Rh}(\text{Ind})(\text{COE})_2]$ (**2.2**) were synthesised according to literature procedures by the reaction of LiInd with the respective $[\text{Rh}(\mu\text{-Cl})(\text{alkene})_2]_2$ dimers.^{206, 213} Reaction with SIPr was found to require heating at 80°C to proceed in a timely manner to afford $[\text{Rh}(\text{Ind})(\text{SIPr})(\text{C}_2\text{H}_4)]$ (**2.5**) and $[\text{Rh}(\text{Ind})(\text{SIPr})(\text{COE})]$ (**2.6**, **Scheme 2.8**). Both were found to be easily crystallised from benzene or toluene, but are insoluble in alkane solvents. $^{13}\text{C}\{^1\text{H}\}$ NMR spectroscopic analysis showed resonances at δ 215.4 and 213.9 ppm for **2.5** and **2.6** respectively for the carbenic carbon with $^1J_{\text{Rh-C}}$ coupling of 68.6 and 70.1 Hz observed. The bound alkene C=C carbons are observed at 35.6 ppm and 61.5 ppm respectively for **2.5** and **2.6**, with $^1J_{\text{Rh-C}}$ values of 15.1 and 15.3 Hz. The difference in chemical shift may be explained due to differences in the alkenes, however, the very similar J -couplings suggest that the degree of interaction between the Rh and the alkene is very similar in **2.5** and **2.6**. The alkene resonances for **2.5** and **2.6** are shifted upfield in their ^1H NMR spectra upon coordination, with coordinated ethene at 2.26 ppm (5.25

ppm in free ethene) and the coordinated cyclooctene at 2.59 ppm (5.65 ppm in free cyclooctene). The shift in these resonances arises due to coordination to the electron rich Rh(I). The metal centre donates electron density into the C=C π^* orbital thus making the alkene more electron rich which leads to the upfield shift.



Scheme 2.8: Reactions between indenylrhodium bis(alkene) complexes and SIPr.

Single crystal X-ray diffraction studies were carried on complexes **2.5** (Figure 2.3) and **2.6** (Figure 2.4). Both show binding of the indenyl, NHC and alkene to the Rh centre in a ‘two-legged’ piano stool geometry.

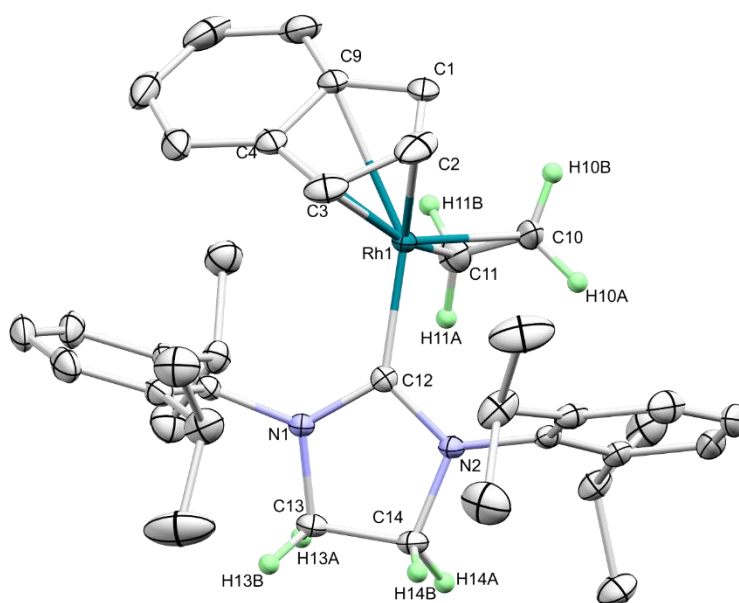


Figure 2.3: X-ray determined molecular structure of complex **2.5** (thermal ellipsoids at 50%). All H atoms except for H10A/B, H11A/B, H13A/B and H14A/B have been omitted for clarity.

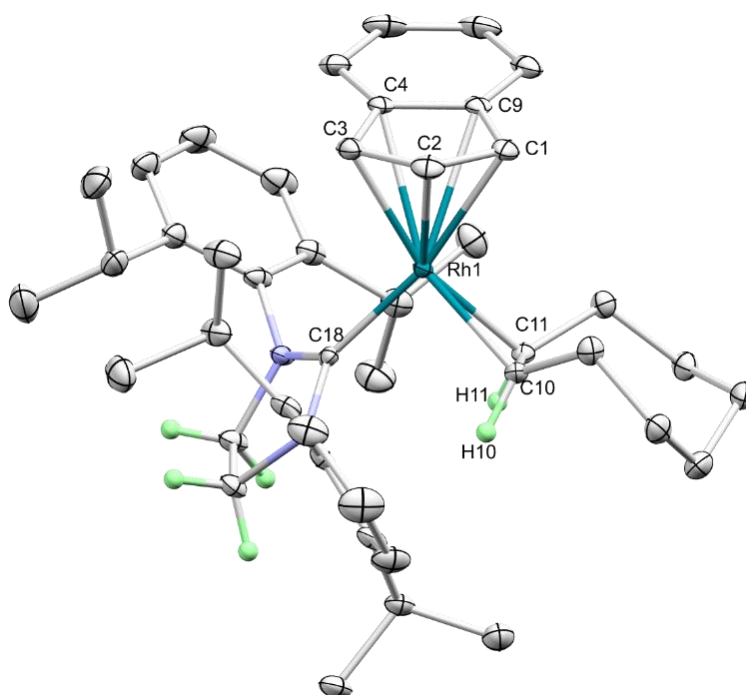
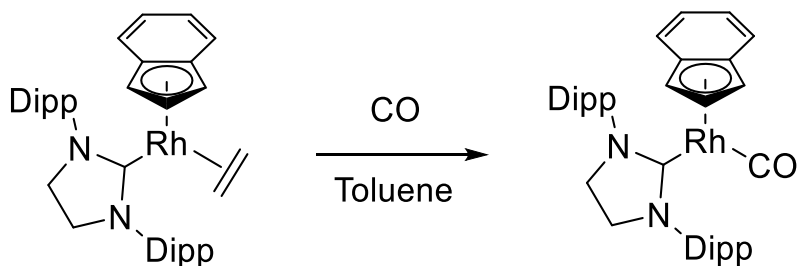


Figure 2.4: X-ray determined structure of complex **2.6** (thermal ellipsoids at 50%). All H atoms except for H10, H11, H19A/B and H20A/B have been omitted for clarity.

The rhodium-NHC bond distance is the same within error for **2.5** and **2.6** [1.989(1) and 1.988(2) Å respectively]. This indicates that the difference in alkene has minimal effect on the NHC bonding interaction. The Rh-C_{alkene} distances are equivalent in **2.5** [2.120(1) and 2.120(2) Å], while there is a slight distortion in the bonding in **2.6** with Rh-C(10) = 2.116(2) Å and Rh-C(11) = 2.140(2) Å. The C=C bond distance in **2.5** is 1.399(2) Å, which is longer than the distance for free ethene of 1.33 Å. In **2.6**, the C=C bond distance is 1.409(2) Å, which is elongated compared to free COE C=C distance (computational determined as 1.331 Å; level of theory used: B3LYP/cc-pVTZ).²¹⁴ This is to be expected due to π -back-bonding from the rhodium into the C=C π^* antibonding orbital. The C=C distance in **2.5** is shorter than the C=C distance found in [Rh(Cp*)(IMes)(C₂H₄)] of 1.416(6) Å,²⁰¹ which may be due to the electron rich Cp* ligand leading to a higher degree of back-donation compared to indenyl, although the NHC is also different so direct comparison is not possible.

A solution of **2.5** in toluene was treated with CO and clean conversion to [Rh(Ind)(SIPr)(CO)] (**2.7**) was observed (**Scheme 2.9**). The ¹³C{¹H} NMR spectroscopic carbene resonance was observed at 214.8 ppm with $J_{\text{Rh-C}} = 68.8$ Hz; the resonance at 195.1 ppm was assigned to Rh-CO with a 93.3 Hz coupling to Rh. These values are similar to examples in the literature.¹²⁷ From IR spectroscopy, a CO stretching band was observed at 1944 cm⁻¹, which is slightly higher than similar complexes in the literature, 1920 cm⁻¹ for [Rh(Cp)(SIME)(CO)] and 1927 cm⁻¹ for complex **1.97**.^{127, 181} Generally, lower ν_{CO} values indicate greater electron density on the metal centre. The higher CO stretching frequency in **2.7** may be due to the different carbene ligands in these complexes, but could also be related to the differing aromatic ligands (indenyl, Cp, Cp*) and thus cannot be taken as indicative of the donor properties of SIPr.



Scheme 2.9: Reaction of **2.5** with CO to give **2.7**.

Crystals of **2.7** suitable for single crystal X-ray diffraction were grown from a saturated C₆D₆ solution. The Rh-NHC distance in **2.7** is 2.010(2) Å, which is slightly longer than that in **2.5** and **2.6**. It is comparable to the value for [Rh(Cp)(SIME)(CO)] of 1.994(7) Å,¹²⁷ although due to the larger ESD, it is not possible to distinguish between the two values. The Rh-CO distance is 1.828(2) Å, which is longer than that for [Rh(Cp)(SIME₂)(CO)] of 1.795(9) Å, suggesting that the degree of backbonding into the CO antibonding orbital is less in **2.7**. This is because as backdonation increases, the Rh-C bond becomes stronger and thus shorter, while the C-O becomes weaker and therefore longer. Unfortunately, the large error on the C-O distance for [Rh(Cp)(SIME₂)(CO)] negates meaningful comparison [1.16(1) vs 1.154(2) Å].

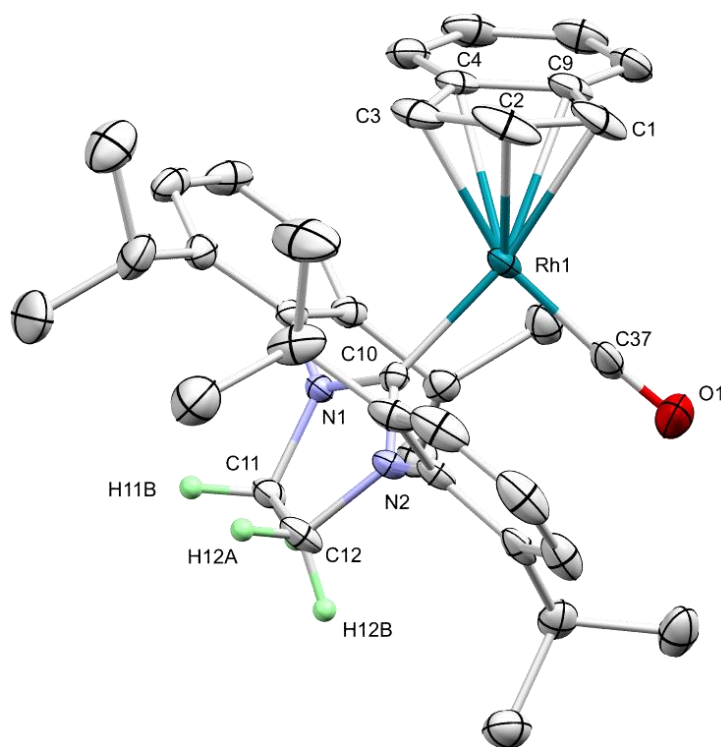
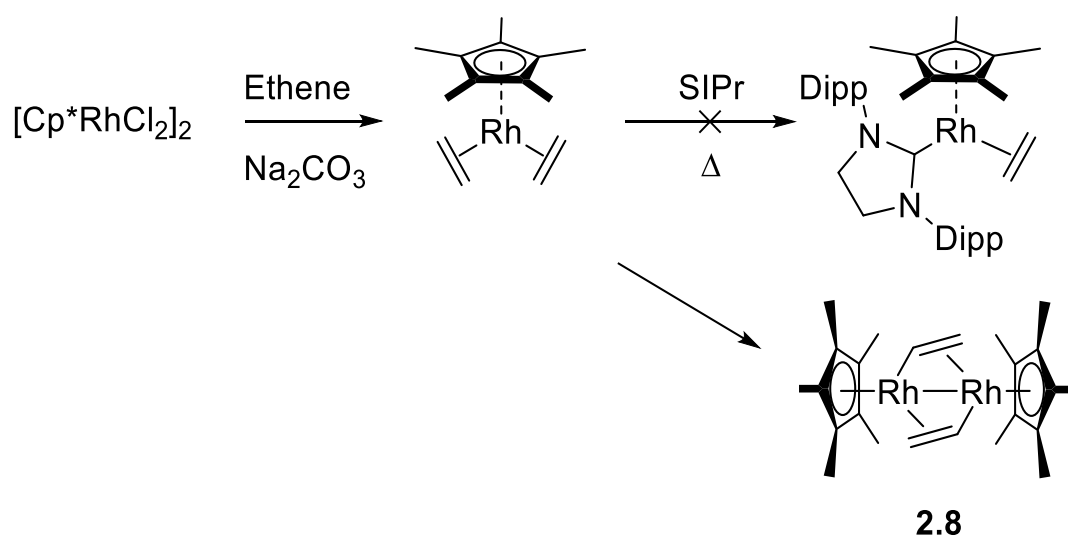


Figure 2.5: X-ray determined structure of complex **2.7** (thermal ellipsoids at 50%). All H atoms except for H11A/B and H12A/B have been omitted for clarity.

In order to enable comparisons between indenylrhodium and pentamethylcyclopentadienylrhodium alkene complexes, [Rh(Cp*)(C₂H₄)₂] was synthesised according to the literature procedure by the reductive ethenylation of [Rh(Cp*)Cl₂]₂.²¹⁵ Previous studies noted the difficulty of coordinating IMes to [Rh(Cp*)(C₂H₄)₂], with prolonged heating required.²⁰¹ Heating SIPr with

$[\text{Rh}(\text{Cp}^*)(\text{C}_2\text{H}_4)_2]$ in toluene at 110°C showed partial consumption of both starting materials by ^1H NMR spectroscopy, however, the resonances associated with the NHC became indistinct. From the concentrated reaction mixture, in addition to crystals of $[\text{Rh}(\text{Cp}^*)(\text{C}_2\text{H}_4)_2]$, crystals of the vinyl-bridged dimer **2.8** were obtained and characterised by X-ray diffraction (**Figure 2.6**). C-H activation of ethene has occurred with subsequent loss of two H atoms, possibly either as H_2 or reduction of the NHC to an imidazoline, however, the exact mechanism is yet to be determined. The resultant ethenyl groups are η^2 L-type ligands to one Rh and η^1 X-type ligands to the other Rh centre. From the X-ray determined structure, it can be observed that the methyl groups on the Cp^* rings are in a staggered configuration (**Figure 2.7**).



Scheme 2.10: Attempted reaction of SIPr with $[\text{Rh}(\text{Cp}^*)(\text{C}_2\text{H}_4)_2]$ to yield a $\text{Cp}^*\text{Rh}(\text{NHC})$ complex.

The Rh-Rh distance in **2.8** is $2.6947(5)$ Å, which is consistent with a Rh-Rh bond as $[\text{Rh}(\text{Cp}^*)\text{Cl}]_2$ has a Rh-Rh distance of $2.617(1)$ or $2.628(1)$ Å (respectively, the staggered and the eclipsed form).^{216, 217} Generally, Rh-Rh distances have a high degree of variation depending on the attached ligands.^{218, 219} The alkene C=C distance is $1.412(4)$ Å which is elongated compared to the C=C distance in **2.6** but shorter than the analogous distance in $[\text{Rh}_2(\text{C}_2\text{H}_3)\{\text{MeC}=\text{CMe}(\text{H})\}(\text{MeInd})_2]$.²²⁰

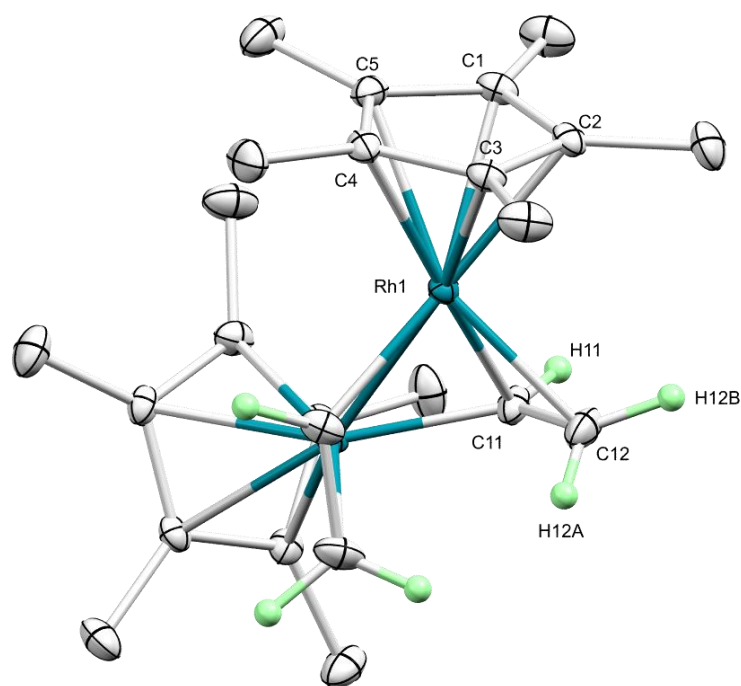


Figure 2.6: X-ray determined structure of Cp* Rh ethene dimer **2.8** (thermal ellipsoids at 50%). All H-atoms, except for H11 and H12A/B, have been omitted for clarity.

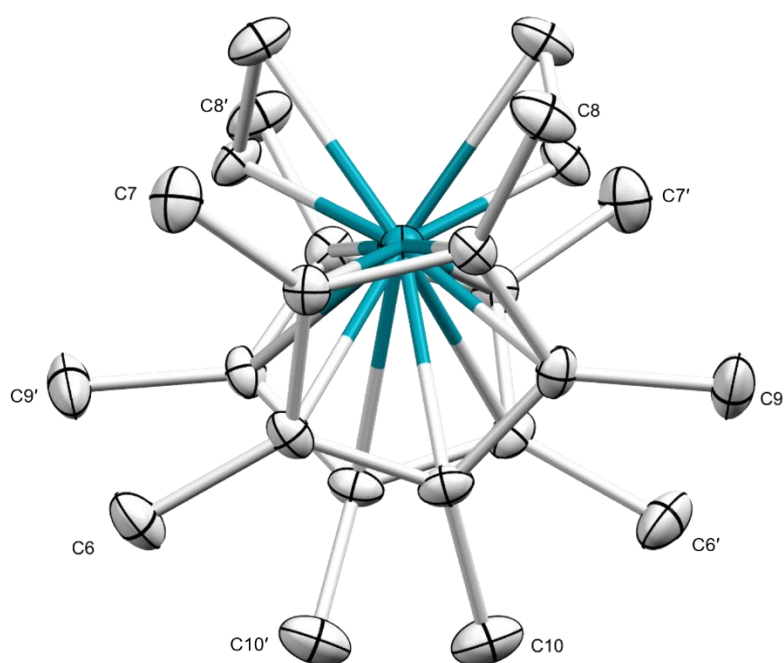
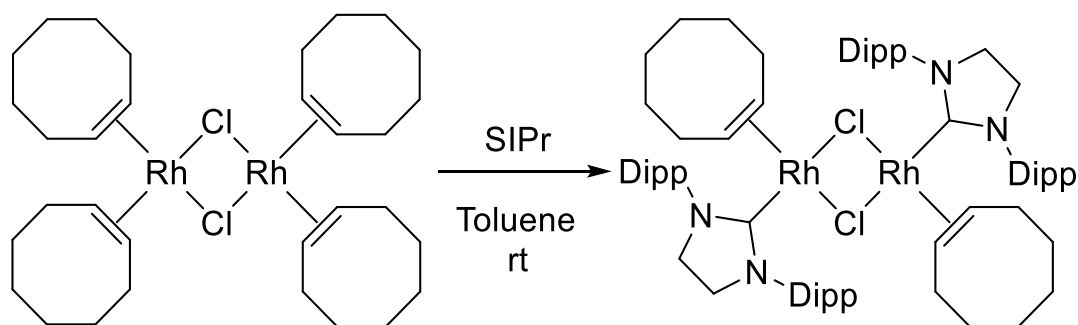


Figure 2.7: View along the Rh-Rh bond in **2.8** showing the staggered conformation of the Cp* methyl groups.

The formation of **2.8** indicates the difficulty in adding bulky NHCs to Cp*Rh fragments.²⁰¹ This is in contrast to indenyl systems where substitution occurs at a much reduced reaction temperature. This is consistent with the so called ‘indenyl effect’, with the variable coordination of the indenyl ring inducing a higher reactivity, allowing for increased rates of substitution such as the type attempted here.^{81, 82, 84, 85, 221}

The reaction of two equivalents of SIPr with $[\text{Rh}(\text{COE})_2\text{Cl}]_2$ led to the elimination of two COE ligands affording the Rh chloride dimer **2.9** (**Scheme 2.11**). This contrasts with the observed reactivity for $[\text{Rh}(\text{C}_2\text{H}_4)_2\text{Cl}]_2$ with IMes where the monomeric bis alkene product was formed. However, this matches the reactivity previously observed for IPr and IMes with $[\text{Rh}(\text{COE})_2\text{Cl}]_2$,²²² as well as with I'Bu and IBioxMe₄.^{202, 223} This may be due to the larger size of both SIPr and COE disavouring the formation of the mononuclear bis(alkene) complex due to steric-crowding effects.



Scheme 2.11: Addition of SIPr to $[\text{Rh}(\text{COE})_2\text{Cl}]_2$ to give **2.9**.

Single crystal X-ray diffraction studies on **2.9** show that both Rh centres have square planar geometries with the NHC ligands situated anti to one another (**Figure 2.8**). The COE ligands are orientated with the alkene H substituents facing the NHC, which minimises steric clashes with the isopropyl methyl groups. The Rh-NHC distance is 1.950(1) Å, which is similar to those observed in the literature for $[\text{Rh}(\text{NHC})(\text{C}_2\text{H}_4)\text{Cl}]_2$ complexes [1.973(2), 1.9681(17), and 1.943(3) when NHC = SIPr, IPr, SIMes, respectively].^{224, 225} The Rh-Cl distances are observed to be 2.3910(5) and 2.4621(6) Å. This distortion likely arises from the different trans influences of the NHC and COE ligands and can thus be a measure by which the X,L formalisation is applied, with the shorter interaction between Rh(1)-Cl(1) (trans to the COE) being assigned the X type bond and the longer Rh(1)-Cl(1') (trans to the NHC) the L type. The alkene double bond

C(28)-C(29) is 1.407(2) Å which is within error the same distance found in **2.6**, indicating a similar amount of π -back bonding.

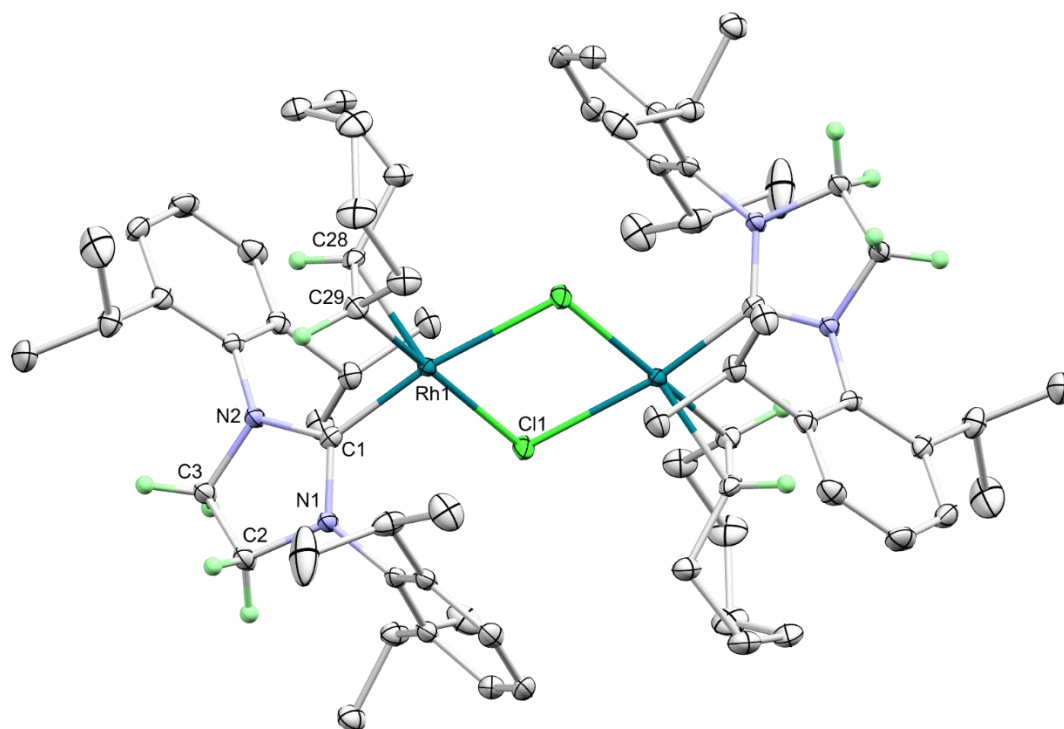
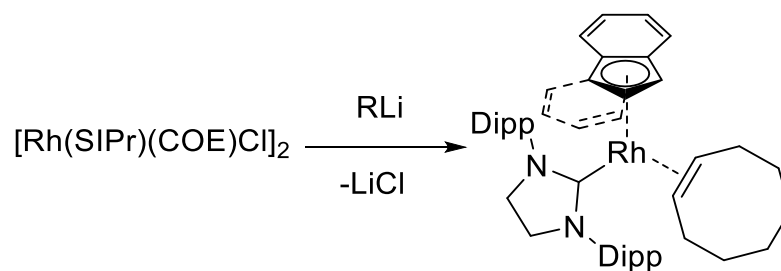


Figure 2.8: X-ray determined structure of **2.9** (thermal ellipsoids at 50%). All H-atoms, except for H2A/B, H3A/B, H28 and H29, and a benzene solvate molecule have been omitted for clarity.

Addition of LiInd to **2.9** was trialed to test how well this alternative synthetic route works (**Scheme 2.12**). On mixing, the reaction mixture briefly turned homogeneous before a fine precipitate was observed (LiCl) and the colour of the solution matched that observed for **2.6**. The ^1H NMR spectrum of this crude mixture showed relatively clean conversion to **2.6** (90%), with only a few minor impurities.



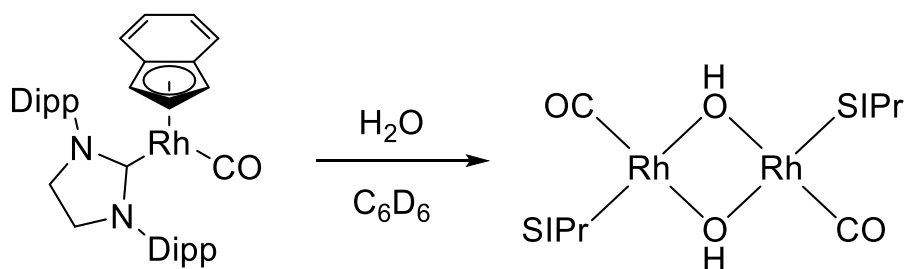
Scheme 2.12: Addition of LiR to **2.9** (R = Ind, Flu) to give **2.6**.

With the success of the LiInd reaction, it was decided to test the coordination of fluorenyl as the Cp-type donor because fluorenyl Rh complexes are relatively unknown in the literature and the tethered complexes described in Chapter 4 feature a fluorenyl donor. Addition of LiFlu to **2.9** gave a deep-red solution that darkened over the course of several hours. ^1H NMR spectroscopy indicated the formation of free COE and no clear signals were observed that could be associated with the expected product. No carbene resonance was observed by both direct observation $^{13}\text{C}\{^1\text{H}\}$ NMR spectroscopy and by ^1H - ^{13}C HMBC experiments, indicating that the target Rh complex was not formed in contrast to the reaction with LiInd, and suggesting that the NHC had degraded in the presence of the LiFlu/ $[\text{Rh}(\text{SIPr})(\text{COE})\text{Cl}]_2$ mixture.

2.3 Reactivity

2.3.1 Stability

The stability of **2.6** and **2.7** was tested in non-inert conditions. Complex **2.6** was dissolved in normal (i.e. non-dry) C_6D_6 and $CDCl_3$ and 1H NMR spectra were recorded at regular intervals. While **2.6** was observably stable in dry C_6D_6 (see below), degradation was observed in wet solvents with the reaction proceeding quickly in $CDCl_3$ (no starting material after overnight in solution) and significantly more slowly in C_6D_6 . In $CDCl_3$, the products show weak and complicated resonances in the region where isopropyl CH peaks typically appear, and there are weak resonances in the region where isopropyl methyl groups and cyclooctene CH_2 groups are observed. Free cyclooctene was observed in the 1H NMR spectra, indicating that the degradation proceeds with dissociation of cyclooctene. Reaction of **2.7** with water led to the formation of **2.10** with the loss of indene (Scheme 2.13).



Scheme 2.13: Reaction of **2.7** with water to generate hydroxide bridged Rh dimer **2.10**.

Single crystal X-ray diffraction studies on **2.10** show both Rh centres as having square planar geometries with the NHC ligands anti to one another (Figure 2.9). The Rh-NHC distance is 1.961(2) Å, which is longer than in **2.9**. The Rh carbonyl distance is 1.792(2) Å, which is shorter than the Rh-CO distance found in **2.7**. This suggests that the relative degree of backbonding is more in **2.10**, however, the different geometry may also play a role. The two Rh-O distances are unsymmetrical, with Rh-O(2) = 2.073(2) Å and Rh-O(2') = 2.092(2) Å. The square planar geometry is distorted with the angle between O(2)-Rh-O(2') being 77.66(6)°, a 12° deviation from the 90° expected for square planar geometry. The angle between the NHC and the nearest OH [C(1)-Rh-O(2)] is the closest value to 90° at 91.60(7)°, while C(1)-Rh-C(28) 93.76(8)° and C(28)-Rh-O(2) 96.97(8)°.

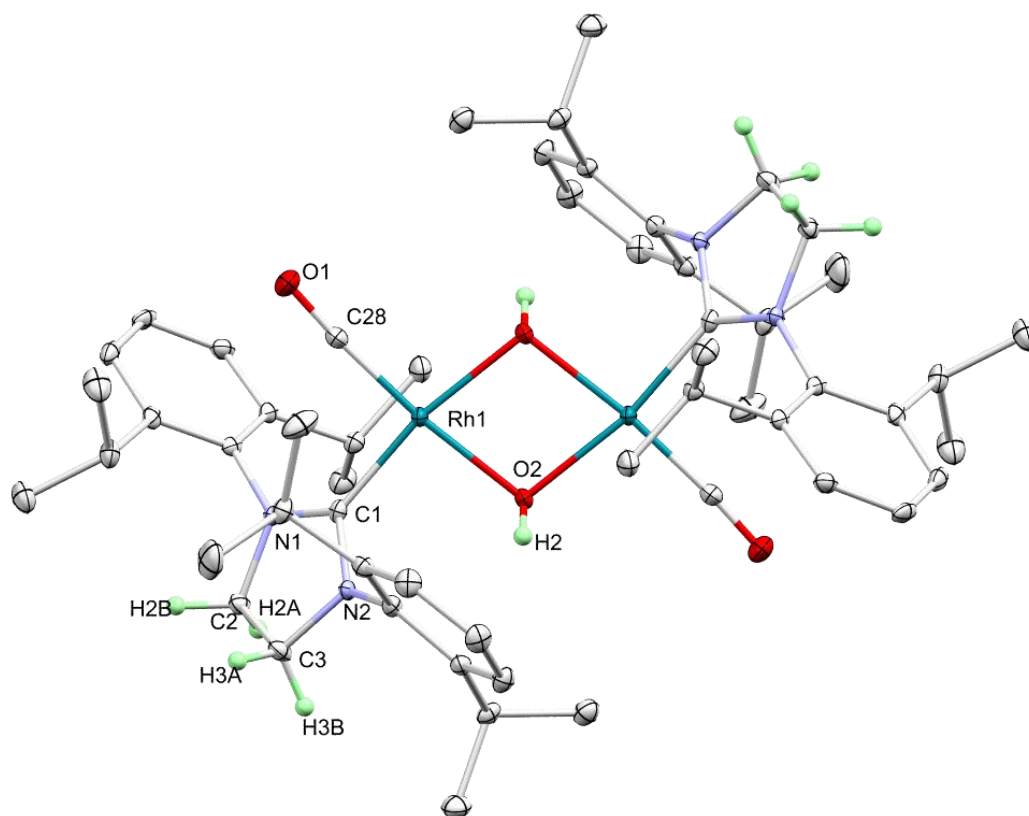
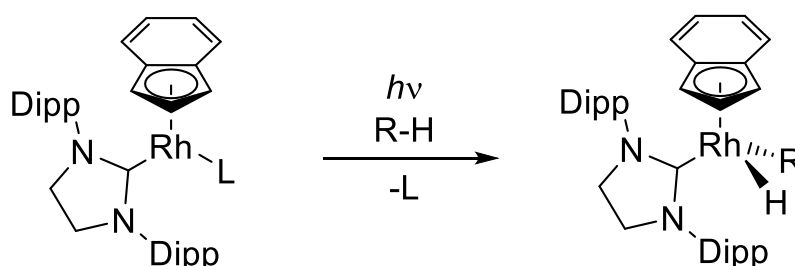


Figure 2.9: X-ray determined structure for complex **2.10** (thermal ellipsoids at 50%). All H atoms, except for H2, H2A/B and H3A/B have been removed for clarity in addition to two benzene solvate molecules.

The thermal stability of complexes **2.5** – **2.7** was tested by heating NMR samples at 80 °C using dry C₆D₆ and were found to be stable at this temperature for at least 24 hrs. This observation is supported by the synthesis of **2.5** and **2.6** occurring at this temperature. Thus, it was concluded that purely thermal activation of these complexes to enable C-H activation was not possible and alternative conditions were therefore investigated.

2.3.2 Photolysis studies

Work by Perutz and co-workers has shown that cyclopentadienylrhodium complexes with a photo-labile ligand, such as C_2H_4 or CO , can undergo C-H activation upon photolysis.^{38-40, 194} Ethene is a more weakly bound ligand than CO , but the $Rh-CO$ is more cleanly cleaved whereas ethene can C-H activate to give ethenyl hydride species. These have been observed for the photolysis of $[Ir(Cp)(C_2H_4)_2]$ and were involved in H/D exchange for $[Rh(Cp)(C_2H_4)]$ with C_2D_4 .^{39, 194, 226} Similar photo-activated C-H activation reactivity was also observed for Cp^* and indenyl Ir(III) species such as $[Ir(Cp^*)(PMe_3)(H)_2]$, which undergo reductive elimination of H_2 to generate the reactive Ir(I) intermediate.^{34, 35, 37, 86, 87, 226-228} Phosphines have been used as co-ligands and thus can be compared to the NHC complexes above to see how the different bonding interactions affect the rate and selectivity of C-H activation. A range of substrates could be trialled such as arenes, alkanes, silanes and boranes (**Scheme 2.14**).



Scheme 2.14: General photochemical reaction for Rh complexes with R-H substrates [R = H, Ph, SiR'₃].

In order to test whether complexes **2.5** – **2.7** are potential candidates for photochemical reactions, their UV/vis spectra were recorded along with $[Rh(Ind)(COE)_2]$ (**2.2**) for comparison (**Figure 2.10**). These showed that **2.5** – **2.7** have a noticeable absorption band at around 400 – 420 nm, while **2.2** absorbs less strongly in this region (**Table 2.1**). As **2.5** – **2.7** are shifted compared to **2.2**, it can be concluded that this shift is due to the coordination of the NHC. This is supported by the observed UV-vis spectra for $[Ir(Cp^R)(PMe_3)(H)_2]$ ($Cp^R = Cp, Cp^*$) that have negligible absorption above 350 nm,⁸⁶ while $[Ir(Ind)(PMe_3)(H)_2]$ has shoulder bands at 313 ($\epsilon = 1.4 \times 10^3 \text{ dm}^3\text{mol}^{-1}\text{cm}^{-1}$) and 345 nm ($\epsilon = 8.9 \times 10^2 \text{ dm}^3\text{mol}^{-1}\text{cm}^{-1}$). $[M(Cp)(C_2H_4)_2]$ ($M = Rh, Ir$) also have no bands above 350 nm (Rh: 239, 310 (minor), Ir: 202, 231, 261 nm).^{38, 39} The presence of

absorption bands at wavelengths greater than 380 nm allow photolysis experiments using visible light and thus avoids the need for the use of UV wavelengths.

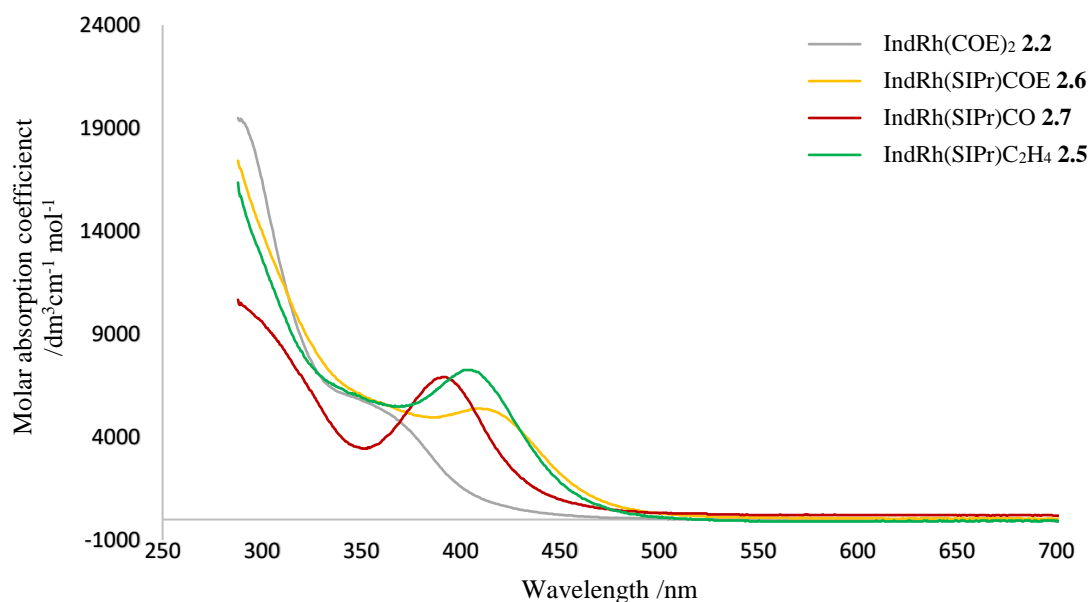


Figure 2.10: UV-vis spectra for **2.2** and **2.5 – 2.7** obtained from a solution in toluene. The solvent cut-off for toluene occurs at 284 nm; data from this wavelength or lower is therefore omitted.

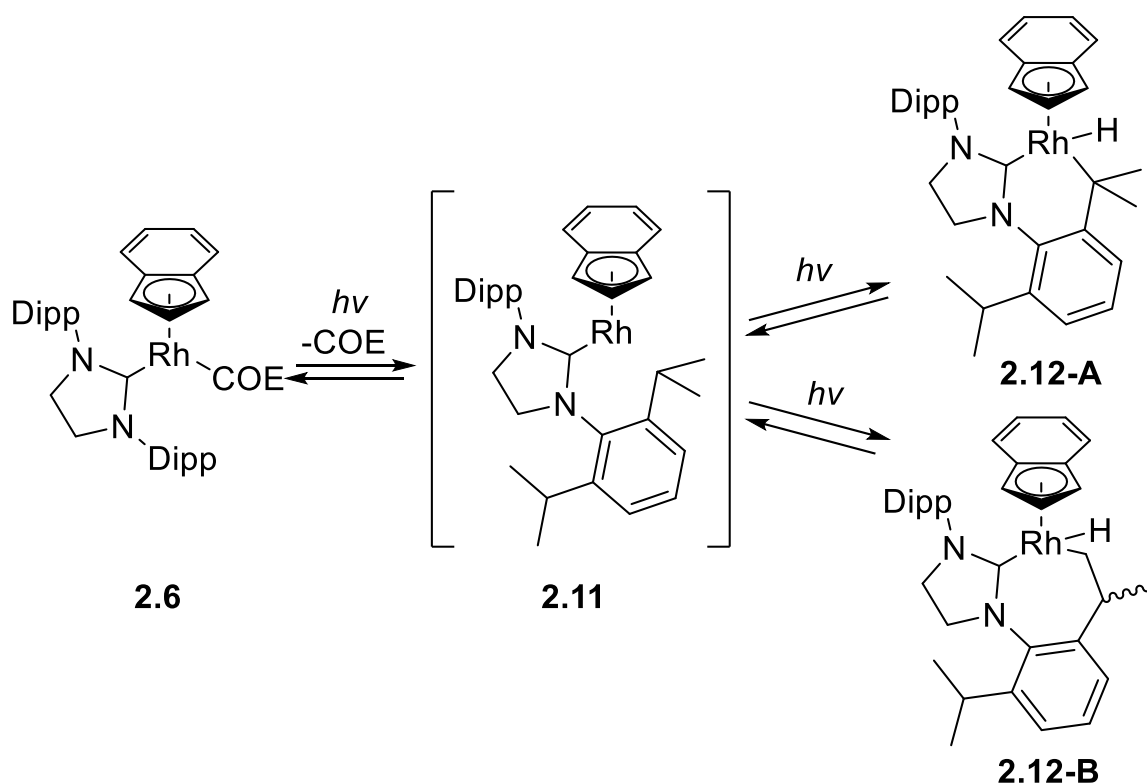
Table 2.1: Local λ_{\max} for complexes **2.2** and **2.5 – 2.7** with their respective molar absorption coefficients.

Complex	λ_{\max} /nm	Molar absorption coefficient/ $\text{dm}^3\text{mol}^{-1}\text{cm}^{-1}$
2.2	354.5	5617.8
2.5	404	7251.6
2.6	409	5391.6
2.7	392	6909.4

Photolysis reactions with **2.5** – **2.7** were trialled using either a 400 nm LED (5 W) or a 420 nm LED bank (33 W) in C₆D₆ solution. CO complex **2.7** showed no change upon photolysis (monitored by ¹H NMR spectroscopy), suggesting that CO is too strongly bound in the excited state to be removed readily by photolysis with either relatively low intensity light sources or low energy visible-light photons (mercury arc lamps produce a range of UV-photon energies and are typically greater than 100 W). Complex **2.2** also did not change upon photolysis indicating that absorption at these wavelengths is not strong enough to enable photoactivation. In contrast, both **2.6** and **2.7** do show change upon irradiation (within 20 mins), with the solutions darkening in colour. ¹H NMR spectroscopy showed the formation of free alkene (5.25 for ethene and 5.65 ppm for COE). Also observed were resonances in the upfield region of -15 – -17ppm, which are indicative of the formation of Rh hydrides. Two resonances are observed with **2.5**: the major species is a doublet at -16.72 ppm ($J = 36.0$ Hz) and the minor product a doublet at -15.35 ppm ($J = 36.0$ Hz), with the ratio between the two species changing over time. Initially it is 3:1 in favour of the species with a resonance at -16.72 ppm, changing to 2:1 upon further photolysis. This could arise from interconversion between the two species, or that the formation of the minor product is a slower process. For **2.6**, only one resonance at -16.72 ppm was observed. For **2.5**, no indenyl resonances could be found that gave satisfactory integrals to the hydride at -15.35 ppm (the minor product), while for **2.5** and **2.6** two resonances were observed that integrate 1:1 with the hydride at -16.72 ppm, a doublet at 5.21 ppm ($J = 2.7$ Hz) and doublet of doublets at 5.83 ppm ($J = 4.8, 2.7$ Hz); these are in the region observed for the 5-membered ring. The loss of symmetry could lead to the C1/C3 indenyl C-H no longer being equivalent by NMR. Another indenyl C-H resonance should be present but this resonance could be coincident with the free COE resonances, or others. For both reactions, conversion was low (less than 25%); this may be due to the products absorbing light in a similar region to the starting materials, as well as the darker colour of the reaction mixture preventing light from reaching the whole of the sample effectively. Alternatively, a photo-stationary state may have been achieved where the forward and backward reactions are both promoted by light and the rates are equal.²²⁹ Attempts at observing ¹³C NMR resonances for the photoproducts proved unsuccessful due to the low concentrations of the products leading to indistinct spectra.

The presence of hydridic resonances in the ¹H NMR spectra rules out the addition of the deuterated solvent to the Rh (the amount of residual H in C₆D₆ is considered too low to be observable). The formation of the free alkene suggests that oxidative addition into a

C-H bond of the alkene did not occur. One remaining possibility is cyclometallation of the isopropyl groups, which could occur at either the methyl group – forming a 7-membered metallacycle in **2.12-B** – or at the methine C-H bond forming a 6-membered metallacycle, **2.12-A** (**Scheme 2.15**). These products would be unsymmetrical and would match the observed indenyl C-H peaks for the major product. The reaction is proposed to proceed via **2.11**; this species would be coordinatively and electronically unsaturated and thus could readily cyclometallate the available isopropyl C-H bonds. Such a species could exist in a photostationary state, with the rate for the formation of **2.11** equal to the rate of its reaction. Such a species will only occur in very low concentrations and thus is difficult to observe by NMR spectroscopy, especially in the relatively busy spectra observed for the reaction with **2.6**. Addition of the free alkene to **2.11** could reform **2.5/2.6**. This process would be dependent on the relative concentration of **2.11** and the alkene, with high concentrations favouring the re-addition and low concentrations disfavoring it. When leaving the reaction mixture at ambient conditions for 16 hours, no degradation of the products was observed suggesting the photoproducts are thermally stable and do not undergo reductive elimination back to **2.5/2.6**.



Scheme 2.15: Proposed photochemical products from the photolysis of **2.6**. One diisopropylphenyl group is displayed for clarity.

An interesting observation is that over longer time periods (greater than 5 hours) upon further photolysis of **2.5**, the hydride resonance at -16.72 ppm decreases in intensity while a singlet at 0.79 ppm starts to grow in. For **2.6** the growth of a similar singlet at 1.49 ppm was observed. Comparison to the literature suggests that these resonances correspond to ethane and cyclooctane, respectively. Supporting this is a decrease in the intensity for the corresponding free alkenes. The use of LIFDI (Liquid Injected Field Desorption Ionisation) mass spectrometry was trialled to see if information could be obtained on the minor species observed in these reaction mixtures. The LIFDI technique features very soft ionisation with the molecular ion peaks of reactive species regularly observed as $[M^+]$ rather than protonated ions as often found with ESI or APCI/ASAP methods. This means that the effects of fragmentation are minimised, and the observed peaks are indicative of the actual sample rather than artefacts of the ionisation. Mass spectra for the photolysis reaction mixtures of **2.5** and **2.6** revealed the presence of peaks at m/z 606 and 608 (**Figure 2.11**). The latter fits for the cyclometallated species **2.12** (isomers would have the same m/z , only one is shown for clarity), while $m/z = 606$ matches for the loss of H_2 that leads to the proposed alkene complex **2.13**. The dehydrogenation of isopropyl groups in Rh complexes has been observed previously for $[Rh(P^iPr_3)_3][BAR^F_4]$.²³⁰ This is in agreement with the observed reduction of the corresponding alkenes to their respective alkanes (observation of peaks at 0.8 and 1.5 ppm that fit the expected chemical shifts for ethane and cyclooctane, accounting for chemical shift differences between solvents).

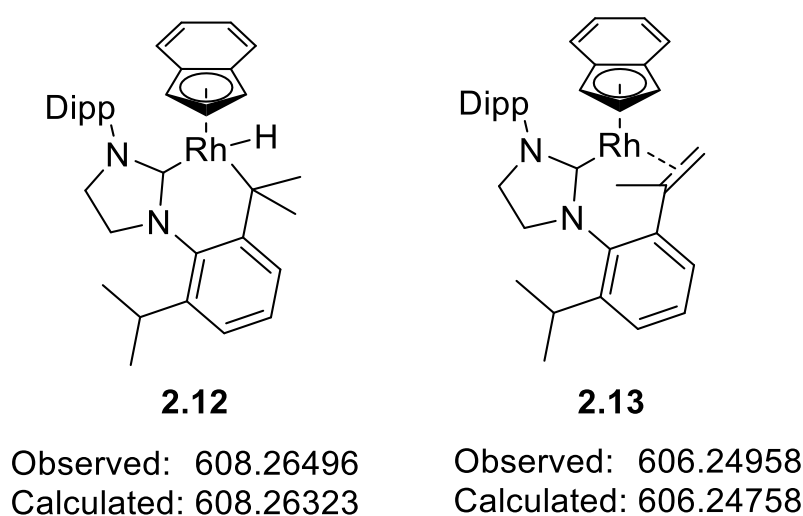


Figure 2.11: Proposed structures for the species observed by LIFDI mass spec.

Following the photolysis of **2.6** by UV-vis spectroscopy (**Figure 2.12** & **Figure 2.13**) showed the reaction to proceed quickly, with the band associated with **2.6** at 409 nm bleached instantaneously upon photolysis and new, but broad, bands growing in at 326 nm and 480 nm. The increased reaction rate compared to that observed by NMR spectrometry is likely due to the much lower concentration of the reaction compared to the NMR scale reaction (0.0345 mM for photolysis in a UV-vis cuvette compared to 41.7 mM for NMR-scale reactions). Photochemical reactions favour low concentration due to the requirement for the light to reach the entire sample and to minimise the negative effect of the product absorbing in the same region as the starting material.

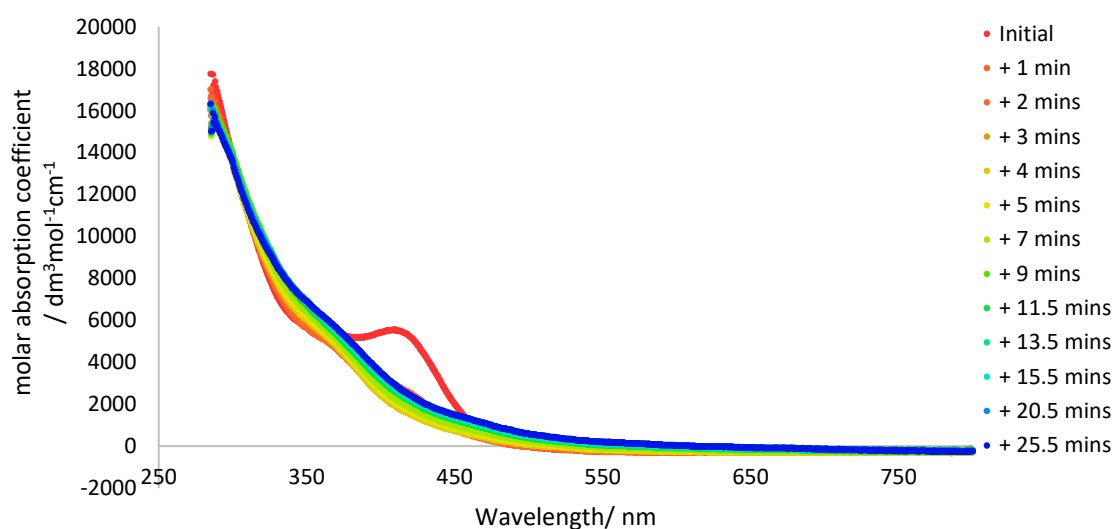


Figure 2.12: UV-vis spectra following the photolysis of **2.6** in toluene.

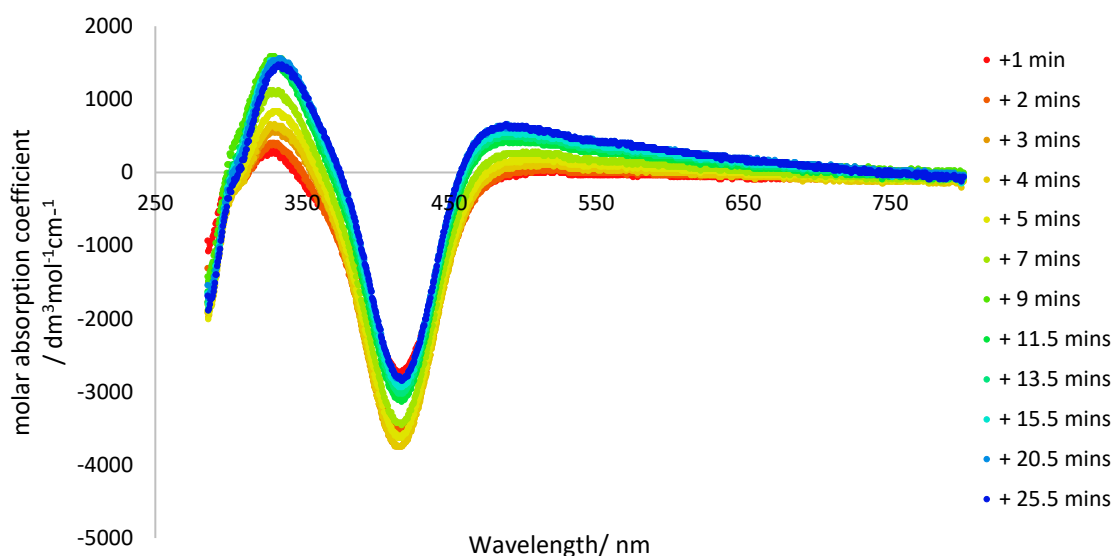
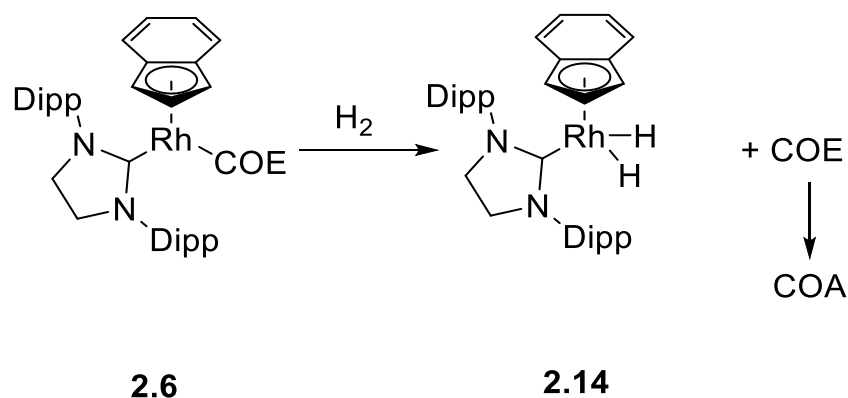


Figure 2.13: UV-vis difference spectra showing change upon photolysis of **2.6** ($t=0'$). Positive values indicate increased absorption relative to the initial spectrum of **2.6** in toluene, negative values indicate decreased absorption relative to the initial spectrum.

As shown by **Figure 2.12**, the photolysis products absorb in a similar region to the starting complex **2.6**, which supports one of the reasons for the slow rate and low conversion observed for the NMR scale photolysis reactions. Dilution would, in theory, help improve the conversion, however, it would have a negative effect on NMR spectral quality and signal-to-noise, making the use of this characterisation technique less favourable. Additionally, concentration of the reaction mixture post-photolysis via low pressure could have a negative effect on the sensitive photolysis products.

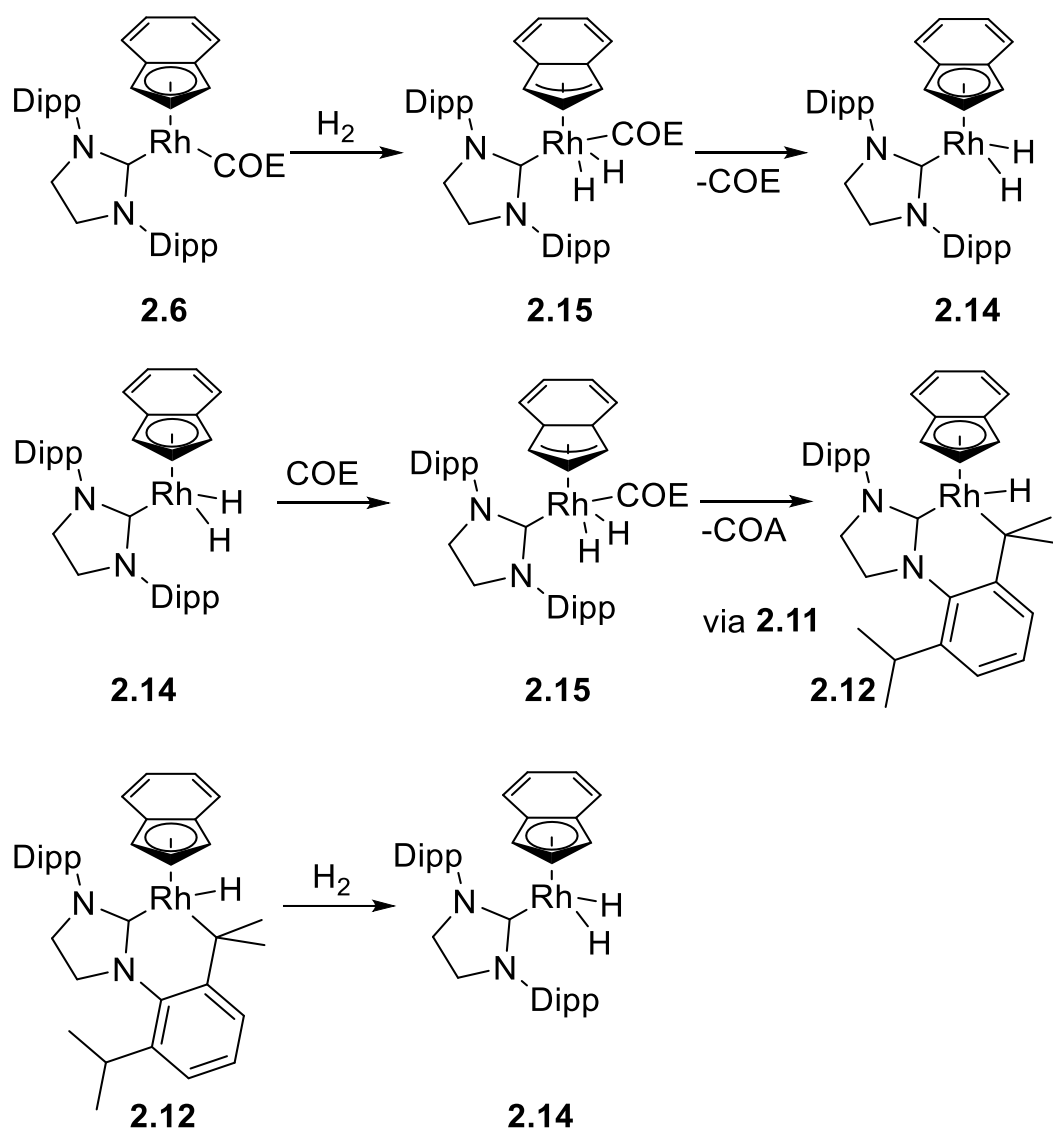
2.3.3 Hydrogenation and reaction with silanes

Complexes **2.5** and **2.6** were placed under an atmosphere of H_2 with the anticipation of forming a dihydride complex (**Scheme 2.16**); these reactions were kept away from light where possible to prevent competing photochemical reactions. The hydrogen was obtained from a hydrogen generator which produces hydrogen via electrolysis of water, however, no water contamination was observed in the 1H NMR spectra of the reaction mixtures (water occurs at δ_H 0.4 ppm in C_6D_6).²³¹



Scheme 2.16: The anticipated addition of H₂ to **2.6** with the formation of cyclooctane (COA).

Upon addition of H₂, a doublet at -16.72 ppm was observed in the ¹H NMR spectrum for both reactions (**2.5** and **2.6**); this is the same resonance observed for the photolysis reaction suggesting that the reaction could proceed via the same metallacycle complex for both reactions. Further reaction of H₂ led to the formation of a second doublet at -15.91 ppm ($J = 50.5$ Hz). This could tentatively be assigned as the Rh(III) dihydride species **2.14**. Also observed in the ¹H NMR spectra were singlets associated with ethane (0.80 ppm) and cyclooctane (1.51 ppm) for the hydrogenation of **2.5** and **2.6** respectively, however, these only grow in later in the course of the reaction, suggesting that they could be formed by the reaction of the respective alkene and the Rh(III) dihydride. A proposed mechanism for this reaction would be that H₂ adds to **2.6** (**Scheme 2.17**), which forms the dihydride complex **2.14** via ring-slipped indenyl coordination (from η^5 to η^3) to give the intermediate **2.15**. Alkene loss would be favourable, thus the dihydride complex with η^5 -indenyl coordination would be formed. Complex **2.14** could then react with the alkene leading to reduction to the observed alkane and the formation of **2.12** via intermediate **2.11**. Addition of H₂ to **2.12** would then form dihydride complex **2.14**. If the hydrogenation of the alkene occurs readily then the formation of **2.14** would be dependent on the reaction between **2.12** and H₂, which may be slow due to the constrained geometry around the Rh. A prolonged reaction time with an increased amount of H₂ would favour the formation of the alkane thus should lead to clean formation of **2.14**, however, this would require further work.

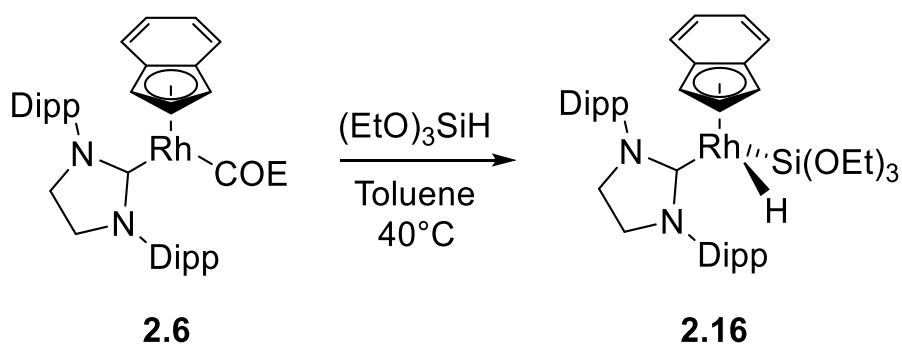


Scheme 2.17: Proposed steps in the reaction between **2.6** and H_2 . Only one isomer of **2.12** and one diisopropylphenyl group is displayed for clarity where appropriate.

Aside from the distinctive hydride resonances, also observed in the ^1H NMR spectra for reactions of **2.5** and **2.6** with hydrogen gas is the formation of two doublets at 1.17 and 1.50 ppm (12 H, $J = 7.0$ Hz and 12 H, 6.8 Hz, respectively), a quintet at 1.78 ppm ($J = 7.4$ Hz), a triplet at 2.69 ppm ($J = 7.4$ Hz) and a singlet at 3.38 ppm (4 H). Additionally, there are weak resonances growing in underneath the septet for **2.5/2.6** that can be assigned to isopropyl CHs, however, due to overlap, the integrals have little meaning. The integrals for the two doublets and the singlet fit a 3:3:1 pattern, which are compatible with each doublet being equivalent to 12 H each and the singlet to 4 H. This is the standard pattern for SIPr-substituted complexes with the doublets arising from the isopropyl methyls and the singlet being the backbone CH_2 . However, the integrals do not match recognisable integer ratios to the hydride peak or the triplet and quintet suggesting

these are separate species. The ratios for the doublets and singlet indicate that the species these correspond to have a symmetrical NHC ligand and thus is not cyclometallated or similar. As the triplet at 2.69 ppm and quintet at 1.78 ppm occur in both hydrogenation reactions with **2.5/2.6**, the alkene is not involved in this species, which rules out a Rh hydride complex involving the alkene (either an alkenyl complex from the oxidative addition of the alkene across the metal centre or alkyl which could be formed in the presence of H₂). Closer inspection of the ¹H NMR spectra for the photolysis of **2.5/2.6** contain the same triplet and quintet, albeit in much weaker intensities. The alkene resonances for the proposed Rh alkene complex **2.13** would be in the same region due to the coordination to Rh. Coordination to the Rh would also affect the nature of the ¹H-¹H *J*-coupling due to the backdonation into alkene anti-bonding orbital. Thus, it is possible that the triplet and quintet could be associated with **2.14** if the magnitude of the Rh-H *J*-coupling is similar to that of the ²*J* vicinal coupling. However, this assignment requires further investigation, as 2D correlation experiments would be able to detect possible interactions from the arene ring to the alkene which could support the proposed structure.

The reaction of **2.6** and (EtO)₃SiH under gentle heating overnight leads to the formation of **2.16** (Scheme 2.18). In the ¹H NMR spectrum, there is a doublet at -15.07 ppm with ¹*J*_{RhH} = 30.6 Hz, which is similar to literature Rh silyl hydride complexes.^{232, 233} It also displays satellite peaks from coupling to ²⁹Si with ²*J*_{SiH} of 14.8 Hz, which also compares well with literature values. This reaction appears to be relatively clean, with only a minor resonance appearing at -16.75 ppm (*J* = 35.9 Hz), which is similar to a resonance observed in the photolysis of **2.6**. The ²⁹Si{¹H} NMR spectrum shows a doublet at -13.77 ppm (¹*J*_{Rh-Si} = 67.3 Hz). In both ¹H and ¹³C NMR spectra, a number of resonances appear broad in nature and there are more than would be expected. Integration of these broad resonances to the sharper resonances provide reasonable values when taken as a ‘doubling’ effect. Such an effect is typically observed when there is a dynamic process involved. The rotation of the indenyl ring around the M-Ind centroid leads to averaging of signals for the indenyl group even when there are multiple different ligands on the metal. As the silane in **2.16** is very bulky in size (Figure 2.14), it is possible that the rotation of the indenyl ring around the M-Ind centroid is now restricted at the normal operating temperature of the NMR spectrometer (298 K). The use of variable temperature NMR would be able to prove this possibility, however this was not possible due to time constraints.



Scheme 2.18: Reaction between **2.6** and $(\text{EtO})_3\text{SiH}$ forming **2.16**.

Single crystals of **2.16** suitable for X-ray diffraction were grown from a saturated benzene solution (**Figure 2.14**). The indenyl coordination has two short, one intermediate and two longer Rh-C interactions, with a fold distortion of 8.8° . The Rh-Si ($2.2691(8) \text{ \AA}$) bond length is shorter than for $[\text{Rh}(\text{Cp})(\text{Si}^i\text{Pr}_3)(\text{H})(\text{PMe}_3)]$ ($2.3617(3) \text{ \AA}$)²³³ and $[\text{Rh}(\text{Cp})(\text{Si}^i\text{Pr}_3)(\text{H})(\text{PPh}_3)]$ ($2.386(2) \text{ \AA}$).²³⁴ However, the Rh-H distances ($1.45(3) \text{ \AA}$ in **2.16**) are indistinguishable within experimental uncertainty. The $\text{Si}1 \cdots \text{H}43$ distance (2.239 \AA) as well as the unequal H-Rh-C_{carbene} and H-Rh-Si angles suggest some residual H \cdots Si interaction,^{235, 236} as was concluded for $[\text{Rh}(\text{Cp})(\text{Si}^i\text{Pr}_3)(\text{H})(\text{PMe}_3)]$ (H \cdots Si = $2.278(17) \text{ \AA}$).²³³ The Rh-NHC distance ($2.014(3) \text{ \AA}$) is marginally longer than in **2.5** ($1.9886(12) \text{ \AA}$) or **2.6** ($1.9881(15)$ and $1.9946(15) \text{ \AA}$) and within error of the distance in **2.7** ($2.010(2) \text{ \AA}$).

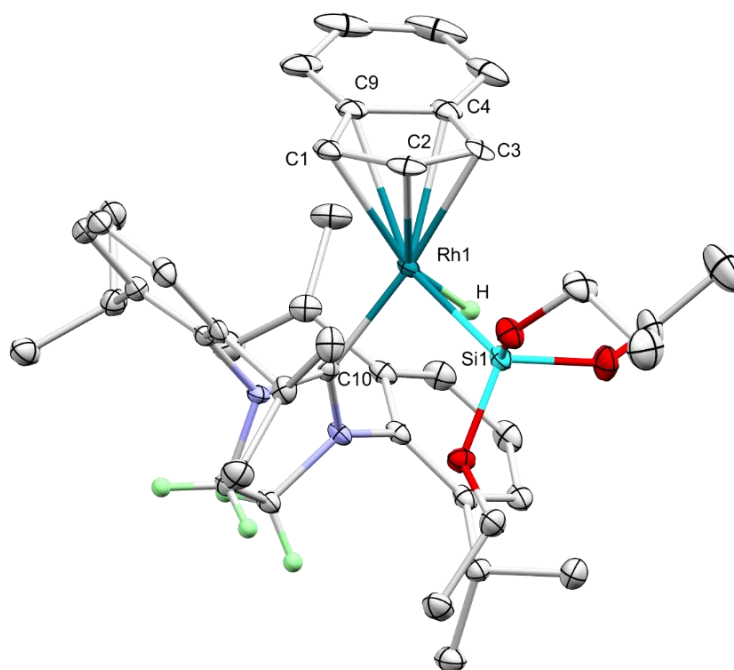
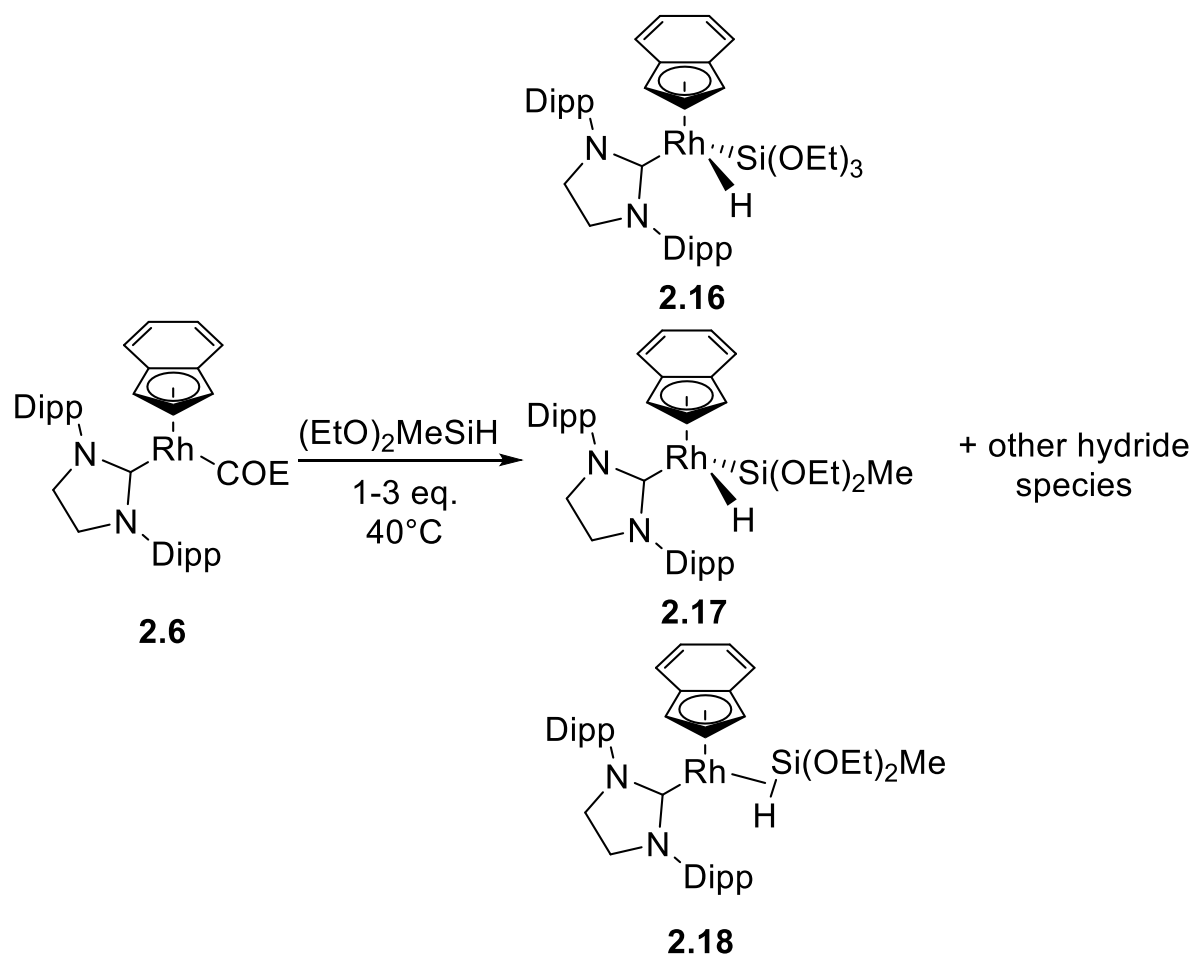


Figure 2.14: X-ray determined structure for Rh silyl hydride complex **2.16** (thermal ellipsoids at 50%). All H atoms except for the hydride and NHC backbone have been removed for clarity.

The reaction of **2.6** with $\text{HSi}(\text{OEt})_2\text{Me}$ contrasts greatly with $\text{HSi}(\text{OEt})_3$ as there are multiple different Rh hydride resonances observed in the ^1H NMR spectrum and the reaction is not complete even after heating overnight. A Rh hydride resonance was present at -15.08 ppm (d, $J = 30.7$ Hz), which was still growing in even after heating for 16 hours. This is effectively the same as the resonance in **2.16**; a noticeable difference in chemical shift would be expected from changing from three ethoxy groups to 2 ethoxy and a methyl on the silicon, thus the similarity suggests an exchange process is occurring, scrambling the Si substituents and leading to $\text{Si}(\text{OEt})_3$. Single crystals obtained from the reaction mixture of **2.6** with $\text{HSi}(\text{OEt})_2\text{Me}$ were found to be **2.16** from X-ray diffraction experiments, corroborating the above findings. To form **2.16**, C-Si bonds are required to be activated which has been observed occurring with electron-rich Pt, Ni, Pd, Ir and Rh complexes.²³⁷⁻²³⁹ The major resonance is a doublet at -15.59 ($J = 34.1$ Hz), which could be assigned to the expected Rh silyl hydride complex **2.17**. There is a minor doublet at -5.13 ppm with a 22.1 Hz coupling (**Scheme 2.19**). This could be a Rh η^2 -silane complex **2.18** as these can have similar chemical shifts and J -coupling values, with $\delta_{\text{H}} = -6.62$ ppm ($^1J_{\text{HRh}} = 21.2$ Hz) observed for $[\text{Rh}(\text{H})(\eta^2\text{-HSiEt}_3)(\text{dipp})]$ and -6.23 ppm ($^1J_{\text{HRh}} = 19.6$ Hz) observed for $[\text{Rh}(\text{H})(\eta^2\text{-HSi}^i\text{Pr}_3)(\text{dipp})]$ ($\text{dipp} = 1,3$ -bis(diisopropylphosphino)propane).²⁴⁰ This peak disappears as the reaction proceeds

suggesting that it is a possible intermediate or only occurs when there is a relatively large amount of silane in solution. There are in addition two further hydridic resonances at -15.88 ($J = 35.9$ Hz), and -16.05 ppm ($J = 35.9$ Hz). These could be intermediates in the formation of **2.16** via Si-C bond activation from **2.17** and rearrangement. The later two resonances disappear almost completely upon further heating (two nights at 40°C) while the doublet at -15.59 ppm changes relatively little in intensity as the Rh silyl hydride peak at -15.07 ppm increases in intensity.



Scheme 2.19: Reaction between **2.6** and $(\text{EtO})_2\text{MeSiH}$.

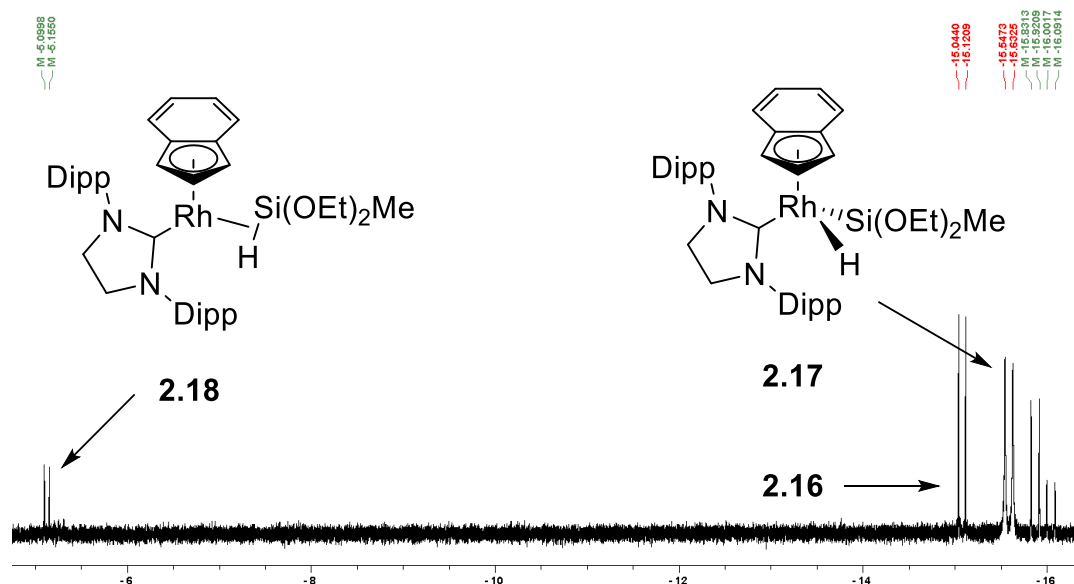


Figure 2.15: ^1H NMR spectrum of the hydride region for the reaction between **2.6** and $(\text{EtO})_2\text{MeSiH}$.

Upon the addition of Ph_3SiH to **2.5** & **2.6**, the formation of cyclooctane is observed and the most intense hydridic resonance occurs at -15.36 ppm ($J = 31.6$ Hz), which can be assigned as the corresponding Rh silyl hydride complex **2.19** (Figure 2.16). Also observed are minor doublets at -16.72 ppm, which is the same resonance observed from the photolysis of **2.5/2.6**, -12.62 ppm ($J = 37.7$ Hz) and -6.05 ppm ($J = 28.2$ Hz), the latter of which is similar to the potential η^2 -silane complex observed for the reaction with $(\text{EtO})_2\text{MeSiH}$ and thus could be silane complex **2.20**. Additionally, in the reaction of Ph_3SiH with **2.5**, a doublet at -15.91 ppm with a 50 Hz coupling is observed, which is the same doublet observed for the reaction with H_2 . Silanes are used for reductions thus could generate the dihydride species **2.14**. Investigations to find the most cleanly reducing silane would potentially provide an alternative to H_2 gas, which is troublesome to handle.

Reactions of **2.6** with PhMe_2SiH proceed with the formation of cyclooctane and generated doublets at -15.94 ppm and -16.72 ppm, which are respectively the resonances associated with the tentatively assigned Rh(III) dihydride **2.14** and the metallacycle **2.12**. As these are the only hydridic species, it may be that PhMe_2SiH is more reducing than Ph_3SiH (stronger +I effect of Me over Ph) and thus favour the formation of the Rh(III) dihydride species over oxidative addition of the silane to the Rh. It is probable that the formation of **2.14** occurs via **2.12** reacting with the silane in analogous reaction to that between **2.6** and H_2 . In the ^{29}Si NMR spectrum, resonances were observed at 9.0, -8.3 , and -21.8 ppm. The resonance at -21.8 ppm can be assigned to $\text{PhMe}_2\text{SiSiMe}_2\text{Ph}$,²⁴¹ and is presumably

formed via a dehydrogenative process which has been observed with other silanes in reactions with Ir complexes.²⁴² The formation of $\text{PhMe}_2\text{SiSiMe}_2\text{Ph}$ agrees with the formation of **2.14**.

Reaction of **2.6** with Et_3SiH once more leads to the formation of cyclooctane and the following hydridic ^1H NMR resonances: -7.53 ($J = 29.0$ Hz), which is likely to be the η^2 -silane complex **2.21**, -15.94 ($J = 50.5$) which is the dihydride complex **2.14**, -16.74 ($J = 36.0$ Hz), and -17.20 ($J = 37.9$ Hz). Excess Et_3SiH led to formation of additional minor doublets at -16.73 ppm ($J = 36.1$ Hz) and -17.22 ppm ($J = 37.1$ Hz). These additional species could arise from oxidative addition of the alkyl groups on the silane. Additionally, Et_3SiH could undergo elimination reaction on the ethyl side chains whereas Ph_3SiH and PhMe_2SiH cannot, which could explain the increased variation in products from the reaction with Et_3SiH . There is no peak that can definitely be assigned to the oxidative addition product $[\text{Rh}(\text{Ind})(\text{SiPr})(\text{H})(\text{SiEt}_3)]$ as the peaks at -16 and -17 either appear in the photolysis reactions and/or have noticeably different J -coupling values as values for **2.16**, **2.17** and **2.19** are 30.6, 30.7 and 31.6 Hz respectively. The ^{29}Si NMR spectrum showed only two singlets at 1.65 ppm and -22 ppm; free Et_3SiH has $\delta_{\text{Si}} = 0.2$ ppm which was not observed.²⁴³ The resonance at -22 ppm is $\text{Et}_3\text{SiSiEt}_3$ and is formed in the analogous way to the reaction between **2.6** and PhMe_2SiH .

In summary, it was found that reducing silanes would favour the formation of the dihydride complex **2.14** and η^2 -silane complexes (**Figure 2.16**). Less reducing silanes, particularly those with alkoxy substituents, lead to the formation of the oxidative addition products with **2.16** the only product when using $(\text{EtO})_3\text{SiH}$.

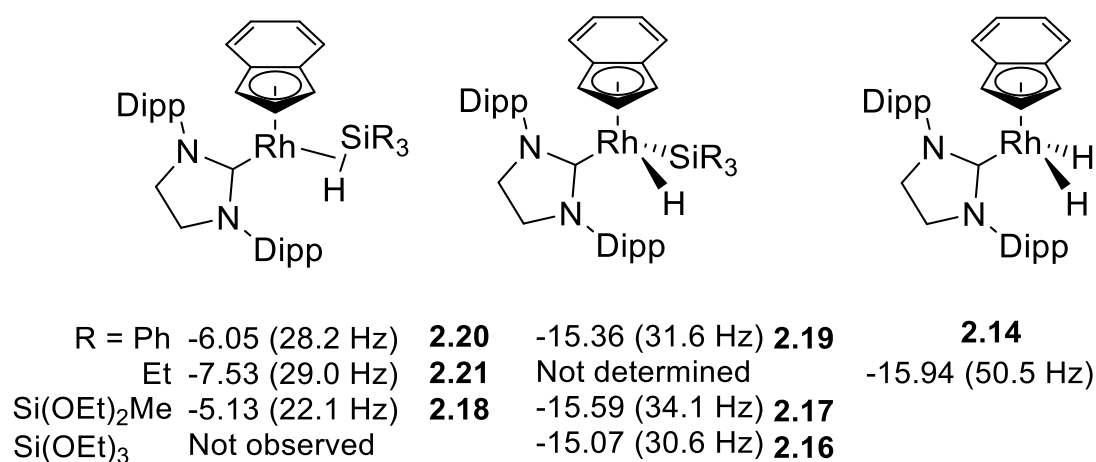


Figure 2.16: Summary of proposed products with the associated hydridic resonance chemical shift and J -coupling values for the reaction of **2.6** with trisubstituted silanes.

2.4 Conclusions

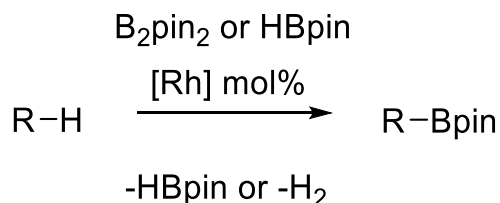
A range of indenylrhodium(I) complexes featuring the NHC SIPr were synthesised in good yields (60-80%). This was achieved via the addition of the free NHC to the indenylrhodium(I) bis alkene complexes. The analogous route with pentamethylcyclopentadienyl ligands was unsuccessful, highlighting the increased reactivity observed for indenyl complexes over Cp/Cp* complexes. The formation of a NHC alkene Rh(I) chloride dimer allowed the testing of an alternative route for the formation of the indenylrhodium(I) complexes via addition of indenyllithium to the dimer, which was successful. Attempts to access the analogous fluorenyl complex were unsuccessful. This route could be used to access other Cp-type complexes for comparison of ligand effects.

Photolysis of these complexes along with reactions with H₂ and silanes suggest that loss of the alkene is favoured and show evidence that cyclometallation of the NHC's isopropyl groups occurs as a common intermediate. The reaction with H₂ is likely to lead to a Rh(III) dihydride complex, which is also partially formed by the reaction with reducing silanes. Trialkoxy silanes form the oxidative addition product, a Rh silyl hydride complex, which has been crystallographically characterised. Mixed alkoxy-alkyl silanes form a mixture of products. Other alkylsilanes, such as Et₃SiH, form a mixture of products suggesting that reactions could occur with the alkyl chains. Tuning the electronic properties of the silane may allow access to the dihydride without the need for H₂ gas.

Chapter 3: Catalytic borylation

3.1 Introduction

The catalytic borylation of arenes with transition metals usually proceeds via borylation with diborane(4) derivatives (B_2R_4) or dehydrogenative borylation with secondary boranes, HBR_2 (**Scheme 3.1**). The former reaction is generally easier due to the B-B bond being relatively weak and the thermodynamic driving force from the formation of stronger H-B bonds in the form of HBR_2 .



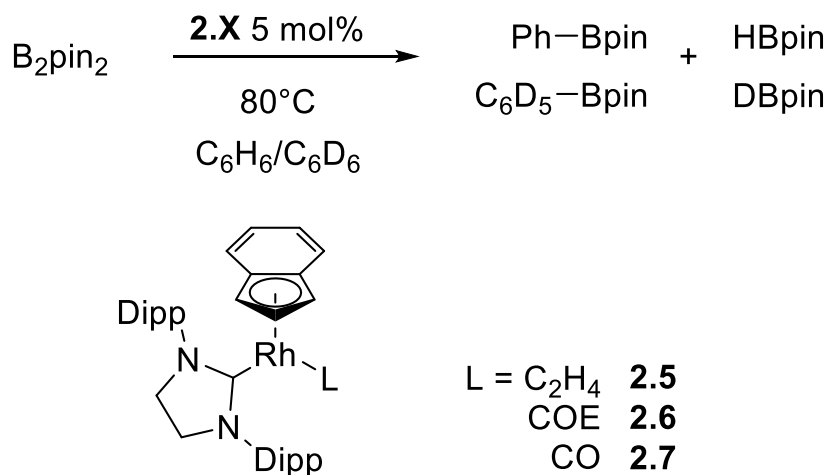
Scheme 3.1: General reaction for the borylation of arenes and alkanes with bis(pinacolato)diborane(4) (B_2pin_2) and pincolborane ($HBpin$) using a rhodium complex.

A variety of different metals have been used for the catalytic borylation of arenes and alkanes,^{64, 244, 245} with examples including Ir,^{246, 247} Rh,^{22, 66}, and Co.²⁴⁸ There are examples of borylation that occur with ‘directed’ mechanisms, where a functional group interacts with the metal and leads to the preferential activation of a particular site. ‘Undirected’ mechanisms are controlled by steric interactions or electronic preferences of the catalyst system, which guides the selectivity of the reaction. Activation of arene C-H bonds proceeds more readily than for alkanes, due to the formation of strong M-C(sp²) bonds providing a greater driving force for activation, and the presence of M-arene intermediates which allow substrates to be coordinated prior to activation. This leads to the borylation of arenes occurring more readily and at lower temperatures than for alkanes, and thus initial catalytic studies focussed on arene substrates to probe the effectiveness of the rhodium complexes before attempts at more challenging substrates were attempted.

3.2 Borylation of arenes

The borylation of benzene was used as a standard test for the activity of complexes **2.5** – **2.7**, and was conducted on small scales in NMR spectroscopy tubes sealed with J. Young taps for convenience, with the course of the reaction being followed by ¹H and ¹¹B NMR

spectroscopy (**Scheme 3.2**). To enable the spectrometer to lock to a deuterium signal, and to determine additional information about the catalytic reaction, a 3:1 mixture of C₆H₆:C₆D₆ was used. Typically, 5 mol% of the rhodium complex (*ca.* 5.0 mM) was used with B₂pin₂ (*ca.* 100 mM) and an excess of benzene. Observable by ¹H NMR spectroscopy as the reaction progressed were two new CH₃ resonances at 1.11 and 0.99 ppm for PhBpin and HBPin respectively, as well as a broad 1:1:1:1 quartet at 4.3 ppm which can be assigned to H-Bpin. In the ¹¹B{¹H} NMR spectra, a singlet resonance was observed at 28 ppm, which is a doublet in the coupled ¹¹B NMR spectrum (¹J_{H-B} = 173 Hz), which corresponds to the formation of HBpin. The formation of PhBpin was demonstrated by the growth of an aryl resonance at 8.15 ppm in the ¹H NMR spectrum, which displayed the typical second-order effects observed for mono-substituted arenes.



Scheme 3.2: Borylation with complexes **2.5** – **2.7**.

In benzene solvent, the ¹¹B resonance for PhBpin (31 ppm) was observed to overlap with the resonance for B₂pin₂, which limits the ability to monitor formation of PhBpin by ¹¹B NMR spectroscopy, although the concomitant formation of HBpin is an indication of the reaction proceeding. Also observable in the ¹¹B NMR spectra is an additional resonance at 28 ppm (**Figure 3.1**) which can be assigned to DBpin formed by borylation of C₆D₆ rather than C₆H₆. The resonance appears as a distorted triplet with a *J*-coupling of 22 Hz from coupling between the two quadrupolar nuclei. d₅-PhBpin is also produced but the boron resonance cannot be distinguished from PhBpin in the ¹¹B NMR spectra, and the methyl resonance is indistinguishable from PhBpin. Mass spectrometry analysis on

C_6H_6/C_6D_6 reaction mixtures confirmed the formation of PhBpin and d_5 -PhBpin ($m/z = 204.1$ and 209.2 , respectively) (**Figure 3.2**). The observed peaks are within the distribution expected for the two products with no isotropic scrambling, although the presence of $^{10}B/^{11}B$ and only a 5 Da difference makes this less distinguished. It is also noteworthy that as the reaction proceeds the reaction mixture changes from yellow-orange to dark orange.

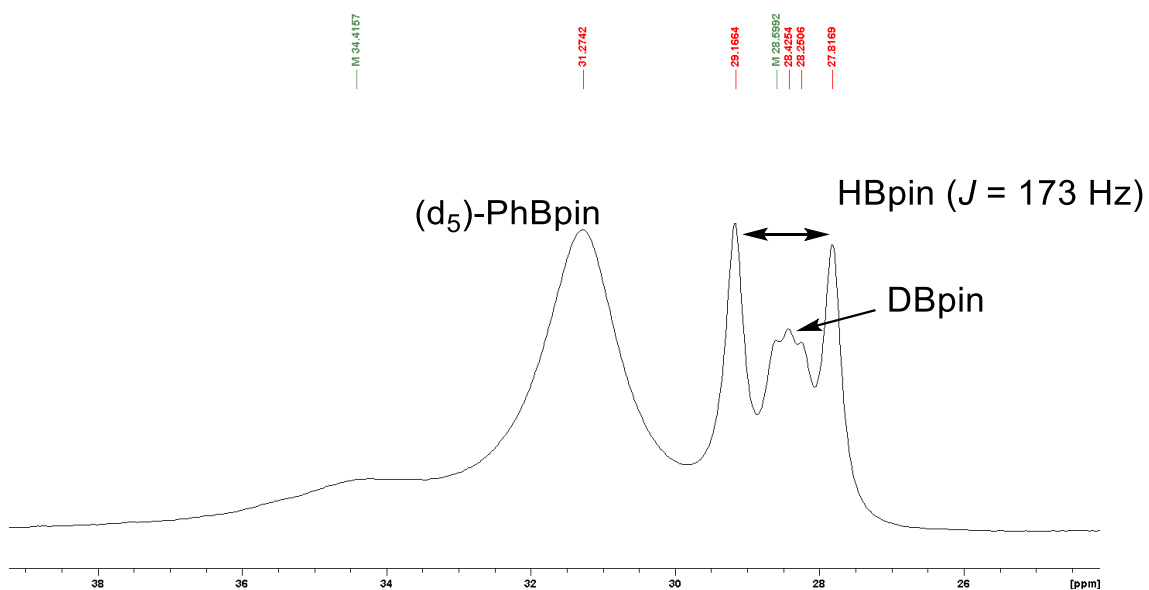


Figure 3.1: ^{11}B NMR spectrum of reaction of B_2pin_2 with **2.6** in C_6H_6/C_6D_6 .

The relative abundance of the protio- and deutrio-products in the mass spectrum fits the 3:1 ratio of C_6H_6/C_6D_6 solvent (48% for PhBpin and 16% for d_5 -PhBpin). This would indicate a kinetic isotope effect of 1 suggesting that the C-H activation of benzene is not the rate determining step.

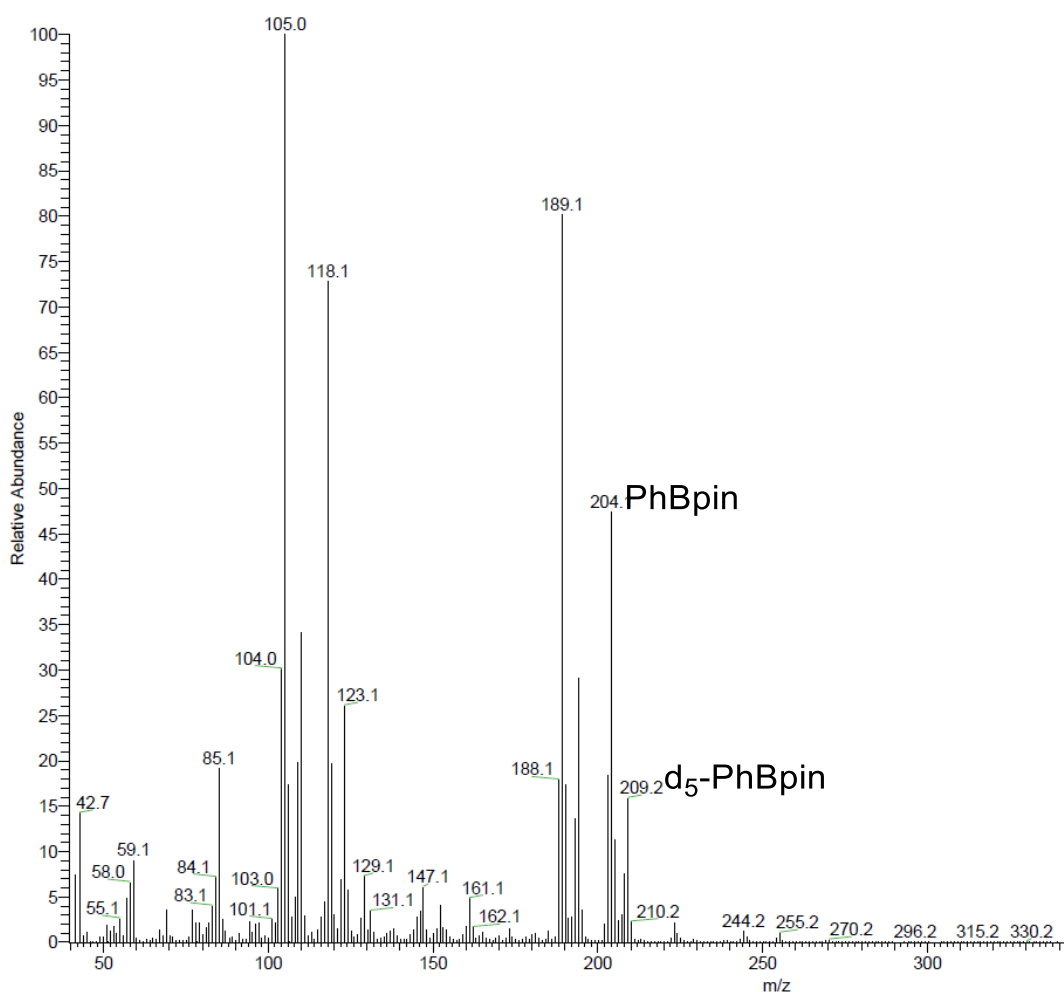


Figure 3.2: Mass spectrum (EI) for the borylation of C_6H_6/C_6D_6 with **2.6**.

In the low field region of the 1H NMR spectrum, two resonances were observed: a broad doublet at -16.88 ppm ($J \approx 38$ Hz) and a sharp doublet at -18.66 ppm ($J = 40.3$ Hz). The broad resonance is most likely a Rh boryl hydride (**Figure 3.3**), as the presence of quadrupolar B typically leads to broad resonances. Related literature comparisons include $[Rh(Cp^*)(H)_2(Bpin)_2]$ and $[Rh(Cp^*)(H)(Bpin)_3]$ which have resonances at -11.9 ppm ($J = 40.5$ Hz) and -11.3 ppm ($J = 39.0$ Hz) respectively.^{22, 158} The sharper resonance could be a Rh phenyl hydride species as it is similar in terms of chemical shift and J-coupling to resonances observed for reactions with silanes that produced Rh silyl hydride species, but obviously do not match any of those that were observed. Attempts at further characterisation of the phenyl hydride in the reaction mixture were hampered by its low concentration precluding useful ^{13}C NMR analysis.

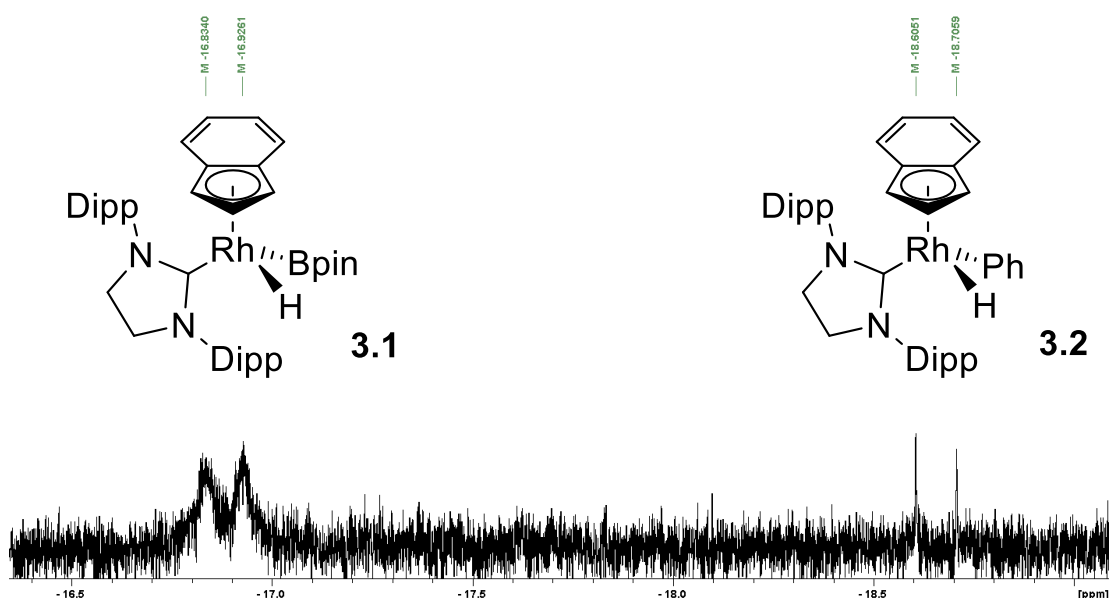


Figure 3.3: Low-field region of the ^1H NMR spectrum in a reaction between B_2pin_2 and **2.5**, including possible assignments.

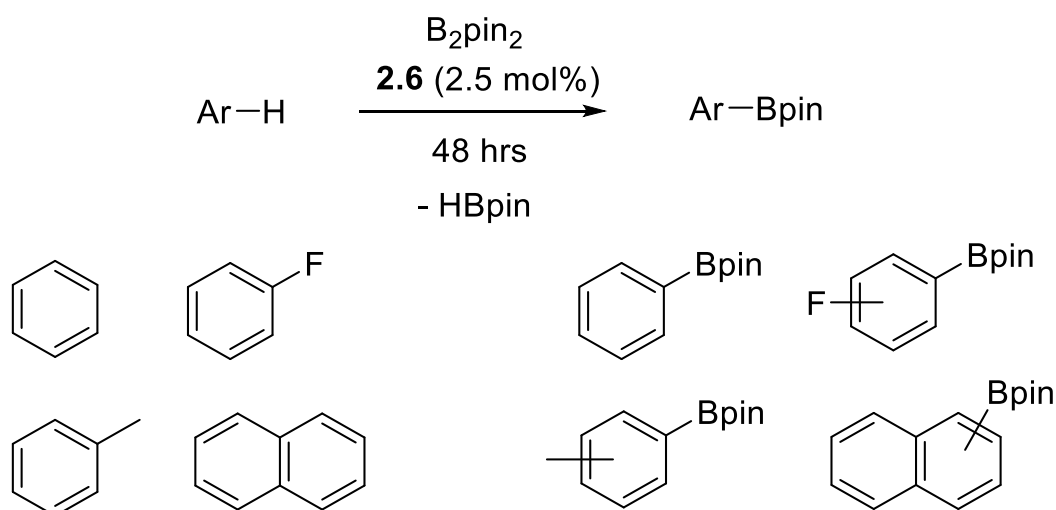
Reactivity of complexes **2.5** and **2.6** were found to be similar with the final conversions being within experimental error (**Table 3.1**). Complex **2.7**, however, showed no conversion, even with extended heating, and the reaction mixture remained the same colour throughout. This suggests that either CO is too strongly bound to Rh or the loss of the alkenes is facilitated by reaction with B_2pin_2 , which could borylate the alkene and prevent it from re-associating to the metal centre. It also shows the relative thermal stability of **2.7** as it does not show signs of degradation even in the presence of a reactive substrate. For convenience of scale, 5 mol% of the complex with respect to B_2pin_2 was used. Conversions to greater than 90% within 24 hours were deemed acceptable at the catalyst loading used. To compare the effects from the presence of the NHC, $[\text{Rh}(\text{Ind})(\text{COE})_2]$ was also tested, and was found to be competent at the borylation of benzene, however, it took significantly longer at greater than 40 hrs to achieve similar conversions. Thus it suggests that the presence of the NHC ligand is important for the active Rh species in solution. Additionally, in ^1H NMR spectra from the borylation reactions of $[\text{Rh}(\text{Ind})(\text{COE})_2]$, a broad doublet was observed at -13.96 ppm ($J = 34.6$ Hz), which is different from the resonances observed for **2.6** demonstrating that a different intermediate was formed.

Table 3.1: Conversion of benzene to phenylboronic acid pinacol ester by complexes **2.5** – **2.7** in NMR scale reactions.

Complex (L)	Temperature / °C	Time / hrs	Conversion / % ^a
2.5 (C ₂ H ₄)	80	24	93
2.6 (COE)	80	24	97
2.7 (CO)	80	48	0
[Rh(Ind)(COE) ₂]	80	40	90

^a Conversion based upon integration of the CH₃ resonances in ¹H NMR spectra.

Complex **2.6** was chosen for the scaled-up reactions with a number of different arene substrates (**Scheme 3.3**). This was because the synthesis of **2.6** was found to be more reliable and gave higher yields than that of **2.5**. Due to the increase in scale, a reduction in catalyst loading was conducted to test the effectiveness of reduced catalytic loadings upon conversion and yields, which was not practical on the smaller NMR scale. As was observed for the NMR scale reactions, the reaction mixtures darken upon heating with the mixture being essentially black within 10 mins.



Scheme 3.3: Preparative-scale borylation of arenes with **2.6**.

Using benzene as the substrate gave good conversions and yields (81%) within the reaction time when 2.5 mol% of **2.6** was used at 80 °C (**Table 3.2**). When using 1 mol%,

a reduced yield of 40% was observed for the same reaction time and temperature. Thus, catalytic loadings of 2.5 mol% were used going forward to allow good yields in reasonable timescales. When $[\text{Rh}(\text{Ind})(\text{COE})_2]$ (2.5 mol%) was used instead on a preparative scale, a yield of 38% was obtained after 48 hrs at 80 °C, which further proves the benefit of the addition of the NHC. Toluene was found to require higher reaction temperatures of 110 °C as opposed to 80 °C for benzene. Clearly, an electron-donating substituent does not increase the reactivity of the substrate. Product selectivity favours the meta isomer with a distribution of ortho:meta:para isomers being 1:14.2:6.0 (based upon integration of the tolyl methyl group). The ortho isomer is usually disfavoured due to sterics while there are two meta positions to one para, so the distribution is mostly statistical in nature with little additional selectivity.

Fluorobenzene gave good conversions by ^1H NMR spectroscopy; however, isolated yields were reduced (33%), which was observed on repeated occasions and thus suggests possible instability during the purification with column chromatography. The product selectivity in the crude mixture showed a slight preference for the meta isomer with a o:m:p ratio of 4.8:5.3:1 (based upon integration of ^{19}F resonances with the identity of the resonances determined by *J*-coupling pattern), which also means that compared to toluene, the ortho:para ratio has switched around. The meta position would be the most electron-poor position suggesting that the reaction may favour electron-deficient substrates. Additionally, fluorine is significantly smaller than a methyl group, approximately the size of hydrogen atom thus the ortho position is no longer disfavoured due to steric interactions. Naphthalene was observed to have a lower conversion and a lower isolated yield as well (38%), with the 2-isomer being the favoured product in a ratio of 14.6:1 over the 1-isomer, which would be the more sterically encumbered position. The lower conversion may be explained by the tendency for naphthalene to sublime up the side of the reaction flask, causing issues with reaction mixing.

Table 3.2: Borylation of a range of arenes with B₂pin₂ catalysed by **2.6**.

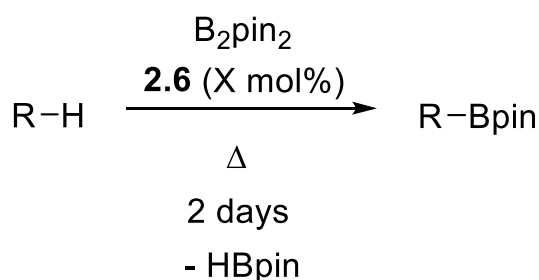
Arene	Temperature / °C	Conversion / % ^a	Isolated yield / % ^b
C ₆ H ₆	80	95	81
Toluene	80	87	54
Toluene	110	95	76
PhF	80	95	33
Naphthalene	80	79	38

^a Conversion based upon integration of CH₃ resonances in ¹H NMR spectra; ^b isolated yields are based upon conversion of B₂pin₂ into one equivalent of product.

In comparison to literature examples it appears that catalysis with **2.6** is slower than that observed for [Rh(Cp*)(η⁴-C₆Me₆)] (92% after 2.5 hrs at 2 mol%), but faster than that observed for [Ir(Cp*)(PMe₃)(H)(Bpin)] for the borylation of benzene (53% after 120 hrs at 20 mol%).²⁴⁹ Using the conversions determined by ¹H NMR spectroscopy, the turnover number (TON) for **2.6** was 38.0 while the turnover frequency (TOF) was 0.79 hr⁻¹. [Rh(Cp*)(η⁴-C₆Me₆)] has a TON for benzene of 46 with the TOF being 18.4 hr⁻¹, while [Ir(Cp*)(PMe₃)(H)(Bpin)] has a TON for benzene of **2.7** with the TOF being 0.02 hr⁻¹. For 0.5[Ir(COD)OMe]₂/bpy, a TON of 16.7 was observed with a TOF of 4.2 hr⁻¹. For toluene, **2.6** gave a similar yield to [Rh(Cp*)(η⁴-C₆Me₆)] but is slower (48 hrs against 3.5 hrs). Isomer selectivity is broadly the same, although the meta/para ratio is slightly greater for **2.6** at 2.4 compared to 1.83 and 1.93 for the Cp*Ir and Cp*Rh complexes respectively. Other Ir-based complexes such as [{Ir(COE)₂Cl}₂] or [Ir(Bpin)₃(η⁶-mes)] with the addition of bipyridine ligands give catalytic systems that could achieve good yields at room temperature.^{247, 250} From the TON and TOF values, it is clear that arene borylation catalysis with **2.6** is behind that of the state-of-the-art systems. However, it is noted that the borylation of arenes is considerably more favourable than other substrates for most catalytic systems.

3.3 Borylation of alkanes

Following the successful use of **2.6** in the borylation of arenes, it was decided to investigate **2.6** as a catalyst for the borylation of alkanes. As alkanes are generally more difficult to borylate than arenes, it was likely that more forcing conditions would be required to enable these reactions to precede in a timely manner. Thus, octane and decane were chosen as their relatively high boiling points (125 °C and 174 °C, respectively) would enable more forcing conditions to be used (**Scheme 3.4**) while not posing risks of overheating lower-chain alkanes such as pentane or hexane.



Scheme 3.4: Borylation of alkanes.

Initial attempts at the catalytic borylation of alkanes with **2.6** and B₂pin₂ showed that the reaction was possible with **2.6** as the catalyst, but required higher temperatures and an increase in catalyst loading (**Table 3.3**). Borylation of decane with 2.5 mol% **2.6** and at 120 °C gave no isolated product with the crude reaction mixture showing mostly B₂pin₂ in the ¹H NMR spectrum. Increasing the catalyst loading and temperature gave the expected products, however, the yields were relatively low. The products were obtained after column chromatography with CH₂Cl₂ (**Figure 3.5** and **Figure 3.5**). The most distinctive resonances other than the pinacol-derived singlet from the Me groups are the two triplet resonances that occur around 0.8 ppm, which correspond to the terminal CH₃ and the CH₂ group attached to the Bpin substituent. The other CH₂ resonances overlap and display more complex coupling patterns. Additionally, high-resolution mass spectra were obtained for both crude reaction mixtures that show decylBpin and octylBpin as the most prominent signals (**Figure 3.6** and **Figure 3.7**).

Table 3.3: Borylation of alkanes using **2.6**.

Alkane (R =)	Catalysis loading/ mol%	Temperature/ °C	Isolated yield/%
Decane (Decyl)	2.5	120	N/A
	10	150	18
Octane (Octyl)	5	130	7

Isolated yields are based upon use of B₂pin₂, and are after purification with column chromatography.

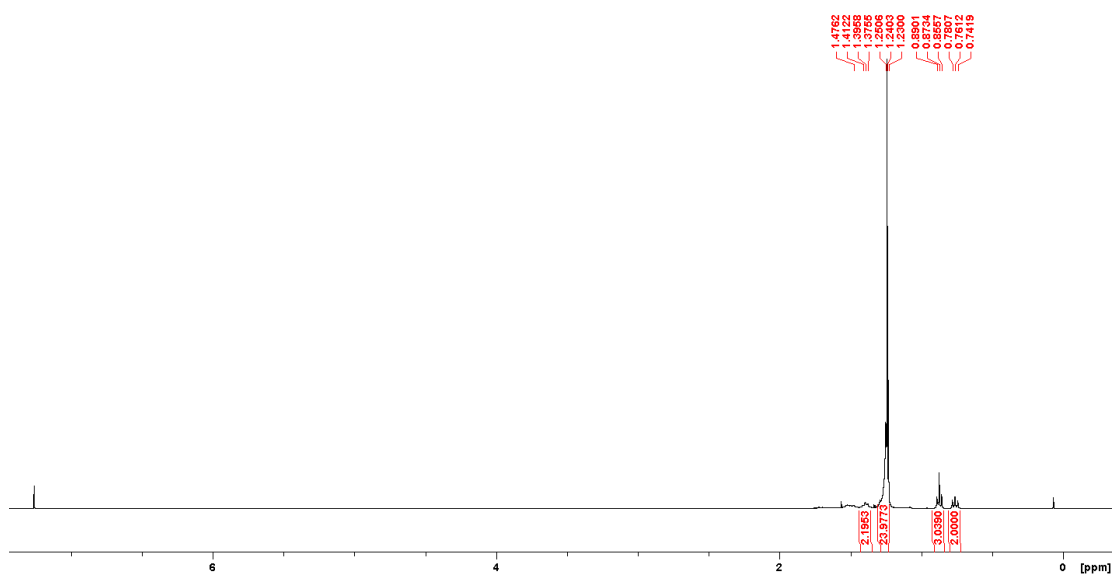


Figure 3.4: ¹H NMR spectrum of decylBpin obtained after purification.

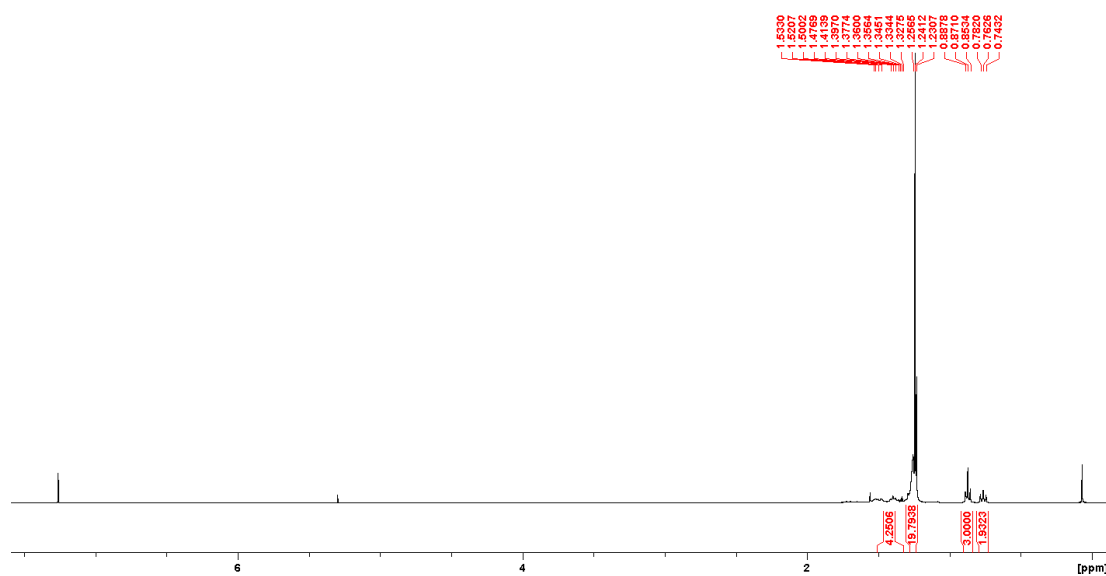


Figure 3.5: ^1H NMR spectrum of octylBpin obtained after purification.

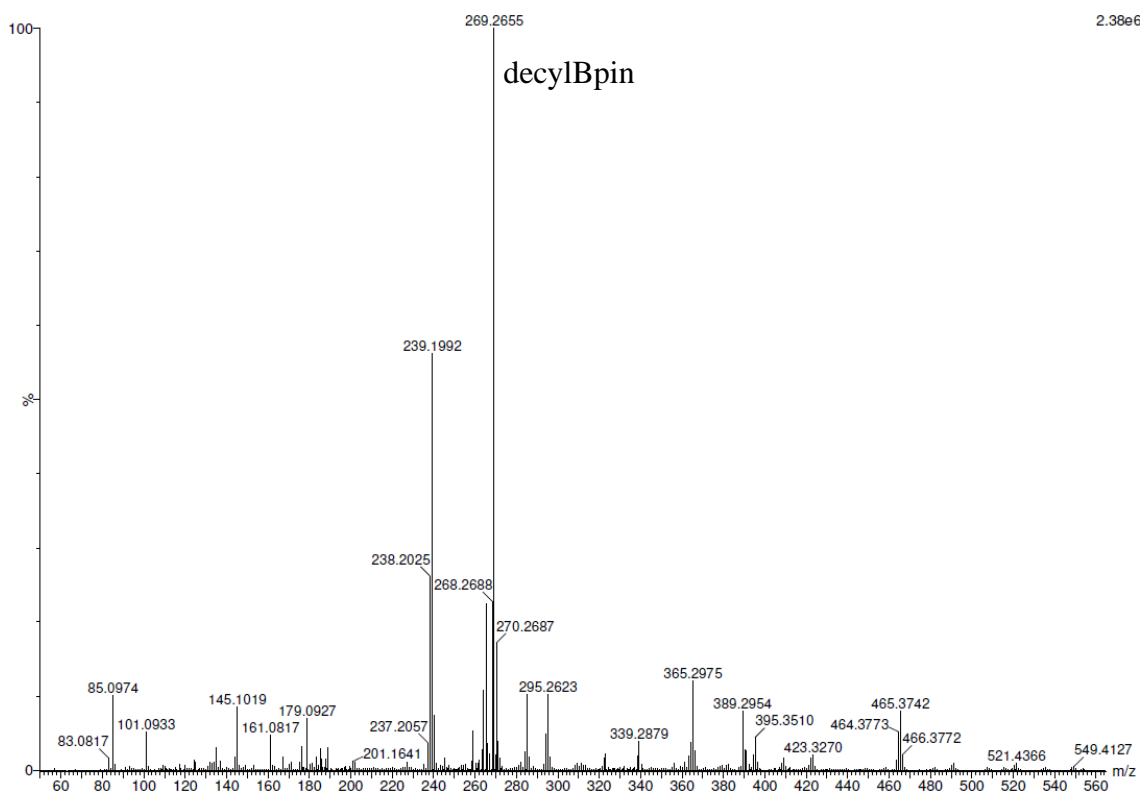


Figure 3.6: Mass spectrum for the crude reaction mixture of the borylation of decane with B_2pin_2 .

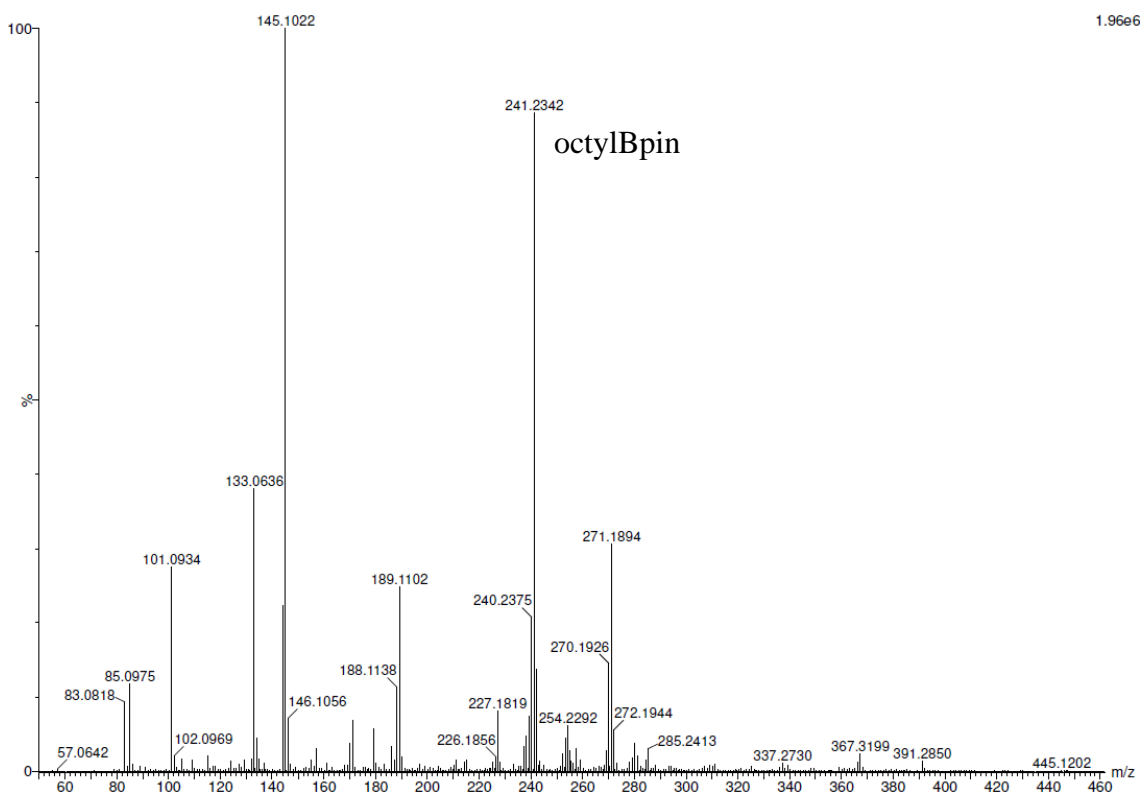


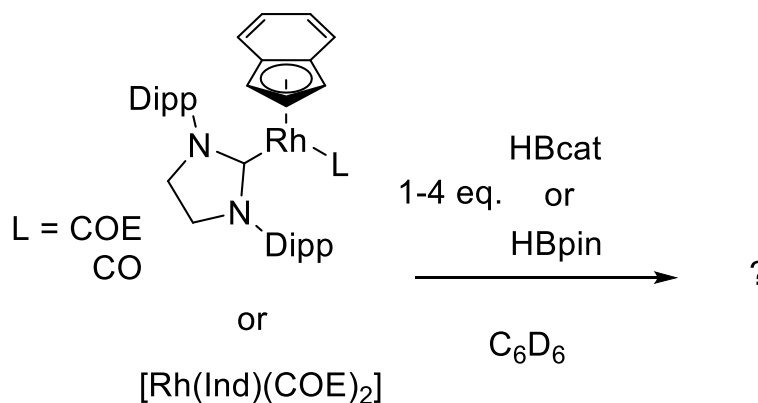
Figure 3.7: Mass spectrum for the crude reaction mixture of the borylation of octane with B_2pin_2 .

These are very promising initial results for what is considered to be a very difficult reaction to achieve. Further optimisation of these reactions is required, with increased reaction time one possible improvement, or investigation of modified catalysts. It should be noted that currently there are only eight catalysts described in the literature,^{22, 73-76} and these have been shown to require forcing conditions to enable borylation of alkanes temperatures above 150 °C typically required for yields greater than 50% compared to reaction temperatures of 150 °C or less used in this work. The reaction time falls into the range observed in the literature of between 5 hours and 10 days. Thus, even these modest results are encouraging as they indicate that the complexes can perform the catalytic borylation of alkanes which has proven to be a challenging transformation.

3.4 Stoichiometric reactions

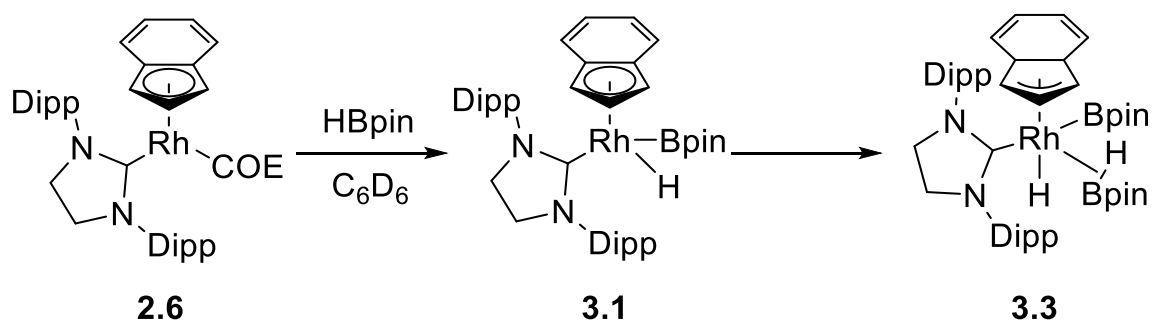
To further probe the nature of the intermediates in these catalytic borylation reactions, a series of small-scale NMR reactions were trialled with HBcat and HBpin to see any similarities and differences with the species observed in the catalytic reaction mixtures (**Scheme 3.5**). These were chosen as stoichiometric reactions with B_2pin_2 did not lead to

better or clearer spectra compared to direct spectroscopic analysis of the catalytic reactions mixtures. Additionally, HBpin has been used in literature examples of C-H borylation and there are many similarities between reaction intermediates generated with B₂Pin₂ and HBpin, even if the exact products are different.²²



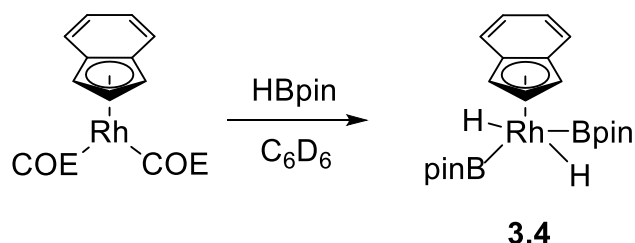
Scheme 3.5: Stoichiometric NMR-scale reactions.

Addition of HBpin to **2.6** initially, upon heating at 50 °C, gives rise to four hydridic resonances: a broad doublet at -15.09 ppm ($J \approx 42$ Hz) (*c.f.* the catalytic reaction which showed a broad doublet at -16.88 ppm, $J \approx 38$ Hz), a doublet at -15.95 ppm ($J = 50.7$ Hz) that matches the resonance observed for the tentative Rh dihydride **2.14**, a doublet at -16.75 ppm ($J = 35.7$ Hz) and a doublet at -18.65 ppm ($J = 40.6$ Hz) that was the same resonance as observed in the catalytic reactions. The broad doublet is at a notably different chemical shift when compared to the broad resonance observed in the catalytic reactions, and is thus clearly from a different species, but has similar J -coupling and shape. One possibility is that one of the species has more than one H-Bpin units. In the literature, [Rh(Cp*)(H)₂(Bpin)₂] and [Rh(Cp*)(H)(Bpin)₃] have very similar ¹H chemical shifts and J -couplings.²² Another possibility is a complex where the indenyl ligand has ring slipped and generated a vacant coordination site in which HBpin could coordinate in an η^2 -coordination mode (**Scheme 3.6**). The resonance at -15.09 ppm disappears over time and a resonance at -16.88 ppm appears with the same J -coupling as the resonance observed for the in-situ catalytic reactions. This growth is more pronounced with increasing equivalents of HBpin which supports the suggestion that it corresponds to a multi-boryl species.



Scheme 3.6: Reaction between **2.6** and HBpin and potential products.

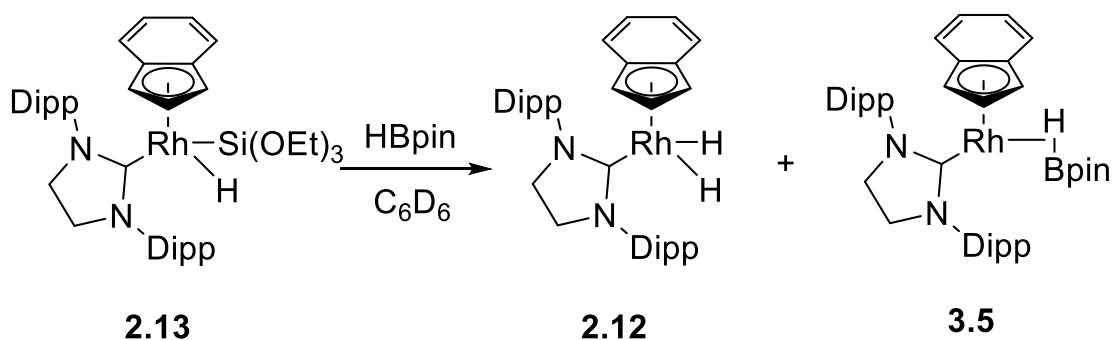
Addition of HBpin to $[Rh(Ind)(COE)_2]$ led to the slow formation of a broad doublet at -13.96 ppm, which is the same as from the NMR scale borylation of benzene with $[Rh(Ind)(COE)_2]$ and B_2pin_2 (**Scheme 3.7**). This could be the Rh(V) complex **3.4** (alternatively described as a Rh(III) σ -complex) due to the aforementioned similar chemical shift and J -coupling to those observed for $[Rh(Cp^*)(H)_2(Bpin)_2]$ and $[Rh(Cp^*)(H)(Bpin)_3]$. The σ -complex description has been suggested to be more accurate for $[Rh(Cp^*)(H)_2(Bpin)_2]$ and $[Rh(Cp^*)(H)(Bpin)_3]$ due to the presence of short B-H distances in the X-ray determined structure and computational studies showing the relative ease of interconversion.²²



Scheme 3.7: Reaction of $[Rh(Ind)(COE)_2]$ and HBpin.

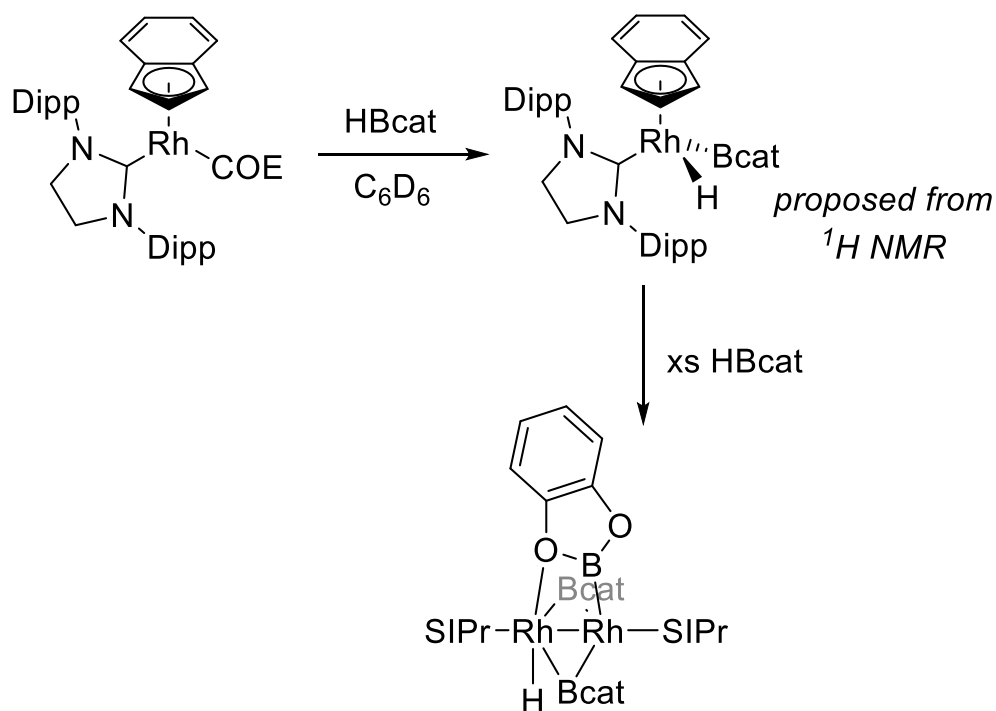
An additional test was the reaction of **2.16** with HBpin to see if any of the proposed intermediates were formed, as the reaction of HBpin at the Rh(III) species may occur more readily than the reactions with the Rh(I) alkenes which were characterised to be quite slow. After 2 hrs at 75 °C, **2.13** was no longer present with hydridic 1H NMR resonances present at -5.12 (d, $J = 22.2$ Hz), -15.88 (d, $J = 50.7$ Hz) and -15.94 (d, $J = 50.4$ Hz). The latter would appear to be the Rh dihydride species **2.14**, which was observed for other silane reactions but not for $(EtO)_3SiH$. The resonance at -5.12 ppm is

in the region where proposed σ -complexes of silanes and boranes occur, thus the proposed structure for this resonance is borane complex **3.5** (**Scheme 3.8**).



Scheme 3.8: Reaction of **2.13** with HBpin and the proposed products.

Upon addition of HBcat to **2.6** at room temperature, a hydridic species in the ^1H NMR spectrum was observed at -14.84 ppm with 40.1 Hz J -coupling. This resonance is broad in nature, but sharpens when a ^{11}B proton-decoupled NMR spectrum is recorded, which suggests the product contains a Rh boryl hydride. Due to the similar chemical shift when compared to **2.13**, and the presence of indenyl peaks of the correct integrals, the proposed structure is the oxidative addition product **3.6** (**Scheme 3.9**). The reaction is complete after 5 hours at room temperature, as judged by ^1H NMR spectroscopy. In the ^{11}B NMR spectrum, a broad resonance was observed at 43.9 ppm, which is consistent with a metal boryl species; resonances at 40.4 and 39.9 ppm were observed for $[\text{Rh}(\text{Cp}^*)(\text{H})_2(\text{Bpin})_2]$ and $[\text{Rh}(\text{Cp}^*)(\text{H})(\text{Bpin})_3]$ respectively.²² An additional resonance at 36.2 ppm was observed, which is in the region for alkyl boranes suggesting that this resonance arises from cyclooctylcatecholborane formed from the borylation of COE. Attempts to crystallise **3.6** from benzene/pet ether led to the isolation of crystals of **3.7** instead, likely to be a degradation product. The crystals obtained were suitable for X-ray diffraction (**Figure 3.8**).



Scheme 3.9: Reaction between **2.6** and HBcat, with the proposed oxidative addition product **3.6** and the isolated dirhodium complex **3.7**.

The compound contains two Rh atoms joined by a Rh-Rh bond. The SIPr ligands are still present as terminal ligands to each of the Rh centres, but the indenyl ligands have been lost and been replaced with three Bcat units, two of which are bridging via the B atom. The other Bcat ligand bridges the two Rh via the B atom to one centre and an O atom to the other. The Rh-Rh distance is shorter than that observed in **2.8**, at 2.6824(8) compared to 2.6947(5) Å. The formal oxidation states would both be Rh(II). The two Rh-NHC distances are identical within error, Rh(1)-C(1) 2.069(2) and Rh(2)-C(28) 2.073(2) Å, and are longer than those observed for the half-sandwich complexes **2.5** – **2.7** & **2.16** and the square planar complex **2.10**. The Rh-H distance of 1.31(4) Å is shorter than that observed for **2.13** (1.45(3) Å). The Rh-B distances for B(1) are the same within error {Rh(1)-B(1) 2.082(3) Å and Rh(2)-B(1) 2.079(3) Å}, while B(2) has Rh distances of 2.060(3) Å and 2.098(3) Å respectively, thus showing a noticeable difference.

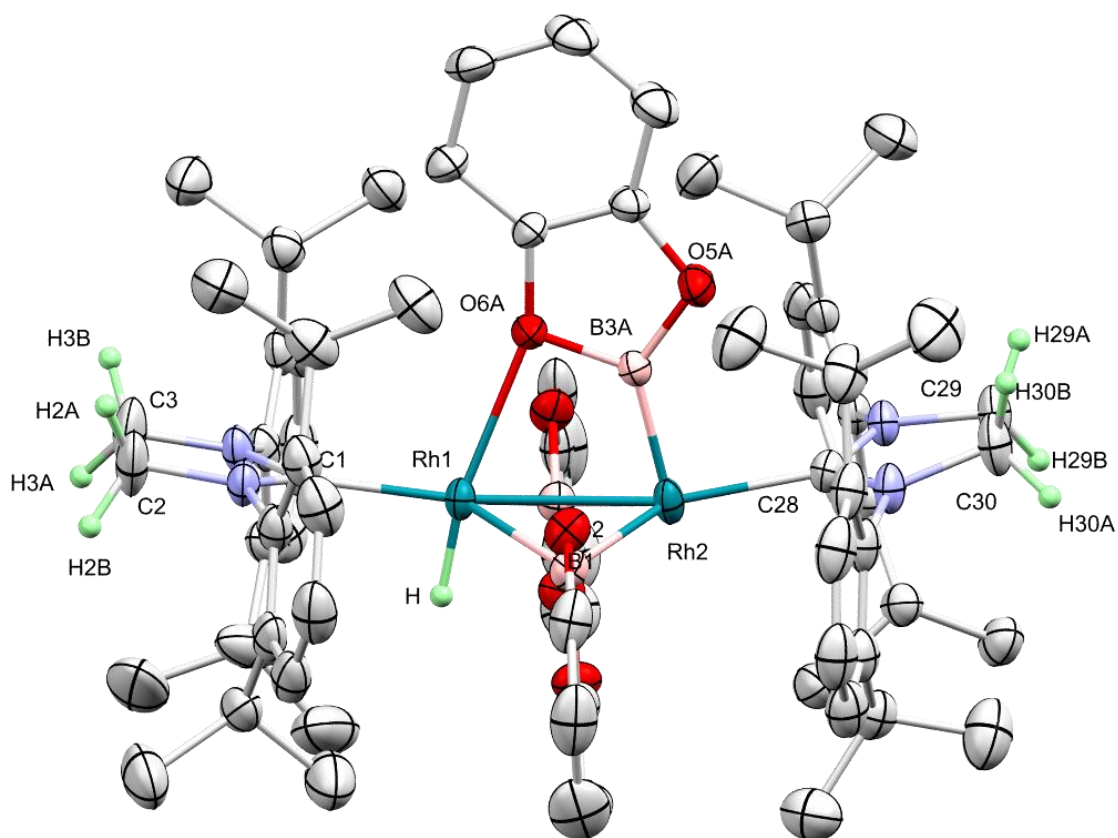


Figure 3.8: X-ray determined structure for Rh boryl hydride complex **3.7** (thermal ellipsoids at 50%). All H atoms except for the hydride and NHC backbone have been removed for clarity in addition to a benzene solvate molecule.

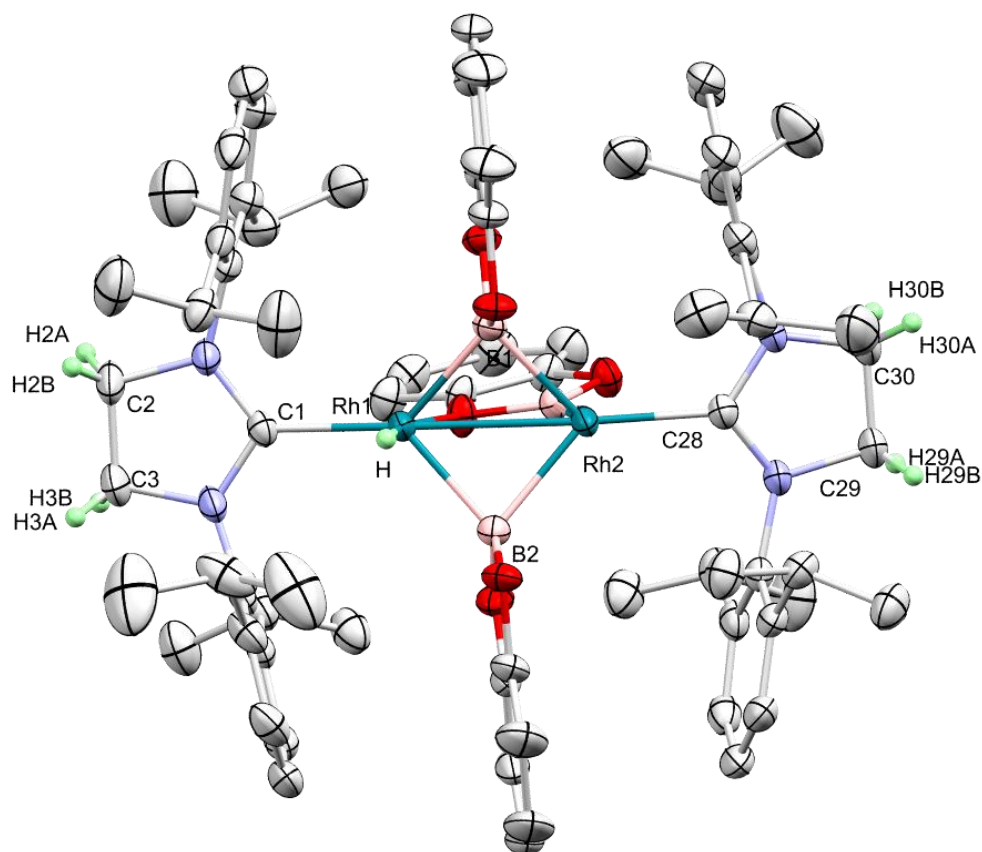


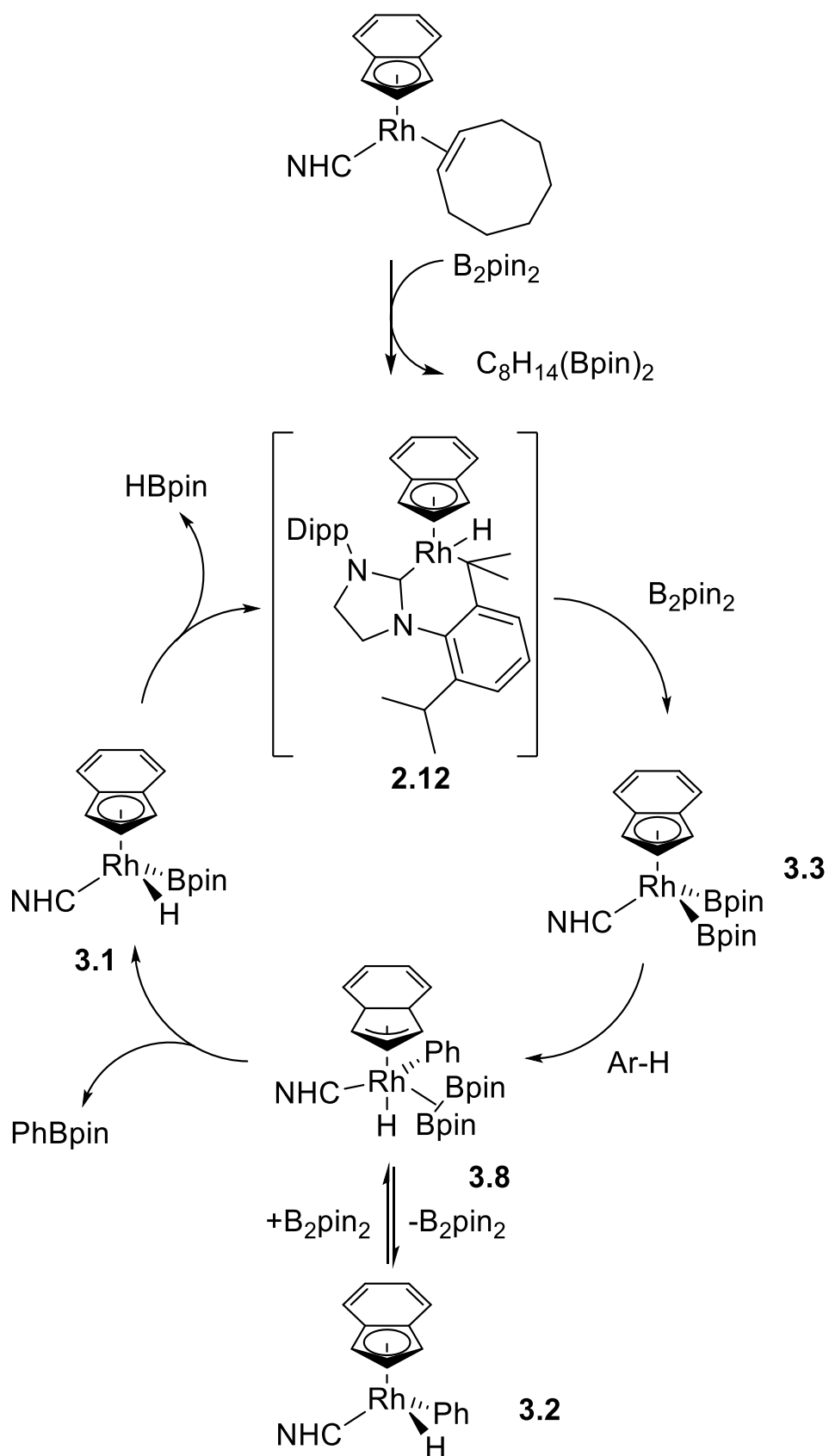
Figure 3.9: Alternative view of **3.7** showing the bridging boryl groups.

No reaction was observed between **2.7** and HBpin, even upon heating at 80 °C, which fits for the low reactivity observed for **2.7** (**Chapter 2**) and HBpin being less reactive than HBcat. Reaction of **2.7** with HBcat, with heating, leads to the formation of a new species, which has a triplet resonance at -9.52 ppm ($J = 20$ Hz) in the ^1H NMR spectrum. Resonances in this region are typically associated with metal σ -borane complexes,²⁵¹ and thus is similar to reactions with silanes (**Chapter 2**). However, it cannot be the simple oxidative addition product due to the resonance being a triplet as only a doublet would be expected, and is different from what was observed for the reaction between **2.6** and HBcat. Upon further heating, the initially observed resonance decreased in intensity and further resonances appeared at -8.96 ppm (t, $J = 34.8$ Hz) and -12.94 ppm (t, $J = 22.0$ Hz). The different J -coupling suggests that these are all different species which are all likely to be Rh boryl hydride complexes. There are indenyl resonances which grow in along with the hydridic resonances suggesting that indenyl is present in (at least some of) the products, however, low overall conversion means that distinguishing the new resonances are difficult due to the presence of starting material resonances. The triplet nature of these resonances suggests that two rhodiums are present with either both Rh equivalent or

similar in nature to give an apparent triplet. A possibility could be a species similar in nature to **3.6**, however, this requires further work.

3.5 Potential catalytic cycle

The mechanism by which borylation with **2.6** occurs could have a number of variations (**Scheme 3.10**). As can be seen from differences between the catalytic borylation of benzene with **2.6** compared to $[\text{Rh}(\text{Ind})(\text{COE})_2]$, the NHC is likely to still be coordinated and play a role in the active species in solution, and thus is unlikely to be lost as part of the mechanism. As metallacycle **2.12** was a favoured shared intermediate in photolysis reactions and reactions with H_2 and silanes, it is likely that this species is involved in the borylation process. The coordinated alkene could react with B_2pin_2 , forming a 1,2-diboronic ester, which can no longer coordinate to Rh. Given the ease of formation of **2.12**, it is unlikely that the addition of the isopropyl C-H would be the rate-determining step, which agrees with the observed lack of KIE though further studies would be required to probe this in detail. The indenyl can undergo ring-slippage from η^5 to η^3 , creating a vacant coordination site on the Rh for substrates to coordinate and react. The mechanism proposed has the active species as Rh(III) which undergoes σ -CAM-type reactions with arenes and diboranes to lead to the borylation of benzene. Thus, this mechanism does not invoke the presence of Rh(V). The proposed **3.1** is an intermediate in this cycle, and while **3.2** is not, it could be an off-cycle product from the dissociation of B_2pin_2 from **3.8**. Little isotopic scrambling was observed from the MS of the borylation of mixture of C_6H_6 and C_6D_6 . This suggests reaction of the solvent with **3.2** or **3.4** is disfavoured.



Scheme 3.10: Proposed catalytic cycle for the borylation of arenes with B_2pin_2 .

3.6 Conclusions

Complexes **2.5** and **2.6** have both been shown to be catalytically competent for the borylation of arenes in good to acceptable yields. The selectivity seems to be similar to literature complexes, while the conversion was comparable but rate of reaction slower than that previously reported for Cp**Rh* catalysts. Complex **2.6** was also shown to be able to borylate alkanes, which is a difficult reaction to perform. Comparison of ¹H NMR spectra for the catalysis reactions and stoichiometric reactions provide evidence that the intermediates are boryl hydride complexes.

Chapter 4: Fluorenyl-tethered NHC complexes

4.1 Introduction

The potential advantages of tethered ligand systems include possible increased stability due to the chelate effect, hemilability when one of the donors is weaker than the other, and changing the energy of various orbitals via geometric constraints.^{96, 252, 253} The hemilabile effect can be achieved if, for the π -aromatic donor, indenyl or fluorenyl is used as these have a propensity to ‘ring slip’, leading to vacant coordination sites. The ability to constrain the geometry and the frontier orbitals is related to the linker length between the two groups, with optimisation of the length required to match the desired metal complex geometry. Indenyl- and fluorenyl-tethered NHCs have been explored previously but these have so far been based on unsaturated NHCs.^{109, 163, 169, 254, 255} Catalysis with rhodium complexes has been limited to hydroformylation of 1-octene and the carbonylation of methanol,¹⁸¹ and these complexes have not been examined for C-H activation. Fluorenyl-, indenyl- and cyclopentadienyl-tethered systems with saturated NHCs have not been reported and thus require a new synthetic route. Saturated systems were chosen to match the work conducted with the monodentate systems. The targeted rhodium complexes have a range of variable groups (**Figure 4.1**), with different Cp-type donors potentially offering different reactivity. The oxidation state of rhodium could be changed from +1 to +3 which will also lead to different reactivity.

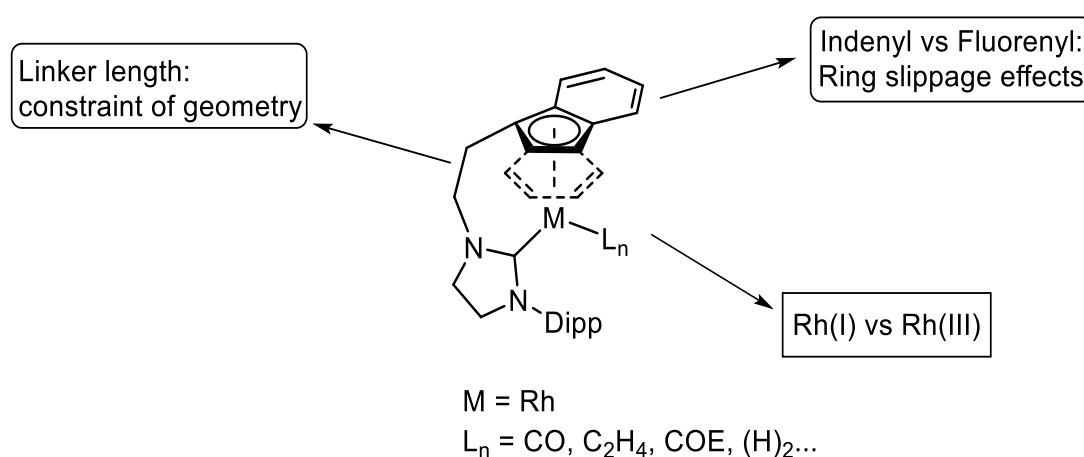
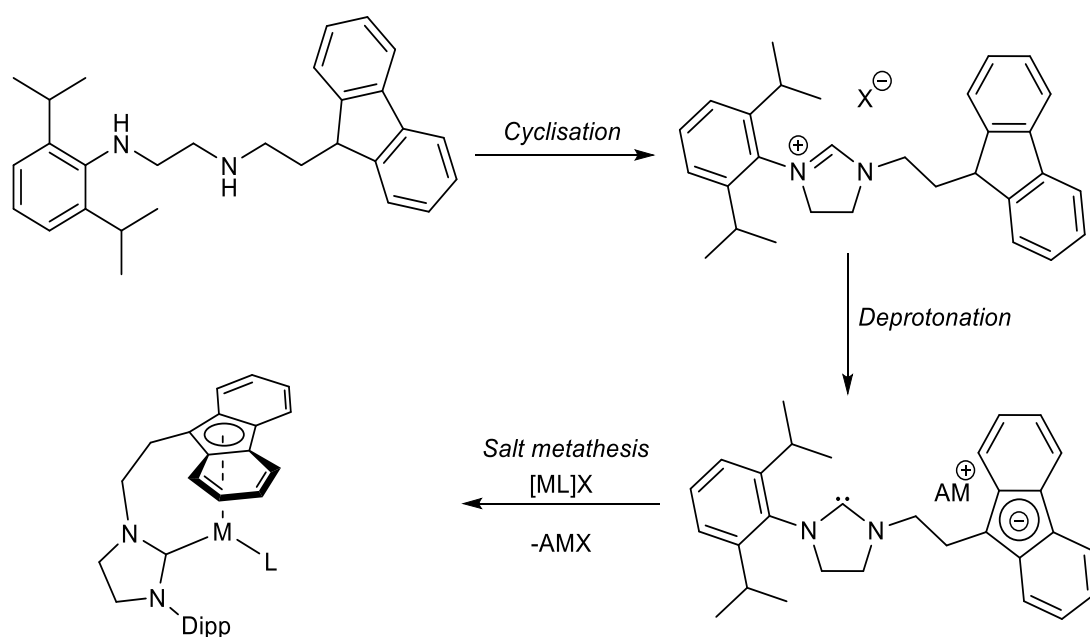


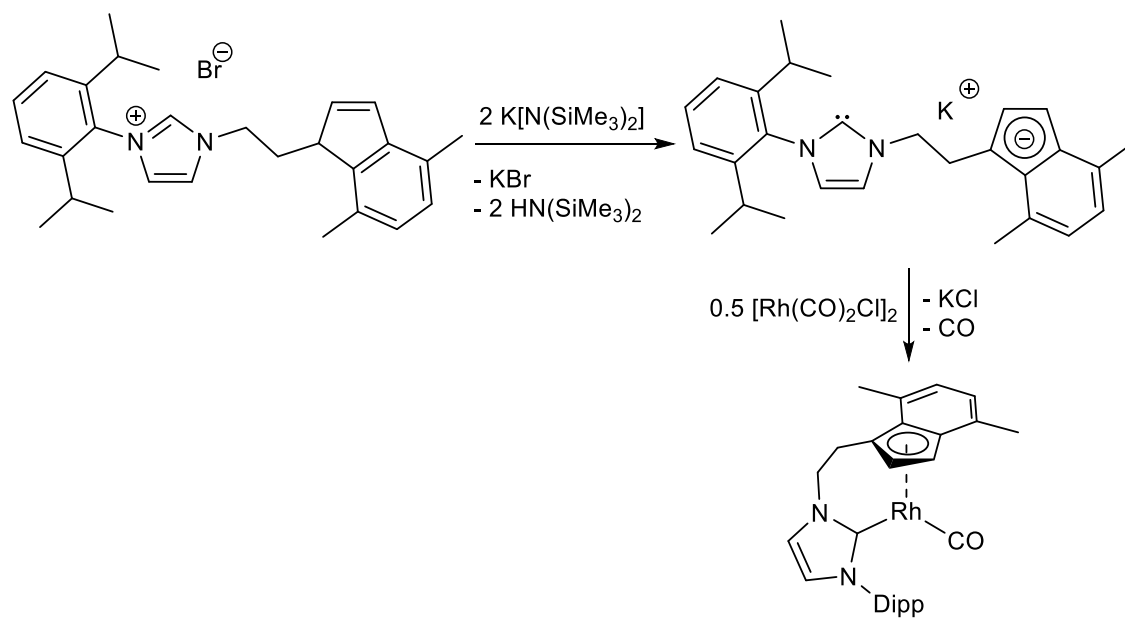
Figure 4.1: Tethered indenyl/fluorenyl-NHC complexes with important features highlighted.

Synthesis of the targeted pro-ligand required the synthesis of a substituted imidazolium salt and then its subsequent deprotonation to an NHC-tethered fluorenyl anion salt that can then be coordinated to transition metals (**Scheme 4.1**). Different methodologies have been developed for the synthesis of functionalised NHCs,^{122, 256} which depend heavily on the nature of the substitution, the stability of the different groups to the reaction conditions and whether saturated or unsaturated carbenes are desired. From previous work in the group on substituted N-heterocyclic stannylenes,²¹⁰ a shared intermediate (a diamino-substituted fluorene) was identified which could allow for access to a suitable imidazolium salt.



Scheme 4.1: Proposed synthetic pathway to tethered-NHC transition metal complexes. AM is an alkali metal, M is a transition metal and L is a suitable ligand such as COE, C_2H_4 or CO.

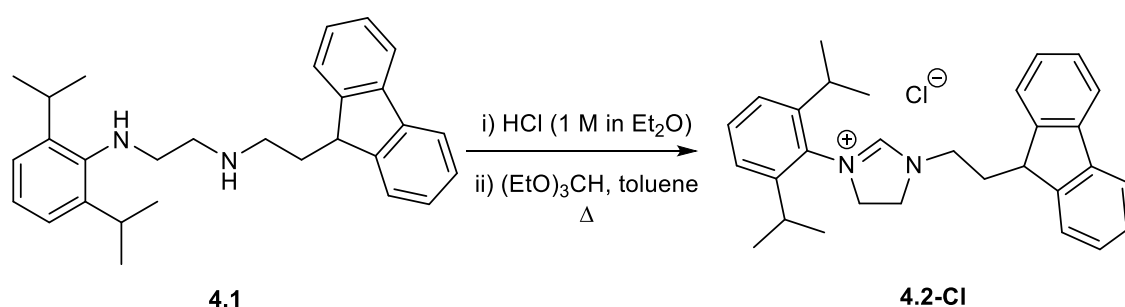
From the substituted imidazolium salt, double deprotonation to the alkali metal salt of a fluorenyl-tethered NHC was anticipated to occur in an analogous manner to the unsaturated complexes,¹⁶³ and then salt metathesis to the desired transition-metal fragment (**Scheme 4.2**).¹⁸¹ This would form the target tethered half-sandwich complex with several different co-ligands accessible which will change the reactivity of these complexes. The synthesis has additional advantages in that the N-substituent could be altered by using a different substituted aniline.



Scheme 4.2: Previously synthesised indenyl-tethered NHC Rh complexes by Danopoulos and co-workers.¹⁸¹

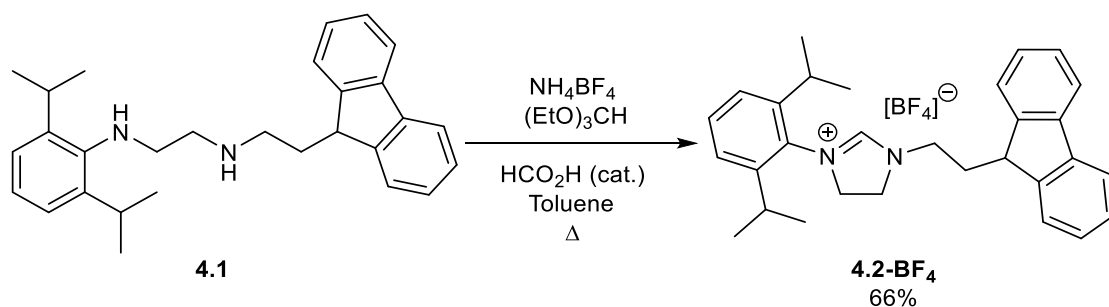
4.2 Synthesis of imidazolinium salts and spirocyclic compounds

Initially, the synthesis of the target imidazolinium salt with a chloride counterion was attempted (**Scheme 4.3**) from known diamine **4.1**²¹⁰ via orthoformate cyclisation with $(\text{EtO})_3\text{CH}$. While ^1H NMR spectroscopy of the crude reaction mixture indicated product formation based on the indicative downfield shift of the imidazolinium CH resonance at 9.38 ppm, the product was found to be very difficult to purify due to it being obtained as an oil. Attempts to precipitate the product or purify it by column chromatography were unsuccessful.



Scheme 4.3: Initial synthesis of imidazolinium salt **4.2-Cl**.

While counterion exchange for iodide did not aid purification, exchange for $[\text{BF}_4]^-$ obtained the product **4.2-BF₄** as a colourless crystalline solid after recrystallisation from either $\text{CH}_2\text{Cl}_2/\text{Et}_2\text{O}$ or $\text{MeCN}/\text{Et}_2\text{O}$. Of note is the 1.5 ppm chemical shift difference for the imidazolinium CH when changing the counterion from Cl^- to $[\text{BF}_4]^-$ (9.36 ppm and 7.80 ppm respectively), presumably indicating a reduced interaction between the counterion and imidazolinium moiety. The use of ^{19}F and ^{11}B NMR spectroscopy demonstrated that the product indeed featured the $[\text{BF}_4]^-$ counterion (-151.8 ppm and -1.17 ppm respectively). While synthesis of **4.2-BF₄** can be conducted via orthoformate cyclisation with HCl followed by counterion exchange on the crude product, it was found that **4.2-BF₄** could be directly synthesised from the diamine using orthoformate cyclisation with NH_4BF_4 , a readily available reagent that acts as both a proton and counterion source for the reaction (**Scheme 4.4**). This allowed a more expedient synthesis of imidazolinium salt **4.2-BF₄**.



Scheme 4.4: Improved synthesis of imidazolinium salt **4.2 BF₄**.

Single crystals of **4.2-BF₄** suitable for X-ray diffraction were grown from hot C₆H₆. They were exceedingly fine needles in habit, but utilising the National Crystallography Service at Southampton, data was acquired that confirmed the connectivity (**Figure 4.2**). Of note, there are short contacts between the imidazolinium H and the F atoms of the [BF₄]⁻, H16···F1 2.222 Å and H16···F2 2.548 Å. These interactions likely arise from [BF₄]⁻ acting as a hydrogen bond acceptor due to its weak Lewis acid properties, which has been observed in other systems.²⁵⁷⁻²⁵⁹

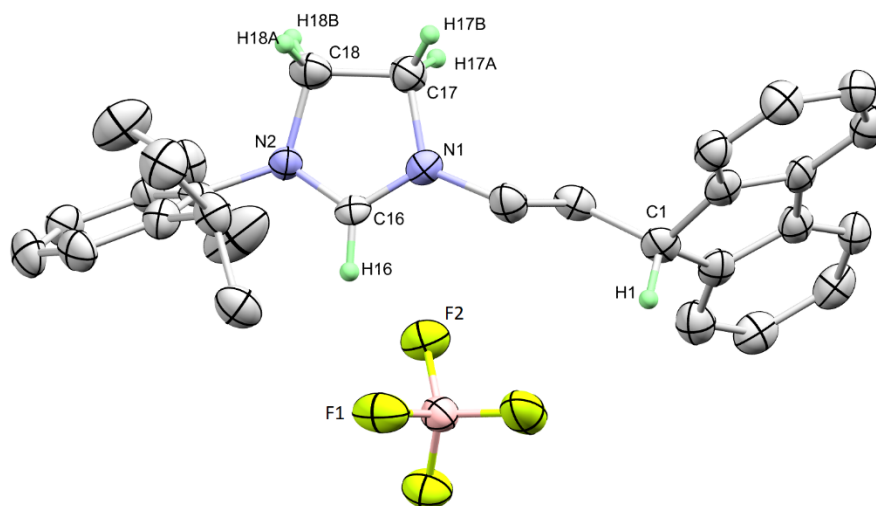
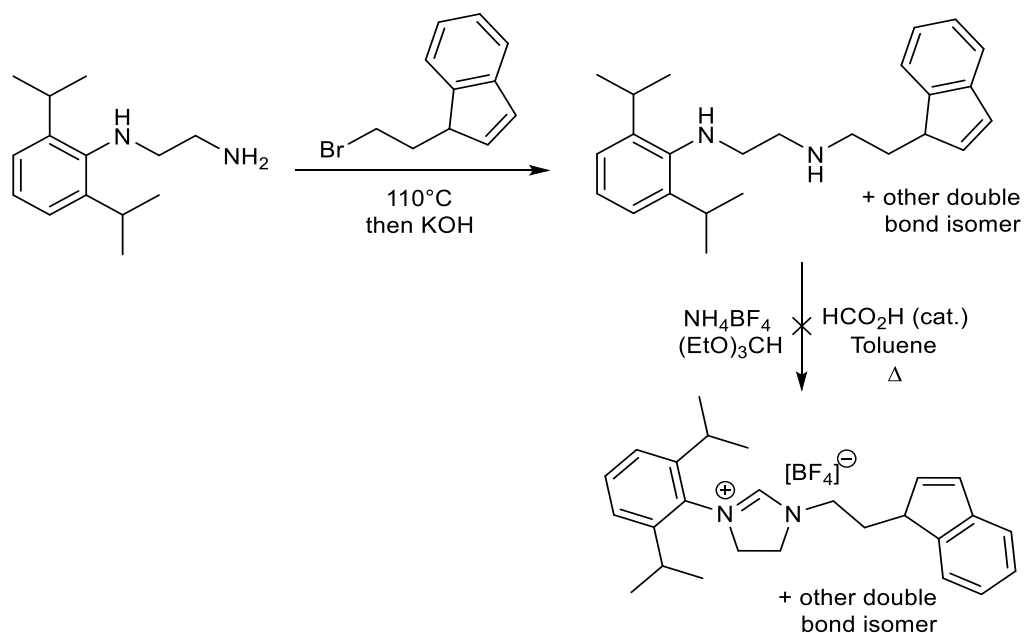


Figure 4.2: Molecular structure for **4.2-BF₄** (thermal ellipsoids at 50%). All H-atoms except for H1, H16, H17A/B and H18A/B have been omitted for clarity.

Attempts at synthesising the analogous indenyl imidazolinium salt were not as successful (**Scheme 4.5**). While the indenyl-substituted diamine could be synthesised by the addition of diamine and (bromoethyl)indene in satisfactory yield and purity according to

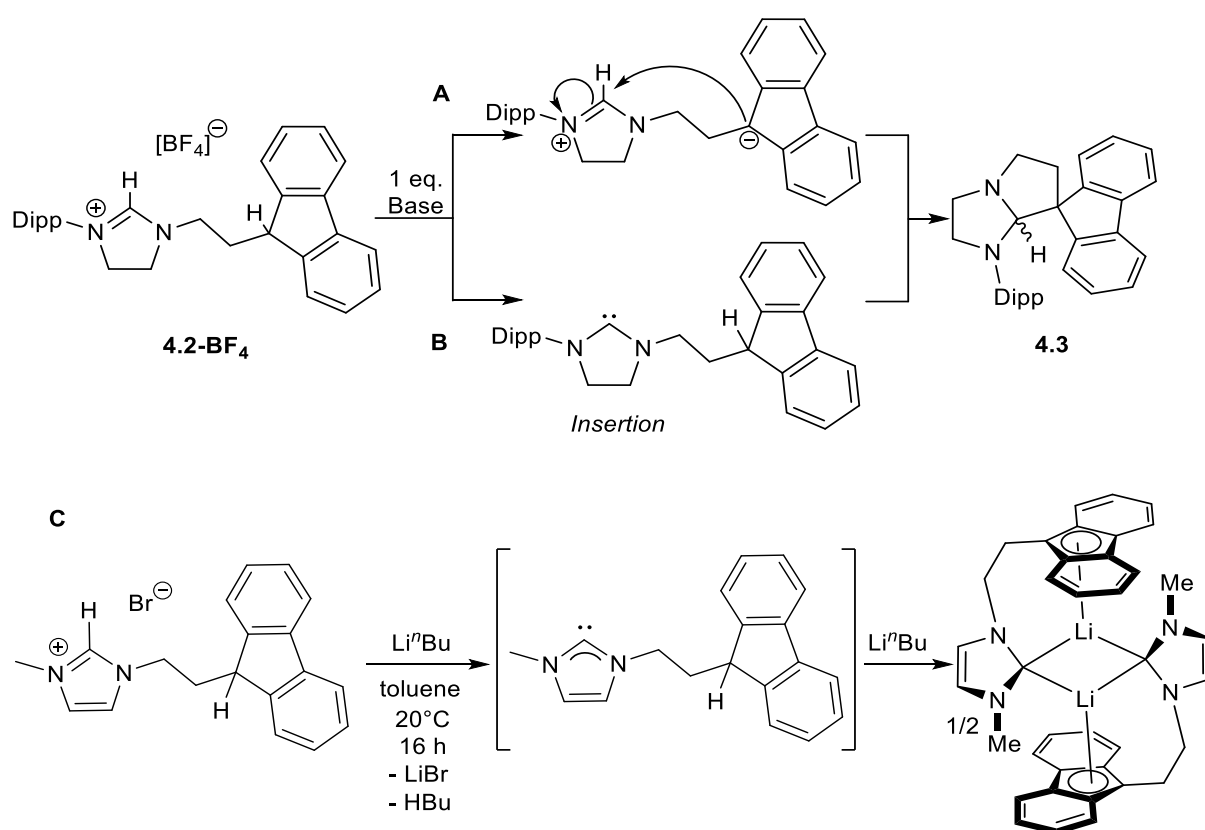
a previous synthesis,^{210, 260} the subsequent cyclisation step was not effective. From ¹⁹F and ¹¹B NMR spectroscopy, it was observed that a [BF₄]⁻ salt had been formed, however, it was not possible to purify this compound despite numerous attempts at crystallisation and column chromatography, with analysis additionally hampered by a mixture of double isomers in the indene moiety being present in both the starting material and the product. It was decided to focus work on **4.2** and its subsequent reactions.



Scheme 4.5: Attempted synthesis of indenyl-tethered NHC proligands.

Deprotonation of **4.2-BF₄** was found to generate the spirocyclic compound **4.3** (**Scheme 4.6**). This reactivity contrasts with the unsaturated analogues where sequential deprotonation occurs (**Scheme 4.6, C**),^{163, 261} but is similar to that observed in a synthetic route to a saturated alkoxy-carbene species.²⁶² This difference in reactivity could be explained from the increased electrophilicity/nucleophilicity of saturated NHCs compared to unsaturated ones due to higher HOMO and lower LUMO energies.²⁶³ Thus, saturated NHCs have an increased ability to donate electron density as well as accept it. The mechanism by which cyclisation occurs could either proceed via the deprotonation of the fluorene proton and then its nucleophilic attack onto the iminium carbon (**A**), or via deprotonation to form the NHC and subsequent carbene insertion into the C-H bond causing cyclisation (**B**). The relative pK_a of an alkylfluorene is ≈22 (in DMSO).²⁶⁴ Imidazolium salts (unsaturated NHC precursors) are typically 18-23 depending on substituents as electron rich imidazolium salts display higher pK_a values whereas electron

deficient species have lower values. N-Aryl imidazoliums are observed to have pK_a values in a similar range (19-22).²⁶⁵ It is likely that the imidazolium salt used here follows a similar pattern, thus it is possible that both the fluorene and the imidazolium moieties have similar pK_a values. It was observed that upon initial mixing the reaction mixture briefly turned orange-red in colour, which quickly disappeared, and a blue colour was also briefly observed, before the mixture turned colourless and the corresponding tetrafluoroborate salt precipitated out. The red-orange colour would be consistent with a fluorenyl anion as this is the colour observed when synthesising the precursors, suggesting that initial deprotonation occurs at the fluorene group.



Scheme 4.6: Formation of spirocycle **4.3** from the single deprotonation of **4.2-BF₄** via either deprotonation at the fluorenyl (pathway A) or deprotonation at the imidazolium (pathway B), compared to the double deprotonation of N-methyl imidazolium **C**.

The ¹H NMR spectrum for **4.3** is distinctive with the imidazoline CH being the only singlet (5.45 ppm in C₆D₆). The four methyl groups are inequivalent and the CH₂ resonances showing second order effects to give a complicated ¹H NMR spectrum. Crystallisation of **4.3** was achieved from a saturated pet ether solution and the molecular

structure is shown in **Figure 4.3** (**4.3** is highly soluble in most organic solvents due to the large amount of hydrophobic substituents). The molecular structure shows a spirocyclic species around C1 of the fluorene group. **4.3** is chiral, although both enantiomers are presumably formed in the reaction. Due to saturation, there is no delocalisation between the NCN unit and thus the atoms have tetrahedral sp^3 geometry. The formation of the stereogenic centre is interesting as it suggests that with indene-substituted imidazolium salts, a diastereomeric product would be formed which potentially would assist isolation as well as providing information about selectively and possible mechanism.

Optimisation of the deprotonation conditions with a range of bases identified $n\text{BuLi}$ as the optimum choice to remove LiBF_4 and butane conveniently, together with its ready availability (**Scheme 4.7**).

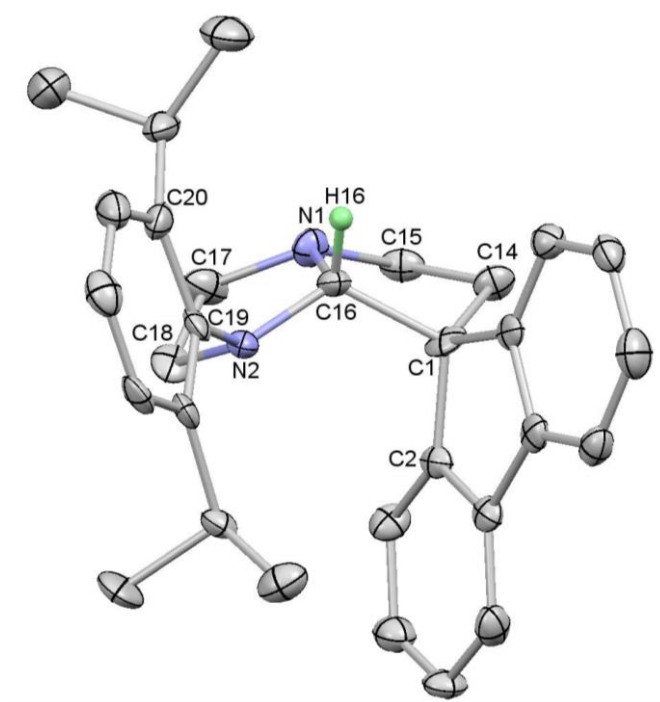
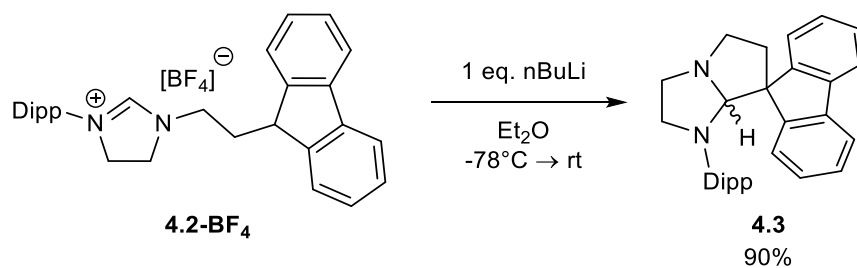
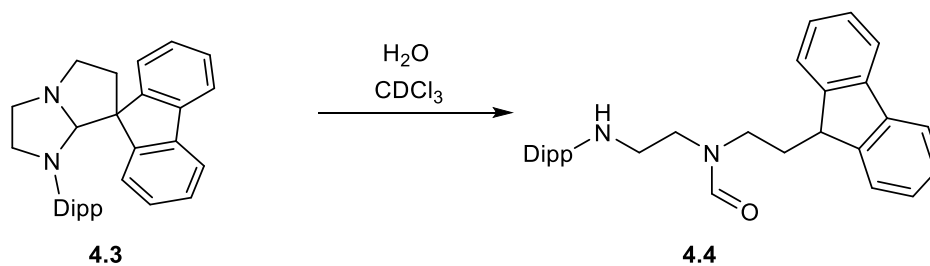


Figure 4.3: X-ray determined structure of spirocycle **4.3** (thermal ellipsoids at 50% probability). All H-atoms (except imidazoline H16) have been removed for clarity.



Scheme 4.7: Optimised synthesis of spirocycle **4.3**.

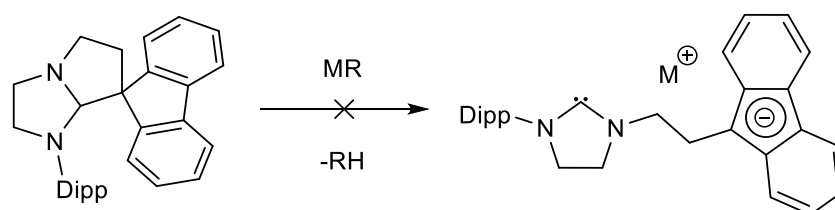
The stability of **4.3** was tested by dissolution in wet CDCl_3 , and it was found that after 2 weeks **4.3** had mostly reacted, as monitored by ^1H NMR spectroscopy. The new species lacked the complex resonances for the CH_2 groups of **4.3** indicating that the bicyclic structure had been broken up, and a fluorenyl 9-C H resonance was also apparent. The presence of a singlet at 8.02 ppm matched the chemical shift associated with a formamide group (DMF in CDCl_3 : 8.02 ppm)²³¹ and HRMS found m/z matches for the amino formamide **4.4** [$(\text{M}+\text{H})^+$ cal. 441.2900 m/z , obs. 441.2897] (**Scheme 4.8**). Thus, compound **4.3** needs to be kept free of moisture, and hence was stored and handled in a glovebox.



Scheme 4.8: Reaction of spirocycle with water **4.3** to generate formamide **4.4**.

4.3 Deprotonation and metallation attempts

Due to the similarities between **4.3** and well-known alcohol-carbene adducts,²⁶² it was proposed that **4.3** could be deprotonated/ring-opened in a similar fashion with strong bases such as nBuLi and rare-earth homoleptic amides etc. (**Scheme 4.9**). Deprotonation of the spirocycle was therefore attempted with a range of bases (**Table 4.1**). While some reactivity was observed with some of the bases (several reactions displayed carbene resonances by ¹³C NMR spectroscopy with the expected chemical shift), no readily-isolated compound was obtained.



Scheme 4.9: Attempts to deprotonate **4.3** to generate an anionic NHC salt (MR is a generic alkyl metal reagent).

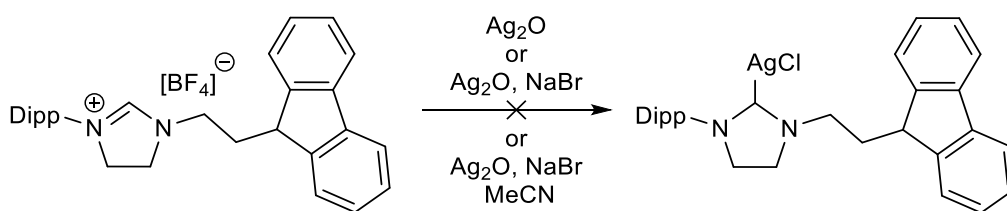
In addition, and as a comparison to literature alcohol-carbene adducts, **4.2-BF₄** and **4.3** were both reacted with [Y{N(SiMe₃)₂}₃]. The former reaction led to the formation of the spirocycle as the major organic component suggesting that cyclisation is preferable to metallation. The latter reaction did not proceed, even with heating, indicating that the spirocycle is significantly less reactive than that the alcohol carbene adducts towards ring-opening/deprotonation. In the alcohol-carbene adducts, the imidazoline H is acidic due to the presence of three electronegative atoms: two N and O. This makes the imidazoline H relatively activated, while in **4.3** the fluorenyl group is not as electronegative and therefore the imidazoline H is not as activated with only two N substituents, hence the increased difficulty in the deprotonation/ring-opening step.

Table 4.1: Summary of initial deprotonation attempts of **4.3**

Base used	Conversion	Product observed
ⁿ BuLi ^[a]	0	Only BuLi observed in ⁷ Li NMR
ⁿ BuLi/TMEDA ^[a]	0	Only BuLi/TMEDA species observed in ⁷ Li NMR
ⁿ BuLi/TMEDA ^[b]	>99	Unknown, indistinct ¹ H and no peaks in ⁷ Li NMR
KBn ^[c]	10	Mostly spirocycle
KBn + 18-crown-6	80	¹³ C NMR indicated formation of carbene shift at 241 ppm. Product was unable to be crystallised
LiPh ^[d]	50	Slow consumption with heating leading to unidentified product
ⁿ BuLi/KO ^t Bu	30	Product had carbene peak at δ_C 231ppm. Unable to purify

[a] 1 eq. in toluene, [b] 80°C, [c] THF, [d] 80°C

Alternative methods of NHC-metal complex synthesis include silver carbene complexes,²⁶⁶ which can then be transmetallated to the targeted TM. Thus, **4.2-BF₄** was treated with Ag₂O in DCM in the absence of light for 18 hours (**Scheme 4.10**). However, no reaction was observed by ¹H NMR spectroscopy. This could be due to **4.2** being the BF₄ salt while silver carbene syntheses are usually conducted with a halide anion present, and thus the formation of the silver complex is disfavoured. Repeat reactions with the addition of NaBr²⁶⁷ was attempted as this has been used to form NHC silver bromide complexes from imidazolium BF₄ salts, presumably via in-situ counterion exchange. Again, no reaction was observed when trialled with **4.2-BF₄**.



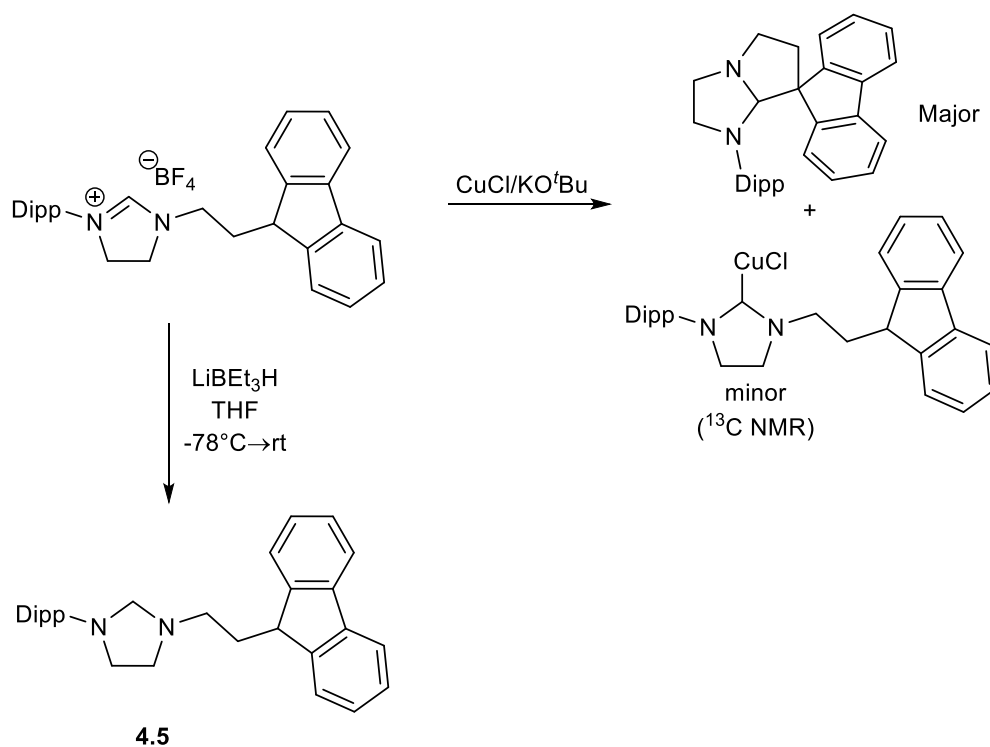
Scheme 4.10: Attempted reactions of **4.2-BF₄** with Ag₂O.

To test whether it would be possible to metallate in the presence of a more coordinating solvent, MeCN was used instead of CH₂Cl₂, as it could possibly form the MeCN adduct cation with BF₄ as the counterion. However, under the same conditions as previously used, no reaction was observed. In an attempt to combine the previous three methods, **4.2-BF₄** was treated with Ag₂O with NaBr in MeCN, but once again no reaction was observed by ¹H NMR spectroscopy.

CuCl/KO^tBu has been used to form NHC copper transfer agents.^{132, 268} One potential issue is the need for a base (ie KO^tBu) which could lead to the formation of the spirocycle. This was indeed the major product observed when the reaction was trialled with 1 eq. CuCl/KO^tBu and **4.2-BF₄** (**Scheme 4.11**). In the ¹³C{¹H} NMR spectrum, a low intensity resonance was observed at 210 ppm which could be assigned to a carbene-Cu species. Repeat reactions were attempted with the order of addition of reagents varied, however, these were unable to improve the formation of the Cu species, highlighting the preference for the formation of **4.3**. The formation of the Cu-NHC adduct suggests that the deprotonation occurs at the imidazolium C-H generating the free NHC which could be trapped with a suitable reagent, i.e. CuCl, or undergo self-cyclisation via carbene insertion into the fluorenyl C-H bond forming **4.3**. The preference for the formation of **4.3** suggests that the rate of self-cyclisation is higher than that of the carbene trapping.

Borane-protected NHCs have been used in the formation of tethered NHC complexes with indenyl.^{108, 269} This would then allow for metallation to a TM either with the fluorenyl first or the NHC, followed by the coordination of the other group. The borane is introduced by reaction of LiBEt₃H, a common strong reducing agent, with an imidazolium salt to give an unsaturated NHC adduct.¹⁰⁹ As it is a reducing agent rather than a base it may avoid the formation of **4.3**, although the formation of the NHC-borane adduct must go via a free carbene. Treatment of **4.2-BF₄** with LiBEt₃H led neither to the formation of the spirocycle or the desired NHC-borane adduct, rather to the formation of

the reduced imidazoline compound **4.5** instead, characterised by the loss of imidazolium CH resonance at 7.80 ppm and the appearance of a CH₂ resonance at 3.86 ppm. Similar reactivity has been observed for imidazolinium salts with LiAlH₄,¹⁰⁶ and highlights the differences in reactivity observed for saturated and unsaturated NHC architectures as the former is reduced rather than deprotonated under identical conditions.



Scheme 4.11: Reactions of **4.2-BF₄** with CuCl/KO^tBu and reduction with LiBEt₃H.

4.4 Lithium amide complexes

The recent rise of synergic bimetallic bases has drawn attention to the potential advantages that such systems provide. Examples include regioselective metallation of ferrocene in a single reaction by a Na/Mg amide rather than mono- or di-metallation with nBuLi and TMEDA,²⁷⁰ and the selective meta-metallation of toluene rather than at the benzyl or ortho positions.^{271, 272} Thus, the use of these reagents may enable transformations that are not possible by other means, and offer milder conditions in contrast to traditional reagents that require harsh conditions which may have detrimental effects to sensitive groups. With the inability of the previously tried bases to perform the deprotonation/ring-opening step, it was decided to investigate the possibility of bimetallic bases in the synthesis of the required alkali metal NHC-fluorenyl salts.

In a different project in the group, the new reagent LiPh/LiTMP (**4.6**, see **Figure 4.4** for molecular structure) was synthesised by the combination of LiPh and LiTMP (TMP = 2,2,6,6-tetramethylpiperidide) in benzene or toluene.²⁷³ A 4:2 adduct is formed with a Li₂Ph₂ core and LiTMP units forming η^6 interactions with phenyl rings of the Li₂Ph₂ unit, which is similar to the coordination in LiPh and helps explain why **4.6** is molecular in nature rather than polymeric as observed for LiPh. While pure LiTMP did not react with **4.3**, LiPh did to some degree and it was theorised that **4.6** could act as a better base.

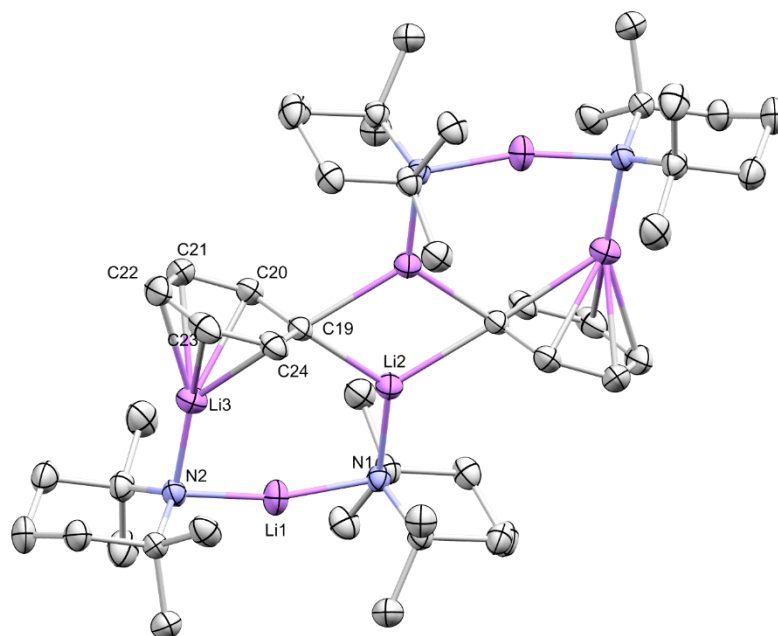
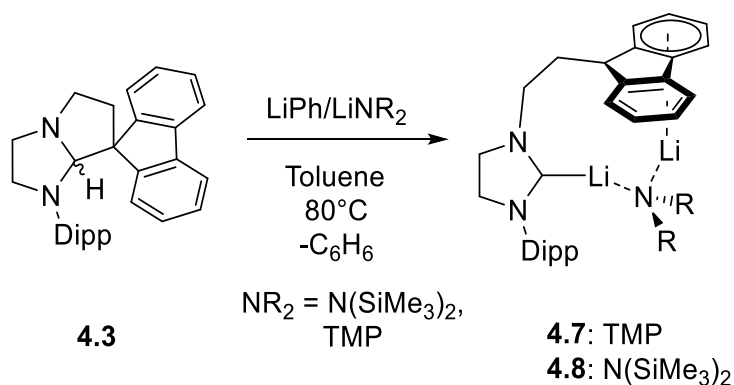


Figure 4.4: X-ray determined molecular structure of the LiPh/LiTMP aggregate **4.6** (thermal ellipsoids at 50% probability).²⁷³ All H atoms have been omitted for clarity.

Reaction of spirocycle **4.3** with the LiPh/LiTMP adduct **4.6**²⁷³ gave rise to the dilithium amide species **4.7** as red-orange crystals (**Scheme 4.12**). The ⁷Li NMR spectrum displayed two singlets at 0.09 ppm and -5.40 ppm, assigned to the NHC-bound Li and the fluorenyl-bound Li respectively. This suggests that there is little exchange between the two Li cations as the lithium peaks are sharp and distinct for a low symmetry environment. The product can be formalised as the LiTMP adduct of the lithium NHC-salt, which along with the observation of the formation of benzene in the ¹H NMR spectrum, led to successful repeats of the reaction using a 1:1 LiPh/LiTMP in-situ mixture. This reaction occurred noticeably quicker than with **4.6**, due to the poor solubility of isolated **4.6**.

Changing the lithium amide from LiTMP to LiHMDS, (which is a weaker base at p*K*_a ≈ 26 rather than 37) gave the analogous complex **4.8**, with similar ⁷Li NMR spectroscopic resonances at -0.86 and -5.68 ppm. The ¹³C{¹H} NMR spectrum shows a broad resonance at 219 ppm for the carbenic carbon which is broad due to coordination to the quadrupolar Li (⁶Li: I = 1, ⁷Li: I = -3/2).



Scheme 4.12: Synthesis of dilithium amide complexes **4.7** and **4.8** with phenyl lithium/lithium amide mixtures.

Single crystal suitable for X-ray diffraction of **4.7** and **4.8** were grown from benzene. Their molecular structures (**Figure 4.5** and **Figure 4.6**, respectively) show similar structures with a lithium cation bound η^6 to a fluorenyl group, the other lithium cation bound to the NHC and a bridging amide ligand. The NHC-Li bond distances for **4.7** and **4.8** are the same within error [2.118(3) and 2.109(4) Å respectively] and both display a Li- η^6 arene interaction to the side rings of the fluorenyl group. The C-9 fluorenyl position is sp²-hybridised and thus carries a formal negative charge, which is interesting as the Li

is separated from it. This could be due to the amide bridge requiring too much space and the linker not being flexible enough to allow the Li to reach the centre ring, thus it coordinates to the neighbouring ring that is less steric constrained than the centre. However, fluorenyl shows a number of different bonding modes to the alkali metals, and is much more flexible in its coordination geometry compared to Cp.^{210, 274}

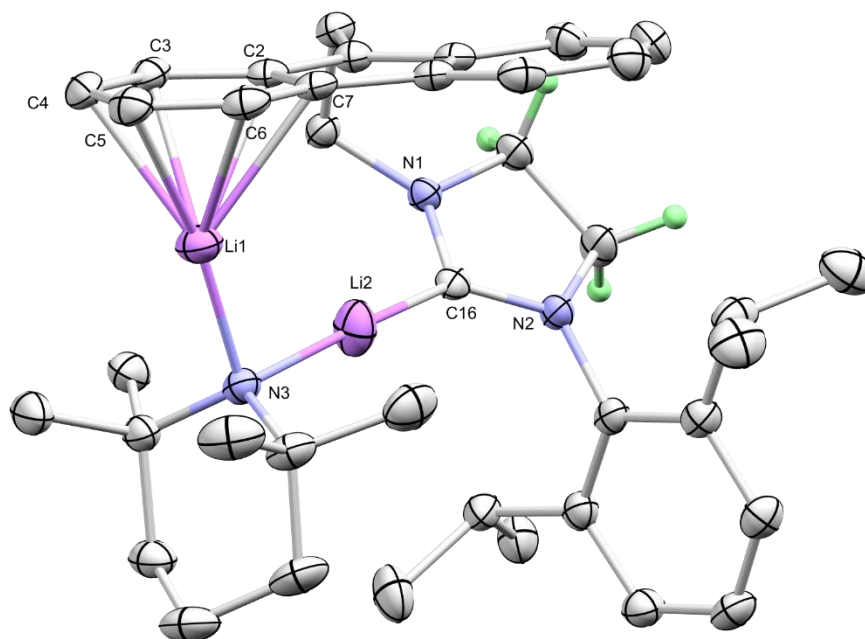


Figure 4.5: X-ray determined structure of dilithium complex **4.7** (thermal ellipsoids at 50% probability). All H-atoms (except for those on the NHC backbone) have been omitted for clarity.

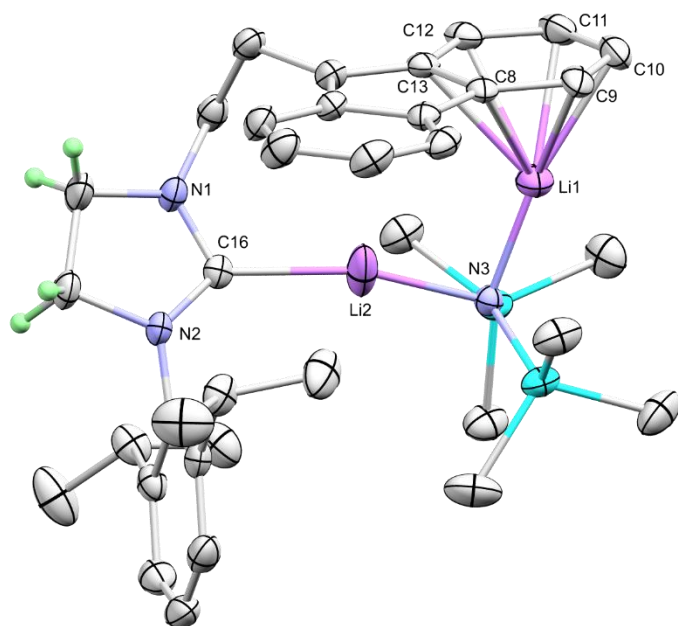
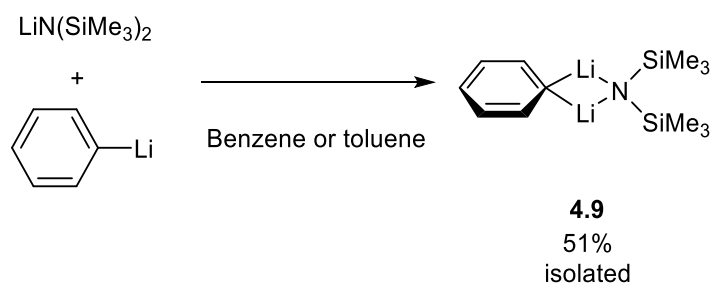


Figure 4.6: X-ray determined structure of dilithium complex **4.8** (thermal ellipsoids at 50% probability). All H-atoms (except for those on the NHC backbone) have been omitted for clarity.

The reaction between **4.3** and LiPh/LiN(SiMe₃)₂ was found to proceed at room temperature albeit much more slowly; after 48 hours it had reached 20% conversion (judged by ¹H and ⁷Li NMR spectroscopy). Using two equivalents of LiHMDS instead of LiPh/LiN(SiMe₃)₂, the reaction reached 25% conversion to **4.8** by 6 hours at 80°C, but did not proceed anymore even after 24 hours at 80°C. Thus the need for both LiPh and LiN(SiMe₃)₂ is highlighted.

During the course of these experiments, it was observed that mixing LiPh and LiHMDS in benzene or toluene led to a clear solution whereas pure LiPh is not soluble. Crystallisation from benzene obtained the LiPh/LiHMDS 1:1 adduct **4.9** as colourless crystals (**Scheme 4.13**).



Scheme 4.13: Formation of **4.9** from mixing LiPh and LiHMDS.

The ^7Li NMR spectrum showed a single resonance at -0.55 ppm indicating a symmetrical environment with both Li cations equivalent. This is confirmed by the X-ray determined structure which is similar to that found for LiPh by powder diffraction,²⁷⁵ with a Li_2X_2 [$\text{X}=\mu^2\text{-Ph}$, $\mu^2\text{-N}(\text{SiMe}_3)_2$] core, which then stacks with neighbouring Ph rings to form an extended polymeric structure (**Figure 4.7**). The Li–C1 distances in **4.9** are symmetrical [2.204(3) Å] and shorter than those in Li_2Ph_2 [2.242(14) and 2.322(14) Å], whereas the close contacts to the neighbouring phenyl ring [η^3 : 2.527(2)–2.679(2) Å] are longer than in $[\text{Li}_2\text{Ph}_2]_n$ [ipso and ortho C: 2.401(12)–2.534(14) Å, meta and para C: 2.745(15)–2.862(14) Å]. Li-(η^3 -Ph) interactions are already known in the literature.²⁷⁶ The weaker interactions between Li_2X_2 units and the presence of SiMe_3 groups may explain the greatly increased solubility of **4.9** in aromatic solvents compared with LiPh.

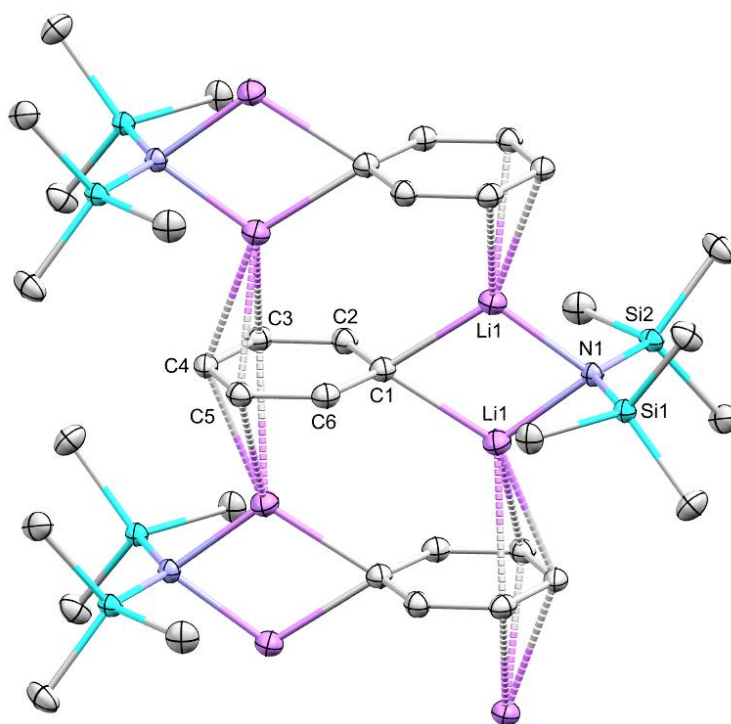


Figure 4.7: X-ray determined structure of LiPh/LiN(SiMe₃)₂ 1:1 adduct **4.9** with the interactions to neighbouring units shown (thermal ellipsoids at 50% probability). All H-atoms have been omitted for clarity.

It was found that the isolated LiPh/LiN(SiMe₃)₂ adduct could be used to deprotonate the spirocycle **4.3** although no differences in reactivity over in-situ mixing was observed, thus both methods could be used interchangeably in deprotonation reactions. Subsequently, a 1:1 ⁿBuLi/LiN(SiMe₃)₂ mixture was trialled to see whether the higher pK_a of ⁿBuLi compared to LiPh would lead to the reaction proceeding at room temperature. After 2 days at ambient temperature, noticeable solid was observed and after washing with pentane, an isolated yield of 56% was obtained indicating that this mixture can also be used for the deprotonation/ring-opening reaction.

Despite the highly reactive nature of the bimetallic base and heating required for the LiPh/LiN(SiMe₃)₂ reactions, no degradation of the NHC is observed. This is in contrast with the reactions of saturated NHCs and alkali metal silylalkyl reagents where ring-opening of the NHC was observed.^{277, 278} This points to the bimetallic lithium bases being more selective in nature.

4.5 Sodium and potassium amide complexes

The heavier group 1 analogues were synthesised by the reaction of spirocycle **4.3** with a 1:1 mixture of $\text{MCH}_2\text{Ph}/\text{MN}(\text{SiMe}_3)_2$ ($\text{M} = \text{Na}, \text{K}$) in benzene (**Figure 4.8**). The reactions were complete after 24 hours at room temperature, while at 80°C only 30 minutes was required. Longer reaction times were detrimental to the yield and purity, with dark solutions obtained and no product observed. Toluene was trialled as the solvent, however, this did not give satisfactory results.

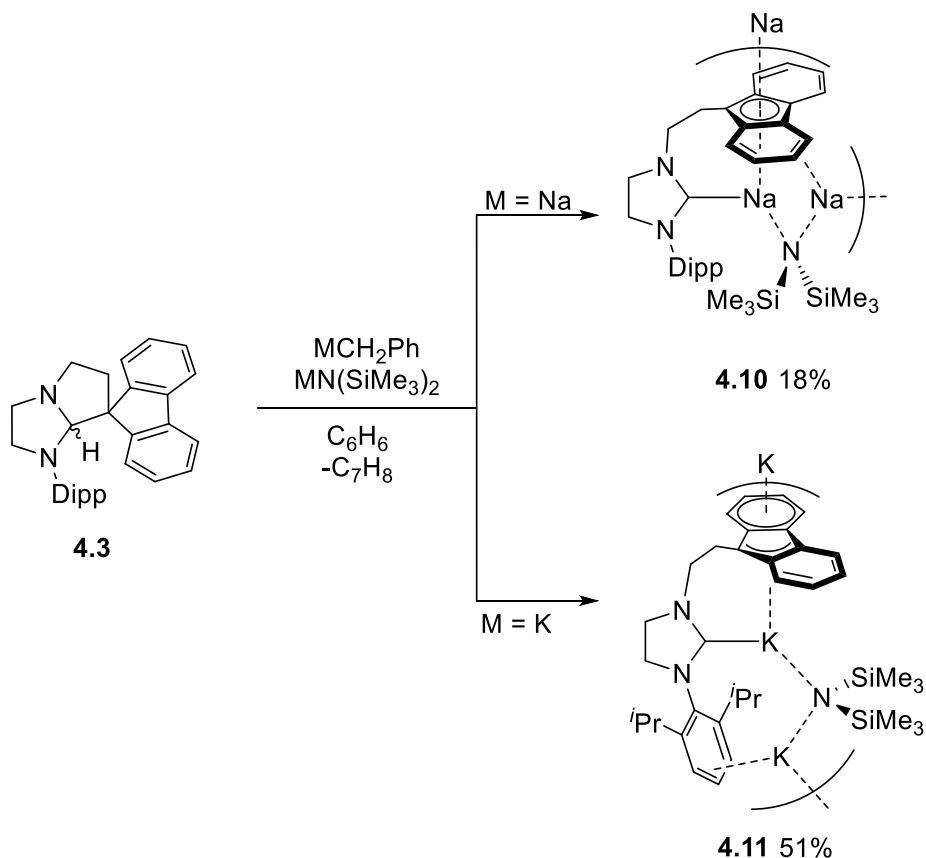


Figure 4.8: Reactions of spirocycle **4.3** with MCH_2Ph and $\text{MN}(\text{SiMe}_3)_2$ ($\text{M} = \text{Na}, \text{K}$).

Crystallisation of the sodium reaction from a saturated benzene solution obtained the polymeric amide-bridged disodium structure **4.10**. The larger sodium cation prevents both metals from sitting within the fluorenyl-NHC pocket, thus one of them (Na_2 in **Figure 4.9**) is pushed out and forms interactions with the fluorenyl on a neighbouring unit to complete its coordination sphere. Three different arene coordination modes of sodium are present: η^5 with Na_1 , and η^2 and η^4 for Na_2 . The larger size of Na seems to make it the right size to sit in the central ring pocket with η^5 -coordination to the fluorenyl and also chelated by the NHC, in contrast to the structures with the smaller cations in **4.7** and **4.8** and larger K (**4.11**). The Na-carbene distance of $2.578(3) \text{ \AA}$ closely matches those

observed previously for Na-NHC complexes.^{212, 279, 280} While the Na-NHC angles show deviation from linearity and planarity, this has been observed in other bidentate systems previously and is likely to be explained by the NHC-Na interaction having little covalent character and being mostly electrostatic in nature.

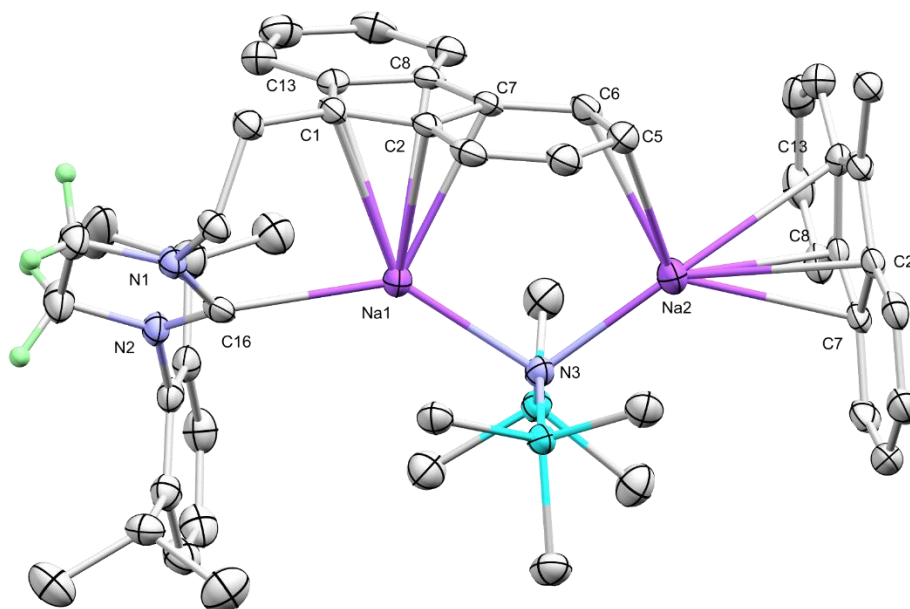


Figure 4.9: X-ray determined structure of disodium complex **4.10** with interactions of Na2 to the neighbouring unit shown (thermal ellipsoids at 50% probability). All H-atoms (except for those on the NHC backbone) in addition to solvating benzene molecules have been omitted for clarity.

From the potassium reaction, a polymeric amide-bridged dipotassium structure (**4.11**) was observed. In this case K1 (**Figure 4.10**) is displaying an η^4 -interaction to the central ring of the fluorenyl group suggesting K is too big to sit perfectly in the central pocket, while K2 is bound η^2 to the arene ring of the Dipp group and η^4 to a fluorenyl moiety on a neighbouring unit. This gives the repeat unit an alternating column structure in the extended crystalline lattice. It is interesting to note the presence of the amide bridge in all structures suggesting that there is a preference for its formation. The K-carbene bond length of 3.011(5) Å fits within the range for previously reported K-NHC complexes.^{163, 279-283} Comparison of the pitch and yaw angles (**Table 4.2**) reveals that as the cation increases in size, so do these angles. As NHC-alkali metal interactions are mostly electrostatic in nature with negligible covalence, there is little need for the NHC to be planar and linear with respect to the metal as would occur with late transition metals.

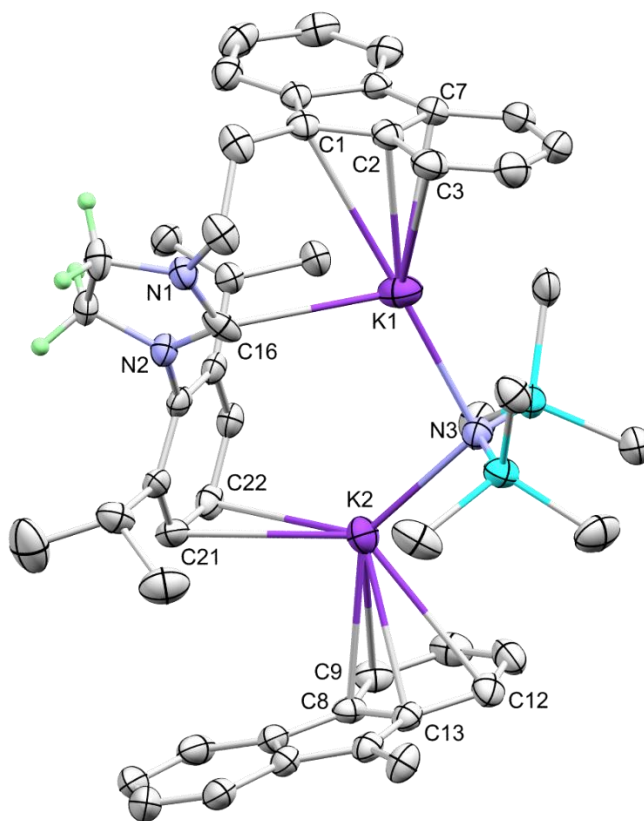


Figure 4.10: X-ray determined structure of dipotassium complex **4.11** with interactions of K2 to the neighbouring unit shown (thermal ellipsoids at 50% probability). All H atoms (except for those on the NHC backbone) in addition to solvating benzene molecules have been omitted for clarity.

Table 4.2: Key bond lengths and angles for **4.8**, **4.10** and **4.11**

	4.8	4.10	4.11
M–NHC [Å]	2.109(3)	2.578(3)	3.011(5)
M–NHC pitch angle [°] ^[a]	11.1	18.7	23.3
M–NHC yaw angle [°] ^[b]	7.1	7.2	8.9
M1–N [Å]	1.949(3)	2.424(3)	2.795(3)
M2–N [Å]	1.967(3)	2.361(2)	2.727(3)

[a] Deviation from planarity of M to the NCN plane. [b] Deviation from linearity of the M–NHC angle.

4.6 Mixed-metal attempts

Attempts to synthesise mixed-metal (heterobimetallic) NHC complexes were trialled by changing either the metal amide or metal alkyl reagent (**Figure 4.11**). Reaction of **4.3** with LiPh/NaN(SiMe₃)₂ led to the formation of **4.8** as observed in the ¹H NMR and ⁷Li NMR spectra (**Figure 4.12** and **Figure 4.13**). This presumably proceeds via cation exchange forming LiN(SiMe₃)₂ in situ which then reacts on to give **4.8**. The reaction of **4.3** with LiPh/KN(SiMe₃)₂ also formed **4.3** as observed by ⁷Li NMR spectroscopy (**Figure 4.14** and **Figure 4.15**). This pattern was also observed for MCH₂Ph/LiN(SiMe₃)₂ mixture reactions, suggesting that dilithium **4.8** is the more favourable product from the reactions and that cation exchange occurs readily.

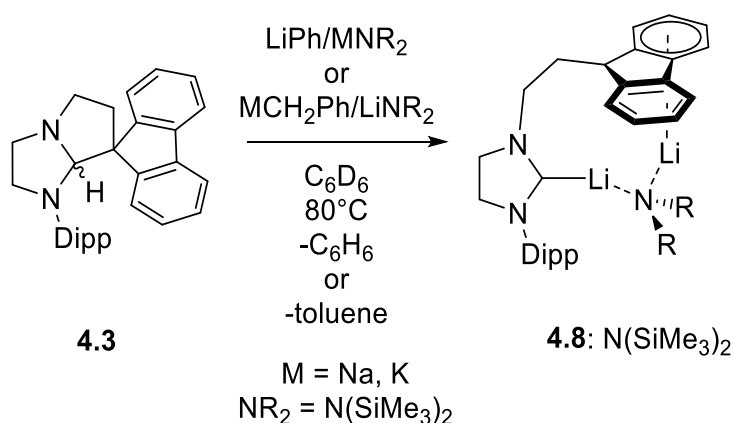


Figure 4.11: Attempted reactions of **4.3** with mixed bimetallic bases with Li.

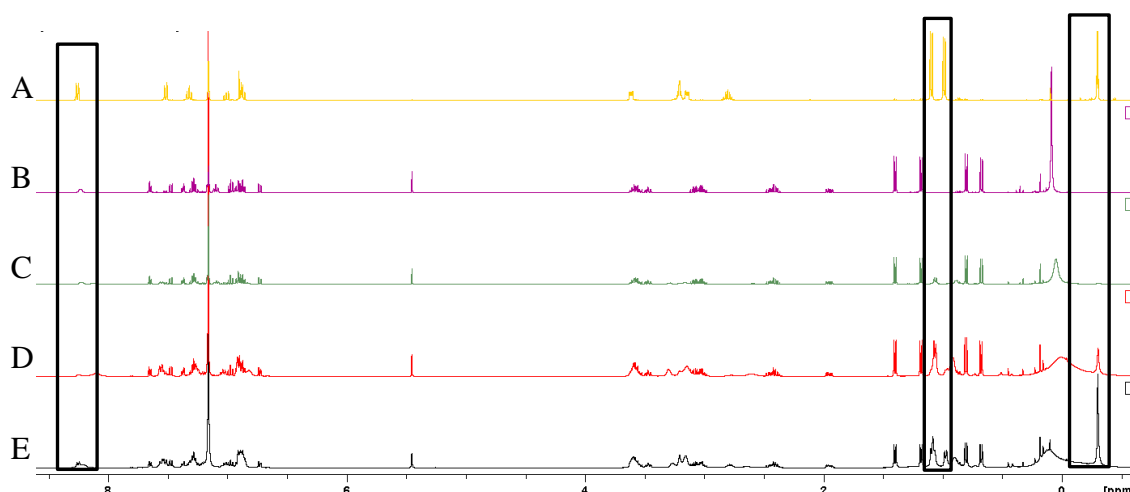


Figure 4.12: ¹H NMR (400 MHz, C₆D₆) spectra for the reaction between **4.3** and LiPh/NaN(SiMe₃)₂, with highlighted similarities. **A** is isolated **4.8**, **B-E** shows the reaction upon heating up to 20 hrs.

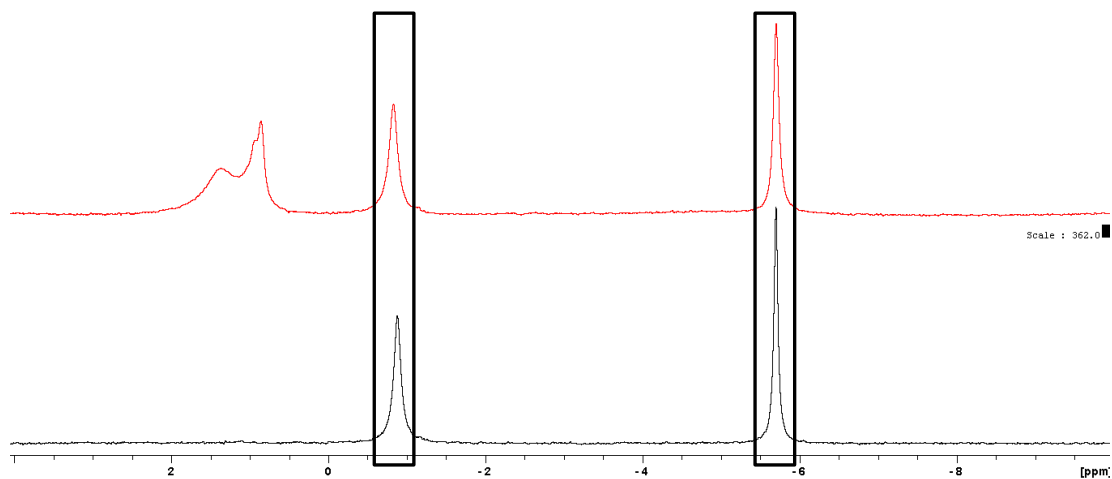


Figure 4.13: ^7Li NMR (155 MHz, C_6D_6) spectra for the reaction between **4.3** and $\text{LiPh/NaN}(\text{SiMe}_3)_2$ (red) compared to **4.8** (black).

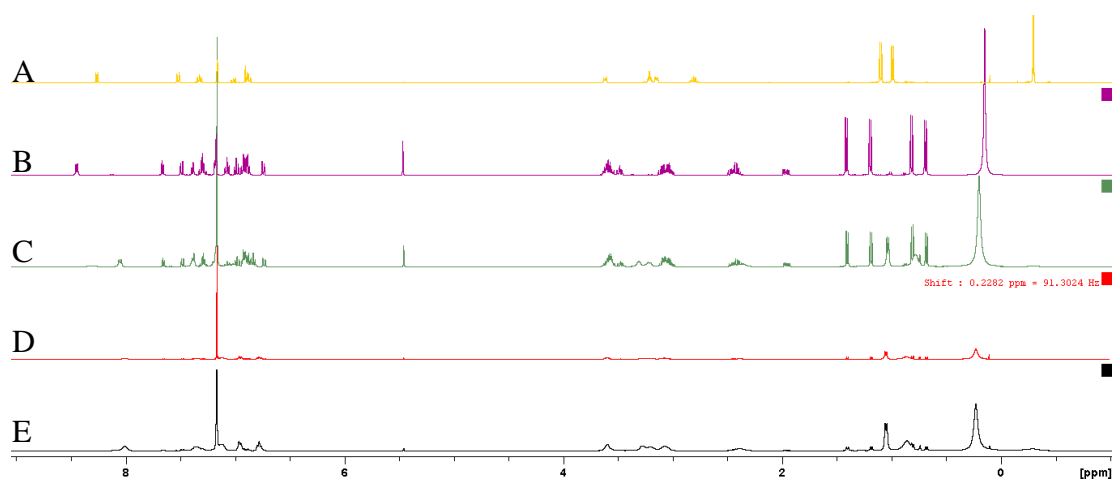


Figure 4.14: ^1H NMR (400 MHz, C_6D_6) spectra for the reaction of **4.3** with $\text{LiPh/KN}(\text{SiMe}_3)_2$ compared to the spectrum for isolated **4.8** (A).

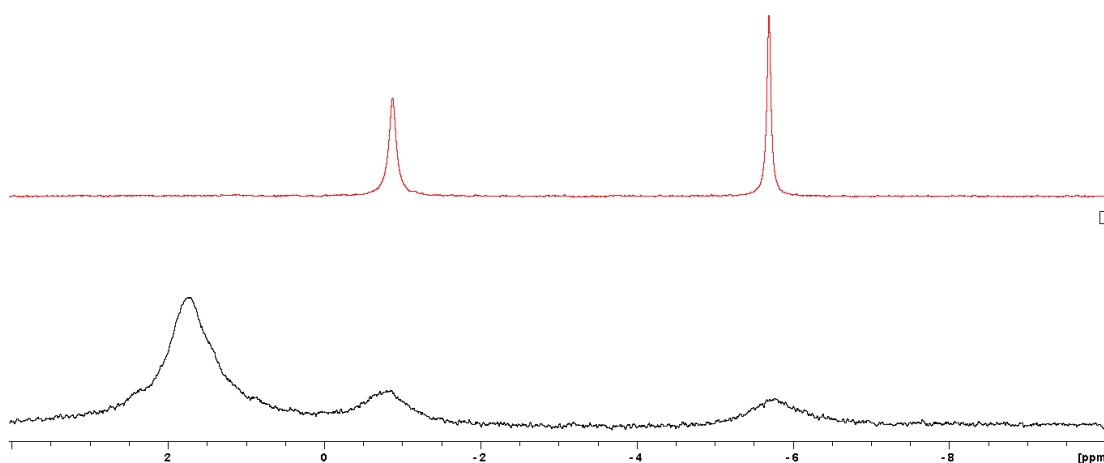


Figure 4.15: ^7Li NMR (155 MHz, C_6D_6) spectra comparing the reaction between $\text{LiPh}/\text{KN}(\text{SiMe}_3)_2$ and **4.3** with spectrum for **4.8**.

With $\text{NaCH}_2\text{Ph}/\text{KN}(\text{SiMe}_3)_2$ and $\text{NaN}(\text{SiMe}_3)_2/\text{KCH}_2\text{Ph}$, the same features were observed by ^1H NMR spectroscopy (**Figure 4.16**), which suggests that the bases are exchanging in-situ, thus leading to similar products to the homobimetallic reactions. In addition, a crystal of **4.11** was isolated from a mixed reaction. However, it is not clean and thus there is some uncertainty to the exact nature of the reactions.

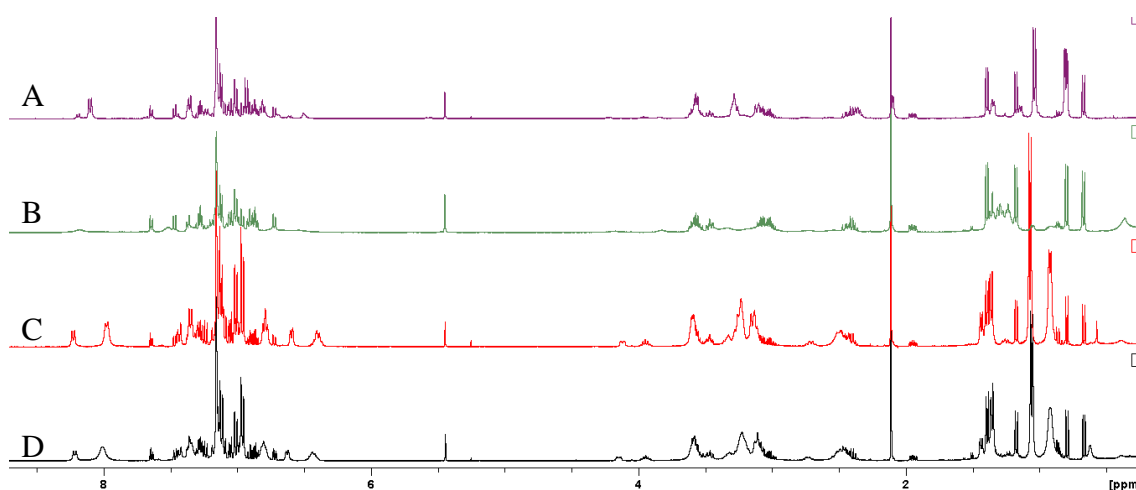
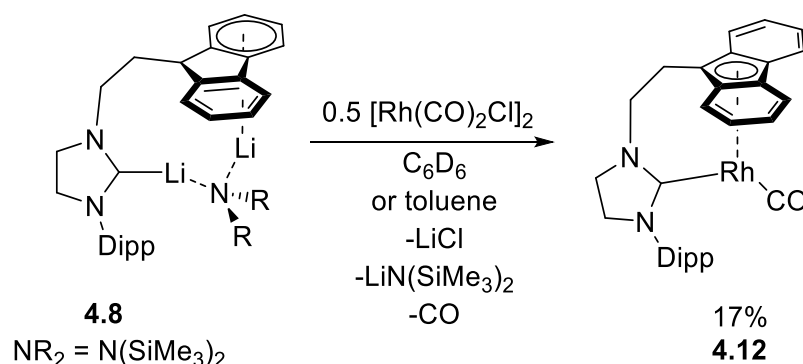


Figure 4.16: Stacked plot of ^1H NMR (400 MHz, C_6D_6) spectra for NMR scale reactions of **4.3** with **A:** $\text{KCH}_2\text{Ph}/\text{KHMDS}$, **B:** $\text{NaCH}_2\text{Ph}/\text{NaHMDS}$, **C:** $\text{KCH}_2\text{Ph}/\text{NaHMDS}$, **D:** $\text{NaCH}_2\text{Ph}/\text{KHMDS}$. The spectra for **C** and **D** are very similar in nature suggesting the same product(s) are being formed.

4.7 Complexation to rhodium

With suitable proligands available, reactions to coordinate this tethered ligand to Rh were attempted. The targeted tethered complexes with rhodium would include an L-type co-ligand such as CO, ethene or cyclooctene. The presence of an additional equivalent of metal amide was concerning, as it could potentially lead to different reactivity, but on the other hand it may not affect the course of the reaction. Thus the salt metathesis of dilithium **4.8** with suitable rhodium chloride complexes was trialled using $[\text{Rh}(\mu\text{-Cl})(\text{CO})_2]_2$ as the metal precursor (**Scheme 4.14**).



Scheme 4.14: Reaction of **4.8** with $[\text{Rh}(\text{CO})_2\text{Cl}]_2$.

^1H NMR spectroscopy showed complete consumption of **4.8** and the formation of a new species, **4.12**, with a change in the isopropyl methyl groups' chemical shift particularly noticeable. The $^{13}\text{C}\{^1\text{H}\}$ NMR spectrum showed the formation of two doublets at δ 214.0 ($J = 78.7$ Hz) and δ 192.9 ($J = 90$ Hz) which can be assigned to the carbene and CO resonances respectively; the magnitude of the Rh-C J -coupling match similar complexes in the literature.¹²⁷ The chemical shift for the carbene and the carbonyl in **4.12** are similar to **2.7** (214.8 ppm and 195.1 ppm). The $J_{\text{Rh-CO}}$ coupling magnitude for **2.7** and **4.12** is also similar (93.3 Hz vs 90.0 Hz), which suggests a similar interaction between the CO and the Rh centre. A greater difference is observed in the magnitude of the $J_{\text{Rh-carbene}}$ between **2.7** and **4.12** (68.8 Hz and 78.7 Hz) which may arise from the NHC bonding in a different orientation in **4.12** compared to **2.7**. Additionally, an intermediate was observed with resonances at δ 205.1 (d, $J = 49.3$ Hz), 187.6 (d, $J = 62.0$ Hz) and 186.0 ppm (d, $J = 57.8$ Hz) (**Figure 4.17**), which converted to the product over the course of 48 hrs. These values compare well to literature values for NHC and CO ligands in $[\text{RhX}(\text{NHC})(\text{CO})_2]$ complexes,²⁸⁴ suggesting that coordination of the ligand occurs via

salt metathesis to form a square planar intermediate, from which CO is lost to form the tethered half-sandwich complex.

For the final product, an IR stretching band was found at 1946 cm^{-1} which is in the region observed for rhodium half-sandwich complexes including **2.7**.^{127, 181} Thus, the spectroscopic data supports the structure of **4.12** as being a half-sandwich complex. The observed band of 1946 cm^{-1} for **4.12** is only slightly greater than 1944 cm^{-1} for **2.7**, which suggests that **4.12** has a similar level of electron density on Rh as **2.7**. It should be noted that both the NHC and aromatic donor are different between **4.12** and **2.7**, thus it is possible that changes in ligand have cancelled out (the mixed alkyl-aryl NHC would potentially be a better donor than a bis-aryl NHC but fluorenyl might be a poorer donor than indenyl). To be able to separate these two components, either the monodentate fluorenyl complex or the indenyl-substituted tethered NHC complex would be required.

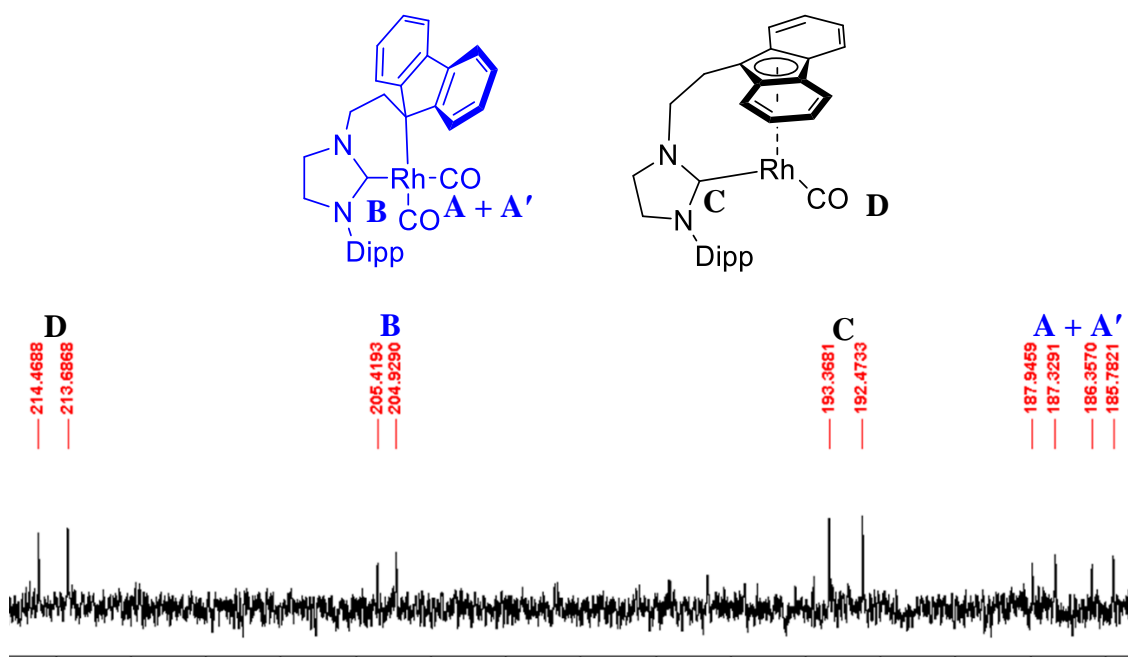


Figure 4.17: $^{13}\text{C}\{^1\text{H}\}$ NMR (101 MHz, C_6D_6) spectrum of the reaction between **4.8** and $[\text{Rh}(\text{CO})_2\text{Cl}]_2$, with peaks assigned to different structures.

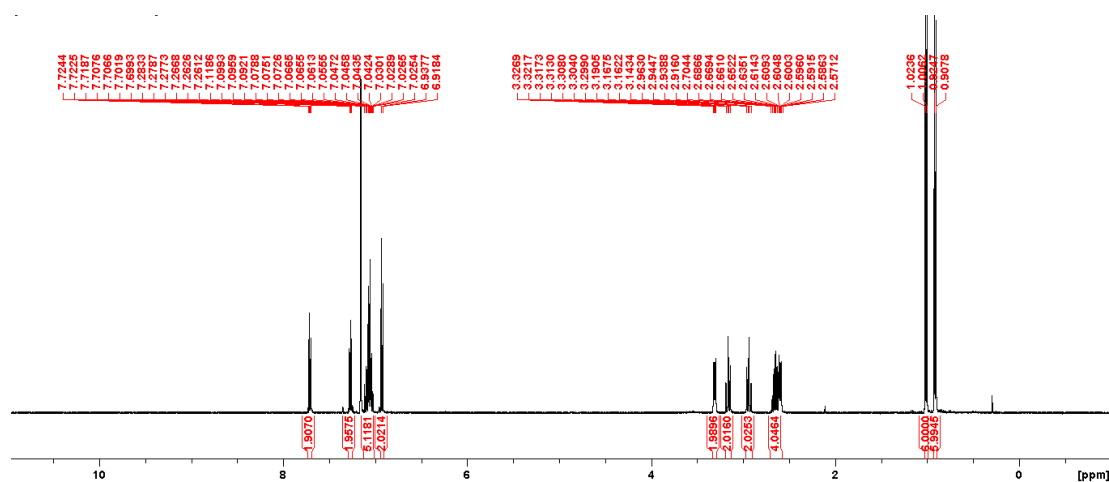


Figure 4.18: ^1H NMR (400 MHz, C_6D_6) spectrum of isolated **4.12**.

Single crystals of **4.12** suitable for X-ray diffraction were grown from a saturated benzene solution. The Rh-NHC distance is 1.985(2) Å, which is within error the same as the Rh-NHC distances found in **2.5** and **2.6**, but shorter than that for **2.7**. The Rh-CO distance for **4.12** is longer than **2.7** with 1.849(2) and 1.828(2) Å respectively, which suggests that the degree of π -backbonding is less for **4.12** than **2.7**, which may arise from the differences in NHC, the use of fluorenyl rather than indenyl, or a combination of both factors. The CO bond length is similar with the larger error for **4.12** preventing more detailed analysis [1.160(7) vs 1.154(2) Å].

The fluorenyl-rhodium interaction in **4.12** is slightly distorted away from symmetrical η^5 coordination (**Figure 4.19**), with Rh(1)-C(1) shortest at 2.188(2) Å. The other distances are similar: Rh-C(2) 2.332(2), Rh-C(7) 2.375(2), Rh-C(8) 2.376(2) and Rh-C(13) 2.345(2) Å. This is similar to what has been observed previously for fluorenyl-rhodium complexes with the C(1) distances being shorter than the others.²¹⁰ However, comparison of the distances with the sum of the covalent radii indicate that all five atoms are within the range expected for interactions.²⁸⁵ The Rh-C(1) distance is shorter than the indenyl-Rh distances in **2.7** [2.221(2)-2.485(1) Å], suggesting the Rh-C(1) interaction is stronger than those in **2.7**.

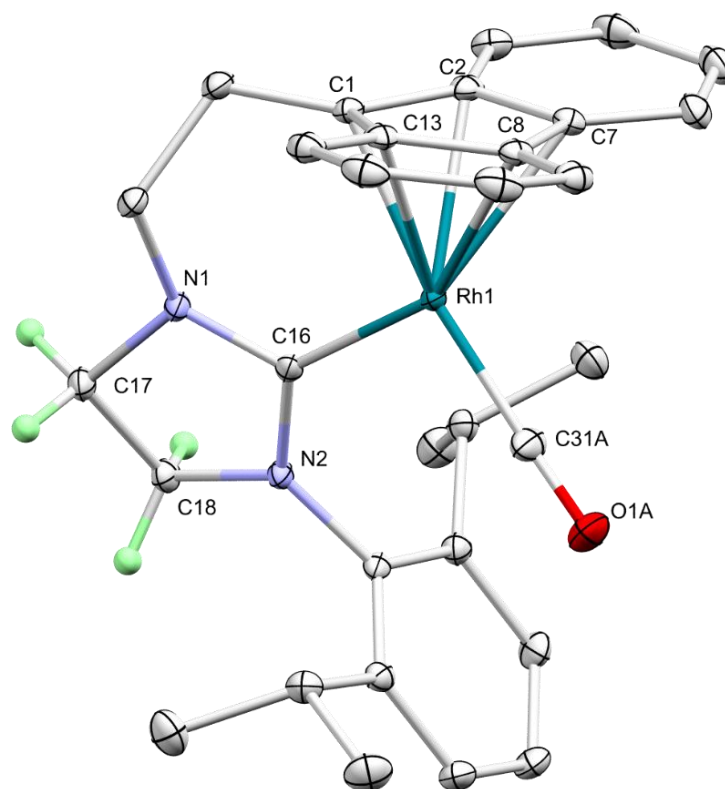
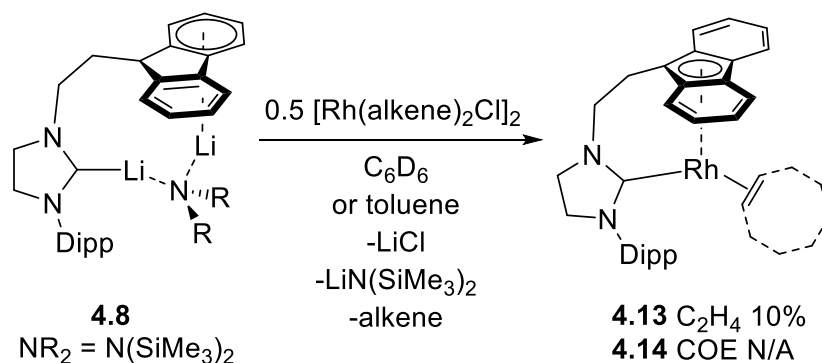


Figure 4.19: X-ray determined structure of rhodium carbonyl complex **4.12** (thermal ellipsoids at 50% probability). All H-atoms (except for those on the NHC backbone) have been omitted for clarity.

Despite the successful small-scale crystallisation for X-ray diffraction, attempts at scaled-up synthesis of **4.12** have so far been challenging. The crude products have an appreciable amount of **4.3** that is difficult to remove due to its solubility being similar to that of **4.12**. Additionally, filtration through silica or alumina was not successful with degradation of the complex observed. Filtration through celite was able to remove dark impurities and crystallisation from a concentrated toluene solution obtained **4.12** in a low yield of 17%.

Reaction of **4.8** with rhodium bis(alkene) chloride dimers gave the corresponding tethered NHC alkene complexes (**Scheme 4.15**). ^{13}C NMR spectroscopy showed that metallation to Rh was achieved for the carbene moiety as both complexes display doublets at δ 213.0 and 210.8 ppm respectively for **4.13** and **4.14**. The coordinated alkene resonances were observed at δ 44.7 and 61.4 ppm respectively, with similar $^1J_{\text{Rh-C}}$ values of 13.6 Hz and 13.5 Hz respectively that match similar complexes in the literature.²⁰¹ The alkene chemical shift of monodentate complex **2.6** was the same within error of that for **4.14** at 61.5 ppm, while the J -coupling was slightly lower at 13.5 Hz (compared to 15.3 Hz for

the monodentate complex), which may arise from slightly poorer overlap between the alkenes and the Rh in the tethered system. However this difference is rather small suggesting that the monodentate and tethered systems have very similar electronic properties, which agrees with the IR_{CO} comparison between **2.7** and **4.12**. The coordinated ethene chemical shift for **4.13** is different from the monodentate complex (44.7 ppm to 35.6 ppm), while the J -coupling value for **4.13** is slightly lower at 13.6 Hz rather than 15.1 Hz for **2.5**, which is a similar change to the COE substituted complexes. Unfortunately, similar to **4.12**, it proved very difficult to obtain the two complexes cleanly, with both complexes proving to be unstable on silica and alumina. Complex **4.14** is more soluble in alkane solvents than **4.12**, thus making it very difficult to remove any **4.3** present. In an attempt to see if the use of the lithium bases was the issue, the analogous reaction was conducted using $\text{NaCH}_2\text{Ph}/\text{NaN}(\text{SiMe}_3)_2$ with **4.3** instead, followed by metallation with $[\text{Rh}(\text{COE})_2\text{Cl}]_2$. This, however, gave a similar result to the use of lithium reagents, with a mixture obtained which could not be separated.



Scheme 4.15: Reaction of **4.8** with $[\text{Rh}(\text{alkene})_2\text{Cl}]_2$.

A small amount of **4.13** was crystallised from toluene after standing for several months, giving a yield of 10%. The crystals were suitable for X-ray diffraction and the molecular structure was obtained (**Figure 4.20**). The molecular structure shows the desired η^5 coordination of the fluorenyl group to rhodium in a half-sandwich geometry with the NHC and ethene both coordinated as well. The Rh-NHC distance is shorter for **4.13** than for **2.5** [1.967(2) and 1.989(1) Å respectively], and for **4.12**. This observation may be due to ethene being a weaker π -acceptor than CO that leads to increased electron density on the Rh centre, leading to the NHC acting as a π -acceptor. This would lead to increased C-N distances due to the backdonation into the NHC's C p-orbital. The C-N distances are similar within error [**4.12**: C(16)-N(1) 1.357(2) Å, C(16)-N(2) 1.360(2) Å; **4.13**: C(16)-N(1) 1.367(4) Å, C(16)-N(2) 1.367(3) Å]. Additionally, the Rh is bound

unsymmetrically to the ethene with Rh-C(31) 2.118(3) and Rh-C(32) 2.168(3) Å, which is in contrast to **2.5** where the distances are the same. However, the C-C double bond distances in **4.13** and **2.5** are the same within error [1.402(4) and 1.399(1) Å], which indicates there is minimal difference in back donation into the C-C π^* antibonding orbital, which could be used as a measure of the electron density on the metal and thus is indication of the combined donation of the NHC and the fluorenyl group. The slipped nature of the alkene is similar to **2.6** where the Rh-C distances are 2.116(2) and 2.140(2) Å, which means **4.13** is more distorted from symmetrical binding than **2.5**.

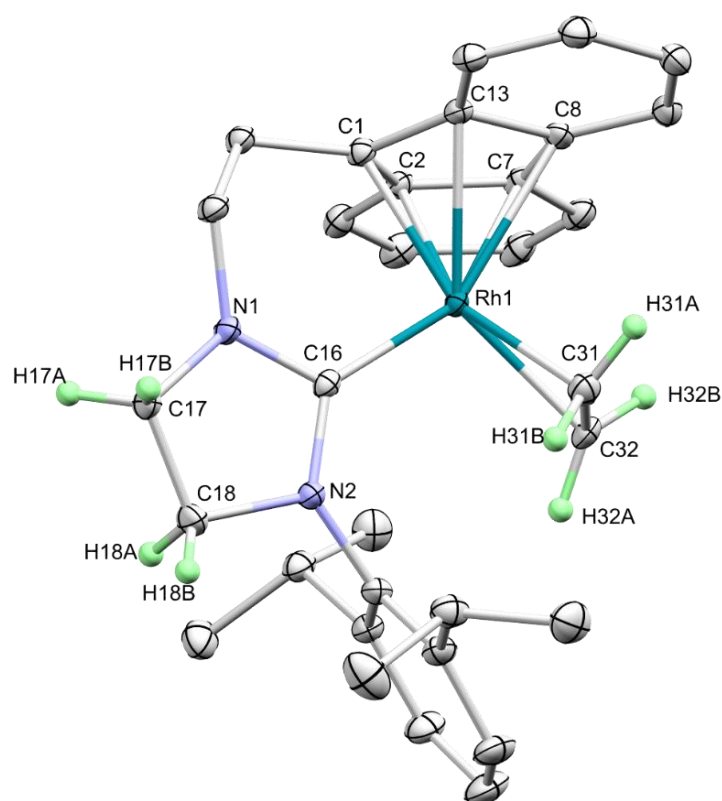


Figure 4.20: X-ray determined structure of rhodium ethene complex **4.13** (thermal ellipsoids at 50% probability). All H-atoms (except for H17A/B, H18A/B, H31A/B and H32A/B) have been omitted for clarity.

It was not possible to isolate **4.14**, though the NMR data suggests it is formed by the reaction of **4.8** and $[\text{Rh}(\text{COE})_2\text{Cl}]_2$ (**Figure 4.21**) with resonances assignable to the coordinated NHC and coordinated COE observed.

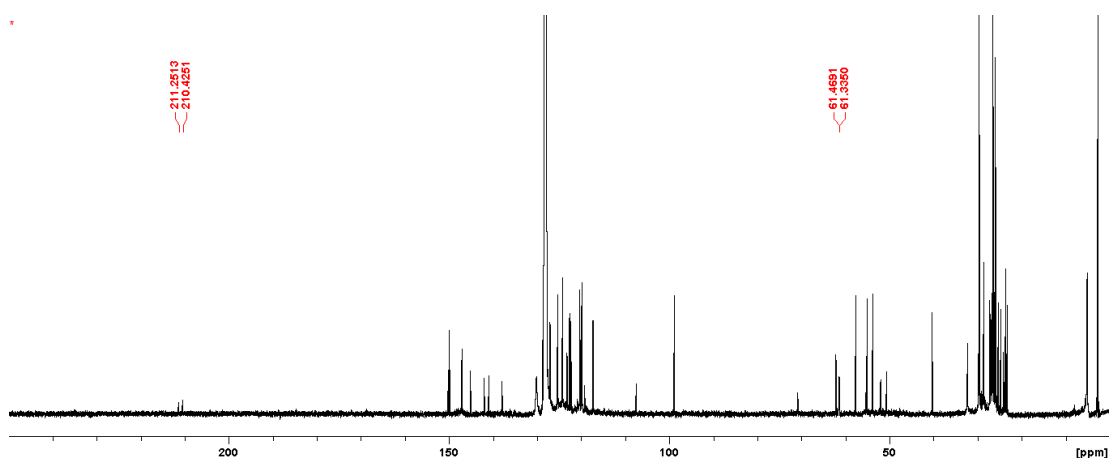
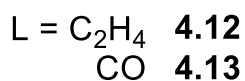
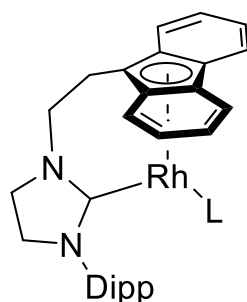
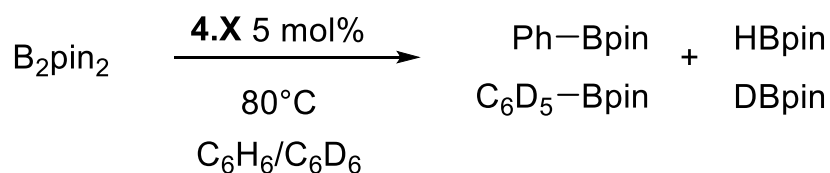


Figure 4.21: $^{13}\text{C}\{^1\text{H}\}$ NMR (101MHz, C_6D_6) spectrum for the reaction of **4.8** with $[\text{Rh}(\text{COE})_2\text{Cl}]_2$ with the carbene and bound alkene resonances highlighted.

4.8 Initial catalytic studies for tethered complexes

Complexes **4.12** and **4.13** were trialed for the borylation of benzene (**Scheme 4.16**). As was observed for monodentate carbonyl complex **2.7**, no borylation was observed with **4.12** (**Table 4.3**), which further suggests that CO is a poor ligand choice for borylation when using the catalyst in the form used in this work.



Scheme 4.16: Borylation of benzene with **4.12/4.13**.

Complex **4.13** was observed to catalyse the borylation of benzene, however, it was significantly slower than the reactions with **2.5** and **2.6**. After 24 hrs only 9% of PhBpin was observed with **4.13** while **2.5** had achieved 93 % in the same time. After a 100 hrs, the reaction had reached 32%, and thus was significantly slower than the monodentate complexes.

Table 4.3: Initial catalytic results of the borylation of benzene with **4.12** and **4.13**.

Complex	Conversion after 24 hrs /% ^a	Conversion after 100 hrs /% ^a
4.12	0	0
4.13	9	32

^a Conversion based upon integration of CH₃ resonances in ¹H NMR spectra.

In the mechanism with **2.5** or **2.6**, the borylation is proposed to proceed via a metallacycle **2.12**. With **4.13**, the formation of such a metallacycle would be disfavoured due to the different orientation of the NHC and the tether preventing the cyclometallation occurring. Thus, it is unlikely to proceed via such an intermediate which may explain the reduced reactivity as the pathway for catalysis with **4.13** would have to be different.

4.8 Conclusions

Using the previously reported fluorenyl diamine **4.1**,²¹⁰ the fluorenyl- and Dipp-substituted imidazolinium tetrafluoroborate **4.2-BF₄** was synthesised and characterised using multinuclear NMR spectroscopy, elemental analysis and by X-ray diffraction to obtain its molecular structure. Deprotonation of **4.2-BF₄** formed spirocycle **4.3**, which was found to be a general reaction occurring with a range of bases. Characterisation of **4.3** was performed by multinuclear NMR spectroscopy and by X-ray diffraction for its molecular structure.

After unsuccessful attempts at deprotonation/ring-opening of **4.3** with conventional bases, the use of bimetallic lithium amide complexes **4.6**²⁷³ and **4.9** led to the successful formation of dilithium tethered fluorenyl NHC amide complexes **4.7** and **4.8**. Complexes **4.7** – **4.9** were characterised by multinuclear NMR spectroscopy and by X-ray diffraction to obtain their molecular structures. Lithium-arene coordination modes of η^3 and η^6 were observed, both of which have been observed previously.

Reactions with heavier group 1 reagents (sodium and potassium) gave rise to bimetallic fluorenyl-tethered NHC amide complexes **4.10** and **4.11**, which were found to have polymeric structures by X-ray diffraction. A variety of M-arene coordination modes are present with η^2 , η^4 and η^5 observed.

The reaction of dilithium **4.8** with Rh(I) chloride sources was found to be partially successful with **4.12** and **4.13** crystallised to obtain X-ray structures. This showed successful formation of the chelated half-sandwich complex, and confirmed the observations from ¹H and ¹³C NMR spectroscopy, the latter of which displayed characteristic doublets for the carbene and CO donors due to coupling to ¹⁰³Rh (100%, I = ½). Evidence for the formation of **4.14** was obtained by ¹³C{¹H} NMR spectroscopy, indicated by the formation of doublets for the carbene and the coordinated alkene carbons which *J*_{Rh-C} coupling constants are similar to **4.12** and **4.13** and those observed in the literature. Whilst NMR data in solution and single crystal structures were obtained, purification of complexes **4.12-4.14** was found to be difficult with low yields of **4.12** and **4.13** obtained.

Chapter 5: Conclusions

A range of indenylrhodium(I) complexes featuring the SIPr NHC ligand were synthesised in good yields (60-80%). This was achieved via the addition of the free NHC to indenylrhodium(I) bisalkene complexes, and the products were fully characterised. The presence of an NHC ligand led to lengthening of the coordinated C=C bond due to backbonding from the metal centre. The analogous route with a pentamethylcyclopentadienyl ligand was unsuccessful, highlighting the increased reactivity observed for indenyl complexes over Cp/Cp* complexes. The formation of an NHC alkene Rh(I) chloride dimer allowed the testing of an alternative synthetic route for the formation of indenylrhodium(I) complexes via addition of indenyllithium to the dimer, which was successful. Attempts to access the analogous fluorenyl complex were unsuccessful. This route could be used to access other Cp-type complexes for comparison of ligand effects.

Photolysis of these complexes, along with reactions with H₂ and silanes, suggest that loss of the alkene is favoured and show evidence that cyclometallation of the NHC's isopropyl groups occurs as a common intermediate. The reaction with H₂ is likely to lead to a Rh(III) dihydride complex with the cyclometallated species an observed intermediate. The dihydride complex was also partially formed by the reaction with reducing alkyl- and aryl-silanes. In contrast, a trialkoxysilane formed the oxidative addition product, a Rh silyl hydride complex, which has been crystallographically characterised. Mixed alkoxy-alkyl silanes formed a mixture of products with a redistribution reaction observed such that the reaction with (EtO)₂MeSiH gave the oxidative addition product of (EtO)₃SiH, indicating the reactivity of the Rh centre towards other bond-activation reactions. Other alkylsilanes, such as Et₃SiH, formed a mixture of products suggesting that C-H activation reactions could occur with the alkyl chains. Tuning the electronic properties of the silane may allow access to the dihydride without the need for H₂ gas.

[Rh(Ind)(SIPr)(C₂H₄)] and [Rh(Ind)(SIPr)(COE)] were shown to be catalytically competent for the borylation of arenes using B₂pin₂ in good to acceptable yields, while [Rh(Ind)(SIPr)(CO)] was found to be inactive, suggesting that carbonyl ligands are not suitable for borylation using the catalyst system used in this work. The selectivity is similar to literature complexes, while the conversion was comparable but with a slower rate of reaction than that previously reported for Cp*Rh catalysts. [Rh(Ind)(SIPr)(COE)] was also shown to be able to borylate alkanes, which is still a difficult reaction to perform.

Although this reaction requires further optimisation of reaction conditions, there is great promise in these initial results because the introduction of an NHC now allows for ligand variation and tuning of the reactivity of the complex, unlike previous Cp*Rh species that lose all the other coligands in order to generate the catalytically active species. Comparison of ^1H NMR spectra between the catalysis reactions and stoichiometric reactions provide evidence that the intermediates are boryl hydride complexes, with the NHC still bound to the Rh and involved in the catalytic cycle due to different intermediates observed for the catalysis and stoichiometric reactions with $[\text{Rh}(\text{Ind})(\text{COE})_2]$.

Using the previously reported fluorenyl diamine **4.1**,²¹⁰ the fluorenyl-tethered and Dipp-substituted imidazolinium tetrafluoroborate salt **4.2-BF₄** was synthesised and characterised using multinuclear NMR spectroscopy, elemental analysis and by X-ray diffraction to obtain its molecular structure. Deprotonation of **4.2-BF₄** formed the spirocycle **4.3**, which was found to be a general reaction occurring with a range of bases. Characterisation of **4.3** was performed by multinuclear NMR spectroscopy and by X-ray diffraction for its molecular structure.

After unsuccessful attempts at deprotonation/ring-opening of **4.3** with conventional bases, the use of bimetallic lithium amide complexes **4.6**²⁷³ and **4.9** led to the successful formation of dilithium salts of the fluorenyl-tethered NHC ligand containing a bridging amide ligand, complexes **4.7** and **4.8**. Therefore, it has been demonstrated that a synergic combination of two bases has synthetic advantages over conventional single-component systems. Complexes **4.7** – **4.9** were characterised by multinuclear NMR spectroscopy and by X-ray diffraction to obtain their molecular structures. Lithium-arene coordination modes of η^3 and η^6 were observed, both of which have been observed previously. Reactions with heavier group 1 reagents (sodium and potassium benzyl and amide reagents) gave rise to the homobimetallic fluorenyl-tethered NHC amide complexes **4.10** and **4.11**, which were found to have polymeric structures by X-ray diffraction. A variety of M-arene coordination modes were present with η^2 , η^4 and η^5 interactions observed.

Reactions of the dilithium salt **4.8** with Rh(I) chloride sources were found to be only partially successful due to persistently low yields, but several Rh complexes (**4.12** and **4.13**) were obtained as single crystals suitable for X-ray diffraction allowing their molecular structures to be obtained supporting the NMR data which showed their formation. Initial catalytic studies with **4.12** and **4.13** confirm that CO is not a suitable

ligand for catalysis with the catalytic system used here, while **4.13** indicates that the tethering effect has reduced the effectiveness towards borylation with a significantly slower conversion observed. This is proposed to occur due to the inability to form cyclometallated species which were observed for the monodentate complexes. Thus, in this work the act of tethering has reduced the reactivity of the system.

Chapter 6: Future work

6.1 Expansion of catalysis substrate scope

The range of substrates explored for the borylation catalysis was limited by the time available. Thus a more expanded range would be useful from a synthetic point of view as it would explore the functional groups that the catalysis with **2.6** is tolerant to (**Figure 6.1**). The presence of functional groups such as ethers and amines can be problematic for transition metal catalysis due to coordination to the metal. Thus being tolerant to these groups is advantageous. Heterocycles are pharmaceutically relevant appearing in numerous drug molecules and thus the activation of such groups is of particular interest. Many have inherent selectivity problems and may cause issues with transition metal catalysis due to catalyst poisoning.

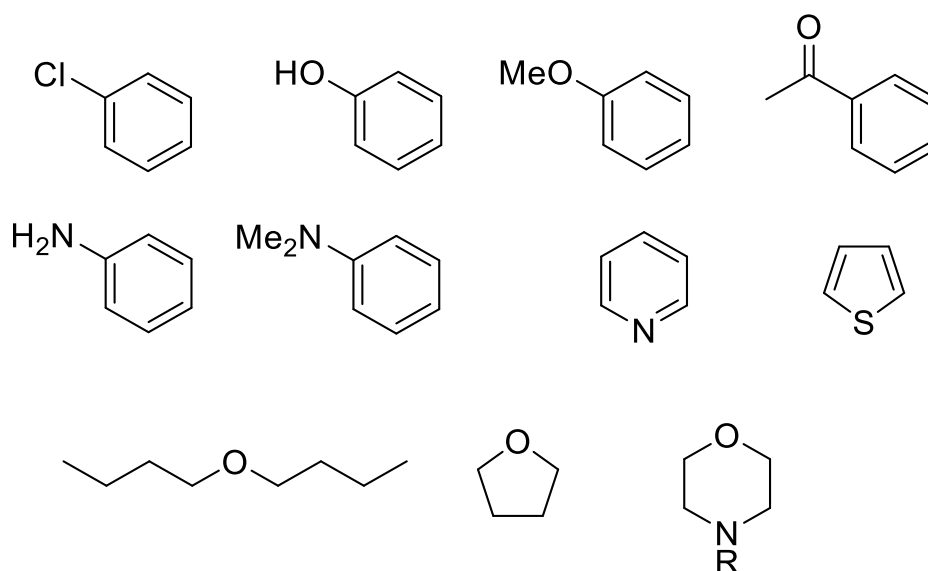


Figure 6.1: An expanded range of substrates for borylation.

The activation of alkanes and other sp^3 hybridised species is more challenging, and the initial studies on alkane activation need to be developed further. More experiments probing the effect of temperature, time, reaction solvent (whether or not a cyclic hydrocarbon containing only methylene groups is resistant to activation) would be beneficial. Catalyst initiation is another key problem that will be focused upon, as it is possible that better precatalysts can be found that circumvent potential problems with catalyst initiation. This includes discrete hydride, alkyl and boryl complexes.

6.2 Ligand modification

Variation of the NHC ligand in the monodentate complexes may be advantageous due to the varying steric and electronic parameters that are possible with NHC ligands (**Figure 6.2**). The NHC IPr shares common starting materials with SIPr, but is unsaturated which will affect the bonding interactions. IMes and SIMes are smaller than the Dipp-based NHCs and can be synthesised in an analogous manner to the Dipp-substituted NHCs. Another commonly used NHC is IMe₄ which is significantly smaller than the Dipp and Mes based NHCs and thus a useful probe for the effects of changing the steric parameters of the NHC ligand. Thus, it would be expected that the target ethene and COE complexes could be synthesised by displacement reactions of the NHC with the indenyl Rh bis(alkene) complexes in an analogous manner to the reaction with SIPr. The different N-substituents will likely affect the formation of cyclometallated species, as the mesityl has only one available position rather than the possible two of Dipp, while cyclometallation of IMe₄ would form a strained 4-membered metallocycle and thus is unlikely to occur.

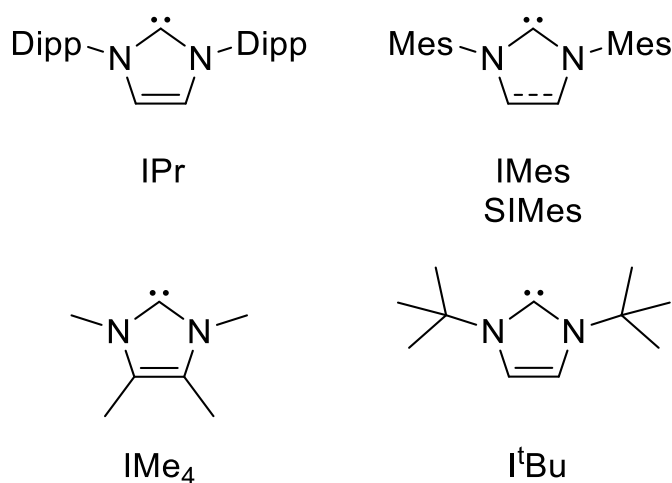


Figure 6.2: Common NHC ligands.

While initial attempts at forming the Cp* analogue of the complexes was unsuccessful, the use of the Rh NHC alkene chloride could allow access to these complexes,²⁰¹ which would allow comparison of the effect of the anionic π -donor and investigation of the influence of the indenyl effect on the reactivity and catalytic potential. In addition to Cp*, other donors such as Cp (smaller and does not favour ring slippage) and tetrahydroindene (similar in size to indene but does not favour ring slippage) would allow a range of complexes with different reactivities which would help the comparison (**Figure 6.3**).

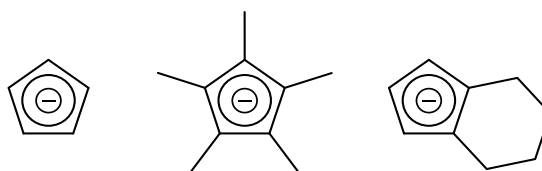


Figure 6.3: Alternative anionic donors.

Modification of the tethered NHC ligand would allow further testing of the effects of tethering and variation of steric and electronics (**Figure 6.4**). Some work in the literature has been conducted on tethered unsaturated NHC with indenyl in Rh complexes,¹⁸¹ however, these were not alkene complexes and the Rh complexes were not examined for C-H borylation catalysis. Thus their reactivity is unexplored and would provide an interesting comparison to the saturated tethered complexes synthesised in this work. Changing the N-substituent to smaller, less solubilising groups may enable the synthesis of indenyl-functionalised tethered NHC ligands which would enable better comparison between the monodentate and tethered ligand complexes.

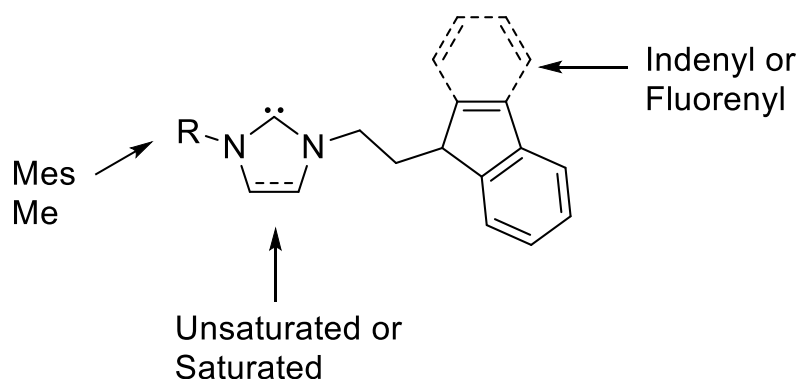
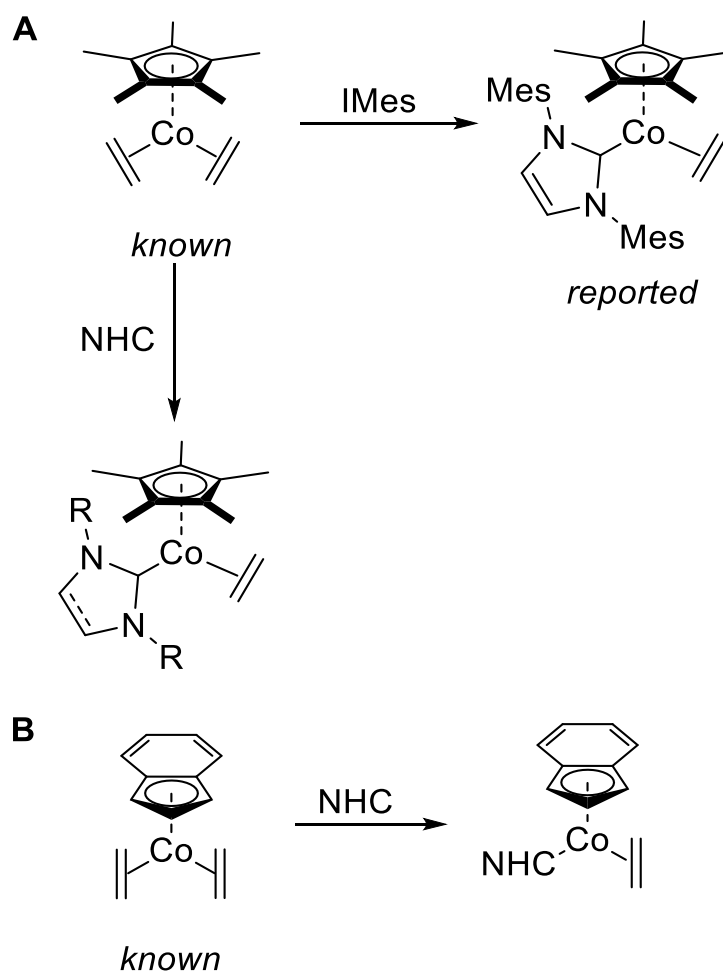


Figure 6.4: Variation of tethered NHC ligands.

6.3 Alternative metals

Changing the metal from rhodium may be beneficial due to accessing different reactivity/selectivity as well as use of more abundant metals improving the sustainability of the catalytic reactions. Moving up group 9, cobalt half-sandwich complexes have been reported with Cp and Cp* (**Scheme 6.1, A**),²⁰¹ but no testing for activity in borylation was carried out. The formation of the Cp and Cp* cobalt complexes with NHCs was found to occur under much milder conditions than with rhodium (ambient temperature rather than 80 °C). The analogous indenyl species have not been reported but the bis(ethene) complex is reported in the literature (**Scheme 6.1, B**),^{286, 287} providing a possible starting point for the synthesis of these complexes.



Scheme 6.1: Possible monodentate Co half-sandwich complexes with NHCs, with Cp* (A) and indenyl (B).

Other possible candidates for half-sandwich based catalysis could be manganese or iron, but these may require different ligands due to the different oxidation states from group 9 complexes.

Chapter 7: Experimental

7.1 General remarks

All reactions requiring inert conditions were performed using standard Schlenk line techniques or in a glovebox under an atmosphere of dinitrogen. Dry toluene, THF and MeCN were obtained from a solvent purification system (MBraun SP-300), degassed and stored over 4 Å molecular sieves prior to use. Petroleum ether (40-60°C) was dried over sodium wire, distilled and stored over 4 Å molecular sieves prior to use. Diethyl ether was dried over sodium/benzophenone, distilled and stored over 4 Å molecular sieves prior to use. Fluorobenzene, octane and decane were dried over 4 Å molecular sieves and degassed via freeze-pump-thaw cycles prior to use. C₆D₆ and C₆H₆ were dried over molten potassium, distilled and stored in the glovebox prior to use. (C₁₃H₉)C₂H₄N(H)C₂H₄N(H)(Dipp) was synthesised as previously reported.²¹⁰ Hydrogen gas used at the University of York was obtained from a hydrogen generator. Pinacolborane (HBpin) was purchased from Acros Organics, and was distilled and stored in the glovebox freezer prior to use. Catecholborane (HBcat) was purchased from Sigma Aldrich, and was distilled and stored in the glovebox freezer prior to use. Bis(pinacolato)diborane (B₂pin₂) was purchased from Fluorochem and stored in the glovebox. Triethylsilane was purchased from Sigma Aldrich and stored in the glovebox prior to use. Triethoxysilane, diethoxymethylsilane and dimethylphenylsilane were purchased from Alfa Aesar and stored in the glovebox prior to use. Lithium bis(trimethylsilyl)amide (LiHMDS), sodium bis(trimethylsilyl)amide (NaHMDS) and potassium bis(trimethylsilyl)amide (KHMDS) were purchased from Sigma Aldrich and stored in the glovebox prior to use. Phenyllithium²⁸⁸ and lithium 2,2,6,6-tetramethylpiperidide²⁸⁹ were synthesised accordingly to literature procedures and stored in the glovebox. [Rh(CO)₂Cl]₂, [Rh(C₂H₄)₂Cl]₂ and [Rh(COE)₂Cl]₂ were synthesised, from RhCl₃·xH₂O supplied by Johnson Matthey, according to literature procedures and were stored in the glovebox freezer prior to use.^{198, 199, 290} 1,3-Bis(diisopropylphenyl)imidazolidinylidene (SIPr) was synthesised according to literature procedures and stored in the glovebox.¹⁰⁶ [Rh(Ind)(COE)₂] and [Rh(Ind)(C₂H₄)₂] were synthesised according to literature procedures and stored in the glovebox.^{206, 213} LiInd and LiFlu were synthesised according to literature procedures and stored in the glovebox.²⁹¹

NMR spectra were obtained on either a Bruker AV 400, AVIII 400 or AVIIIHD 400 spectrometer. ^1H NMR spectra were recorded at 400 MHz and the spectra referenced to the residual solvent peak (7.26 ppm for CDCl_3 , 7.16 ppm for C_6D_6 and 1.94 ppm for CD_3CN). Multiplicity is quoted as singlet (s), doublet (d), triplet (t), quartet (q), quintet (quin), broad (br.) and apparent (app.). $^{13}\text{C}\{^1\text{H}\}$ NMR spectra were recorded at 101 MHz and the spectra referenced to the internal solvent peak (77.16 ppm for CDCl_3 , 128.06 ppm for C_6D_6 and 118.26 ppm for CD_3CN). Assignments are based on DEPT spectra as well as cross-referencing connectivity from ^1H - ^{13}C HSQC and HMBC experiments. ^7Li NMR spectra were recorded at 155 MHz and referenced to an external standard of LiCl in D_2O . ^{11}B NMR spectra were recorded at 128 MHz, with additional $^{11}\text{B}\{^1\text{H}\}$ spectra recorded as required. ^{19}F NMR spectra were recorded at 377 MHz. $^{29}\text{Si}\{^1\text{H}\}$ NMR spectra were recorded at 75.9 MHz using an INEPT pulse sequence and referenced to an external standard of Me_4Si .

Melting points were recorded on a Stuart SMP-10 instrument and are quoted with the solvent of crystallisation.

Mass spectrometry was conducted at the National Mass Spectrometry Facility at Swansea University or at the University of Edinburgh using the techniques stated for the compounds listed in this chapter. Additional mass spectrometry was also conducted at the University of York using the LDFI technique during a research visit.

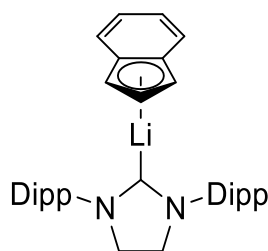
Elemental analyses were performed by Dr Brian Hutton (Heriot-Watt University, non air-sensitive) and Mr Stephen Boyer (London Metropolitan University, air sensitive). For the homobimetallic alkali metal compounds, great difficulties were experienced in obtaining satisfactory elemental analyses for these highly air-sensitive compounds. Compound **2.8** (with $\text{Li}[\text{N}(\text{SiMe}_3)_2]$, $\text{pK}_a = 26$) required multiple analyses to get satisfactory data with widely differing results despite high purities of the samples (as judged by multinuclear NMR spectroscopy). Despite many attempts, satisfactory analyses for the other compounds were not achieved. The much higher pK_a values for LiPh (43) and LiTMP (37) are likely to reflect their higher sensitivities.

Single crystal X-ray diffraction experiments were conducted at Heriot-Watt University using a Bruker X8 APEXII or a Bruker D8 Venture diffractometer, at the University of Edinburgh on an Oxford Diffraction diffractometer, or at the EPSRC National Crystallography Service at the University of Southampton.

7.2 Synthetic methods

7.2.1 Monodentate complexes

η^5 -Indenyl lithium SIPr, 2.3



In a glovebox, LiInd (24.4 mg, 0.200 mmol) and SIPr (78.1 mg, 0.200 mmol) were combined in C_6H_6 (3 cm^3). The reaction mixture was heated at 80°C for 30 mins to dissolve all of the starting materials and then left to crystallise for 3 days at room temperature. The product was isolated by filtration and dried yielding an off-white solid (25.0 mg, 0.0488 mmol, 24%).

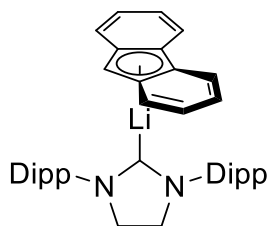
1H NMR (400 MHz, C_6D_6 , 298 K): δ = 7.46 (dd, 2H, J = 6.2, 3.1 Hz, ArH), 7.23 (t, 2H, J = 7.7Hz, ArH), 7.07 (d, 4H, J = 7.7Hz, ArH), 6.82 (dd, 2H, J = 6.3, 3.1 Hz, ArH), 6.36 (t, 1H, J = 3.4Hz, Ind-H), 6.02 (d, 2H, J = 3.3 Hz, Ind-H), 3.05 (br s, 4H, NCH_2CH_2N), 2.69 (br s, 4H, $CH(CH_3)_2$), 1.23 (d, 12H, J = 6.8 Hz, CH_3), 1.11 (br d, 12H, J = 6.5 Hz, CH_3).

$^{13}C\{^1H\}$ NMR (101 MHz, C_6D_6 , 298 K): δ = 223 (v. br., carbene), 146.8 (ArH), 129.4 (Ar), 128.7 (Ar), 125.9 (Ar), 124.4 (ArH), 120.9 (ArH), 116.6 (ArH), 114.1 (ArH), 92.3 (Ind-H), 53.4 (NCH_2CH_2N), 28.8 ($CHMe_2$), 24.8 (CH_3), 24.3 (CH_3).

7Li NMR (155 MHz, C_6D_6 , 298 K): δ = -9.75.

Elemental analysis $C_{42}H_{51}N_2Li$: calcd. C 84.34, H 8.85, N 5.46; found C 84.21, H 8.86, N 5.20.

η^5 -Fluorenyl lithium SIPr, 2.4



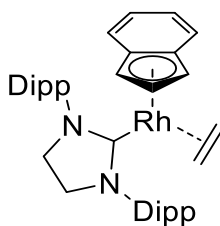
In a glovebox, LiFlu (34.4 mg, 0.2 mmol) and SIPr (78.1 mg, 0.2 mmol) were combined in C_6H_6 (3 cm^3). The reaction mixture was heated at 80°C for 30 mins to dissolve all of the starting materials, forming an orange solution. The reaction was then left to crystallise for 3 days at room temperature. The product was isolated by filtration and dried yielding a yellow microcrystalline solid (61.0 mg, 0.108 mmol, 54%).

1H NMR (400 MHz, C_6D_6 , 298 K): δ = 8.03 (d, 2H, J = 8.0 Hz), 7.38 (d, 2H, J = 8.3 Hz), 7.29-7.19 (m, 4H), 7.00 (t, 6H, J = 7.1 Hz), 6.83 (t, 2H, J = 7.1 Hz), 6.12 (br s, 1H), 2.93 (br s, 4H), 2.50 (br s, 4H), 1.19 (br s, 12H), 1.06 (br s, 12H).

$^{13}C\{^1H\}$ NMR (101 MHz, C_6D_6 , 298 K): δ = 220 (v. br., carbene), 146.5, 143.6, 142.3, 131.8, 129.5, 128.6, 127.1, 127.0, 125.3, 124.4, 122.2, 120.7, 120.2, 118.9, 117.4, 113.8, 79.6 (Ar and Flu C), 53.3 (NCH₂CH₂N), 37.0, 28.8 (CHMe₂), 24.8 (CH₃), 24.3 (CH₃).

7Li NMR (155 MHz, C_6D_6 , 298 K): δ = -8.95.

η^5 -Indenyl rhodium SIPr η^2 -ethene, 2.5



[Rh(Ind)(C₂H₄)₂] (95 mg, 0.347 mmol) and SIPr (135 mg, 0.347 mmol) were combined in a Schlenk flask together with toluene (5 cm^3) in the glovebox. The solution was heated at 80°C for 16 h. The solvent was removed in vacuo and the residue washed with pentane (3 x 10 cm^3). The residue was dried under vacuum to obtain the product as an orange solid (140 mg, 0.220 mmol, 64 %). Crystals suitable for X-ray diffraction were obtained from a concentrated C_6D_6 solution.

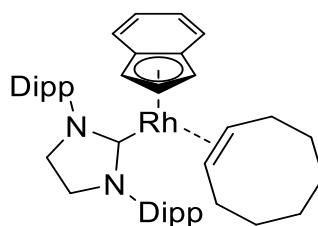
^1H NMR (400 MHz, C_6D_6 , 298 K): δ = 7.23 (d, 1H, J = 8.3 Hz, ArH), 7.21 (d, 1H, J = 8.3 Hz, ArH), 7.11 (d, 4H, J = 8.1 Hz, ArH), 6.69-6.71 (m, 2H, IndH), 6.39-6.42 (m, 2H, IndH), 6.35 (q, 1H, J = 2.7 Hz, IndH), 4.92 (d, 2H, J = 2.8 Hz, IndH), 3.39 (app. sept., 4H, J = 6.7 Hz, CHMe₂), 3.25 (s, 4H, NCH₂CH₂N), 2.27 (br s., 4H, C₂H₄), 1.38 (d, 12H, J = 6.8 Hz, CH(CH₃)₂), 1.10 (d, 12H, J = 6.9 Hz, CH(CH₃)₂).

$^{13}\text{C}\{^1\text{H}\}$ NMR (101 MHz, C_6D_6 , 298 K): δ = 215.5 (d, J = 68.6 Hz, carbene), 147.0, 139.5, 128.7, 124.9, 121.4, 120.9, 116.4, 96.0 (d, J = 6.1 Hz, Ind), 72.9 (d, J = 3.9 Hz, Ind), 54.0 (d, J = 2.0 Hz, NCH₂CH₂N), 35.6 (d, J = 15.2, C₂H₄), 28.9 (CHMe₂), 26.3 (CH(CH₃)₂), 23.5 (CH(CH₃)₂).

UV-vis: 7251.6 dm³mol⁻¹cm⁻¹ at λ_{max} 404 nm

Elemental analysis C₃₈H₄₉H₂Rh: calcd C 71.68, H 7.76, N 4.40; found C 71.73, H 7.85, N 4.45.

η^5 -Indenyl rhodium SIPr η^2 -cyclooctene, **2.6**



Method A: [Rh(Ind)(COE)₂] (303 mg, 0.694 mmol) and SIPr (271 mg, 0.694 mmol) were added to a Schlenk flask in the glovebox. Toluene (5 cm³) was added and the mixture heated at 80°C for 16 h. After this time, the solvent was removed in vacuo. Pentane (5 cm³) was added and the mixture stirred for 10 mins before all volatiles were removed in vacuo. The residue was washed with pentane (3 x 10 cm³) and the solid dried under vacuum to afford the product as a yellow-orange solid (349 mg, 0.485 mmol, 70 %). Crystals suitable for X-ray diffraction were obtained from a concentrated benzene solution.

Method B: **2.9** (10 mg, 7.82 μmol) and IndLi (1.9 mg, 0.0156 mmol, 2 eq.) were combined in C_6D_6 (0.7 cm³). Following the reaction by ^1H NMR spectroscopy, the reaction was complete within 1 hr with the resonances matching those observed for **2.6**, and the reaction mixture turned from cloudy yellow to clear yellow-orange.

¹H NMR (400 MHz, C₆D₆, 298 K): δ = 7.25 (d, 1H, J = 8.3 Hz, ArH), 7.23 (d, 1H, J = 8.3 Hz, ArH), 7.14 (d, 4H, J = 8.2 Hz, ArH), 6.74-6.78 (m, 2H, IndH) 6.39-6.41 (m, 3H, IndH), 4.95 (d, 2H, J = 2.9 Hz, IndH), 3.50 (appr. sept., 4H, J = 6.7 Hz, CHMe₂), 3.28 (s, 4H, NCH₂CH₂N), 2.58-2.60 (m, 2H, alkene), 1.89-1.93 (m, 2H, COE CH₂), 1.57-1.72 (m, 6H, COE CH₂), 1.41 (d, 12H, J = 6.7 Hz, CH(CH₃)₂), 1.27-1.37 (m, 4H, COE CH₂), 1.10 (d, 12H, J = 6.8 Hz, CH(CH₃)₂).

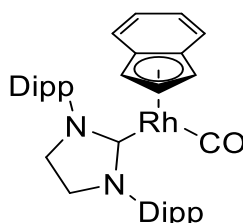
¹³C{¹H} NMR (101 MHz, C₆D₆, 298 K): δ = 214.9 (d, J = 70.1 Hz, carbene), 146.7, 140.2, 128.5, 124.9, 123.1, 121.0, 117.0, 97.4 (d, J = 6.3 Hz, Ind), 74.2 (d, J = 4.1 Hz, Ind), 61.5 (d, J = 15.3 Hz, alkene), 54.5 (d, J = 2.0 Hz, NCH₂CH₂N), 33.1 (COE CH₂), 32.4 (COE CH₂), 28.9 (CHMe₂), 27.1 (COE CH₂), 26.3 (CH(CH₃)₂), 23.8 (CH(CH₃)₂).

UV-vis: 5391.6 dm³mol⁻¹cm⁻¹ at λ_{\max} 409 nm

Elemental analysis C₄₄H₅₉N₂Rh: calcd C 73.52, H 8.27, N 3.90; found C 73.48, H 8.29, N 4.00.

HRMS (ASAP/TOF): Calcd. for C₃₆H₄₄N₂Rh⁺: 607.2560, [M-COE-H]⁺, Found: 607.2562 m/z.

η^5 -Indenyl rhodium SIPr carbonyl, 2.7



To a solution of [Rh(Ind)(SIPr)(C₂H₄)] (270 mg, 0.424 mmol) in toluene (5 cm³), CO was bubbled through at the rate of 1 bubble per second for 30 mins. The solution lightened from orange to yellow-orange. After this time, the solvent was removed in vacuo and the product was obtained as a yellow solid (214.0 mg, 0.336 mmol, 79 %). Crystals suitable for X-ray diffraction were obtained from a concentrated benzene solution.

¹H NMR (400 MHz, C₆D₆, 298 K): δ = 7.24 (d, 1H, J = 8.2 Hz, ArH), 7.22 (d, 1H, J = 8.2 Hz, ArH), 7.11 (d, 4H, J = 7.9 Hz, ArH), 6.75-6.78 (m, 2H, IndH), 6.56-6.59 (m, 2H, IndH), 6.01 (q, 1H, J = 2.8 Hz, IndH), 5.06 (d, 2H, J = 2.9 Hz, IndH), 3.34 (s, 4H,

$\text{NCH}_2\text{CH}_2\text{N}$), 3.25 (app. sept., 4H, $J = 6.8$ Hz, CHMe_2), 1.31 (d, 12H, $J = 6.8$, $\text{CH}(\text{CH}_3)_2$), 1.13 (d, 12H, $J = 6.9$ Hz, $\text{CH}(\text{CH}_3)_2$).

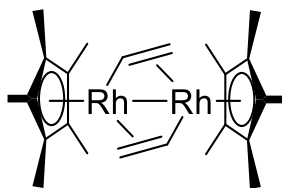
$^{13}\text{C}\{^1\text{H}\}$ NMR (101 MHz, C_6D_6 , 298 K): $\delta = 214.8$ (d, $J = 68.8$ Hz, carbene), 195.1 (d, $J = 93.3$ Hz, CO), 147.3, 139.2, 129.2, 125.1, 122.8, 122.0, 116.8, 99.9 (d, $J = 6.5$, IndH), 71.1 (IndH), 54.0 (d, $J = 2.0$ Hz, $\text{NCH}_2\text{CH}_2\text{N}$), 29.0 (CHMe_2), 26.1 ($\text{CH}(\text{CH}_3)_2$), 23.6 ($\text{CH}(\text{CH}_3)_2$).

IR (thin film)/ cm^{-1} : 1944 (CO).

UV-vis: $6909.4 \text{ dm}^3\text{mol}^{-1}\text{cm}^{-1}$ at λ_{max} 392 nm

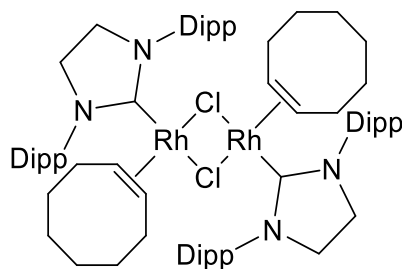
Elemental analysis $\text{C}_{37}\text{H}_{45}\text{N}_2\text{ORh}$: calcd C 69.80, H 7.12, N 4.40; found C 69.72, H 7.21, N 4.29.

η^5 -pentamethylcyclopentadienyl rhodium η^2 ethenyl dimer, **2.8**



$[\text{Rh}(\text{Cp}^*)(\text{C}_2\text{H}_4)_2]$ (372.7 mg, 1.266 mmol) and SIPr (494.7 mg, 1.266 mmol) were combined in toluene (5 cm^3) and the reaction mixture was heated at $110 \text{ }^\circ\text{C}$ for 40 hrs. The solvent was removed in vacuo and pentane (5 cm^3) was added. After stirring for 15 mins, the mixture was filtered and the residue washed with pentane ($3 \times 3 \text{ cm}^3$). The filtrate was concentrated to a third and placed in the freezer for 1 week. During this time crystals had formed and were isolated by filtration of the supernatant solution. The crystals were found to be a mixture of $[\text{Rh}(\text{Cp}^*)(\text{C}_2\text{H}_4)_2]$ and **2.8**. Due to similar solubility it was not possible to fully isolate the product.

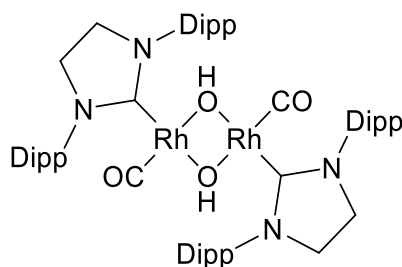
Rhodium SIPr η^2 -cyclooctene chloride dimer, **2.9**



In the glovebox, SIPr (109.0 mg, 0.279 mmol, 2 eq.) and $[\text{Rh}(\text{COE})_2\text{Cl}]_2$ (100 mg, 0.139 mmol) were added to a Schlenk flask along with toluene (5 cm³). The reaction mixture was stirred for 16 h at room temperature. The initial reaction mixture turned from cloudy-orange to clear yellow-orange, and then cloudy yellow. The volatiles were removed in vacuo and the residue was washed with pentane (3 x 5 cm³) and dried thoroughly under vacuum to afford the product as a yellow solid (131.3 mg, 0.103 mmol, 74 %). Crystals suitable for X-ray diffraction were obtained from a concentrated benzene solution. It was noted that **2.9** was poorly soluble in C₆D₆, hampering characterisation by NMR spectroscopy, and decomposes in CDCl₃.

¹H NMR (400 MHz, C₆D₆, 298 K): δ = 7.40-7.27 (m,), 7.00-6.96 (m,), 3.59 (br. sept., J = 6.7 Hz, CH(CH₃)₂), 3.25 (br. s, NCH₂CH₂N), 3.81 (br d, COE alkene), 1.81-1.34 (br m, COE CH₂), 1.15 (d, J = 6.7 Hz).

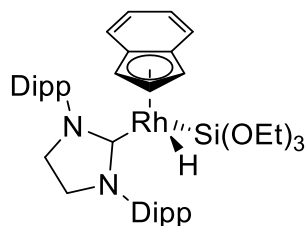
Rhodium SIPr carbonyl hydroxide dimer, **2.10**



To a solution of **2.7** (15 mg) in C₆D₆ (0.7 cm³), water (50 μ L) was added. The reaction was monitored by ¹H NMR spectroscopy over the course of 3 days. The formation of free indene was observed and new resonances for the product of this reaction. Crystals suitable for X-ray diffraction were obtained from a concentrated benzene solution.

¹H NMR (400 MHz, C₆D₆, 298 K): δ = 7.32-7.2 (m, ArH), 7.15-6.95 (m, ArH), 3.33 (s, NCH₂CH₂N), 3.32 (sept., J = 6.9 Hz, CHMe₂), 1.61 (d, 24H, J = 6.7 Hz, CH(CH₃)₂), 1.13 (d, 24H, J = 6.9 Hz, CH(CH₃)₂), -2.6 (s, 2H).

η^5 -Indenyl rhodium SIPr triethoxysilyl hydride, **2.16**



In the glovebox, **2.6** (75.0 mg, 0.104 mmol) was dissolved in toluene (5 cm³) and added to a Schlenk flask. To this solution, (EtO)₃SiH (77 μL, 0.313 mmol, 3 eq.) was added. The reaction mixture was heated to 40 °C and stirred for 16 h. The volatiles were then removed in vacuo and the residue washed with cold pentane (3 x 5 cm³), giving the product as a yellow solid (54.3 mg, 0.0703 mmols, 67 %). Crystals suitable for X-ray diffraction were obtained from a concentrated benzene solution. It was noted that in both the ¹H and ¹³C NMR spectra, broad peaks were observed which point to dynamic exchange e.g. in the ¹³C{¹H} NMR spectra, there are two resonances at 82.1 and 64.0 ppm assignable to the indenyl group rather than one, while the analogous resonance found in **2.5-2.7** occurs at ca. 70 ppm. Thus some assignments are uncertain.

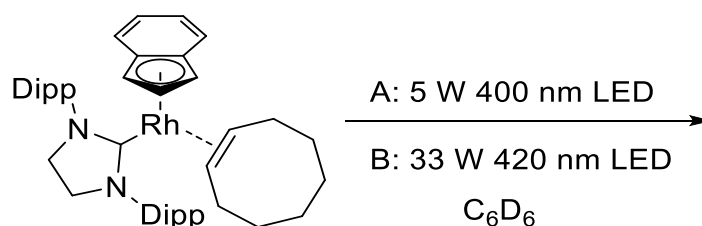
¹H NMR (400 MHz, C₆D₆, 298 K): δ = 7.3 (br, 6H), 7.0 (br m, 2H), 6.9 (br m, 2H) 5.77 (td, 1H, *J* = 2.8, 1.4 Hz, IndH), 4.90 (br ca 1H), 4.49 (br, ca 1H), 3.83 (br, ca 8H), 3.63 (br, 2H), 3.29 (br 2H), 3.07 (br, ca 1H), 2.88 (br, ca 1H), 1.62 (d, *J* = 6.1 Hz), 1.21 (t, *J* = 7.0 Hz), 1.18 (br d), 1.03 (br), 0.71 (br), -15.07 (d, 1H, ¹*J*_{RhH} = 30.6 Hz, Si satellites ²*J*_{SiH} = 15.8 Hz, Rh-H).

¹³C{¹H} NMR (101 MHz, C₆D₆, 298 K): δ = 214.5 (d, *J* = 60.5 Hz, carbene), 147.8 (br), 140.0, 128.3, 128.6, 124.9, 124.3, 122.0, 121.0 100.8 (d, *J* = 3.8 Hz, IndH), 82.1 (br), 64.0 (br), 58.3 (OCH₂CH₃), 53.4 (NCH₂CH₂N), 27.7 (CHMe₂), 26.5 (CH(CH₃)₂), 23.1 (CH(CH₃)₂), 18.5 (OCH₂CH₃).

²⁹Si {¹H} NMR (79.5 MHz, C₆D₆, 298 K): δ = -13.77 (*J* = 67.3 Hz).

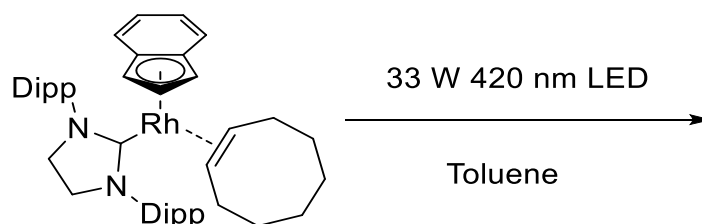
7.2.2 Photolysis

NMR scale



A solution of **2.6** (15.0 mg, 0.0209 mmol) in C_6D_6 (0.7 cm^3) was added to an NMR tube equipped with a J. Young's tap. The tube was suspended adjacent to a blue LED (**Method A**: 400 nm or **B**: 420 nm) at a distance of 3 cm. An appropriately-sized box lined with aluminium foil was used to contain the set-up. The duration of photolysis was initially 5 mins for **A** and 30 s for **B**. The reaction was followed by 1H NMR spectroscopy.

UV-vis scale

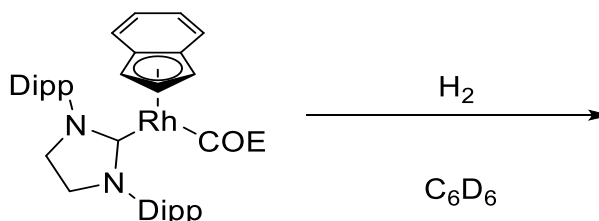


A solution of **2.6** in toluene was prepared such that in the UV-vis spectrum the absorbance at λ_{max} was less than 1 (0.345 mM). A J. Young's tapped quartz cuvette was suspended adjacent to a 420 nm LED in an aluminium lined box. Photolysis was conducted at short intervals with UV-vis spectra recorded quickly after to minimise the effects of ambient light.

7.2.3 Reactions with hydrogen and silanes

General procedure for NMR scale reactions with hydrogen

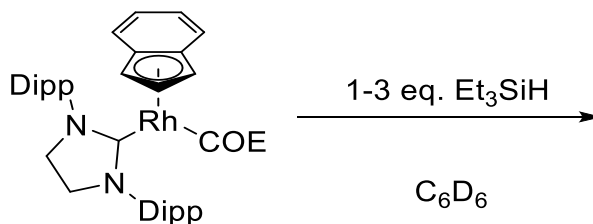
Example: Reaction of **2.6** with hydrogen gas



A solution of **2.6** (15 mg, 0.0209 mmol) in C₆D₆ (0.7 cm³) was added to an NMR tube equipped with a J. Young's tap. The sample is freeze-pump-thaw times to degass the solution, and then H₂ gas is added. The reaction was followed by ¹H NMR spectroscopy at regular intervals. If necessary, further H₂ is added by repeating the degassing step and adding more H₂.

General procedure for NMR scale reactions with silanes

Example: Reaction of **2.6** with triethylsilane

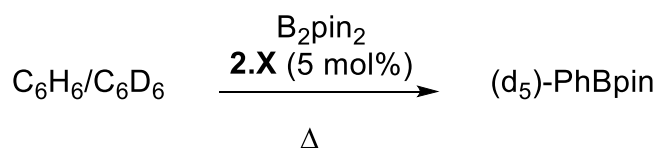


In the glovebox, **2.6** (15 mg, 0.0209 mmol) was dissolved in C₆D₆ (0.5 cm³) and added to an NMR tube equipped with a J. Young's tap. To the sample, triethylsilane (1-3 eq.) was added and the reaction was monitored by ¹H and ²⁹Si NMR spectroscopy. Where necessary, the reaction mixture was heated in an oil bath for increments to facilitate the reaction.

7.2.4 Catalysis

General procedure for NMR-scale catalysis

Example: Benzene-(d₆)

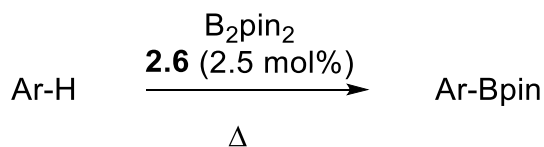


In the glovebox, **2.6** (2.5 mg, 3.48 μmol) and B₂pin₂ (17.7 mg, 0.0696 mmol) were combined in C₆H₆/C₆D₆ (0.7 cm³) and the sample heated at 75°C. The reaction was monitored by ¹H and ¹¹B NMR spectroscopy.

General procedure for preparative scale borylation

Arene

Example: Benzene (Ar = Ph)



In a glovebox, B₂pin₂ (199.4 mg, 0.785 mmol) and **2.6** (12.5 mg, 0.0198 mmol, 2.5 mol%) were dissolved in C₆H₆ (5 cm³) and added to a J. Young's tapped flask. The reaction mixture was heated at 80 °C for 48 hours. The reaction was concentrated in vacuo and the residue extracted with CH₂Cl₂ (2 x 5 cm³). All volatiles were then removed in vacuo to give the crude mixture. The product was purified by column chromatography (SiO₂, CH₂Cl₂), using KMnO₄ to visualise the TLC spots, affording the product as a colourless oil (130 mg, 0.636 mmol, 81 %).

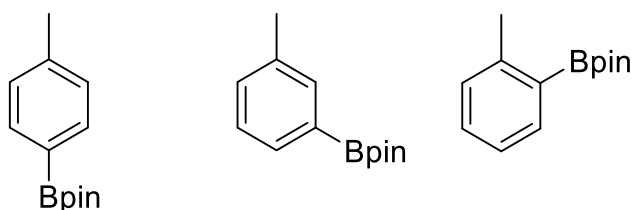
PhBPin, D₅-PhBpin

¹H NMR (400 MHz, CDCl₃, 298 K): δ = 7.81 (dd, 2H, *J* = 8.0, 1.4 Hz, ortho ArH), 7.46 (tt, 1H, *J* = 7.4, 1.5 Hz, para ArH), 7.36 (tt, 2H, *J* = 7.2, 1.2 Hz, meta ArH), 1.35 (s, 12H, Me). ¹H NMR and ¹³C spectral data match literature values.²⁹²

¹¹B NMR (128 MHz, CDCl₃, 298 K): δ = 30.97 (s)

MS (EI/MS): Calcd. for $C_{12}H_{17}BO_2^+$: 204.1 $[M]^+$, Found: 204.1 $[M]^+$ and 189.1 $[M-CH_3]^+$ m/z. Calcd. for $C_{12}H_{12}D_5BO_2^+$: 209.2 $[M]^+$, Found: 209.2 $[M]^+$ and 194.1 $[M-CH_3]^+$ m/z.

TolylBpin

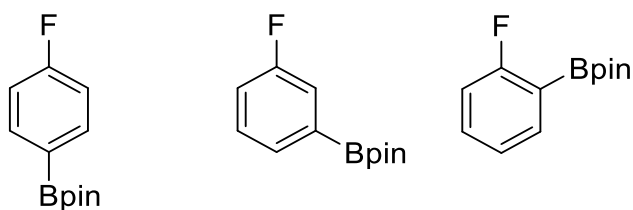


Following the general procedure using toluene (5 cm^3), the product was obtained as colourless oil (130.0 mg, 0.596 mmol, 76 %). 1H NMR spectral data match literature values as a mixture of isomers (o: 0.07, m: 1.00, p: 0.42).^{249, 293}

^{11}B NMR (128 MHz, $CDCl_3$, 298 K): $\delta = 31.0$ (s).

MS (EI/MS): Calcd. for $C_{13}H_{19}BO_2^+$: 218.1 $[M]^+$, Found: 218.1 $[M]^+$ and 203.1 $[M-CH_3]^+$ m/z.

(C_6H_4F)Bpin



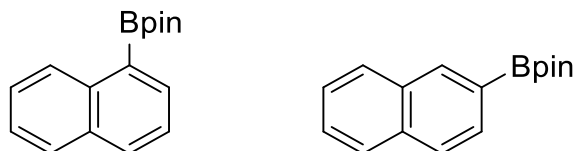
Following the general procedure using fluorobenzene (5 cm^3), the product was obtained as colourless oil (58.1 mg, 0.262 mmol, 33 %). 1H NMR spectral data match literature values as a mixture of isomers (o: 0.91, m: 1, p: 0.18).²⁹³

^{11}B NMR (128 MHz, $CDCl_3$, 298 K): $\delta = 30.5$ (s).

^{19}F NMR ($CDCl_3$, 377 MHz, 298 K): $\delta = -102.63$ (dt, $J = 9.2, 5.9$ Hz, ortho), -108.46 (tt, $J = 9.2, 6.2$ Hz, para), -114.2 (tt, $J = 13.6, 5.6$ Hz, meta).

MS (EI/MS): Calcd. for $C_{12}H_{16}BFO_2^+$: 222.1 $[M]^+$, Found: 222.1 $[M]^+$ and 207.1 $[M-CH_3]^+$ m/z.

NaphthylBpin



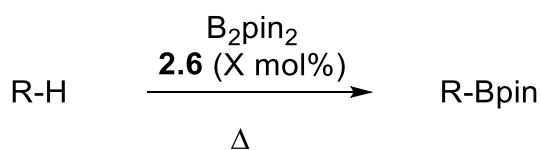
Following the general procedure using naphthalene (201.2 mg, 1.57 mmol, 2 eq.), the product was obtained as colourless oil (76 mg, 0.299 mmol, 38 %). 1H NMR spectral data match literature values as a mixture of isomers (1-position: 0.07, 2-position: 1).^{294, 295}

^{11}B NMR (128 MHz, $CDCl_3$, 298 K): $\delta = 31.1$ (s).

MS (EI/MS): Calcd. for $C_{16}H_{19}BO_2^+$: 254.1 $[M]^+$, Found: 254.1 $[M]^+$ and 239.1 $[M-CH_3]^+$ m/z.

Alkane

Example: Decane (R = decyl)



In a glovebox, B_2pin_2 (121 mg, 0.476 mmol) and **2.6** (34.4 mg, 0.0476 mmol, 10 mol%) were dissolved in decane (5 cm^3) and added to a J. Young's tapped flask. The reaction mixture was heated at 150 °C for 48 h. The reaction was concentrated in vacuo and the residue extracted with CH_2Cl_2 (2 x 5 cm^3). All volatile were then removed in vacuo to give the crude mixture. The product was purified by column chromatography (SiO_2 , CH_2Cl_2), using $KMnO_4$ to visualise the TLC spots, affording the product as a colourless oil (23 mg, 0.0857 mmol, 18 %). The 1H and ^{13}C NMR data match those reported in the literature.²⁹⁶

Borylation of octane: octylBpin

Using the above procedure with **2.6** (17.2 mg, 0.024 mmol, 5 mol%) of at 130 °C the product was obtained as a colourless oil (8 mg, 0.033 mmol, 7%). The ¹H and ¹¹B NMR data match those reported in the literature.⁷⁴

¹H NMR (400 MHz, CDCl₃, 298 K): δ = 1.40-1.20 (m, 24H), 0.87 (t, 3H, *J* = 6.9 Hz, CH₃CH₂), 0.76 (t, 2H, *J* = 7.7 Hz, CH₂Bpin).

¹³C{¹H} NMR (101 MHz, CDCl₃, 298 K): δ = 83.0 (OCMe₂), 32.6, 32.0, 29.6, 29.4, 24.9(CMe₂), 24.2, 22.8, 14.3 (CH₃CH₂), 11.5 (br, CH₂B).

¹¹B NMR (128 MHz, CDCl₃, 298 K): δ = 34.27.

HRMS (ASAP/TOF): Calcd. for C₁₄H₃₀¹⁰BO₂⁺: 240.2375, [M+H]⁺, Found: 240.2375 m/z.

Also, traces of the diborylated product were present: pinBC₈H₁₆Bpin. HRMS (ASAP/TOF): Calcd. for C₂₀H₄₁¹⁰BO₄⁺: 365.3264, [M+H]⁺, Found: 365.3260 m/z.

Borylation of decane: decylBPin

¹H NMR (400 MHz, CDCl₃, 298 K): δ = 1.44-1.13 (m, 28H), 0.87 (t, 3H, *J* = 6.9 Hz, CH₃CH₂), 0.76 (t, 2H, *J* = 7.8 Hz, CH₂Bpin).

¹³C{¹H} NMR (101 MHz, CDCl₃, 298 K): δ = 83.0 (OCMe₂), 32.6, 32.1, 29.8, 29.7, 29.6, 29.5, 24.9 (CMe₂), 24.2, 22.8, 14.3 (CH₃CH₂), 11.3 (br, CH₂B).

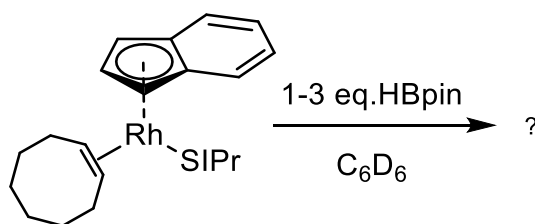
¹¹B NMR (128 MHz, CDCl₃, 298 K): δ = 34.27.

HRMS (ASAP/TOF): Calcd. for C₁₆H₃₄¹⁰BO₂⁺: 268.2688, [M+H]⁺, Found: 268.2688 m/z.

Also, traces of the diborylation product were present: pinBC₁₀H₂₀Bpin. HRMS (ASAP/TOF): Calcd. for C₂₂H₄₅¹⁰BO₄⁺: 394.3540, [M+H]⁺, Found: 394.3539 m/z.

General procedure for stoichiometric NMR scale reactions

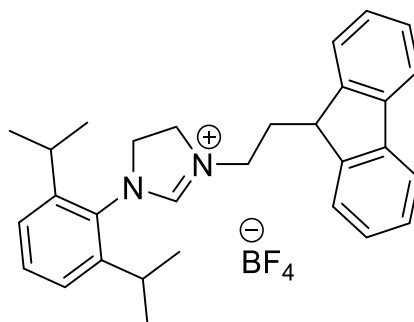
Example: reaction of **2.6** with HBpin



In the glovebox, **2.6** (15 mg, 0.0209 mmol) was dissolved in C₆D₆ (0.5 cm³) and added to an NMR tube equipped with a J. Young's tap. To the sample, HBpin (1-3 eq.) was added and the reaction was monitored by ¹H and ¹¹B NMR spectroscopy. Where necessary, the reaction mixture was heated in an oil bath for increments to facilitate the reaction.

7.2.5 Tethered ligands and complexes

3-(2-(9H-fluoren-9-yl)ethyl)-1-(2,6-diisopropylphenyl)-4,5-dihydro-1H-imidazol-3-ium tetrafluoroborate, 4.2-BF₄



In a Schlenk flask, (C₁₃H₉)C₂H₄N(H)C₂H₄N(H)(Dipp) (5.348 g, 12.96 mmol), NH₄BF₄ (2.10 g, 18.3 mmol, 1.5 eq.) and triethyl orthoformate (20 cm³) were combined in toluene (15 cm³) with a few drops of formic acid. The reaction mixture was heated at 100°C overnight. Upon cooling, the volatiles were removed under reduced pressure and the residue was extracted with CH₂Cl₂ (15 cm³) to remove excess NH₄BF₄. The filtrate was concentrated and diethyl ether added to precipitate the crude product. The crude product was purified with column chromatography (SiO₂, MeCN/CH₂Cl₂, 3:17→1:3 v/v). Recrystallisation from CH₂Cl₂/diethyl ether afforded the product as a colourless solid (4.376 g, 8.57 mmol, 66 %). Single crystals suitable for X-ray diffraction were obtained from slow cooling of a hot C₆H₆ solution.

Rf: 0.24 (MeCN/CH₂Cl₂, 1:4).

MP (CH₂Cl₂/diethyl ether): 166-168°C.

¹H NMR (CD₃CN, 400 MHz, 298 K): δ 7.86-7.88 (m, 2 H, Ar), 7.80 (s, 1 H, NCHN), 7.64-7.67 (m, 2H, Ar), 7.38-7.48 (m, 5H, Ar), 7.31 (d, J = 7.7Hz, 2H, Ar), 4.20 (d, J = 5.6Hz, 1H, Flu-H), 3.99 (m, 4H, overlapping NCH₂CH₂N), 3.30-3.34 (m, 2H, NCH₂CH₂Flu), 2.87 [app. sept, J = 6.8Hz, CH(CH₃)₂], 2.51-2.56 (m, 2H, NCH₂CH₂Flu), 1.23 [d, J = 6.8Hz, 6H, CH(CH₃)₂], 1.17 [d, J = 6.8Hz, 6H, CH(CH₃)₂].

¹³C NMR (CD₃CN, 101 MHz, 298 K): δ 158.6 (Imid CH), 147.9, 146.6, 142.0, 132.1, 131.1, 128.7, 128.4, 125.9, 125.6, 121.2, 54.3 (NCH₂CH₂N), 50.1 (NCH₂CH₂N), 46.3 (NCH₂CH₂), 45.8 (Flu-H), 30.8 (CH₂CH₂Flu), 29.2 (CHMe₂), 24.9 (CH₃), 24.4 (CH₃).

¹⁹F NMR (CD₃CN, 377 MHz, 298 K) δ -151.8 (s).

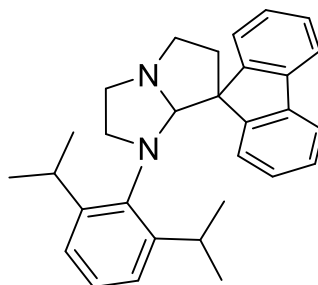
¹¹B NMR (CD₃CN, 128 MHz, 298 K) δ -1.17.

IR (thin film)/cm⁻¹ 3068(w), 2966(w), 1642(s), 1449(m), 1270(w), 1055(s), 740(m).

HRMS (ESI⁺) 423.2788 [M-BF₄]⁺, C₃₀H₃₅N₂ requires 423.2795.

Elemental Analysis C₃₀H₃₅N₂BF₄: calcd. C 70.59, H 6.91, N 5.49; found C 70.59, H 6.92, N 5.20.

**(R)-1'-(2,6-diisopropylphenyl)-1',2',3',5',6',7a'-
hexahydrospiro[fluorene9,7'-pyrrolo[1,2-a]imidazole], 4.3**



To a stirred suspension of **4.2-BF₄** (1.2 g, 2.24 mmol, 1.1 eq.) in diethyl ether (20 cm³), n-BuLi (1.4 ml, 1.512 M, 2.12 mmol, 1 eq.) was added at -78°C. The reaction was allowed to warm to room temperature. A red solution initially formed which slowly faded to a colourless, clear solution. After 2 hours, the solvent was removed under reduced pressure and the resultant white residue dried thoroughly under vacuum. The residue was extracted with pet ether (3 x 10 cm³) and filtered. Removal of the solvent gave the product as a pure, colourless solid (714 mg, 1.63 mmol, 80%). Crystals suitable for X-ray diffraction were obtained from a concentrated pet ether solution.

MP (pet ether): 123-125°C.

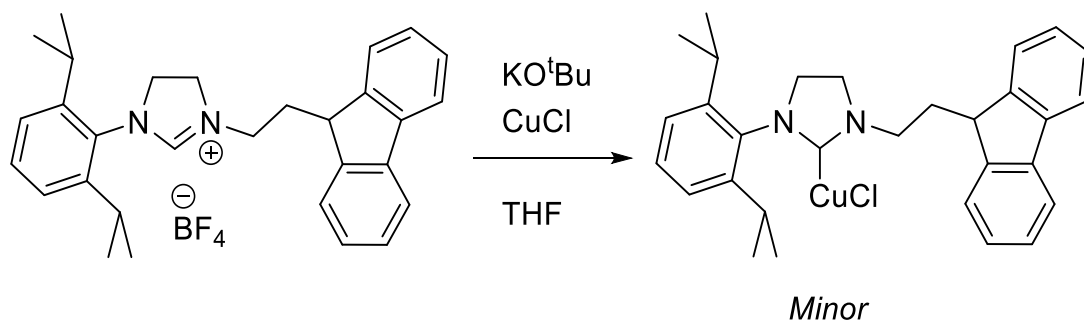
¹H NMR (C₆D₆, 400 MHz, 298 K): δ = 7.66-7.64 (m, 1H, Ar), 7.47 (dq, J = 5.5, 0.6 Hz, 1H, Ar), 7.38-7.36 (m, 1H, Ar), 7.31-7.26 (m, 2H, Ar), 7.17-7.15 (m, 1H, overlap with C₆H₆), 6.99-6.85 (m, 4H, Ar), 6.73 (dd, J = 5.5, 1.8Hz, 1H, Ar), 5.45 (s, 1H, NCHN), 3.63-3.52 (m, 3H), 3.47 (ddd, J = 10.1, 7.8, 2.1 Hz, 1H), 3.11-2.98 (m, 3H), 2.48-2.37 (m, 2H), 1.95 (ddd, J = 13.1, 6.5, 2.2Hz, 1H), 1.40 (d, J = 6.7Hz, CH₃), 1.18 (d, J = 6.8Hz, CH₃), 0.80 (d, J = 6.9Hz, CH₃), 0.68 (d, J = 6.9Hz, CH₃).

^{13}C NMR (C_6D_6 , 101 MHz, 298 K): δ = 150.1 (Dipp-Ar), 149.8, 147.1 (Dipp-Ar), 145.0, 141.9, 140.9, 127.8, 127.1, 127.0, 127.0, 126.9, 125.3, 123.1, 122.3, 120.3, 119.8, 98.8 [CH, NCH(Flu)], 62.1 (4°), 57.6 (NCH₂CH₂N), 55.0 (NCH₂CH₂N), 53.7 (NCH₂CH₂Flu), 40.2 (CH₂Flu), 27.2 (CH), 26.7 (CH), 26.1 (CH₃), 25.2 (CH₃), 24.7 (CH₃), 23.2 (CH₃).

HRMS (ASAP⁺) 423.2800 [M+H]⁺, C₃₀H₃₅N₂ requires 423.2795.

Elemental Analysis C₃₀H₃₄N₂: calcd. C 85.26, H 8.11, N 6.63; found C 85.08, H 8.20, N 6.69.

(1-(2-(9H-fluoren-9-yl)ethyl)-3-(2,6-diisopropylphenyl)imidazolidin-2-yl) copper(I) chloride, **4.4**

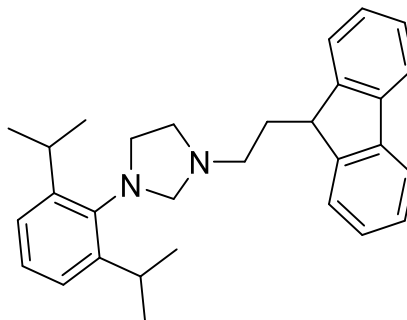


In the glovebox, **4.2-BF₄** (20.0 mg, 0.0392 mmol), CuCl (5.8 mg, 0.0588 mmol) and KO^tBu (4.8 mg, 0.0392 mmol, 1.1 eq.) are combined in THF (1 cm³). After mixing the solution was filtered and solvent removed in vacuo. C₆D₆ (0.5 cm³) was added and ¹H NMR spectrum was recorded. The major product was the spirocycle **4.3**, however, resonances for **4.4** were observed.

^1H NMR (C_6D_6 , 400 MHz, 298 K): δ = (aryl CH overlap with 4.3 resonances) 3.74 (t, J = 4.9 Hz), 2.93 (m), 2.80 (app. sept., J = 6.8 Hz), 2.22 (m), 1.37 (d, J = 6.8 Hz), 1.09 (d, J = 6.6 Hz).

^{13}C NMR (C_6D_6 , 101MHz, 298 K): δ = 202.2 (carbene), 146.9 (Ar C), 146.3, 141.5, 135.3, 129.9, 124.9, 124.7, 53.4 (NCH₂CH₂N), 48.7 (NCH₂CH₂N), 46.5 (Flu-H), 45.3, 32.4, 31.4, 28.7, 28.3 br, 25.4 [CH(CH₃)₂], 24.2 [CH(CH₃)₂].

1-(2-(9H-fluoren-9-yl)ethyl)-3-(2,6-diisopropylphenyl)imidazolidine, 4.5



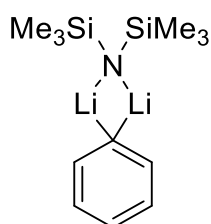
To a stirred suspension of **4.2-BF₄** (510 mg, 1.00 mmol) in THF (10 cm³), LiBEt₃H (1.0 cm³, 1.0 mmol, 1 M in THF) was added dropwise at 0 °C. The reaction mixture was allowed to warm up to room temperature and stirred for 16 h. The volatiles were removed in vacuo and resulting residue was extracted with toluene (3 x 10 cm³). Removal of the solvent under reduced pressure gave the product as a white solid (426 mg, 0.819 mmol, 82 %)

¹H NMR (C₆D₆, 400 MHz, 298 K): δ = 7.63 (d, J = 7.4 Hz, 2H, Flu ArH), 7.36 (d, J = 7.3 Hz, 2H, Flu ArH), 7.10-7.73 (m, 7H, Flu ArH, Dipp ArH + residual C₆H₆), 4.00 (t, J = 5.9 Hz, 1H, Flu CH), 3.86 (s, 2H, NCH₂N), 3.69 (app. sept., J = 6.8 Hz, 2H, CHMe₂), 3.22 (t, J = 5.6 Hz, 2H, NCH₂CH₂N), 2.66 (t, J = 5.6 Hz, 2H, NCH₂CH₂N), 2.36 (t, J = 7.3 Hz, 2H, NCH₂CH₂Flu), 2.01 (q, J = 6.7 Hz, 2H, NCH₂CH₂Flu), 1.22 (d, J = 6.6 Hz, 12H, CH(CH₃)₂).

¹³C NMR (C₆D₆, 101MHz, 298 K): δ = 150.2 (Dipp Ar C), 147.8 (Flu Ar C), 142.8 (Dipp Ar C), 141.6 (Flu Ar C), 127.4 (Flu Ar CH), 127.2 (Flu Ar CH), 125.7 (Ar CH), 124.8 (Ar CH), 124.5 (Ar CH), 120.3 (Ar CH), 76.7 (NCH₂N), 54.7 (NCH₂CH₂N), 53.3 (NCH₂CH₂N), 50.9 (NCH₂CH₂Flu), 45.8 (Flu-H), 32.8 (NCH₂CH₂Flu), 27.9 (CHMe₂), 24.8 (CH₃).

HRMS (ASAP⁺) 425.2960 [M+H]⁺, C₃₀H₃₆N₂ requires 425.2957.

Lithium hexamethyldisilylamide-lithium phenyl adduct, 4.9



LiPh (336 mg, 4.00 mmol) and LiN(SiMe₃)₂ (670 mg, 4.00 mmol) were combined in toluene (10 cm³) and mixed for 5 mins. The solution was then concentrated under reduced pressure and left overnight at 20°C for the product to crystallise out. The supernatant solution was filtered away and the solid washed with cold pet ether (2 x 10 cm³). The solid was dried under vacuum, obtaining the product as an off-white microcrystalline solid (510 mg, 2.03 mmol, 51%). Single crystals suitable for X-ray diffraction were obtained from concentrated C₆H₆ solutions.

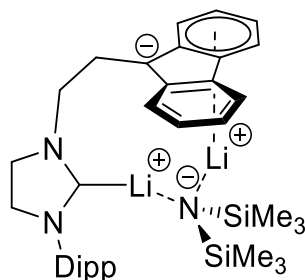
¹H NMR (C₆D₆, 400 MHz, 298 K): δ = 8.06 (dd, J = 7.4, 1.6Hz, 2H, *ortho*-ArH), 7.13 (t, J = 7.4Hz, 2H, *meta*-ArH overlaps with residual solvent peak for C₆D₆), 6.98-6.94 (m, 1H, *para*-ArH), 0.09 (s, 18H, SiMe₃).

¹³C NMR (C₆D₆, 101 MHz, 298 K): δ = 181.2 (Ar-Li), 144.9 (*ortho*-ArH), 128.1 (*meta*-ArH, overlaps with C₆D₆ peak), 126.9 (*para*-ArH), 5.6 (SiMe₃).

⁷Li NMR (C₆D₆, 155.5 MHz, 298 K): δ -0.55 (s).

²⁹Si NMR (C₆D₆, 79.5 MHz, 298 K): δ -10.92 (s).

Fluorenyl-NHC dilithium hexamethyldisilylamide, 4.8



4.3 (400 mg, 0.946 mmol), Li[N(SiMe₃)₂] (174.3 mg, 1.041 mmol) and LiPh (87.5 mg, 1.041 mmol) were combined in toluene (5 cm³) and the sample was heated for 2 days at 80°C. The reaction was allowed to cool and all of the volatiles were removed under reduced pressure. Toluene (1 cm³) and pet ether (20 cm³) were added and the mixture was stirred vigorously for 5 hr. After standing for 30 mins, the resultant red precipitate was isolated by filtration, washed with pet ether (5 cm³) and dried under vacuum affording the product as a red solid (495 mg, 0.831 mmol, 88%). Crystals suitable for X-ray diffraction were obtained from a concentrated C₆H₆ solution.

¹H NMR (C₆D₆, 400 MHz, 298 K): δ = 8.26 (ddd, 2H, *J* = 7.8, 1.1, 0.8 Hz), 7.52 (d, 2H, *J* = 8.2 Hz), 7.32 (ddd, 2H, *J* = 8.1, 6.7, 1.2 Hz), 7.01 (dd, 1H, *J* = 8.3, 7.2 Hz), 6.90-6.85 (m, 4H, overlap), 3.63-3.60 (m, 2H, NCH₂CH₂Flu), 3.25-3.17 (m, 4H, NCH₂CH₂N), 3.16-3.13 (m, 2H, NCH₂CH₂Flu), 2.81 (app. sept, 2H, *J* = 6.8 Hz), 1.10 (d, 6H, *J* = 6.9 Hz), 0.99 (d, 6H, *J* = 6.8 Hz), -0.30 (s, 18H, SiMe₃).

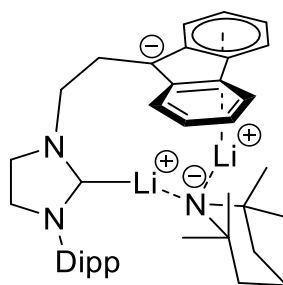
¹³C NMR (C₆D₆, 101 MHz, 298 K): δ = 147.3 (Ar C-CH(CH₃)₂), 137.1 (Ar C-N), 136.2 (Ar C 1 to 9-Flu), 128.8 (Ar CH *para* to N), 124.3 (Ar CH *meta* to N), 121.6 (Ar C 6 to 9-Flu), 121.4 (Ar CH 4 to 9-Flu), 120.8 (Ar CH 5 to 9-Flu), 114.8 (Ar CH 2 to 9-Flu), 109.1 (Ar CH 3 to 9-Flu), 90.8 (9-Flu), 54.1 (NCH₂CH₂N), 52.8 (NCH₂CH₂Flu), 49.4 (NCH₂CH₂N), 28.1 (CH(CH₃)₂), 25.4 (NCH₂CH₂Flu), 25.3 (CH₃), 25.0 (CH₃), 5.1 (SiMe₃).

⁷Li NMR (C₆D₆, 155.5 MHz, 298 K): δ -0.86, -5.68.

²⁹Si NMR (C₆D₆, 79.5 MHz, 298 K): δ -10.00.

Elemental Analysis C₃₆H₅₁Li₂N₃Si₂: calcd. C 72.56, H 8.63, N 7.05; found C 72.46, H 8.67, N 6.91.

Fluorenyl NHC dilithium tetramethylpiperidide, 4.7



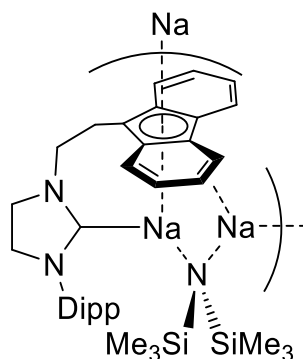
4.3 (400 mg, 0.946 mmol), LiTMP (139.2 mg, 0.946 mmol) and LiPh (79.5 mg, 0.946 mmol) were combined in toluene (5 cm³) and the sample was heated for 1 day at 80°C. The reaction was allowed to cool and all of the volatiles were removed under reduced pressure. Toluene (1 cm³) and pet ether (20 cm³) were added and the mixture was vigorously stirred for 5 hr. After standing for 30 mins, the resultant red precipitate was isolated by filtration, washed with pet ether (5 cm³) and dried under vacuum affording a red solid (349 mg, 0.605 mmol, 64%). Recrystallisation from toluene at -78°C afforded crystalline material which was isolated by filtration and dried under vacuum to give the

product as a red-orange solid (93 mg, 0.16 mmol, 17%). Crystals suitable for X-ray diffraction were obtained from a concentrated C₆H₆ solution.

¹H NMR (C₆D₆, 400 MHz, 298 K): δ = 8.73 (d, 2H, *J* = 7.8 Hz), 7.54 (d, 2H, *J* = 8.2 Hz), 7.32 (app. t, 2H, *J* = 6.9 Hz), 7.01 (t, 1H, *J* = 7.2 Hz), 6.94-6.89 (m, 4H, overlap), 3.57-3.54 (m, 6H, overlap), 3.27-3.21 (m, 2H, NCH₂CH₂Flu), 2.71 (app. sept, 2H, *J* = 6.8 Hz), 1.48-1.45 (m, 1H), 1.34-1.29 (m, 2H), 1.19-1.14 (m, 3H), 1.07 (d, 6H, *J* = 6.9 Hz), 0.99 (d, 6H, *J* = 6.8 Hz), 0.77 (s, 6H, Me), 0.31 (s, 6H, Me).

⁷Li NMR (C₆D₆, 155.5 MHz, 298 K): δ 0.09, -5.40.

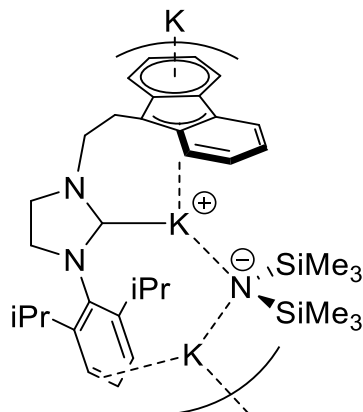
[Na₂{μ-N(SiMe₃)₂}] {μ-(η⁵-C₁₃H₈)C₂H₄N(κ-C)N(C₂H₄)(Dipp)}], **4.10**



4.3 (50 mg, 0.118 mmol), NaN(SiMe₃)₂ (21.7 mg, 0.118 mmol) and NaCH₂Ph (13.5 mg, 0.118 mmol) were combined in toluene (5 cm³). The reaction mixture was heated for 30 mins at 80°C and then left to cool overnight. The mixture was filtered at 0°C and the remaining solid dried under vacuum to obtain the product as an orange solid (14 mg, 0.0214 mmol, 18%). Crystals suitable for X-ray diffraction were obtained from an NMR scale reaction (0.047 mmol) in C₆D₆ after transferring the sample to a vial and leaving it to crystallise for 1 week.

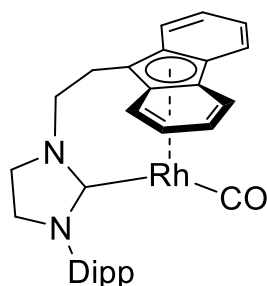
Compound **4.10** (and **4.11**) showed very poor solubility in benzene and toluene precluding NMR spectroscopic analysis.

[K₂{μ-N(SiMe₃)₂}{μ-(C₁₃H₈)C₂H₄N(κ-C)N(C₂H₄)(Dipp)}], 4.11



4.3 (50 mg, 0.118 mmol), KN(SiMe₃)₂ (23.6 mg, 0.118 mmol) and KCH₂Ph (15.4 mg, 0.118 mmol) were combined in toluene (5 cm³). The reaction mixture was heated for 30 mins at 80°C and then left to cool overnight. The mixture was filtered at 0°C and the remaining solid dried under vacuum to obtain the product as an orange solid (40 mg, 0.060 mmol, 51%). Crystals suitable for X-ray diffraction were obtained from an NMR scale reaction (0.047 mmol) in C₆D₆ after transferring the sample to a vial and leaving to crystallise for 3 weeks.

[Rh{(η⁵-C₁₃H₈)C₂H₄N(κ-C)N(C₂H₄)(Dipp)}(CO)], 4.12



In the glovebox, **4.3** (211.3 mg, 0.500 mmol), Li[N(SiMe₃)] (92.0 mg, 0.550 mmol) and LiPh (46.2 mg, 0.550 mmol) were combined in toluene (5 cm³). The sample was heated for 2 d at 80°C. After this time, [Rh(CO)₂Cl]₂ (97.2 mg, 0.250 mmol) in toluene (10 cm³) was added at -78 °C and the reaction was allowed to warm to room temperature and stir over the weekend. The reaction mixture was filtered and all volatiles were removed in vacuo. The residue was washed with pentane (3 x 10 cm³) and the solvent removed in vacuo. The product was extracted with CH₂Cl₂ and filtered; this was repeated with

toluene. The solution was concentrated and left to crystallise, producing the product as red-orange crystals (48.2 mg, 0.0872 mmol, 17 %).

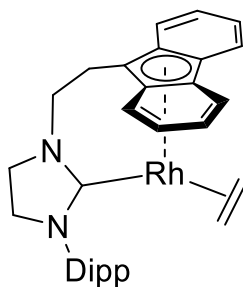
¹H NMR (C₆D₆, 400 MHz, 298 K): δ = 7.70-7.72 (m, 2H, FluH), 7.26-7.28 (m, 2H, FluH), 7.03-7.12 (m, 5H, overlap of FluH + Dipp ArH), 6.93 (d, 2H, *J* = 7.7 Hz, Dipp ArH), 3.30-3.33 (m, 2H, CH₂), 3.14-3.19 (m, 2H, CH₂), 2.92-2.96 (m, 2H, CH₂), 2.59-2.70 (m, 4H, overlap of CHMe₂ + CH₂), 1.02 (d, 6H, *J* = 7.0 Hz, CH(CH₃)₂), 0.92 (d, 6H, *J* = 6.7 Hz, CH(CH₃)₂).

¹³C NMR (C₆D₆, 101 MHz, 298 K): δ = 214.1 (d, *J* = 78.8 Hz, carbene), 192.9 (d, *J* = 90.9 Hz, CO), 147.3, 137.5, 129.3, 128.7, 124.7, 122.5, 121.5, 119.8, 118.1 (d, *J* = 3.2 Hz), 116.6, 102.0, 70.6, 53.8, 51.4, 28.5(CH(CH₃)₂), 25.4 (CH(CH₃)₂), 23.4 (CH(CH₃)₂).

IR (thin film)/cm⁻¹: 1946.

HRMS (ASAP/TOF): Calcd. for C₃₁H₃₄N₂ORh⁺: 553.1721, [M+H]⁺, Found: 553.1714 m/z. Calcd. for C₃₀H₃₃N₂Rh⁺: 524.1699, [M-CO]⁺, Found: 524.1687 m/z. Calcd. for C₃₁H₃₄N₂O₂Rh⁺: 569.1670, [M+OH]⁺, Found: 569.1666 m/z.

[Rh{(η⁵-C₁₃H₈)C₂H₄N(κ-C)N(C₂H₄)(Dipp)}(C₂H₄)], **4.13**



In glovebox, **4.3** (211.3 mg, 0.5 mmol), Li[N(SiMe₃)₂] (92.0 mg, 0.55 mmol) and LiPh (46.2 mg, 0.55 mmol) were combined in toluene (5 cm³). The sample was heated for 2 d at 80°C. After this time, [Rh(C₂H₄)₂Cl]₂ (97.2 mg, 0.25 mmol) in toluene (10 cm³) was added and the reaction mixture was stirred for 72 h. The reaction mixture was filtered and all volatiles were removed in vacuo. The residue was washed with pentane (3 x 10 cm³) and dried in vacuo. The solid was extracted with toluene (15 cm³) and filtered. The solution was concentrated and left to crystallise, producing yellow crystals of **4.13** (15 mg, 0.0271 mmol, 5 %).

¹H NMR (C₆D₆, 400 MHz, 298 K): δ = 7.48-7.50 (m, 2H, FluH), 7.35-7.37 (m, 2H, FluH), 7.11-7.15 (m, 4H, FluH, partial overlap with residual C₆H₆ peak), 7.00 (t, 1H, *J* = 7.8 Hz, Dipp ArH), 6.84 (d, 2H, *J* = 7.6 Hz, Dipp ArH), 3.40-3.44 (m, 2H, CH₂), 2.99-3.07 (m, 2H, CH₂), 2.73-2.87 (m, 6H, overlap of 2x CH₂ and 2x CHMe₂), 1.29 (br. s., 4H, C₂H₄), 0.99 (d, 6H, *J* = 6.7 Hz, CH(CH₃)₂), 0.96 (d, 6H, *J* = 6.9 Hz, CH(CH₃)₂).

¹³C NMR (C₆D₆, 101 MHz, 298 K): δ = 213.0 (d, *J* = 79.5 Hz, carbene), 147.0, 137.6, 128.6, 124.3, 122.2, 120.8, 118.8, 117.3, 116.3, 116.1, 103.3, 72.0 (d, *J* = 5.4 Hz, Flu), 55.1 (d, *J* = 3.0 Hz, CH₂), 51.9 (CH₂), 50.8 (CH₂), 44.7 (d, *J* = 13.6 Hz, ethene), 28.4 (CHMe₂), 26.3 (CH(CH₃)₂), 23.3 (CH(CH₃)₂).

7.3 Tables of crystallographic data

	2.3	2.4
Empirical formula	C ₄₂ H ₅₁ LiN ₂	C ₄₃ H ₅₀ LiN ₂
Formula weight	590.78	601.79
Temperature/K	100.0	100.0
Crystal system	monoclinic	monoclinic
Space group	<i>P</i> 2 ₁ / <i>c</i>	<i>P</i> 2 ₁ / <i>n</i>
<i>a</i> /Å	15.4547(4)	9.4944(3)
<i>b</i> /Å	12.7182(3)	16.7806(5)
<i>c</i> /Å	18.8864(5)	22.8382(7)
α /°	90	90
β /°	102.0690(10)	90.3750(10)
γ /°	90	90
Volume/Å ³	3630.18(16)	3638.54(19)
<i>Z</i>	4	4
ρ_{calc} /cm ³	1.081	1.099
μ /mm ⁻¹	0.061	0.062
<i>F</i> (000)	1280.0	1300.0
Crystal size/mm ³	0.45 × 0.40 × 0.26	0.40 × 0.40 × 0.28
Radiation	MoK α (λ = 0.71073)	MoK α (λ = 0.71073)
2 Θ range for data collection/°	5.658 to 56.606	5.876 to 57.426
Index ranges	-20 ≤ <i>h</i> ≤ 20, -16 ≤ <i>k</i> ≤ 16, -25 ≤ <i>l</i> ≤ 25	-12 ≤ <i>h</i> ≤ 12, -22 ≤ <i>k</i> ≤ 22, -30 ≤ <i>l</i> ≤ 30
Reflections collected	149816	119093
Independent reflections	9006 [<i>R</i> _{int} = 0.0478, <i>R</i> _{sigma} = 0.0166]	9385 [<i>R</i> _{int} = 0.0476, <i>R</i> _{sigma} = 0.0213]
Data/restraints/parameters	9006/0/414	9385/1/393
Goodness-of-fit on <i>F</i> ²	1.036	1.027
Final <i>R</i> indexes [<i>I</i> ≥ 2 σ (<i>I</i>)]	<i>R</i> ₁ = 0.0387, <i>wR</i> ₂ = 0.0931	<i>R</i> ₁ = 0.0663, <i>wR</i> ₂ = 0.1531
Final <i>R</i> indexes [all data]	<i>R</i> ₁ = 0.0500, <i>wR</i> ₂ = 0.1019	<i>R</i> ₁ = 0.0837, <i>wR</i> ₂ = 0.1656
Largest diff. peak/hole / e Å ⁻³	0.31/-0.21	0.65/-0.53
Diffractometer	D8 Venture	D8 Venture

	2.5	2.6
Empirical formula	C ₃₈ H ₄₉ N ₂ Rh	C ₄₄ H ₅₉ N ₂ Rh
Formula weight	636.70	718.84
Temperature/K	120.0(1)	100.0
Crystal system	monoclinic	orthorhombic
Space group	<i>P2₁/c</i>	<i>Pbca</i>
a/Å	10.04226(19)	18.4246(6)
b/Å	19.1446(3)	21.4379(7)
c/Å	17.3168(3)	37.0393(10)
α/°	90	90
β/°	106.327(2)	90
γ/°	90	90
Volume/Å ³	3194.98(11)	14630.0(8)
Z	4	16
ρ _{calc} /g/cm ³	1.324	1.305
μ/mm ⁻¹	0.563	0.500
F(000)	1344.0	6112.0
Crystal size/mm ³	0.394 × 0.312 × 0.215	0.5 × 0.5 × 0.05
Radiation	MoKα (λ = 0.71073)	MoKα (λ = 0.71073)
2θ range for data collection/°	5.852 to 65.942	5.498 to 54.996
Index ranges	-15 ≤ h ≤ 15, -28 ≤ k ≤ 28, -26-21 ≤ l ≤ 23, -48 ≤ 1 ≤ 45	-27 ≤ k ≤ 16, -48 ≤ 1 ≤ 45
Reflections collected	82040	73947
Independent reflections	11529 [R _{int} = 0.0519, R _{sigma} = 0.0354]	16736 [R _{int} = 0.0270, R _{sigma} = 0.0227]
Data/restraints/parameters	11529/0/390	16736/0/882
Goodness-of-fit on F ²	1.061	1.025
Final R indexes [I ≥ 2σ (I)]	R ₁ = 0.0312, wR ₂ = 0.0684	R ₁ = 0.0270, wR ₂ = 0.0599
Final R indexes [all data]	R ₁ = 0.0390, wR ₂ = 0.0718	R ₁ = 0.0358, wR ₂ = 0.0634
Largest diff. peak/hole / e Å ⁻³	0.58/-0.62	0.41/-0.42
Diffractionmeter	University of Edinburgh	Bruker D8 Venture

	2.7	2.8
Empirical formula	C ₃₇ H ₄₅ N ₂ ORh	C ₂₄ H ₃₆ Rh ₂
Formula weight	636.66	530.35
Temperature/K	100.0	100.0
Crystal system	monoclinic	monoclinic
Space group	<i>P</i> 2 ₁ / <i>c</i>	<i>C</i> 2/ <i>c</i>
<i>a</i> /Å	10.0182(2)	11.5282(15)
<i>b</i> /Å	19.3666(5)	12.5724(16)
<i>c</i> /Å	17.1516(4)	15.699(2)
α /°	90	90
β /°	106.8980(10)	105.622(5)
γ /°	90	90
Volume/Å ³	3184.05(13)	2191.4(5)
Z	4	4
ρ_{calc} /cm ³	1.328	1.608
μ /mm ⁻¹	4.561	1.511
F(000)	1336.0	1080.0
Crystal size/mm ³	0.42 × 0.22 × 0.18	0.25 × 0.20 × 0.12
Radiation	CuK α (λ = 1.54178)	MoK α (λ = 0.71073)
2 Θ range for data collection/°	7.06 to 144.256	6.508 to 66.312
Index ranges	-12 ≤ <i>h</i> ≤ 12, -23 ≤ <i>k</i> ≤ 23, -19 ≤ <i>l</i> ≤ 21	-17 ≤ <i>h</i> ≤ 17, 0 ≤ <i>k</i> ≤ 19, 0 ≤ <i>l</i> ≤ 24
Reflections collected	45288	5672
Independent reflections	6185 [R _{int} = 0.0255, R _{sigma} = 0.0167]	5672 [R _{int} = twinned data, R _{sigma} = 0.0136]
Data/restraints/parameters	6185/0/378	5672/0/133
Goodness-of-fit on F ²	1.069	1.200
Final R indexes [<i>I</i> ≥ 2 σ (<i>I</i>)]	R ₁ = 0.0224, wR ₂ = 0.0594	R ₁ = 0.0185, wR ₂ = 0.0533
Final R indexes [all data]	R ₁ = 0.0227, wR ₂ = 0.0596	R ₁ = 0.0209, wR ₂ = 0.0651
Largest diff. peak/hole / e Å ⁻³	0.41/-0.70	0.49/-0.76
Diffractometer	Bruker D8 Venture	Bruker D8 Venture

	2.9	2.13
Empirical formula	C ₈₂ H ₁₁₆ Cl ₂ N ₄ Rh ₂	C ₄₂ H ₆₁ N ₂ O ₃ RhSi
Formula weight	1434.50	772.92
Temperature/K	100.0	100.0
Crystal system	monoclinic	monoclinic
Space group	<i>C2/c</i>	<i>Cc</i>
a/Å	16.6682(7)	20.4826(9)
b/Å	21.4373(8)	11.1294(4)
c/Å	20.5528(9)	18.2980(6)
α/°	90	90
β/°	93.971(2)	107.733(2)
γ/°	90	90
Volume/Å ³	7326.3(5)	3973.0(3)
Z	4	4
ρ _{calc} /g/cm ³	1.301	1.292
μ/mm ⁻¹	4.653	4.062
F(000)	3040.0	1640.0
Crystal size/mm ³	0.2 × 0.2 × 0.1	0.58 × 0.22 × 0.06
Radiation	CuKα (λ = 1.54178)	CuKα (λ = 1.54184)
2θ range for data collection/°	6.728 to 150.182	11.116 to 149.146
Index ranges	-20 ≤ h ≤ 20, -26 ≤ k ≤ 26, -25 ≤ l ≤ 25	-25 ≤ h ≤ 25, -13 ≤ k ≤ 13, -21 ≤ l ≤ 22
Reflections collected	134922	59950
Independent reflections	7509 [R _{int} = 0.0293, R _{sigma} = 0.0106]	7781 [R _{int} = 0.0451, R _{sigma} = 0.0333]
Data/restraints/parameters	7509/0/469	7781/2/457
Goodness-of-fit on F ²	1.047	1.045
Final R indexes [I ≥ 2σ (I)]	R ₁ = 0.0179, wR ₂ = 0.0426	R ₁ = 0.0200, wR ₂ = 0.0513
Final R indexes [all data]	R ₁ = 0.0184, wR ₂ = 0.0428	R ₁ = 0.0202, wR ₂ = 0.0514
Largest diff. peak/hole / e ⁻ Å ⁻³	0.31/-0.41	0.42/-0.48
Flack parameter		0.034(6)
Diffractometer	Bruker D8 Venture	Bruker D8 Venture

	2.19	3.7
Empirical formula	C ₆₈ H ₉₀ N ₄ O ₄ Rh ₂	C _{78.5} H _{101.5} B ₃ N ₄ O ₆ Rh ₂
Formula weight	1233.25	1435.38
Temperature/K	100.0	100.0
Crystal system	triclinic	orthorhombic
Space group	<i>P</i> -1	<i>Pbca</i>
<i>a</i> /Å	9.1518(18)	24.8674(4)
<i>b</i> /Å	12.442(3)	21.7758(4)
<i>c</i> /Å	14.300(3)	28.6884(5)
α /°	74.87(3)	90
β /°	78.00(3)	90
γ /°	78.25(3)	90
Volume/Å ³	1518.1(6)	15535.0(5)
Z	1	8
ρ_{calc} /cm ³	1.349	1.227
μ /mm ⁻¹	0.595	3.830
F(000)	648.0	6028.0
Crystal size/mm ³	0.40 × 0.24 × 0.08	0.42 × 0.28 × 0.06
Radiation	MoK α (λ = 0.71073)	CuK α (λ = 1.54178)
2 Θ range for data collection/°	5.984 to 63.366	6.162 to 149.662
Index ranges	-13 ≤ <i>h</i> ≤ 13, -17 ≤ <i>k</i> ≤ 18, -29 ≤ <i>l</i> ≤ 31, -0 ≤ <i>l</i> ≤ 21	-29 ≤ <i>h</i> ≤ 31, -27 ≤ <i>k</i> ≤ 27, -35 ≤ <i>l</i> ≤ 35
Reflections collected	9781	197875
Independent reflections	9781 [R _{int} = twinned data, R _{sigma} = 0.0395]	15899 [R _{int} = 0.0451, R _{sigma} = 0.0193]
Data/restraints/parameters	9781/0/365	15899/48/1010
Goodness-of-fit on F ²	1.051	1.045
Final R indexes [<i>I</i> ≥ 2 σ (<i>I</i>)]	R ₁ = 0.0278, wR ₂ = 0.0522	R ₁ = 0.0359, wR ₂ = 0.1023
Final R indexes [all data]	R ₁ = 0.0333, wR ₂ = 0.0542	R ₁ = 0.0395, wR ₂ = 0.1054
Largest diff. peak/hole / e Å ⁻³	0.50/-0.72	1.22/-1.24
Diffractometer	Bruker D8 Venture	Bruker D8 Venture

	4.2-BF₄	4.3
Empirical formula	C ₃₀ H ₃₅ BF ₄ N ₂	C ₃₀ H ₃₄ N ₂
Formula weight	510.41	422.59
Temperature/K	100.0	100.0
Crystal system	orthorhombic	monoclinic
Space group	<i>Pbca</i>	<i>Cc</i>
a/Å	15.2178(15)	35.165(8)
b/Å	11.8778(10)	9.280(2)
c/Å	30.409(4)	14.963(3)
α/°	90	90
β/°	90	90.931(14)
γ/°	90	90
Volume/Å ³	5496.6(10)	4882(2)
Z	8	8
ρ _{calc} /g/cm ³	1.234	1.150
μ/mm ⁻¹	0.090	0.066
F(000)	2160.0	1824.0
Crystal size/mm ³	0.2 × 0.12 × 0.02	0.6 × 0.35 × 0.03
Radiation	MoKα (λ = 0.71075)	MoKα (λ = 0.71073)
2θ range for data collection/°	4.552 to 49.426	4.54 to 55.408
Index ranges	-17 ≤ h ≤ 17, -13 ≤ k ≤ 13, -35 ≤ l ≤ 35	-45 ≤ h ≤ 45, 0 ≤ k ≤ 12, 0 ≤ l ≤ 18
Reflections collected	32599	5423
Independent reflections	4672 [R _{int} = 0.3287, R _{sigma} = 0.1574]	5423 [R _{int} = twinned data, R _{sigma} = 0.1087]
Data/restraints/parameters	4672/0/338	5423/2/586
Goodness-of-fit on F ²	1.099	1.062
Final R indexes [I ≥ 2σ (I)]	R ₁ = 0.1306, wR ₂ = 0.2439	R ₁ = 0.0699, wR ₂ = 0.1601
Final R indexes [all data]	R ₁ = 0.2136, wR ₂ = 0.2831	R ₁ = 0.1132, wR ₂ = 0.1890
Largest diff. peak/hole / e Å ⁻³	0.28/-0.35	0.42/-0.42
Flack parameter		0(5)
Diffractometer	NCS	Bruker X8 Apex II

	4.7	4.8
Empirical formula	C ₃₉ H ₅₁ Li ₂ N ₃	C ₃₆ H ₅₁ Li ₂ N ₃ Si ₂
Formula weight	575.70	595.85
Temperature/K	100	100.0
Crystal system	monoclinic	monoclinic
Space group	<i>P2₁/c</i>	<i>P2₁/c</i>
a/Å	13.0403(6)	17.8401(6)
b/Å	12.0336(5)	11.9822(4)
c/Å	22.0611(10)	17.7207(6)
α/°	90	90
β/°	92.317(3)	105.920(2)
γ/°	90	90
Volume/Å ³	3459.0(3)	3642.8(2)
Z	4	4
ρ _{calc} /cm ³	1.105	1.086
μ/mm ⁻¹	0.063	0.124
F(000)	1248.0	1288.0
Crystal size/mm ³	0.22 × 0.22 × 0.04	0.50 × 0.35 × 0.30
Radiation	MoKα (λ = 0.71073)	MoKα (λ = 0.71073)
2θ range for data collection/°	4.744 to 55.13	4.718 to 55.06
Index ranges	-16 ≤ h ≤ 16, -15 ≤ k ≤ 15, -28 ≤ l ≤ 28	--23 ≤ h ≤ 23, -15 ≤ k ≤ 15, -22 ≤ l ≤ 23
Reflections collected	58481	45224
Independent reflections	7934 [R _{int} = 0.0668, R _{sigma} = 0.0600]	8221 [R _{int} = 0.0438, R _{sigma} = 0.0410]
Data/restraints/parameters	7934/0/405	8221/0/415
Goodness-of-fit on F ²	1.008	1.021
Final R indexes [I ≥ 2σ (I)]	R ₁ = 0.0475, wR ₂ = 0.0972	R ₁ = 0.0423, wR ₂ = 0.0959
Final R indexes [all data]	R ₁ = 0.0918, wR ₂ = 0.1117	R ₁ = 0.0686, wR ₂ = 0.1081
Largest diff. peak/hole / e Å ⁻³	0.23/-0.23	0.33/-0.29
Diffractometer	Bruker X8 APEX II	Bruker X8 APEX II

	4.9	4.10
Empirical formula	C ₁₂ H ₂₃ Li ₂ NSi ₂	C ₄₈ H ₆₃ N ₃ Na ₂ Si ₂
Formula weight	251.37	784.17
Temperature/K	100	100.0
Crystal system	orthorhombic	monoclinic
Space group	<i>Pnma</i>	<i>P2₁/c</i>
a/Å	17.7758(10)	16.8915(10)
b/Å	7.1723(3)	24.0748(13)
c/Å	12.3300(7)	11.9226(7)
α/°	90	90
β/°	90	106.457(2)
γ/°	90	90
Volume/Å ³	1571.99(14)	4649.8(5)
Z	4	4
ρ _{calc} /cm ³	1.062	1.120
μ/mm ⁻¹	0.203	0.129
F(000)	544.0	1688.0
Crystal size/mm ³	0.3 × 0.2 × 0.04	0.2 × 0.18 × 0.05
Radiation	MoKα (λ = 0.71073)	MoKα (λ = 0.71073)
2θ range for data collection/°	6.572 to 61.158	4.216 to 50.176
Index ranges	-25 ≤ h ≤ 25, -10 ≤ k ≤ 10, -17 ≤ l ≤ 17	-20 ≤ h ≤ 18, -21 ≤ k ≤ 28, -14 ≤ l ≤ 12
Reflections collected	35485	43256
Independent reflections	2577 [R _{int} = 0.0736, R _{sigma} = 0.0329]	8203 [R _{int} = 0.0873, R _{sigma} = 0.0912]
Data/restraints/parameters	2577/0/98	8203/0/494
Goodness-of-fit on F ²	1.035	1.012
Final R indexes [I ≥ 2σ (I)]	R ₁ = 0.0324, wR ₂ = 0.0771	R ₁ = 0.0540, wR ₂ = 0.1058
Final R indexes [all data]	R ₁ = 0.0537, wR ₂ = 0.0866	R ₁ = 0.1161, wR ₂ = 0.1263
Largest diff. peak/hole / e Å ⁻³	0.35/-0.27	0.38/-0.39
Diffractometer	Bruker X8 APEX II	Bruker X8 APEX II

	4.11	4.12
Empirical formula	C ₃₆ H ₅₁ K ₂ N ₃ Si ₂	C ₃₁ H ₃₃ N ₂ ORh
Formula weight	660.17	552.50
Temperature/K	100.0	100.0
Crystal system	monoclinic	orthorhombic
Space group	<i>P2₁/n</i>	<i>P2₁2₁2₁</i>
a/Å	13.0617(8)	11.3032(6)
b/Å	20.7596(14)	13.6808(7)
c/Å	13.7996(9)	16.3132(8)
α/°	90	90
β/°	102.117(3)	90
γ/°	90	90
Volume/Å ³	3658.5(4)	2522.6(2)
Z	4	4
ρ _{calc} /g/cm ³	1.199	1.455
μ/mm ⁻¹	0.353	0.704
F(000)	1416.0	1144.0
Crystal size/mm ³	0.25 × 0.2 × 0.05	0.44 × 0.34 × 0.3
Radiation	MoKα (λ = 0.71073)	MoKα (λ = 0.71073)
2θ range for data collection/°	3.6 to 50.054	5.3 to 64.926
Index ranges	-15 ≤ h ≤ 15, -24 ≤ k ≤ 22, 15 ≤ l ≤ 16	-17 ≤ h ≤ 12, -20 ≤ k ≤ 19, -24 ≤ l ≤ 16
Reflections collected	39240	18129
Independent reflections	6461 [R _{int} = 0.0927, R _{sigma} = 0.0884]	8590 [R _{int} = 0.0410, R _{sigma} = 0.0634]
Data/restraints/parameters	6461/0/398	8590/0/320
Goodness-of-fit on F ²	1.017	0.997
Final R indexes [I ≥ 2σ (I)]	R ₁ = 0.0609, wR ₂ = 0.1328	R ₁ = 0.0333, wR ₂ = 0.0636
Final R indexes [all data]	R ₁ = 0.1264, wR ₂ = 0.1583	R ₁ = 0.0391, wR ₂ = 0.0659
Largest diff. peak/hole / e Å ⁻³	1.60/-0.67	0.47/-0.47
Flack parameter	N/A	-0.035(18)
Diffractometer	Bruker X8 APEX II	UoEdinburgh

4.13

Empirical formula	C ₃₂ H ₃₇ N ₂ Rh
Formula weight	552.54
Temperature/K	100.0
Crystal system	monoclinic
Space group	<i>P</i> 2 ₁
<i>a</i> /Å	8.6176(5)
<i>b</i> /Å	13.6545(8)
<i>c</i> /Å	11.1334(6)
α /°	90
β /°	91.346(2)
γ /°	90
Volume/Å ³	1309.69(13)
<i>Z</i>	2
ρ_{calc} /cm ³	1.401
μ /mm ⁻¹	0.675
<i>F</i> (000)	576.0
Crystal size/mm ³	0.34 × 0.2 × 0.04
Radiation	MoK α (λ = 0.71073)
2 Θ range for data collection/°	5.592 to 72.774
Index ranges	-14 ≤ <i>h</i> ≤ 14, -22 ≤ <i>k</i> ≤ 22, -18 ≤ <i>l</i> ≤ 18
Reflections collected	95195
Independent reflections	12756 [<i>R</i> _{int} = 0.0709, <i>R</i> _{sigma} = 0.0508]
Data/restraints/parameters	12756/1/336
Goodness-of-fit on <i>F</i> ²	1.022
Final <i>R</i> indexes [<i>I</i> ≥ 2 σ (<i>I</i>)]	<i>R</i> ₁ = 0.0360, <i>wR</i> ₂ = 0.0730
Final <i>R</i> indexes [all data]	<i>R</i> ₁ = 0.0481, <i>wR</i> ₂ = 0.0781
Largest diff. peak/hole / e Å ⁻³	1.19/-1.67
Flack parameter	-0.016(11)
Diffractometer	Bruker D8 Venture

Chapter 8: References

1. R. A. Sheldon, *Chem. Soc. Rev.*, 2012, **41**, 1437-1451.
2. B. M. Trost, *Science*, 1991, **254**, 1471-1477.
3. R. A. Sheldon, *Pure Appl. Chem.*, 2000, **72**, 1233-1246.
4. B. M. Trost, *Angew. Chem. Int. Ed.*, 1995, **34**, 259-281.
5. F. Roudesly, J. Oble and G. Poli, *J. Mol. Catal. A: Chem.*, 2017, **426**, 275-296.
6. S. J. Blanksby and G. B. Ellison, *Acc. Chem. Res.*, 2003, **36**, 255-263.
7. R. G. Bergman, *Nature*, 2007, **446**, 391-393.
8. W. D. Jones, *Science*, 2000, **287**, 1942-1943.
9. T. Cernak, K. D. Dykstra, S. Tyagarajan, P. Vachal and S. W. Krska, *Chem. Soc. Rev.*, 2016, **45**, 546-576.
10. M. Moir, J. J. Danon, T. A. Reekie and M. Kassiou, *Expert Opin. Drug Discovery*, 2019, **14**, 1137-1149.
11. D. E. Yerien, S. Bonesi and A. Postigo, *Org. Biomol. Chem.*, 2016, **14**, 8398-8427.
12. T. Gensch, M. N. Hopkinson, F. Glorius and J. Wencel-Delord, *Chem. Soc. Rev.*, 2016, **45**, 2900-2936.
13. M. C. Bryan, P. J. Dunn, D. Entwistle, F. Gallou, S. G. Koenig, J. D. Hayler, M. R. Hickey, S. Hughes, M. E. Kopach, G. Moine, P. Richardson, F. Roschangar, A. Steven and F. J. Weiberth, *Green Chem.*, 2018, **20**, 5082-5103.
14. J. Halpern, *Acc. Chem. Res.*, 1970, **3**, 386-392.
15. C. Hall and R. N. Perutz, *Chem. Rev.*, 1996, **96**, 3125-3146.
16. B. A. Arndtsen, R. G. Bergman, T. A. Mobley and T. H. Peterson, *Acc. Chem. Res.*, 1995, **28**, 154-162.
17. W. D. Jones, *Acc. Chem. Res.*, 2003, **36**, 140-146.
18. P. L. Watson, *J. Am. Chem. Soc.*, 1983, **105**, 6491-6493.
19. R. Waterman, *Organometallics*, 2013, **32**, 7249-7263.
20. R. N. Perutz and S. Sabo-Etienne, *Angew. Chem. Int. Ed.*, 2007, **46**, 2578-2592.
21. C. E. Webster, Y. Fan, M. B. Hall, D. Kunz and J. F. Hartwig, *J. Am. Chem. Soc.*, 2003, **125**, 858-859.
22. J. F. Hartwig, K. S. Cook, M. Hapke, C. D. Incarvito, Y. Fan, C. E. Webster and M. B. Hall, *J. Am. Chem. Soc.*, 2005, **127**, 2538-2552.
23. S. M. Ng, W. H. Lam, C. C. Mak, C. W. Tsang, G. Jia, Z. Lin and C. P. Lau, *Organometallics*, 2003, **22**, 641-651.

24. A. S. Goldman and K. I. Goldberg, in *Activation and Functionalization of C—H Bonds*, American Chemical Society, 2004, vol. 885, ch. 1, pp. 1-43.
25. J. A. Labinger, *Organometallics*, 2015, **34**, 4784-4795.
26. J. P. Collman, *Acc. Chem. Res.*, 2002, **1**, 136-143.
27. H. M. Omer and P. Liu, *J. Am. Chem. Soc.*, 2017, **139**, 9909-9920.
28. Y. Aihara, M. Tobisu, Y. Fukumoto and N. Chatani, *J. Am. Chem. Soc.*, 2014, **136**, 15509-15512.
29. F. Roudesly, J. Oble and G. Poli, *J. Mol. Catal. A: Chem.*, 2017, **426**, 275-296.
30. D. Balcells, E. Clot and O. Eisenstein, *Chem. Rev.*, 2010, **110**, 749-823.
31. Y. Boutadla, D. L. Davies, S. A. Macgregor and A. I. Poblador-Bahamonde, *Dalton Trans.*, 2009, 5820-5831.
32. O. Dimroth, *Ber. Dtsch. Chem. Ges.*, 1902, **35**, 2032-2045.
33. J. Chatt and J. M. Davidson, *J. Chem. Soc.*, 1965, 843-855.
34. A. H. Janowicz and R. G. Bergman, *J. Am. Chem. Soc.*, 1983, **105**, 3929-3939.
35. A. H. Janowicz and R. G. Bergman, *J. Am. Chem. Soc.*, 1982, **104**, 352-354.
36. X. Yang and M. B. Hall, *Inorg. Chem.*, 2019, **58**, 16553-16558.
37. J. K. Hoyano and W. A. G. Graham, *J. Am. Chem. Soc.*, 1982, **104**, 3723-3725.
38. D. M. Haddleton and R. N. Perutz, *J. Chem. Soc., Chem. Commun.*, 1985, 1372-1374.
39. D. M. Haddleton and R. N. Perutz, *J. Chem. Soc., Chem. Commun.*, 1986, 1734-1736.
40. D. M. Haddleton, A. McCamley and R. N. Perutz, *J. Am. Chem. Soc.*, 1988, **110**, 1810-1817.
41. C.-H. Jun, E.-A. Jo and E.-G. Cho, *Synlett*, 2007, **2007**, 1059-1062.
42. D. A. Colby, R. G. Bergman and J. A. Ellman, *Chem. Rev.*, 2010, **110**, 624-655.
43. V. Ritleng, C. Sirlin and M. Pfeffer, *Chem. Rev.*, 2002, **102**, 1731-1770.
44. P. B. Arockiam, C. Bruneau and P. H. Dixneuf, *Chem. Rev.*, 2012, **112**, 5879-5918.
45. S. Murai, F. Kakiuchi, S. Sekine, Y. Tanaka, A. Kamatani, M. Sonoda and N. Chatani, *Nature*, 1993, **366**, 529-531.
46. F. Kakiuchi and S. Murai, *Acc. Chem. Res.*, 2002, **35**, 826-834.
47. D. Kalyani, N. R. Deprez, L. V. Desai and M. S. Sanford, *J. Am. Chem. Soc.*, 2005, **127**, 7330-7331.
48. A. J. Reay, L. A. Hammarback, J. T. W. Bray, T. Sheridan, D. Turnbull, A. C. Whitwood and I. J. S. Fairlamb, *ACS Catal.*, 2017, **7**, 5174-5179.

49. L. A. Hammarback, A. Robinson, J. M. Lynam and I. J. S. Fairlamb, *J. Am. Chem. Soc.*, 2019, **141**, 2316-2328.
50. B. Zhou, H. Chen and C. Wang, *J. Am. Chem. Soc.*, 2013, **135**, 1264-1267.
51. L. Zhang and D. C. Fang, *J. Org. Chem.*, 2016, **81**, 7400-7410.
52. S. Guo, R. Pan, Z. Guan, P. Li, L. Cai, S. Chen, A. Lin and H. Yao, *Org. Lett.*, 2019, **21**, 6320-6324.
53. D. F. Fischer and R. Sarpong, *J. Am. Chem. Soc.*, 2010, **132**, 5926-5927.
54. C. A. James and V. Snieckus, *J. Org. Chem.*, 2009, **74**, 4080-4093.
55. J. Zhao, M. G. Davidson, M. F. Mahon, G. Kociok-Kohn and T. D. James, *J. Am. Chem. Soc.*, 2004, **126**, 16179-16186.
56. W. Li, D. P. Nelson, M. S. Jensen, R. Scott Hoerrner, D. Cai and R. D. Larsen, *Org. Synth.*, 2005, **81**, 89-97.
57. J. L. Kristensen, M. Lysén, P. Vedsø and M. Begtrup, *Org. Synth.*, 2005, **81**, 134-139.
58. A. B. Charette and H. Lebel, *Org. Synth.*, 1999, **76**, 86-100.
59. L. T. Pilarski and K. J. Szabo, *Angew. Chem. Int. Ed.*, 2011, **50**, 8230-8232.
60. G. A. Molander, S. L. Trice and S. D. Dreher, *J. Am. Chem. Soc.*, 2010, **132**, 17701-17703.
61. J. F. Hartwig, *Acc. Chem. Res.*, 2012, **45**, 864-873.
62. K. M. Waltz, *Science*, 1997, **277**, 211-213.
63. K. M. Waltz, X. He, C. Muhoro and J. F. Hartwig, *J. Am. Chem. Soc.*, 1995, **117**, 11357-11358.
64. H. Chen and J. F. Hartwig, *Angew. Chem. Int. Ed.*, 1999, **38**, 3391-3393.
65. C. N. Iverson and M. R. Smith, *J. Am. Chem. Soc.*, 1999, **121**, 7696-7697.
66. H. Chen, S. Schlecht, T. C. Semple and J. F. Hartwig, *Science*, 2000, **287**, 1995-1997.
67. T. Ishiyama, J. Takagi, J. F. Hartwig and N. Miyaura, *Angew. Chem. Int. Ed.*, 2002, **41**, 3056-3058.
68. J. Y. Cho, M. K. Tse, D. Holmes, R. E. Maleczka, Jr. and M. R. Smith, 3rd, *Science*, 2002, **295**, 305-308.
69. T. Ishiyama, J. Takagi, K. Ishida and N. Miyaura, *J. Am. Chem. Soc.*, 2002, **124**, 390-391.
70. J. A. Kerr, *Chem. Rev.*, 1966, **66**, 465-500.
71. S. W. Benson, *J. Chem. Educ.*, 1965, **42**, 502-518.

72. J. D. Lawrence, M. Takahashi, C. Bae and J. F. Hartwig, *J. Am. Chem. Soc.*, 2004, **126**, 15334-15335.
73. D. H. Woodmansee, X. Bu and G. C. Bazan, *Chem. Commun.*, 2001, 619-620.
74. J. M. Murphy, J. D. Lawrence, K. Kawamura, C. Incarvito and J. F. Hartwig, *J. Am. Chem. Soc.*, 2006, **128**, 13684-13685.
75. C. W. Liskey and J. F. Hartwig, *J. Am. Chem. Soc.*, 2012, **134**, 12422-12425.
76. J. Thongpaen, E. S. T, L. Toupet, V. Dorcet, M. Mauduit and O. Basle, *Chem. Commun.*, 2018, **54**, 8202-8205.
77. M. R. Jones, C. D. Fast and N. D. Schley, *J. Am. Chem. Soc.*, 2020, **142**, 6488-6492.
78. R. Oeschger, B. Su, I. Yu, C. Ehinger, E. Romero, S. He and J. Hartwig, *Science*, 2020, **368**, 736-741.
79. J. Campos, U. Hintermair, T. P. Brewster, M. K. Takase and R. H. Crabtree, *ACS Catal.*, 2014, **4**, 973-985.
80. U. Hintermair, S. W. Sheehan, A. R. Parent, D. H. Ess, D. T. Richens, P. H. Vaccaro, G. W. Brudvig and R. H. Crabtree, *J. Am. Chem. Soc.*, 2013, **135**, 10837-10851.
81. A. J. Hart-Davis and R. J. Mawby, *J. Chem. Soc. A*, 1969, 2403-2407.
82. A. J. Hart-Davis, C. White and R. J. Mawby, *Inorg. Chim. Acta*, 1970, **4**, 441-446.
83. M. E. Rerek and F. Basolo, *J. Am. Chem. Soc.*, 1984, **106**, 5908-5912.
84. M. E. Rerek, L.-N. Ji and F. Basolo, *J. Chem. Soc., Chem. Commun.*, 1983, 1208-1209.
85. L. F. Veiros, *Organometallics*, 2000, **19**, 3127-3136.
86. T. Foo and R. G. Bergman, *Organometallics*, 1992, **11**, 1801-1810.
87. T. Foo and R. G. Bergman, *Organometallics*, 1992, **11**, 1811-1819.
88. K. Tatsumi, A. Nakamura, S. Komiya, A. Yamamoto and T. Yamamoto, *J. Am. Chem. Soc.*, 1984, **106**, 8181-8188.
89. S. Komiya, Y. Abe, A. Yamamoto and T. Yamamoto, *Organometallics*, 1983, **2**, 1466-1468.
90. P. S. Braterman, R. J. Cross and G. B. Young, *J. Chem. Soc., Dalton Trans.*, 1977, 1892-1897.
91. R. J. McKinney and D. C. Roe, *J. Am. Chem. Soc.*, 1985, **107**, 261-262.
92. K. I. Gell and J. Schwartz, *J. Am. Chem. Soc.*, 1981, **103**, 2687-2695.
93. A. G. Orpen and N. G. Connelly, *Organometallics*, 1990, **9**, 1206-1210.

94. N. Fey, A. G. Orpen and J. N. Harvey, *Coord. Chem. Rev.*, 2009, **253**, 704-722.
95. C. M. Lavoie and M. Stradiotto, *ACS Catal.*, 2018, **8**, 7228-7250.
96. S. M. Mansell, *Dalton Trans.*, 2017, **46**, 15157-15174.
97. D. Evans, J. A. Osborn and G. Wilkinson, *J. Chem. Soc. A*, 1968, 3133-3142.
98. R. Martin and S. L. Buchwald, *Acc. Chem. Res.*, 2008, **41**, 1461-1473.
99. C. A. Fleckenstein and H. Plenio, *Chem. Soc. Rev.*, 2010, **39**, 694-711.
100. K. C. Nicolaou, P. G. Bulger and D. Sarlah, *Angew. Chem. Int. Ed.*, 2005, **44**, 4442-4489.
101. G. Bertrand and R. Reed, *Coord. Chem. Rev.*, 1994, **137**, 323-355.
102. A. Igau, H. Grutzmacher, A. Baceiredo and G. Bertrand, *J. Am. Chem. Soc.*, 1988, **110**, 6463-6466.
103. A. J. Arduengo, R. L. Harlow and M. Kline, *J. Am. Chem. Soc.*, 1991, **113**, 361-363.
104. A. J. Arduengo, H. V. R. Dias, R. L. Harlow and M. Kline, *J. Am. Chem. Soc.*, 1992, **114**, 5530-5534.
105. A. J. Arduengo, J. R. Goerlich and W. J. Marshall, *J. Am. Chem. Soc.*, 1995, **117**, 11027-11028.
106. A. J. Arduengo, R. Krafczyk, R. Schmutzler, H. A. Craig, J. R. Goerlich, W. J. Marshall and M. Unverzagt, *Tetrahedron*, 1999, **55**, 14523-14534.
107. M. N. Hopkinson, C. Richter, M. Schedler and F. Glorius, *Nature*, 2014, **510**, 485-496.
108. D. Takaki, T. Okayama, H. Shuto, S. Matsumoto, Y. Yamaguchi and S. Matsumoto, *Dalton Trans.*, 2011, **40**, 1445-1447.
109. Y. Yamaguchi, T. Kashiwabara, K. Ogata, Y. Miura, Y. Nakamura, K. Kobayashi and T. Ito, *Chem. Commun.*, 2004, 2160-2161.
110. D. J. Nelson and S. P. Nolan, *Chem. Soc. Rev.*, 2013, **42**, 6723-6753.
111. A. Gomez-Suarez, D. J. Nelson and S. P. Nolan, *Chem. Commun.*, 2017, **53**, 2650-2660.
112. H. V. Huynh, *Chem. Rev.*, 2018, **118**, 9457-9492.
113. C. A. Tolman, *Chem. Rev.*, 1977, **77**, 313-348.
114. R. Dorta, E. D. Stevens, N. M. Scott, C. Costabile, L. Cavallo, C. D. Hoff and S. P. Nolan, *J. Am. Chem. Soc.*, 2005, **127**, 2485-2495.
115. D. G. Gusev, *Organometallics*, 2009, **28**, 6458-6461.
116. Y. Oonishi, A. Gomez-Suarez, A. R. Martin and S. P. Nolan, *Angew. Chem. Int. Ed.*, 2013, **52**, 9767-9771.

117. V. L. Chantler, S. L. Chatwin, R. F. Jazzar, M. F. Mahon, O. Saker and M. K. Whittlesey, *Dalton Trans.*, 2008, 2603-2614.
118. S. P. Reade, M. F. Mahon and M. K. Whittlesey, *J. Am. Chem. Soc.*, 2009, **131**, 1847-1861.
119. P. M. Gois, A. F. Trindade, L. F. Veiros, V. Andre, M. T. Duarte, C. A. Afonso, S. Caddick and F. G. Cloke, *Angew. Chem. Int. Ed.*, 2007, **46**, 5750-5753.
120. O. Back, M. Henry-Ellinger, C. D. Martin, D. Martin and G. Bertrand, *Angew. Chem. Int. Ed.*, 2013, **52**, 2939-2943.
121. A. Liske, K. Verlinden, H. Buhl, K. Schaper and C. Ganter, *Organometallics*, 2013, **32**, 5269-5272.
122. L. Benhamou, E. Chardon, G. Lavigne, S. Bellemin-Laponnaz and V. Cesar, *Chem. Rev.*, 2011, **111**, 2705-2733.
123. A. Beillard, T. X. Metro, X. Bantreil, J. Martinez and F. Lamaty, *Chem. Sci.*, 2017, **8**, 1086-1089.
124. L. Jafarpour, E. D. Stevens and S. P. Nolan, *J. Organomet. Chem.*, 2000, **606**, 49-54.
125. M. Blumel, R. D. Crocker, J. B. Harper, D. Enders and T. V. Nguyen, *Chem. Commun.*, 2016, **52**, 7958-7961.
126. D. J. Cardin, B. Cetinkaya and M. F. Lappert, *Chem. Rev.*, 1972, **72**, 545-574.
127. D. W. Macomber and R. D. Rogers, *J. Organomet. Chem.*, 1986, **308**, 353-360.
128. B. Cetinkaya, P. B. Hitchcock, M. F. Lappert and P. L. Pye, *J. Chem. Soc., Chem. Commun.*, 1975, 683-684.
129. P. B. Hitchcock, M. F. Lappert and P. L. Pye, *J. Chem. Soc., Dalton Trans.*, 1977, 2160-2172.
130. M. F. Lappert and P. L. Pye, *J. Less-Common Met.*, 1977, **54**, 191-207.
131. J. C. Lin, R. T. Huang, C. S. Lee, A. Bhattacharyya, W. S. Hwang and I. J. Lin, *Chem. Rev.*, 2009, **109**, 3561-3598.
132. R. E. Andrew, C. M. Storey and A. B. Chaplin, *Dalton Trans.*, 2016, **45**, 8937-8944.
133. C. Boehme and G. Frenking, *Organometallics*, 1998, **17**, 5801-5809.
134. I. J. B. Lin and C. S. Vasam, *Coord. Chem. Rev.*, 2007, **251**, 642-670.
135. A. M. Voutchkova, M. Feliz, E. Clot, O. Eisenstein and R. H. Crabtree, *J. Am. Chem. Soc.*, 2007, **129**, 12834-12846.
136. M. V. Baker, P. J. Barnard, S. K. Brayshaw, J. L. Hickey, B. W. Skelton and A. H. White, *Dalton Trans.*, 2005, 37-43.

137. P. L. Arnold and I. J. Casely, *Chem. Rev.*, 2009, **109**, 3599-3611.
138. P. de Frémont, N. Marion and S. P. Nolan, *Coord. Chem. Rev.*, 2009, **253**, 862-892.
139. S. Diez-Gonzalez, N. Marion and S. P. Nolan, *Chem. Rev.*, 2009, **109**, 3612-3676.
140. M. Scholl, S. Ding, C. W. Lee and R. H. Grubbs, *Org. Lett.*, 1999, **1**, 953-956.
141. M. S. Sanford, J. A. Love and R. H. Grubbs, *J. Am. Chem. Soc.*, 2001, **123**, 6543-6554.
142. S. Gessler, S. Randl and S. Blechert, *Tetrahedron Lett.*, 2000, **41**, 9973-9976.
143. J. S. Kingsbury, J. P. A. Harrity, P. J. Bonitatebus and A. H. Hoveyda, *J. Am. Chem. Soc.*, 1999, **121**, 791-799.
144. J. A. Love, J. P. Morgan, T. M. Trnka and R. H. Grubbs, *Angew. Chem. Int. Ed.*, 2002, **41**, 4035-4037.
145. D. J. Walsh, S. H. Lau, M. G. Hyatt and D. Guironnet, *J. Am. Chem. Soc.*, 2017, **139**, 13644-13647.
146. A. Leitgeb, J. Wappel and C. Slugovc, *Polymer*, 2010, **51**, 2927-2946.
147. G. C. Fortman and S. P. Nolan, *Chem. Soc. Rev.*, 2011, **40**, 5151-5169.
148. N. Marion and S. P. Nolan, *Acc. Chem. Res.*, 2008, **41**, 1440-1449.
149. E. A. Kantchev, C. J. O'Brien and M. G. Organ, *Angew. Chem. Int. Ed.*, 2007, **46**, 2768-2813.
150. M. S. Viciu, R. M. Kissling, E. D. Stevens and S. P. Nolan, *Org. Lett.*, 2002, **4**, 2229-2231.
151. M. S. Viciu, R. F. Germaneau and S. P. Nolan, *Org. Lett.*, 2002, **4**, 4053-4056.
152. M. S. Viciu, R. F. Germaneau, O. Navarro-Fernandez, E. D. Stevens and S. P. Nolan, *Organometallics*, 2002, **21**, 5470-5472.
153. A. Fürstner, G. Seidel, D. Kremzow and C. W. Lehmann, *Organometallics*, 2003, **22**, 907-909.
154. W. A. Herrmann, C.-P. Reisinger and M. Spiegler, *J. Organomet. Chem.*, 1998, **557**, 93-96.
155. W. A. Herrmann, M. Elison, J. Fischer, C. Köcher and G. R. J. Artus, *Angew. Chem. Int. Ed.*, 1995, **34**, 2371-2374.
156. J.-Y. Lee, P.-Y. Cheng, Y.-H. Tsai, G.-R. Lin, S.-P. Liu, M.-H. Sie and H. M. Lee, *Organometallics*, 2010, **29**, 3901-3911.
157. J. Huang, G. Grasa and S. P. Nolan, *Org. Lett.*, 1999, **1**, 1307-1309.
158. S. R. Stauffer, S. Lee, J. P. Stambuli, S. I. Hauck and J. F. Hartwig, *Org. Lett.*, 2000, **2**, 1423-1426.

159. K. J. Evans and S. M. Mansell, *Chem. Eur. J.*, 2020, **26**, 5927-5941.
160. S. T. Liddle, I. S. Edworthy and P. L. Arnold, *Chem. Soc. Rev.*, 2007, **36**, 1732.
161. P. L. Arnold, S. A. Mungur, A. J. Blake and C. Wilson, *Angew. Chem. Int. Ed.*, 2003, **42**, 5981-5984.
162. P. L. Arnold, A. C. Scarisbrick, A. J. Blake and C. Wilson, *Chem. Commun.*, 2001, 2340-2341.
163. S. P. Downing and A. A. Danopoulos, *Organometallics*, 2006, **25**, 1337-1340.
164. K. J. Evans, B. Potrykus and S. M. Mansell, *Heteroat. Chem.*, 2019, **2019**, 1-6.
165. B. R. Lake, E. K. Bullough, T. J. Williams, A. C. Whitwood, M. A. Little and C. E. Willans, *Chem. Commun.*, 2012, **48**, 4887-4889.
166. M. R. Chapman, Y. M. Shafi, N. Kapur, B. N. Nguyen and C. E. Willans, *Chem. Commun.*, 2015, **51**, 1282-1284.
167. J. C. Garrison and W. J. Youngs, *Chem. Rev.*, 2005, **105**, 3978-4008.
168. B. Royo and E. Peris, *Eur. J. Inorg. Chem.*, 2012, **2012**, 1309-1318.
169. S. P. Downing, S. C. Guadaño, D. Pugh, A. A. Danopoulos, R. M. Bellabarba, M. Hanton, D. Smith and R. P. Tooze, *Organometallics*, 2007, **26**, 3762-3770.
170. H.-M. Sun, D.-M. Hu, Y.-S. Wang, Q. Shen and Y. Zhang, *J. Organomet. Chem.*, 2007, **692**, 903-907.
171. L. Postigo, R. Lopes and B. Royo, *Dalton Trans.*, 2014, **43**, 853-858.
172. L. Postigo and B. Royo, *Adv. Synth. Catal.*, 2012, **354**, 2613-2618.
173. C. Zhang, F. Luo, B. Cheng, B. Li, H. Song, S. Xu and B. Wang, *Dalton Trans.*, 2009, 7230-7235.
174. A. P. da Costa, J. A. Mata, B. Royo and E. Peris, *Organometallics*, 2010, **29**, 1832-1838.
175. A. Pontes da Costa, M. Viciano, M. Sanaú, S. Merino, J. Tejada, E. Peris and B. Royo, *Organometallics*, 2008, **27**, 1305-1309.
176. M. H. S. A. Hamid, P. A. Slatford and J. M. J. Williams, *Adv. Synth. Catal.*, 2007, **349**, 1555-1575.
177. A. J. Watson and J. M. Williams, *Science*, 2010, **329**, 635-636.
178. A. P. da Costa, M. Sanau, E. Peris and B. Royo, *Dalton Trans.*, 2009, 6960-6966.
179. K. Fujita, T. Fujii and R. Yamaguchi, *Org. Lett.*, 2004, **6**, 3525-3528.
180. K.-i. Fujita, Z. Li, N. Ozeki and R. Yamaguchi, *Tetrahedron Lett.*, 2003, **44**, 2687-2690.
181. S. P. Downing, P. J. Pogorzelec, A. A. Danopoulos and D. J. Cole-Hamilton, *Eur. J. Inorg. Chem.*, 2009, 1816-1824.

182. D. Roberto, E. Cariati, R. Psaro and R. Ugo, *Organometallics*, 1994, **13**, 4227-4231.
183. A. E. C. McConnell, D. F. Foster, P. Pogorzelec, A. M. Z. Slawin, D. J. Law and D. J. Cole-Hamilton, *Dalton Trans.*, 2003, 510-512.
184. A. C. McConnell, P. J. Pogorzelec, A. M. Slawin, G. L. Williams, P. I. Elliott, A. Haynes, A. C. Marr and D. J. Cole-Hamilton, *Dalton Trans.*, 2006, 91-107.
185. C. White, A. Yates, P. M. Maitlis and D. M. Heinekey, *Inorg. Synth.*, 1992, **29**, 228-234.
186. A. Archambeau and T. Rovis, *Angew. Chem. Int. Ed.*, 2015, **54**, 13337-13340.
187. T. A. Davis, C. Wang and T. Rovis, *Synlett*, 2015, **26**, 1520-1524.
188. G. Liu, Y. Shen, Z. Zhou and X. Lu, *Angew. Chem. Int. Ed.*, 2013, **52**, 6033-6037.
189. T. K. Hyster, K. E. Ruhl and T. Rovis, *J. Am. Chem. Soc.*, 2013, **135**, 5364-5367.
190. J. Jayakumar, K. Parthasarathy and C. H. Cheng, *Angew. Chem. Int. Ed.*, 2012, **51**, 197-200.
191. S. Rakshit, F. W. Patureau and F. Glorius, *J. Am. Chem. Soc.*, 2010, **132**, 9585-9587.
192. S. Rej and N. Chatani, *Angew. Chem. Int. Ed.*, 2019, **58**, 8304-8329.
193. R. B. King, *Inorg. Chem.*, 1963, **2**, 528-531.
194. S. T. Belt, S. B. Duckett, D. M. Haddleton and R. N. Perutz, *Organometallics*, 1989, **8**, 748-759.
195. J. Knight and M. J. Mays, *J. Chem. Soc. A*, 1970, 654-658.
196. G. Giordano, R. H. Crabtree, R. M. Heintz, D. Forster and D. E. Morris, *Inorg. Synth.*, 1990, **28**, 88-90.
197. A. Van Der Ent, A. L. Onderdelinden and R. A. Schunn, *Inorg. Synth.*, 1990, **28**, 90-92.
198. J. A. McCleverty, G. Wilkinson, L. G. Lipson, M. L. Maddox and H. D. Kaesz, *Inorg. Synth.*, 1990, **28**, 84-86.
199. R. Cramer, J. A. McCleverty and J. Bray, *Inorg. Synth.*, 1990, **28**, 86-88.
200. R. Cramer, J. A. McCleverty and J. Bray, *Inorg. Synth.*, 1974, **15**, 14-18.
201. E. Fooladi, B. Dalhus and M. Tilset, *Dalton Trans.*, 2004, 3909-3917.
202. A. B. Chaplin, *Organometallics*, 2014, **33**, 3069-3077.
203. J. Terasawa, Y. Shibata, Y. Kimura and K. Tanaka, *Chem. Asian J.*, 2018, **13**, 505-509.
204. N. Semakul, K. E. Jackson, R. S. Paton and T. Rovis, *Chem. Sci.*, 2017, **8**, 1015-1020.

205. M. Hussain, S. Kohser, K. Janssen, R. Wartchow and H. Butenschön, *Organometallics*, 2009, **28**, 5212-5221.
206. H. Eshtiagh-Hosseini and J. F. Nixon, *J. Less-Common Met.*, 1978, **61**, 107-121.
207. N. Dunwoody, S.-S. Sun and A. J. Lees, *Inorg. Chem.*, 2000, **39**, 4442-4451.
208. M. Prinz, L. F. Veiros, M. J. Calhorda, C. C. Romão, E. Herdtweck, F. E. Kühn and W. A. Herrmann, *J. Organomet. Chem.*, 2006, **691**, 4446-4458.
209. D. Johnels, A. Andersson, A. Boman and U. Edlund, *Magn. Reson. Chem.*, 1996, **34**, 908-912.
210. M. Rosello-Merino and S. M. Mansell, *Dalton Trans.*, 2016, **45**, 6282-6293.
211. A. J. Arduengo, M. Tamm, J. C. Calabrese, F. Davidson and W. J. Marshall, *Chem. Lett.*, 1999, **28**, 1021-1022.
212. M. S. Hill, G. Kociok-Kohn and D. J. MacDougall, *Inorg. Chem.*, 2011, **50**, 5234-5241.
213. C. N. Garon, D. I. McIsaac, C. M. Vogels, A. Decken, I. D. Williams, C. Kleeberg, T. B. Marder and S. A. Westcott, *Dalton Trans.*, 2009, 1624-1631.
214. S. E. Barrows and T. H. Eberlein, *J. Chem. Educ.*, 2005, **82**, 1334-1339.
215. K. Moseley, J. W. Kang and P. M. Maitlis, *J. Chem. Soc. A*, 1970, 2875-2883.
216. D. W. Hoard and P. R. Sharp, *Inorg. Chem.*, 1993, **32**, 612-620.
217. P. R. Sharp, D. W. Hoard and C. L. Barnes, *J. Am. Chem. Soc.*, 1990, **112**, 2024-2026.
218. X. Yi, B. Liu, K. Chen, W. Chen and W. Chen, *Dalton Trans.*, 2019, **48**, 3835-3839.
219. N. Fey, M. F. Haddow, R. Mistry, N. C. Norman, A. G. Orpen, T. J. Reynolds and P. G. Pringle, *Organometallics*, 2012, **31**, 2907-2913.
220. P. Caddy, M. Green, L. E. Smart and N. White, *J. Chem. Soc., Chem. Commun.*, 1978, 839-841.
221. M. J. Calhorda, C. C. Romão and L. F. Veiros, *Chem. Eur. J.*, 2002, **8**, 868-875.
222. X.-Y. Yu, B. O. Patrick and B. R. James, *Organometallics*, 2006, **25**, 4870-4877.
223. N. M. Scott, R. Dorta, E. D. Stevens, A. Correa, L. Cavallo and S. P. Nolan, *J. Am. Chem. Soc.*, 2005, **127**, 3516-3526.
224. O. V. Zenkina, E. C. Keske, R. Wang and C. M. Crudden, *Organometallics*, 2011, **30**, 6423-6432.
225. O. V. Zenkina, E. C. Keske, R. Wang and C. M. Crudden, *Angew. Chem. Int. Ed.*, 2011, **50**, 8100-8104.

226. T. W. Bell, S. A. Brough, M. G. Partridge, R. N. Perutz and A. D. Rooney, *Organometallics*, 1993, **12**, 2933-2941.
227. D. P. Klein, J. C. Hayes and R. G. Bergman, *J. Am. Chem. Soc.*, 1988, **110**, 3704-3706.
228. L. J. Newman and R. G. Bergman, *J. Am. Chem. Soc.*, 1985, **107**, 5314-5315.
229. J. W. Verhoeven, *Pure Appl. Chem.*, 1996, **68**, 2223-2286.
230. A. B. Chaplin, A. I. Poblador-Bahamonde, H. A. Sparkes, J. A. Howard, S. A. Macgregor and A. S. Weller, *Chem. Commun.*, 2009, 244-246.
231. G. R. Fulmer, A. J. M. Miller, N. H. Sherden, H. E. Gottlieb, A. Nudelman, B. M. Stoltz, J. E. Bercaw and K. I. Goldberg, *Organometallics*, 2010, **29**, 2176-2179.
232. S. B. Duckett, D. M. Haddleton, S. A. Jackson, R. N. Perutz, M. Poliakoff and R. K. Upmacis, *Organometallics*, 1988, **7**, 1526-1532.
233. M. V. Câmpian, J. L. Harris, N. Jasim, R. N. Perutz, T. B. Marder and A. C. Whitwood, *Organometallics*, 2006, **25**, 5093-5104.
234. S. N. Heaton, M. G. Partridge, R. N. Perutz, S. J. Parsons and F. Zimmermann, *J. Chem. Soc., Dalton Trans.*, 1998, 2515-2520.
235. J. S. Price, D. J. H. Emslie and B. Berno, *Organometallics*, 2019, **38**, 2347-2362.
236. J. Y. Corey, *Chem. Rev.*, 2016, **116**, 11291-11435.
237. P. Hofmann, H. Heiss, P. Neiteler, G. Müller and J. Lachmann, *Angew. Chem. Int. Ed.*, 1990, **29**, 880-882.
238. S. J. Mitton, R. McDonald and L. Turculet, *Angew. Chem. Int. Ed.*, 2009, **48**, 8568-8571.
239. H. Kameo, S. Ishii and H. Nakazawa, *Dalton Trans.*, 2013, **42**.
240. L. Zámostná, M. Ahrens and T. Braun, *J. Fluorine Chem.*, 2013, **155**, 132-142.
241. K. A. Trankler, J. Y. Corey and N. P. Rath, *J. Organomet. Chem.*, 2003, **686**, 66-74.
242. C. E. Johnson and R. Eisenberg, *J. Am. Chem. Soc.*, 1985, **107**, 6531-6540.
243. S. Park, B. G. Kim, I. Göttker-Schnetmann and M. Brookhart, *ACS Catal.*, 2012, **2**, 307-316.
244. J. F. Hartwig, *Chem. Soc. Rev.*, 2011, **40**, 1992-2002.
245. L. Xu, G. Wang, S. Zhang, H. Wang, L. Wang, L. Liu, J. Jiao and P. Li, *Tetrahedron*, 2017, **73**, 7123-7157.
246. T. Ishiyama, J. Takagi, K. Ishida, N. Miyaoura, N. R. Anastasi and J. F. Hartwig, *J. Am. Chem. Soc.*, 2002, **124**, 390-391.

247. T. M. Boller, J. M. Murphy, M. Hapke, T. Ishiyama, N. Miyaura and J. F. Hartwig, *J. Am. Chem. Soc.*, 2005, **127**, 14263-14278.
248. W. N. Palmer, J. V. Obligacion, I. Pappas and P. J. Chirik, *J. Am. Chem. Soc.*, 2016, **138**, 766-769.
249. J.-Y. Cho, C. N. Iverson and M. R. Smith, *J. Am. Chem. Soc.*, 2000, **122**, 12868-12869.
250. C. W. Liskey, C. S. Wei, D. R. Pahls and J. F. Hartwig, *Chem. Commun.*, 2009, 5603-5605.
251. K. Pandey, *Coord. Chem. Rev.*, 2009, **253**, 37-55.
252. H. Butenschon, *Chem. Rev.*, 2000, **100**, 1527-1564.
253. U. Siemeling, *Chem. Rev.*, 2000, **100**, 1495-1526.
254. B. Wang, D. Cui and K. Lv, *Macromolecules*, 2008, **41**, 1983-1988.
255. S. Li, D. Liu, Z. Wang and D. Cui, *ACS Catal.*, 2018, **8**, 6086-6093.
256. O. Kuhl, *Chem. Soc. Rev.*, 2007, **36**, 592-607.
257. S. J. Grabowski, *Crystals*, 2020, **10**.
258. N. N. Wang, Q. G. Zhang, F. G. Wu, Q. Z. Li and Z. W. Yu, *J. Phys. Chem. B*, 2010, **114**, 8689-8700.
259. Y. Xu, T. Li, C. Peng and H. Liu, *Ind. Eng. Chem. Res.*, 2015, **54**, 9038-9045.
260. T. Bischof, K. J. Evans, M. F. Haddow and S. M. Mansell, *Acta Crystallogr., Sect. E: Crystallogr. Commun.*, 2020, **76**, 254-256.
261. K. J. Evans, C. L. Campbell, M. F. Haddow, C. Luz, P. A. Morton and S. M. Mansell, *Eur. J. Inorg. Chem.*, 2019, **2019**, 4894-4901.
262. P. L. Arnold, I. J. Casely, Z. R. Turner and C. D. Carmichael, *Chem. Eur. J.*, 2008, **14**, 10415-10422.
263. S. Fantasia, J. L. Petersen, H. Jacobsen, L. Cavallo and S. P. Nolan, *Organometallics*, 2007, **26**, 5880-5889.
264. M. H. Dunn, N. Konstandaras, M. L. Cole and J. B. Harper, *J. Org. Chem.*, 2017, **82**, 7324-7331.
265. N. Konstandaras, M. H. Dunn, E. T. Luis, M. L. Cole and J. B. Harper, *Org. Biomol. Chem.*, 2020, **18**, 1910-1917.
266. H. M. J. Wang and I. J. B. Lin, *Organometallics*, 1998, **17**, 972-975.
267. M. Iglesias, D. J. Beetstra, J. C. Knight, L.-L. Ooi, A. Stasch, S. Coles, L. Male, M. B. Hursthouse, K. J. Cavell, A. Dervisi and I. A. Fallis, *Organometallics*, 2008, **27**, 3279-3289.
268. M. R. Furst and C. S. Cazin, *Chem. Commun.*, 2010, **46**, 6924-6925.

269. T. Okayama, T. Watanabe, Y. Hatayama, S. Ishihara and Y. Yamaguchi, *Inorg. Chim. Acta*, 2016, **448**, 1-6.
270. W. Clegg, K. W. Henderson, A. R. Kennedy, R. E. Mulvey, C. T. O'Hara, R. B. Rowlings and D. M. Tooke, *Angew. Chem. Int. Ed.*, 2001, **40**, 3902-3905.
271. A. J. Martinez-Martinez, A. R. Kennedy, R. E. Mulvey and C. T. O'Hara, *Science*, 2014, **346**, 834-837.
272. P. C. Andrikopoulos, D. R. Armstrong, D. V. Graham, E. Hevia, A. R. Kennedy, R. E. Mulvey, C. T. O'Hara and C. Talmard, *Angew. Chem. Int. Ed.*, 2005, **44**, 3459-3462.
273. S. G. Rachor, P. A. Cleaves, S. D. Robertson and S. M. Mansell, *J. Organomet. Chem.*, 2018, **857**, 101-109.
274. K. J. Evans and S. M. Mansell, *Chem. Eur. J.*, 2019, **25**, 3766-3769.
275. R. E. Dinnebier, U. Behrens and F. Olbrich, *J. Am. Chem. Soc.*, 1998, **120**, 1430-1433.
276. C. Strohmann, K. Strohfeldt, D. Schilbach, M. J. McGrath and P. O'Brien, *Organometallics*, 2004, **23**, 5389-5391.
277. A. Hernan-Gomez, A. R. Kennedy and E. Hevia, *Angew. Chem. Int. Ed.*, 2017, **56**, 6632-6635.
278. M. Uzelac and E. Hevia, *Chem. Commun.*, 2018, **54**, 2455-2462.
279. A. Koch, H. Gorls, S. Kriek and M. Westerhausen, *Dalton Trans.*, 2017, **46**, 9058-9067.
280. A. J. Martinez-Martinez, M. A. Fuentes, A. Hernan-Gomez, E. Hevia, A. R. Kennedy, R. E. Mulvey and C. T. O'Hara, *Angew. Chem. Int. Ed.*, 2015, **54**, 14075-14079.
281. R. W. Alder, M. E. Blake, C. Bortolotti, S. Bufali, C. P. Butts, E. Linehan, J. M. Oliva, A. Guy Orpen and M. J. Quayle, *Chem. Commun.*, 1999, 241-242.
282. P. L. Arnold, M. Rodden and C. Wilson, *Chem. Commun.*, 2005, 1743-1745.
283. A. A. Danopoulos and P. Braunstein, *Chem. Commun.*, 2014, **50**, 3055-3057.
284. H. Türkmen and B. Çetinkaya, *Appl. Organometal. Chem.*, 2011, **25**, 226-232.
285. B. Cordero, V. Gomez, A. E. Platero-Prats, M. Reves, J. Echeverria, E. Cremades, F. Barragan and S. Alvarez, *Dalton Trans.*, 2008, 2832-2838.
286. P. Binger, R. Milczarek, R. Mynott, C. Krüger, Y.-H. Tsay, E. Raabe and M. Regitz, *Chem. Ber.*, 1988, **121**, 637-645.
287. R. Benn, K. Cibura, P. Hofmann, K. Jonas and A. Rufinska, *Organometallics*, 1985, **4**, 2214-2221.

288. A. J. Roberts, A. R. Kennedy, R. McLellan, S. D. Robertson and E. Hevia, *Eur. J. Inorg. Chem.*, 2016, **2016**, 4752-4760.
289. M. F. Lappert, M. J. Slade, A. Singh, J. L. Atwood, R. D. Rogers and R. Shakir, *J. Am. Chem. Soc.*, 1983, **105**, 302-304.
290. C.-I. Lee, N. A. Hirscher, J. Zhou, N. Bhuvanesh and O. V. Ozerov, *Organometallics*, 2015, **34**, 3099-3102.
291. C.-T. Chen, M. E. Fischer, C. Windsor, I. C. Vei, D. G. Calatayud, M. L. H. Green and S. I. Pascu, *Polyhedron*, 2016, **119**, 532-547.
292. T. Ishiyama, M. Murata and N. Miyaura, *J. Org. Chem.*, 1995, **60**, 7508-7510.
293. F. Mo, Y. Jiang, D. Qiu, Y. Zhang and J. Wang, *Angew. Chem. Int. Ed.*, 2010, **49**, 1846-1849.
294. W. Srimontree, L. Guo and M. Rueping, *Chem. Eur. J.*, 2020, **26**, 423-427.
295. H. Kinuta, M. Tobisu and N. Chatani, *J. Am. Chem. Soc.*, 2015, **137**, 1593-1600.
296. C. E. Tucker, J. Davidson and P. Knochel, *J. Org. Chem.*, 1992, **57**, 3482-3485.